Polarisation Resolved Spectroscopy of Laser Produced Plasmas

A thesis submitted for the degree of:

DOCTOR OF PHILOSOPHY

DUBLIN CITY UNIVERSITY (DCU)

College of Science and Health

School of Physical Science

National Center for Plasma Science and Technolgy (NCPST)

MILITARY UNIVERSITY OF TECHNOLOGY (MUT)

Institute of Optoelectronics (IOE)

Author

Getasew Admasu Wubetu

Master of Nanophysics, University of Antwerp, Belgium (2009)

M.Sc in Nanomaterials, University of Ulm, Germany (2004)

B.Ed in Physics, Alemaya University, Ethiopia (2000)

Research Supervisors

Prof. John T. Costello

Prof. Henryk Fiedorowicz

Co-Supervisors

Dr. Mossy Kelly

Dr. Wojciech Skrzeczanowski

August 2017

POLARISATION RESOLVED SPECTROSCOPY OF LASER PRODUCED PLASMAS

Thesis presented by

Getasew Admasu Wubetu

Prof. John Costello
(Promoter) &
Dr. Mossy Kelly
(Assistant Promoter)

Dublin City University

Prof. Henryk Fiedorowicz
(Co-Promoter)
Dr Wojciech Skrzeczanowski
(Assistant Promoter)

Military University of Technology

Doctoral Studies Panel Membership:
Prof. John Costello
Prof. Henryk Fiedorowicz
Dr. Mossy Kelly
Dr. Wojciech Skrzeczanowski
Erasmus Mundus Joint Doctorate, EXTATIC

August 2017

Declaration

I hereby certify that this material, which I now submit for assessment on the programme of study leading to the award of Doctor of Philosophy is entirely my own work, and that I have exercised reasonable care to ensure that the work is original, and does not to the best of my knowledge breach any law of copyright, and has not been taken from the work of others save and to the extent that such work has been cited and acknowledged within the text of my work.

Signed: _____

ID No.: ____13212916_____

Date: _____

Dedicated to my wife Wub and my son Michael

Acknowledgements

I would like to thank all of those people who have helped me in various ways during my doctoral studies. First and foremost, my sincere gratitude goes to my supervisor Prof. John Costello for his constant guidance, theoretical and experimental discussions and all-round assistance throughout my study. John is always there to help during difficult times in regard to both personal and educational matters. He has done his level best to assist with my personal long-time goal of becoming a research qualified experimental physicist.

My sincere thanks to my co-supervisor Prof. Henryk Fiedorowicz at the Institute of Optoelectronics, Military University of Technology for the chance to work in his research group. Thanks, are also due to Dr Wojciech Skrzeczanowski, Dr Bartnik Andrzej and Dr Przemyslaw Wachulak for discussions and help with experiments at MUT. I would also like to express my appreciation to EXTATIC students Mesfin, Alfio and Ismail for making life in Poland enjoyable.

I would also like to thank, Dr Mossy Kelly, who gave me the laser plasma spectroscopy training from the get go. Thank you for the invaluable scientific discussions, guidance and constant advice during my study.

I always remember Dr Paul van Kampen for his kind help during my arrival and registration at DCU. Thanks also to DCU group students William, Ben, Steve, Hu, Mohammed, Sadaf, Lazarus, Tejawi and Columb for their friendship. I would like to thank, Dr Paddy Hayden, Dr Colm Fallon, Dr Nicky Walsh, and Dr Pramod Pandey for being supportive and great colleagues to work with.

I would like to acknowledge the EXTATIC management, Irene, Sheila and Fiona for their hospitality and administrative work in my study period. I thank also the technical people like Des Lavelle, Pat Wogan and Alan Hughes for their kind help.

I would like to express my deepest appreciation to Paula, Colin and Shane for the kind hospitality. You guys have made staying at your place feel like home. I consider Paula and her family as my Irish relatives. I appreciate also Girum for his friendship and the discussion we had on atomic and plasma physics. We discussed with each other physics in addition to creating the chance to converse in our mother tongue abroad. I appreciate the mass group in the Saint Marry Ethiopian Orthodox Church at Dublin for their heart warming and refreshing weekly program.

Finally, I would like to express my sincere thanks to my dad Likegubae Admasu and mom Yimegnushal, my wife Wub, my son Michael, my sister Hager, my cousins Tsegaye and Sisay, my friend Amanuel for their love and support during the entire period of my PhD work. At last, I want to express my thanks to the Almighty God for the bright light on my way.

Table of Contents

List of Tables

List of Figures

Symbolic Notation

Symbol	Meaning	Page
λ	Wavelength	xxvii
n_e	Electron density	11
n_q	Ion density	11
q	Charge state of ion	11
λ_D	Debye length	11
ε_0	Electric permittivity constant	11
k_B	Boltzmann constant	11
T_e	Electron temperature	11
e	Charge of electron	11
N_D	Number of electron in Debye sphere	11
ω_e	Characteristic plasma electron frequency	12
m_e	Mass of electron	12
ω_p	Plasma frequency	12
ω_i	Ion frequency	12
n_c	Critical density	12
α_{IB}	Absorption coefficient	15
E	Kinetic energy	16
v_e	Velocity of electron	16
h	Planck's constant	16
v	frequency	16
I_p	Ionization potential	16
τ	Electron ion/atom characteristics time	19

r	Impact parameter	19
a	Acceleration	19
ΔE	Energy at maximum acceleration	20
W	Power radiated per unit of electron	20
$f(v)$	Maxwellian electron distribution function	20
P_{ff}	Power per unit of volume of free to free transition	20
P_{fb}	Power per unit of volume of free to bound transition	20
P_{bb}	Power per unit of volume of bound to bound transition	21
τ_{ff}	Characteristics time of free to free transition	21
τ_{fb}	Characteristics time of free to bound transition	21
τ_{bb}	Characteristics time of bound to bound transition	21
S	Collisional ionization rate	24
α_r	Rate of recombination	24
$\chi_{\mathbf{q}}$	Ionisation potential	25
$\xi_{\mathbf{q}}$	Electron occupying in the outer shell	25
α_{3B}	Rate of three body recombination	25
P	Degree of Polarisation	26
I_H	Intensity parallel to the quantisation axis of the laser	26
I_V	Intensity perpendicular to quantisation axis of the laser	26
v_H	Velocity along the parallel direction	28
v_V	Velocity along the perpendicular direction	28
T_H	Temperature along the parallel direction	28
T_V	Temperature along the perpendicular direction	28
$\tilde{\Pi}(\omega)$	Degree of linear polarisation of recombination radiation	29
γ	Growth rate	31

A_t	Atwood constant	31
α	Set of all quantum number in the upper state	31

List of Abbreviations

Abbreviation	Meaning	Page
Nd: YAG	Neodymium Doped Yttrium Aluminium Garnet	xxviii
ICCD	Intensified Charge-Coupled Device	xxviii
EVDF	Electron Velocity Distribution Function	xxviii
RT	Rayleigh-Taylor	xxviii
PRLIBS	Polarisation Laser Induced Breakdown Spectroscopy	1
LOD	Limit of Detection	1
PPS	Plasma Polarisation Spectroscopy	1
LIBS	Laser Induced Breakdown Spectroscopy	1
PLD	Pulsed Laser Deposition	2
SBR	Signal to Background Ratio	2
LPPS	Laser Plasma Polarisation Spectroscopy	5
LTE	Local Thermodynamic Equilibrium	10
IB	Inverse Bremsstrahlung	12
F-F	Free-Free	14
F-B	Free-Bound	14
B-B	Bound-Bound	14
CE	Coronal Equilibrium	25
CRE	Collisional Radiative Equilibrium	25
CRM	Collisional Radiative Model	25
MBD	Maxwell Boltzmann Distribution	27
RR	Radiative Recombination	86
3B	Three Body Recombination	86

Abstract

Getasew Admasu Wubetu

Polarisation Resolved Spectroscopy of Laser Produced Plasmas

The degree of polarisation of the light emitted from laser produced plasmas has been studied using time-resolved imaging along with time- and polarisation-resolved spectroscopy in the visible spectral range. A Q-switched Nd: YAG laser (λ = 1064 nm, pulse width = 14 ns) was used to ablate the target. Optical spectra were obtained using a Czerny-Turner spectrometer equipped with an intensified charge-coupled device (ICCD) readout. A Wollaston prism split the emitted radiation into orthogonally polarised states for simultaneous spectral acquisition.

Polarisation anisotropy in line emission is the result of a non-statistical distribution of population amongst the available magnetic sublevels in the upper state of the transition of interest. The origin of the non-statistical distribution lies in an anisotropy in the electron velocity distribution function (EVDF) which is the most often described by a bi-Maxwellian function. For the continuum emission, it is found that the main contributor is recombination radiation and once again an EVDF anisotropy is the origin. In this case the partially preferred direction of motion of the recombining electrons is transferred into a partially preferred polarisation direction.

The imaging results reveal stronger plasma emission polarisation in air than in vacuo. They also showed stronger polarisation of the continuum emission compared to line emission at higher pressure for Al^0 (at 396.15 nm) and Al^+ (466.3 nm) features. In vacuo, the degree of polarisation (P_λ) of all charge states studied oscillates with time. It is suggested that this oscillation is a result of self-generated magnetic fields which cause the plasma itself to undergo compression and rarefraction cycles. In this case the EVDF will also oscillate and hence the degree of polarisation will do so. The magnetic field itself is thought to arise from Rayleigh-Taylor (RT) instability.

The effects of target geometry and incident laser polarisation on the emission were also studied. A greater effect was observed for continuum radiation compared to line emission. It is also observed that the laser polarisation has the greatest effect for oblique incidence on the target.

Streszczenie

Getasew Admasu Wubetu

Spektroskopia polaryzacyjna plazmy wytwarzanej laserem

Stopień polaryzacji światła emitowanego z plazmy wytwarzanej metodą laserową badano przy użyciu obrazowania z rozdzielczością w czasie wraz z polaryzacyjną spektroskopią w widzialnym zakresie widma. Do ablacji materiału tarczy i wytwarzania tarczy użyto lasera Nd: YAG typu Q (λ = 1064 nm, długość impulsu = 14 ns). Widma optyczne uzyskano stosując spektrometr Czerny-Turnera wyposażony w kamerę z układem ICCD. Do rozdzielania wiązki promieniowania na prostopadłe składowe polaryzacji zastosowano pryzmat Wollastona.

Stwierdzono anizotropię polaryzacji w emisji promieniowania liniowego, która jest wynikiem niestatystycznego rozkładu obsadzeń wśród dostępnych podpoziomów magnetycznych dla górnego poziomu przejścia. Przyczyną nierównomiernego rozkładu jest anizotropia funkcji rozkładu prędkości elektronów (EVDF), która jest najczęściej opisywana przez funkcję Bi-Maxwellian. W przypadku emisji promieniowania ciągłego stwierdzono, że jego głównym składnikiem jest promieniowanie rekombinacyjne, a źródłem anizotropii polaryzacji jest anizotropia EVDF.

Wyniki obrazowania plazmy wykazują silniejszą polaryzację emisji w powietrzu aniżeli w próżni. Wykazały one również silną polaryzację emisji ciągłej w porównaniu z emisją linii przy wyższym ciśnieniu w przypadku atomów Al^0 (dla 396,15 nm) i Al^+ (dla 466,3 nm). W próżni stopień polaryzacji (P_λ) wszystkich badanych stanów ładowania oscyluje w czasie. Zasugerowano, że ta oscylacja jest rezultatem spontanicznych pól magnetycznych, które powodują, że sama plazma ulega cyklom ściskania i rozprężania. W tym przypadku rozkład EVDF również oscyluje i powoduje polaryzację. Można przypuszczać, że pole magnetyczne powstaje w wyniku niestabilności Rayleigha-Taylora (RT).

Badano również wpływ geometrii tarczy oraz polaryzacji wiązki laserowej na emisję promieniowania. Zaobserwowano większy wpływ w przypadku promieniowania ciągłego w porównaniu z liniowym. Stwierdzono również, że wpływ polaryzacji wiązki laserowej jest największy w przypadku ukośnego podania wiązki laserowej na tarczę.

1 Introduction

In this chapter, Polarisation Resolved Laser Induced Breakdown Spectroscopy (PRLIBS) is introduced along with the motivation for this specific PhD project and its potential relationship to improving the limit-of-detection (LOD) for LIBS. Although there are only a limited number of articles on plasma polarisation spectroscopy (PPS), especially in the optical region of the electromagnetic spectrum, the historical evolution of this topic is outlined, including reference to some of the more important pieces of literature relevant to the work presented in this thesis. The basic physics of PPS is explained outlining the processes underlying partial polarisation of continuum and line emission, which will be discussed in greater detail in the next chapter. Finally, the specific objectives of this project and the outline of the thesis are provided.

1.1 Motivation

When a pulsed laser is focused to vaporise and ionise a target material (solid, liquid or gas), and when the laser irradiance is greater than the threshold energy of the target material, a plasma is formed [1]. The emitted plasma radiation comprises of a mix of continuum and line spectra. The continuum emission is the result of both bremsstrahlung radiation (free to free electron transitions) and recombination radiation (free to bound electron transitions) [1], [2]. On the other hand, line radiation arises from bound to bound transitions [2].

The primary motivation of this PhD project is the systematic study of time and polarisation resolved imaging and spectroscopy of laser produced aluminium plasmas for well-defined laser and target properties. The key parameter measured is the degree of polarisation of the emitted plasma radiation which is determined by the plasma's electron velocity distribution function (EVDF). There are a number of previous studies on polarised emission from laser produced plasmas. However, they often look at a single spectrum line, or continuum only or in other wavelength ranges, e.g., the X-ray spectra range and are carried out for different laser parameters (e.g., ns, ps and fs pulses) and target environments (background gases, etc.). Also, most existing studies only offer suggestions for the physical origin of the polarisation of plasma radiation and ignore key theoretical papers which tackle this very problem.

The secondary motivation is Laser-induced breakdown spectroscopy (LIBS) which is a subfield of laser plasma spectroscopy and a widely used analytical technique which permits the classification, and potentially the quantification, of atomic elements in a host material referred to as a matrix [1]–[5]. LIBS has become a popular analytical technique for numerous applications in pulsed laser deposition (PLD) [6], material science [7], bio-medicine [6] and space exploration [7]. The advantages of LIBS include no or minimal sample preparation along with fast data acquisition and detection [2], [3]. However, LIBS suffers from issues such as reproducibility, accuracy and sensitivity compared to other analytical techniques [3]. One of the reasons for this is the interference between continuum and line emission which degrades the signal-to-background ratio (SBR).

There are significant efforts currently being made worldwide to increase the main performance parameter of LIBS, namely the limit of detection (LOD). For example, single and double pulse LIBS in a background gas has been found to enhance the sensitivity of the LIBS technique. In our laboratory, vacuum ultraviolet (VUV) LIBS in both single pulse [8] and double pulse [3] configurations has been explored in the framework of improving the LOD which is determined by the signal to background ratio (SBR). Gated LIBS has been used in many labs to increase the SBR and hence improve the LOD [6], [9], [10]. For nanosecond ablation of solids, continuum emission at the early stage of plasma evolution lasts on average for approximately 100 ns [2]. By delaying the opening of the intensified charge-coupled device (ICCD) shutter with respect to the laser pulse, one can reduce the level of the background continuum which increases the SBR and hence improves the LOD [6], [9], [10]. However, this technique is highly dependent on the choice of material to be studied. Recently, it has been reported that polarisation resolved laser induced breakdown spectroscopy (PRLIBS) allows for a reduction in the level of continuum observed in laser plasma emission spectra [10]. PRLIBS works by placing a polariser in front of the detector [10], [11]. In femtosecond ablation experiments, the continuum has been found to be highly polarised, above 90 % in some cases [10]. In the case of nanosecond ablation, the degree of polarisation of the continuum has been shown to be dependent on the laser fluence [12]. In addition, studying the polarisation of the emitted radiation can also reveal information about the spatial distribution of the electron velocities within the plasma [13].

The focus of previous PRLIBS studies can be categorised into three areas: -

(1) The electrons in the plasma do not follow a single Maxwell-Boltzmann distribution. This is sometimes called an anisotropic electron velocity distribution [13], [14].
(2) Self generated or external, electric and magnetic fields exist which can alter the electron velocity distribution and break the magnetic sub-level degeneracy [14].
(3) The improvement of the performance of LIBS [9]–[11].

Several reasons for the partial polarisation of radiation emitted by laser produced plasmas have been put forward. These include anisotropy due to radiative recombination [15] and

anisotropy due to an imbalance of populations in the magnetic sublevels of the atoms and ions in the plasma [9], [10]. It has also been suggested that perhaps the laser polarisation direction is imprinted onto the plasma emission [9] and/or perhaps light reflected inside the plasma becomes partially polarised [11]. In all cases, however, the general agreement is that for light to be partially polarised from a plasma, the plasma must be out of equilibrium [14].

1.2 Background

Historically, the field of spectroscopy in external fields was amongst the first to be awarded the Nobel Prize in Physics. The 1902 Nobel Prize was awarded for the Zeeman effect while the Stark effect gained the 1919 Nobel Prize. In 1924 Hanle tracked the polarisation of fluorescence from mercury vapour against the applied magnetic field [14]. Later, in the mid. 1960's, plasma polarisation spectroscopy experiments were started by three groups. Lombard and Pebay- Peyrolla [14] were the first to observe polarisation of neutral helium lines from a high-frequency discharge; in 1969, Kalla and Chaika investigated the polarisation state of neon lines in discharge plasmas [16]. They designated the polarisation ''Self-alignment''. Alignment refers to a non-statistical but symmetric distribution of the quantum number m_J. Orientation refers to a non-statistical and asymmetric distribution of the quantum number m_J. Classically one can think of angular momentum vectors which are aligned along some preferred direction 'z'. If they are aligned the numbers pointing up and down are equal and opposite, but may point in different directions in a single plane [17]. On the other hand, if they are oriented they do not cancel. In experiments, one must then define a preferred direction which may be e.g., the direction of a laser beam incident on the atom of molecule or the direction of a polarised laser used to excite atom or polarise an atomic cloud. Scientists in the Soviet Union investigated further the polarisation of discharge plasmas in the 1970s and 1980's [14].

In the mid. 1980's, laser plasma polarisation spectroscopy experiments performed on a highly charged aluminium plasma produced with a picosecond laser, showed the X-ray emission to exhibit a partial polarisation [13]. It was found that resonance and intercombination

transitions are polarised differently. The polarisation of the intercombination lines was attributed to an anisotropic electron velocity distribution function arising from spatially anisotropic electron density profiles. Theoretically, the polarisation of recombination emission has been studied [15] and offered as an explanation for the experimental observation of continuum polarisation. More recent experiments have observed polarisation of the emission from lowly charged ions in aluminium [18], [19] in a low density and low-temperature plasma. Ions, formed in excited states, subsequently decay by spontaneous line emission which is partially polarised due to an asymmetry in the magnetic sublevel populations between such excited states. Time-resolved polarisation measurements on gas confined laser plasmas revealed a strong anisotropy in the radiation emitted [20] particularly for the case of short pulse irradiation (typically, during picosecond ablation). It was found in this study that the anisotropy in the Al^{2+} line (569.6 nm wavelength) is stronger when the pulse duration is shorter [20]. This was correlated to the electron-ion thermalisation time and it was found that when the pulse duration is of the order of this time scale, the anisotropy is stronger. J. Kim and D. E. Kim [21] reported that the degree of the polarisation (P) of the Al^{2+} (569.6 nm) line, emitted in a laser plasma produced by a 6 mJ, 3 ns laser operated at its fundamental wavelength (1064 nm) in air, was 2.1 ± 0.13 % at a distance of 220 μm from target and vanished at 1.3 mm from the target. The underlying mechanism for the partial polarisation measured was explained as being due to electron-ion recombination from Al^{3+} ions into the relevant excited state of Al^{2+} based on a calculation with the Saha equation which predicted an ionisation balance in the plasma favouring a greater abundance of Al^{3+} ions. Time-integrated polarisation emission by nanosecond and femtosecond lasers on solids were reported by different authors. The variation of the degree of polarisation (P) was estimated at different pulse energies [12], [21], pressures [6] and time delays [22] .

1.3 Objective

Laser plasma polarisation spectroscopy (LPPS) signatures depend on many factors including laser fluence, wavelength, pulse width, time interval (time delay and observation time), pressure, target geometry etc. The focus of this thesis is to summarise the experimental results

that have been obtained in the present study by measuring time and polarisation resolved emission spectroscopy of Al, Cu, and Al alloy laser produced plasmas at different background pressures. Emission spectra are measured simultaneously for plasma polarisation components parallel and perpendicular to the quantisation axis of the experiment (which is the normal to the target surface). Line and the nearby continuum radiation were systematically studied over wide parameter spaces for both the neutral and ionic lines, mainly for Al plasmas, as a function of background pressure and time delay at different central wavelengths of a Czerny-Turner plane grating spectrometer. Subsequently, the degree of polarisation (P) was extracted from the sensitivity calibrated emission spectra for both continuum and line radiation, the latter for different charge states of ions in each plasma. The results are discussed in the framework of different origins of plasma radiation polarisation and the potential of this technique for LIBS. The specific objectives of this project are to:

- Develop a simple, stable method to measure the degree of polarisation of both the continuum and the line emission from laser plasmas of single elements and alloys
- Carry out a comprehensive study of degree of polarisation for plasmas formed at different background pressures, time delays, wavelength, and target geometries
- Use a simple plasma model to help explain the origins of continuum and line emission in the laser plasmas studied.

1.4 Organization of the Thesis

The thesis is organised as follows:

Chapter 1 summarises the motivation for the work followed by a brief history of the relevant literature on PPS and PRLIBS experimental work to date. It ends with a summary of the overall and specific objectives.

Chapter 2 describes the basics of laser produced plasmas including atomic processes, plasma radiation parameters and plasma polarisation spectroscopy. Specifically, the main mechanisms for the continuum and line polarisation, are discussed.

Chapter 3 focuses on the experimental system for polarisation resolved spectroscopy. It includes the laser, the spectrometer, the vacuum system, the laser focusing optics, the plasma radiation collection optics, the polariser and the detection system.

Chapter 4 describes the results of time-resolved imaging and time and polarisation resolved spectroscopy studies on Al plasma emission in the visible spectral range. Specifically, the Al^0 (at a central wavelength of 395 nm) and Al^+ (at a central wavelength of 463 nm) lines. Continuum emission nearby these lines is also investigated systematically.

Chapter 5 builds on the previous chapter and is focused mainly the comparison of the Al^0 (at a central wavelength of 395 nm) and Al^{2+} (at a central wavelength of 569 nm) lines. The origin of continuum polarisation is discussed in the framework of power radiation losses due to recombination processes in the expanding plasma.

Chapter 6 illustrates the effect of the target geometry and incident laser polarisation on the time and polarisation resolved emission from an Al plasma in the atmospheric air pressure ($1\times10^{+3}$ mbar). The degree of polarisation (P) was measured for the line at 396.15 nm and the nearby continuum. The underlying mechanism of both the continuum and line emission polarisation is discussed in the frame work of radiation recombination as the result of the EVDF.

Chapter 7 summarises the main conclusions from this experimental investigation and points towards possible future investigations to extend it.

Appendix A contains the partial Grotrian diagrams of Al^0, Al^+ and Al^{2+} respectively.

Appendix B is concerned with the polarisation of Cu plasma emission at low pressures. Continuum and line spectra are compared and contrasted.

Appendix C presents the results of time integrated polarisation measurements on Al plasmas at low pressure.

Appendix D shows the results of time-resolved LIBS and PRLIBS studies of plasmas formed on an Al alloy performed in a wide spectral window by means of an Echelle spectrometer.

References

[1] N. Hans, D. W. and Omenetto, "Laser-Induced Breakdown Spectroscopy (LIBS), Part I: Review of Basic Diagnostics and Plasma-Particle Interactions: Still-Challenging Issues Within the Analytical Plasma Community," *Appl. Spectrosc.*, vol. 64, p. 335A–366A, 2010.

[2] F. Anabitarte, A. Cobo, and J. M. Lopez-Higuera, "Laser-Induced Breakdown Spectroscopy: Fundamentals, Applications, and Challenges," *ISRN Spectrosc.*, vol. 2012, pp. 1–12, 2012.

[3] X. Jiang, P. Hayden, R. Laasch, J. T. Costello, and E. T. Kennedy, "Inter-pulse delay optimization in dual-pulse laser induced breakdown vacuum ultraviolet spectroscopy of a steel sample in ambient gases at low pressure," *Spectrochim. Acta - Part B At. Spectrosc.*, vol. 86, pp. 66–74, 2013.

[4] M. A. Khater, "Trace detection of light elements by laser-induced breakdown spectroscopy (LIBS): Applications to non-conducting materials," *Opt. Spectrosc.*, vol. 115, no. 4, pp. 574–590, 2013.

[5] B. Sallé, D. A. Cremers, S. Maurice, and R. C. Wiens, "Laser-induced breakdown spectroscopy for space exploration applications: Influence of the ambient pressure on the calibration curves prepared from soil and clay samples," *Spectrochim. Acta Part B At. Spectrosc.*, vol. 60, no. 4, pp. 479–490, 2005.

[6] D. Zhao, N. Farid, R. Hai, D. Wu, and H. Ding, "Diagnostics of First Wall Materials in a Magnetically Confined Fusion Device by Polarization-Resolved Laser-Induced Breakdown Spectroscopy," *Plasma Sci. Technol.*, vol. 16, no. 2, pp. 149–154, 2014.

[7] R. Gaudiuso, M. Dell'Aglio, O. De Pascale, G. S. Senesi, and A. De Giacomo, "Laser Induced Breakdown Spectroscopy for Elemental Analysis in Environmental, Cultural Heritage and Space Applications: A Review of Methods and Results," *Sensors*, vol. 10, no. 8, pp. 7434–7468, 2010.

[8] M. A. Khater, J. T. Costello, and E. T. Kennedy, "Optimization of the emission characteristics of laser-produced steel plasmas in the vacuum ultraviolet: Significant improvements in carbon detection limits," *Appl. Spectrosc.*, vol. 56, no. 8, pp. 970–983, 2002.

[9] A. Eslami Majd, A. S. Arabanian, and R. Massudi, "Polarization resolved laser induced breakdown spectroscopy by single shot nanosecond pulsed Nd:YAG laser," *Opt. Lasers Eng.*, vol. 48, no. 7–8, pp. 750–753, 2010.

[10] Y. Zhao, S. Singha, Y. Liu, and R. J. Gordon, "Polarization resolved laser-induced

breakdown spectroscopy," *Opt. Lett.*, vol. 34, no. 4, pp. 494–496, 2009.

[11] J. S. Penczak, Y. Liu, R. D. Schaller, D. H. Rich, and R. J. Gordon, "The mechanism for continuum polarization in laser induced breakdown spectroscopy of Si(111)," *Spectrochim. Acta - Part B At. Spectrosc.*, vol. 74–75, pp. 3–10, 2012.

[12] Y. Liu, J. S. Penczak, and R. J. Gordon, "Nanosecond polarization-resolved laser-induced breakdown spectroscopy.," *Opt. Lett.*, vol. 35, no. 2, pp. 112–114, 2010.

[13] J. C. Kieffer, J. P. Matte, M. Chaker, Y. Beaudoin, C. Y. Chien, S. Coe, G. Mourou, J. Dubau, and M. K. Inal, "X-ray-line polarization spectroscopy in laser-produced plasmas," *Phys. Rev. E*, vol. 48, no. 6, pp. 4648–4658, 1993.

[14] T. Fujimoto and S. A. Kazantsev, "Plasma polarization spectroscopy Review Article," *Plasma Phys. Control. Fusion*, vol. 39, pp. 1267–1294, 1997.

[15] H. M. Milchberg and J. C. Weisheit, "Polarization of recombination radiation from nonequilibrium plasmas," *Phys. Rev. A*, vol. 26, no. 2, pp. 1023–1029, 1982.

[16] A. I. Takashi Fujimoto, *Plasma Polarization Spectroscopy*. 2008.

[17] C. Vallance, "Generation, characterisation, and applications of atomic and molecular alignment and orientation," *Phys. Chem. Chem. Phys.*, vol. 13, no. 32, p. 14427, 2011.

[18] J. Kim and D. E. Kim, "Measurement of the degree of polarization of the spectra from laser produced recombining Al plasmas," *Phys. Rev. E - Stat. Nonlinear, Soft Matter Phys.*, vol. 66, no. 1, pp. 1–4, 2002.

[19] A. K. Sharma and R. K. Thareja, "Anisotropic emission in laser-produced aluminum plasma in ambient nitrogen," *Appl. Surf. Sci.*, vol. 253, no. 6, pp. 3113–3121, 2007.

[20] A. K. Sharma and R. K. Thareja, "Polarization-resolved measurements of picosecond laser-ablated plumes," *J. Appl. Phys.*, vol. 98, no. 3, p. 33304, 2005.

[21] J. S. Penczak, Y. Liu, and R. J. Gordon, "Polarization resolved laser-induced breakdown spectroscopy of Al," *J. Phys. Chem. A*, vol. 113, no. 47, pp. 13310–13317, 2009.

[22] M. E. Asgill, H. Y. Moon, N. Omenetto, and D. W. Hahn, "Investigation of polarization effects for nanosecond laser-induced breakdown spectroscopy," *Spectrochim. Acta - Part B At. Spectrosc.*, vol. 65, no. 12, pp. 1033–1040, 2010.

2 Fundamentals

This chapter is based on a literature survey of the basics of plasmas, atomic physics and polarisation resolved emission spectroscopy of laser produced plasmas. The underlying physical processes in laser produced plasmas formed on solids are complex. Here, the basic principles of plasmas followed by some fundamental concepts of laser solid matter interactions are discussed. Then, the dominant atomic processes relevant to plasma polarisation emission spectroscopy are presented. The details of free-free, free-bound and bound-bound transitions are presented in the framework of radiative and collisional models. The power radiation losses due to these atomic processes are used later to help explain anisotropies in the polarization of laser plasma emission. Plasma equilibria, used to determine the plasma parameters (density and temperature), are also discussed in the framework of local thermodynamic equilibrium (LTE) and non-LTE. Finally, the dominant mechanisms underlying the partial polarisation of the emission from laser produced plasmas on solids are presented, while, the origins of polarised continuum and line emission are addressed separately.

2.1 Basics Physics of Plasmas

Plasma is the fourth state of matter and is overall neutral, consisting of electrons, ions and neutral species that exhibit collective motions, important for its overall physical characteristics, such as exhibiting electron and ion waves [1]–[4]. Plasma appears in different forms which include lightening, solar winds, welding arcs, electrical discharges, laser-produced plasmas, etc. The focus of this thesis is on laser produced plasmas. When a pulsed laser is focused to vaporise and ionise a target material (solid, liquid or gas), and the laser irradiance is greater than the threshold energy of the material, a plasma is formed [5]. Considering the bulk of the plasma, the *electron density* n_e (m^{-3}) is given by [1]–[4]:

$$n_e = \sum_q n_q \tag{2.1}$$

where q is the charge number and n_q is the density of the ions of charge q. There are three key physical parameters that describe this bulk plasma. These include the Debye length, the plasma frequency and the critical density [1], [2]. Unlike gases, plasmas have long range strong Coulombic forces between the charged species which can be expressed in terms of the Debye length. This characteristic length is the distance between a positive ion and the edge of the surrounding electron sheath which has the effect of completely screening the influence of the ion's field from all other species in the plasma [1], [6]. This *Debye length* $\lambda_D(m)$ can be calculated from the electrostatic force by the shielded ions and described below [1]–[4]:

$$\lambda_D = \left(\frac{\varepsilon_0 k_B T_e}{n_e e^2} \right)^{1/2} \approx 69 \left(\frac{T_e}{n_e} \right)^{1/2} \tag{2.2}$$

Where ε_0 is the electric permittivity medium, k_B is the Boltzmann constant, $T_e(K)$ is the temperature, $n_e(m^{-3})$ is the density no of electrons, and e is the electronic charge. The *number of electrons in the Debye sphere* $N_D(m^{-3})$ is given by [1], [4]:

$$N_D = \frac{4}{3}\pi\lambda_D^3 n_e \tag{2.3}$$

These collective motions of ions and electrons are important in defining the characteristics of the plasma. They are wavelike and gives rise to so-called ion-acoustic and electron waves. In contrast to plasma ions, electrons are very light and have a much higher frequency oscillation. The associated *characteristic plasma electron (wave) frequency* $\omega_e \left(s^{-1}\right)$ is given by [1]:

$$\omega_e = \left(\frac{n_e e^2}{m_e \varepsilon_0}\right)^{1/2} \approx 56.4 n_e^{1/2} \tag{2.4}$$

Where n_e *(m^{-3})* is once again the density no of electrons. The so-called *plasma frequency* $\omega_p \left(s^{-1}\right)$, based on the assumption of taking the motion of both the electrons and the ions is given by [2], [7]:

$$\omega_p^2 = \omega_e^2 + \omega_i^2 \tag{2.5}$$

Where ω_i is the ion frequency. As the mass of the electron is typically four orders of magnitude small than that of an ion, the frequency of the collective electron motion is much greater than that of the ion oscillations and hence one can write the plasma frequency simply as $\omega_p \approx \omega_e$ For laser produced plasmas, the so-called critical density is reached when the laser frequency and plasma frequency become equal and is given by [1], [7]:

$$n_c = \frac{\varepsilon_0 m_e \omega_p^2}{e^2} \approx 3.14 \times 10^{-4} \omega_p^2 \tag{2.6}$$

2.2 Laser Produced Plasma Formation

When a nanosecond laser pulse is focused onto a solid target, three major processes take place. Material ablation is initiated during the laser material interaction which creates heating and evaporation when the pulse energy is greater than the ablation threshold energy for the target material [5], [8]. In the initial interaction a dilute plasma, is formed as electrons are liberated from the target surface by photoionisation. These electrons then absorb incoming laser

radiation by inverse bremsstrahlung (IB) so that they are heated up and collide with the target surface causing further ionisation [2]–[4]. The process continues until the electron density becomes so high that the plasma frequency reaches the laser frequency. As stated in the previous subsection, this density is called the *critical density*. At that point, laser light is reflected from the critical density layer and can no longer reach the target. Subsequently the plasma expands, the electron density drops and so the laser can once again penetrate the plasma [4], [9]. Electrons are once again heated up by IB and the plasma density once again increases up to the critical value. The continuous cycling of IB plasma heating and expansion continues right throughout the duration of the laser pulse. Once the heating is over the plasma essentially freely expands into the background gas or vacuum. **Figure 2.1** shows the interaction of a nanosecond laser pulse with a solid.

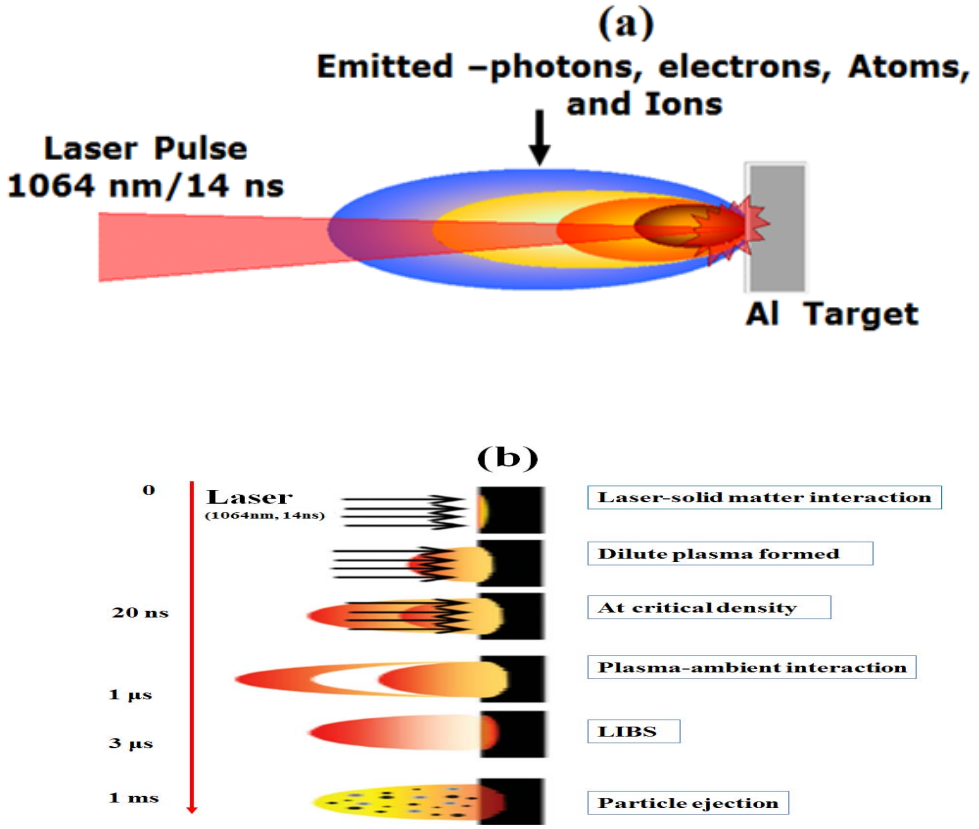

Figure 2.1: (a) Nanosecond laser-solid matter interaction and (b) plasma evolution with time delay (lower panels) [8].

2.3 Atomic Emission Processes in Laser Produced Plasmas

There are several atomic processes that take place in laser produced plasmas involving energy transfer between the plasma species (electrons, neutrals and ions) [2], [4], [10]. Emission from plasma species depends on the entire process which includes the laser-target interaction followed by laser-plasma and plasma-plasma interactions [8]. The processes which give rise to plasma radiation, and are therefore of most interest here, are mainly collisional in nature. These include electron impact excitation (and de-excitation), bremsstrahlung and electron-ion radiative recombination [2]–[4]. These processes allow the plasma to gain or lose energy in different forms as the result of free-free (F-F), free-bound (F-B) and bound-bound (B-B) interactions [4], [10]. Other processes such as di-electronic recombination, ion-ion, and ion-neutral collisions are possible but the rates are usually lower than for electron collisions. **Table 2.1** summarises these atomic processes.

Table 2.1: Classification of main atomic processes [2], [4].

Process	Excitation	De-excitation	Type
F-F	Inverse-Bremsstrahlung	Bremsstrahlung	Collisional
B-F	Photoionsation	Radiative recombination	Radiative
B-F	Impact ionisation	3-body recombination	Collisional
B-B	Impact excitation	Impact de-excitation	Collisional
B-B	Photoabsorption	Spontaneous decay	Radiative

2.3.1 Free to Free Transitions

A free electron that is decelerated in the presence of an ion will give up the excess kinetic energy in the form of a photon, a process known as *Bremsstrahlung emission*. The converse is also possible, i.e., a free electron can absorb a photon in the presence of an ion thereby increasing its energy, so-called *inverse bremsstrahlung* [4].

Bremsstrahlung can be represented by:

$$e_1(E_1) + X^q \rightarrow X^q + e_1(E_2) + h\nu \tag{2.7}$$

Where $E_1 > E_2$ *while Inverse bremsstrahlung* can be represented by:

$$e_1(E_2)+h\nu+X^q \rightarrow e_1(E_1)+X^q \tag{2.8}$$

Where, X^q represents the ion or neutral, E_1 and E_2 represent the free electron energy before and after the interaction (bremsstrahlung) and conversely for inverse bremsstrahlung. **Figure 2.2** illustrates *bremsstrahlung* and *inverse bremsstrahlung* processes [10]. IB is characterised by the absorption coefficient $\alpha_{IB}\left(cm^{-1}\right)$ which depends on the laser wavelength, $\lambda_{laser}=1.064\times10^{-4}cm$ and is given by [11]:

$$\alpha_{IB}=1.37\times10^{-35}\lambda^3 N_e^2 T_e^{1/2} \tag{2.9}$$

Where N_e is the electron density in (cm^{-3}) and T_e is the electron temperature in (K).

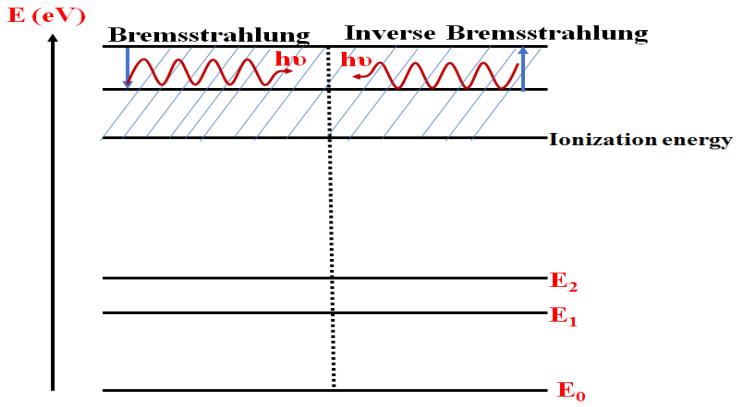

Figure 2.2: Bremsstrahlung and inverse bremsstrahlung processes [10].

2.3.2 Free to Bound Transitions

When a free electron is captured by an ion it gives up its excess energy in the form of a photon in a process known as *radiative recombination* [2], [4], [10]. Since the plasma contains electrons with a continuum of kinetics energies, their capture results in the emission of a continuum of photon energies. Electron capture by an ion also leads to a decrease in the charge state of the ion by unity:

$$e_1+X^q \rightarrow X^{q-1}+h\nu \tag{2.10}$$

Where e_1 is the free electron and X^{q-1}, X^q are successive charge states of the ion, h is the Planck's constant and v is the frequency. Another process is *photoionisation* which occurs when the energy of a photon energy is greater than the ionisation potential of the atom with which it interacts. The kinetic energy of the electron is given by:

$$E = \frac{1}{2} m_e v_e^2 = h\nu - I_p \tag{2.11}$$

Where m_e is the mass of the electron, I_P is the ionisation potential of the parent atom or ion and $h\nu$ is the photon energy. *Photoionisation,* described in terms of the absorption of a photon and release of a bound electron, is represented by:

$$h\nu + X^q \rightarrow X^{q+1} + e^-(E) \tag{2.12}$$

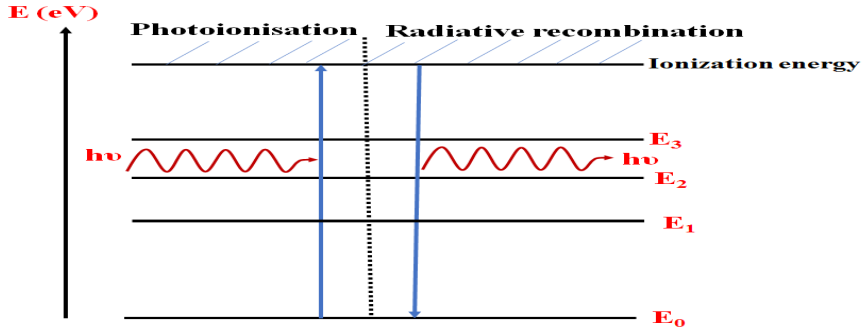

Figure 2.3: Photoionisation and radiative recombination processes [10].

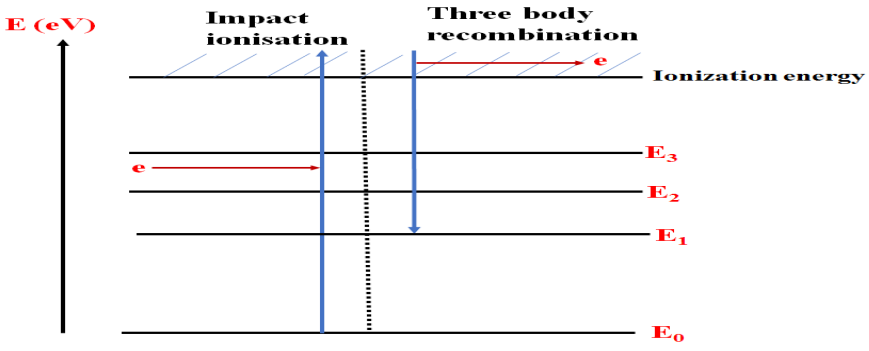

Figure 2.4: Electron impact ionisation and three body recombination processes [10].

Recombination and photoionisation are shown schematically in **Figure 2.3**. When a free electron encounters an ion, it can knock out a bound electron, promoting it into the continuum, a process know as e*lectron impact ionisation*, shown in **Figure 2.4** [4], [10]. On the other hand, when two free electrons in the continuum interact with an ion, one electron can be captured while the other electron gains the excess energy in a process known as *three body recombination*. The equation that governs this collisional process is given by:

$$e(E_1) + e\left(E_2\right) + X^{q+1} \rightarrow X^q + e\left(E_1^{'}\right) \tag{2.13}$$

Where E_1 is the kinetic energy of electron 1 and E_2 is the kinetic energy of electron 2, prior to the collision with ion. $E_1^{'} > E_1$ and $E_1^{'}$ is the kinetic energy of electron 1 post collision.

2.3.3 Bound to Bound Transitions

Transitions between bound states in an atom give rise to discrete lines. Such lines (observed in both absorption and emission spectra) act as characteristic fingerprints of atoms and ions and hence they are very useful in LIBS for the classification and quantification of elements in a material. *Photoabsorption,* resulting in excitation from a lower energy bound state to a higher energy bound state, is given by the equation [10]:

$$e(E_1) + h\upsilon \rightarrow e\left(E_2\right) \tag{2.14}$$

Where $E_2 > E_1$ and $h\nu = E_1 - E_2$.

Figure 2.5 shows spontaneous decay wand the inverse process, namely resonant absorption. De-excitation of an atom from an excited state to a lower bound state results in the emission of a photon radiation to the lower energy bound the state is given by:

$$A^{*}\left(E_2\right) \rightarrow A(E_1) + h\nu \tag{2.15}$$

where $A(E_1)$ and $A^*(E_2)$ represent the atom in lower and upper states, E_1 represents the energy of an electron in the lower bound electronic state 1 and E_2 represents the energy of an electron in the upper bound electronic state 2.

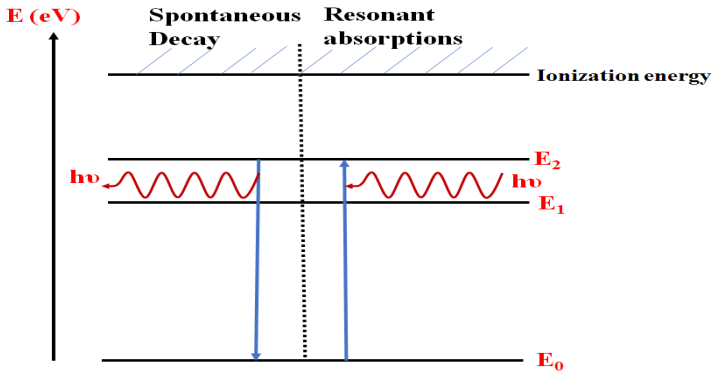

Figure 2.5: Spontaneous emission and resonant absorption [10].

2.4 Plasma Radiation Parameters

Generally, we can categorise the spectral distribution of optical radiation emitted from laser produced plasmas into two classes, namely, continuum and discrete line emission. Continuum emission is usually observed during the early plasma formation and evolution phase and lasts on the order of 100 ns. There are two sources of continuum emission, bremsstrahlung radiation (free to free electron transitions) and radiative recombination (free to bound electron transitions). When the continuum emission decreases, the atomic and ionic lines become clear and sharp due to an increase in their signal to background ratio and a decrease in the Stark broadening [24]. They arise from transitions between bound states in atoms and ions as the plasma cools down [12]. The rates of power radiation loss of *free-free* (P_{ff}), *free-bound* (P_{fb}) *and bound-bound* (P_{bb}) emission are all temperature dependent in a laser plasma [13]–[15].

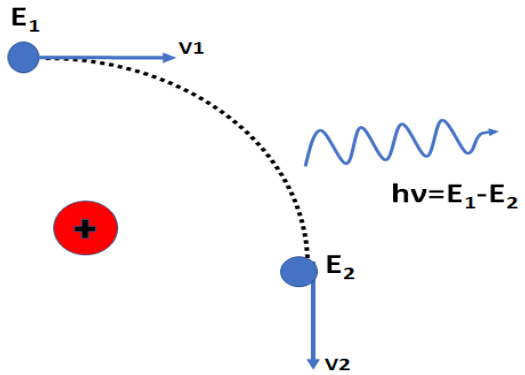

Figure 2.6: Bremsstrahlung radiation produced by the scattering of high energy electrons in atomic or ionic fields.

To approximate the rates of these radiation losses, we derive the equation by starting from a picture of the bremsstrahlung radiation process shown in **Figure 2.6**. Firstly, the characteristic electron-atom/ion interaction time is given by [13]–[15]:

$$\tau = \frac{2r}{v} \tag{2.16}$$

where r is the impact parameter and v is the velocity of the electron. The dominant collision frequency is given by:

$$\nu = \frac{v}{2\pi\tau} = \frac{v}{4\pi r} \tag{2.17}$$

For single impact, the maximum acceleration a is given by:

$$a = \frac{qe^2}{rm} \tag{2.18}$$

where e is the charge of the electron, m is the mass of the electron and q is the charge of the ion. Then, the energy gained at this maximum acceleration is given by:

$$\Delta E = \frac{2e^2a^2\tau}{3c^2} \approx \frac{4q^2e^6}{3m^2c^3r^3v} \tag{2.19}$$

where c is the speed of light. Then the power radiated per electron is given by:

$$W = \int \Delta E_i . 2\pi n_i v r dr \approx \frac{4q^2 e^6}{3m^2 c^3} \int_{r_{\min}}^{r_{\max}} \frac{dr}{r^2} \tag{2.20}$$

Where the maximum impact parameter r_{max} is approximated from the Heisenberg Uncertainty principle and De Broglie wavelength:

$r_{\min} = \frac{h}{2\pi n v}$ and since $r_{min} << r_{max}$ the integration gives:

$$W = \frac{16\pi}{3} \frac{e^6}{mhc^3} q^2 n_i v \tag{2.21}$$

Adding the Maxwellian velocity electron distribution function given by the equation:

$$f(v) = n_e \left(\frac{m_e}{2\pi k_B T} \right)^{3/2} \exp\left[\frac{-m_e v^2}{2k_B T} \right] \tag{2.22}$$

yields, the Bremsstrahlung radiation power per unit volume:

$$P_{ff} = \int_0^\infty W f(v) 4\pi v^2 dv \tag{2.23}$$

Substituting for W and f gives:

$$P_{ff} = 32\pi \frac{q^2 e^6}{mc^3} \frac{n_e n_i}{h} \left(\frac{2k_B T_e}{\pi m} \right)^{1/2} \tag{2.24}$$

A simplified form of the power emitted per unit of volume for the *free-free* electron transitions (*bremsstrahlung radiation*) is given by [14], [15]:

$$P_{ff} \approx 1.5 \times 10^{-26} q^2 n_e n_i T_e^{1/2} \frac{W}{m^3} \tag{2.25}$$

where n_e is electron density, n_i is the ion density and q is the charge of the ion.

The power density per unit of volume of the emitted *recombination radiation* arising from *free to bound* transitions is given in terms of the Bremsstrahlung radiation rate P_{ff} as [14], [15]:

$$P_{fb} = 1.5\times10^{-26} n_e \left(T_e\right)^{1/2} q^2 n_i \left(\frac{E_I}{T_e}\right)\frac{W}{m^3} \tag{2.26}$$

$$P_{fb} = P_{ff}\,\frac{E_I}{T_e}\frac{W}{m^3} \tag{2.27}$$

The emitted power per unit of volume for line radiation arising from bound to bound transitions is given by [14], [15]:

$$P_{bb} = P_{ff}\,\frac{2\times10^7 e^{-\frac{E_r}{T_e}}}{T_e q^2}\frac{W}{m^3} \tag{2.28}$$

where energy and temperature are in eV, n_e is the electron density in m^{-3}, n_i is the ion density in m^{-3}, q is ion charge in C, E_I is the ionisation potential in eV, and E_r is the excitation energy in eV.

In addition, the characteristic transition times are important to explain the collisional excitation and radiative processes in laser produced plasmas. For free-free transition this time is given by the ratio of the total thermal energy to the radiative loss power P_{ff} [15]:

$$\tau_{ff} \approx \frac{1.6\times10^7 \left(T_e\right)^{1/2}}{q^2 n_i}\ \text{sec} \tag{2.29}$$

while the free-bound time constant is given by:

$$\tau_{fb} \approx \tau_{ff}\left(\frac{T_e}{E_I}\right)\text{sec} \tag{2.30}$$

and the bound-bound radiative time constant is given by:

$$\tau_{bb} = 5\times10^{-8}\,\tau_{ff} T_e q^2 e^{\left[\frac{E_r}{T_e}\right]}\ \text{sec} \tag{2.31}$$

2.5 Equilibrium in Plasmas

A plasma in a state of complete equilibrium would satisfy the following thermodynamic relationships [2], [4]:

(1) **Maxwell law:** the plasma species follow the Maxwell velocity distribution function described by the equation:

$$f(E,T) = \frac{4\pi m^2}{\left(2\pi m k_B T\right)} v e^{-\left(E / k_B T\right)} \tag{2.32}$$

where k_B is the Boltzmann constant, E is the electron energy and T is the thermodynamic temperature.

(2) **Boltzmann law:** When the population distribution between levels is dominated by collisions, the distribution function that describes the population ratio between two levels in an atom or ion is given by Boltzmann distribution function [9]:

$$\frac{N_U}{N_L} = \frac{g_U}{g_L} e^{-\left(E / k_B T\right)} \tag{2.33}$$

where N_U and N_L are the numbers of atoms or ions per unit volume in the upper and lower levels separated by an energy $E = E_U - E_L$ while g_u and g_L are the statistical weights of the upper and lower levels respectively.

(3) **Saha law:** This law governs the population ratio of successive ion stages within a plasma and is given by [9]:

$$\frac{N_{i+1} N_e}{N_i} = \frac{2 g_{i+1}}{\wedge g_i} \left(e^{-\left(\frac{E_{i+1} - E_i}{k_B T} \right)} \right) \tag{2.34}$$

where N_i is the density of ions in the i^{th} charge state, g_i is the degeneracy of states in the i^{th} charge state, E_i is the ionisation energy in the i^{th} state, k_B is the Boltzmann constant, Λ is the thermal de Broglie wavelength of an electron and T is the temperature of the ions.

(4) **Planck radiation law:** describes the distribution function of the radiation energy density per unit of frequency and is given by [4]:

$$u(\nu) = \frac{8\pi h\nu^3}{c^3}\left(\frac{1}{e^{-\left(\frac{h\nu}{k_B T}\right)}}\right)d\nu \tag{2.35}$$

Where $u(\nu)$ is the frequency dependent radiation energy density. The energy density per unit volume (in units of Jm^{-3}) is given by the famous Planck radiation law for a blackbody radiator at temperature, T:

$$B_\nu(T) = \frac{2h\nu^3}{c^3}\left(\frac{1}{e^{\frac{h\nu}{k_B T}} - 1}\right) \tag{2.36}$$

Pure thermodynamic equilibrium pertains in a plasma when it behaves like a blackbody, i.e., it satisfies Planck's radiation law, the populations amongst the energy levels in the atoms and ions obey Boltzmann's law, the velocity distribution is Maxwellian and the ionisation balance is described by the Saha equation. In such a closed system, the principle of detailed balance holds for all processes involving particles or photons. In practice only partial equilibrium can be attained in a plasma. These states of partial equilibrium can be classified as follows:

- Local Thermodynamic Equilibrium (LTE)
- Coronal Equilibrium (CE)
- Collisional-Radiative Equilibrium (CRE)

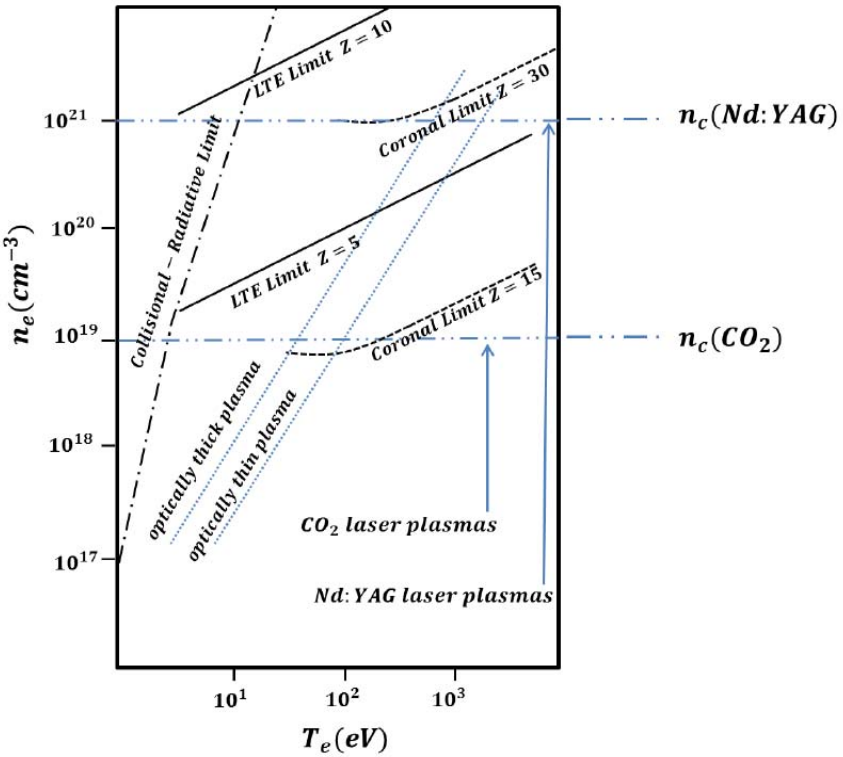

Figure 2.7: Electron density and temperature phase diagram illustrating the limits for different equilibria taken from [7] which was adapted from the source [16].

The state of equilibrium of a plasma is highly dependent on the electron density and temperature at the phase diagram in **Figure 2.7** shows [7,16].

2.5.1 Local Thermodynamic Equilibrium (LTE)

LTE pertains when electron collisional processes are more dominant than radiative ones. This means from the section (**2.1**) that the high density in the plasma results in a high collision frequency and so LTE can be established where the electron energies follow a Maxwell-Boltzmann distribution function and the distribution of the ionisation stages is given by Saha equation.

2.5.2 Coronal Equilibrium (CE)

CE pertains to low electron density (typically < 10^8 cm^{-3}) optically thin plasmas [2]. In such dilute plasmas, the collision frequency is low and collisional excitation/de-excitation can be

neglected. Instead, spontaneous processes dominate and superelastic collisions, can be neglected. However, for laser produced plasmas, where electron densities can exceed 10^{16} cm^{-3}, with typical superelastic collision rates of 10^{10} cm^3 s^{-1}, de-excitation rates of 10^6 s^{-1} result and so such collisional processes are important contributors to the overall radiation budget.

2.5.3 Collisional-Radiative Equilibrium (CRE)

This equilibrium applies to plasmas with moderate electron densities (i.e., typically in the range 10^{19}-10^{21} cm^{-3}) [7]. Using a collisional radiative model (CRM) Colombant and Tonon [16] derived an expression for the population ratio of ions in a laser produced plasma:

$$\frac{n_{q+1}}{n_q} = \left[\frac{S(q,T_e)}{\alpha_r\left(q+1,T_e\right) + n_e\alpha_{3b}} \right] \tag{2.37}$$

where q and T_e are the charge state and the electron temperature, S, α_r, α_{3B} are the collisional ionisation coefficient, the radiative recombination coefficient and the three-body recombination coefficient respectively.

The simplified form of the rate equation for the CRM is given by [16]:

$$\begin{aligned} \frac{dn_{q+1}}{dt} &= n_e n_q S(q,T_e) - n_e n_{q+1}\left[S(q+1,T_e) + \alpha_r(q+1,T_e) + n_e\alpha_{3b}(q+1,T_e)\right] \\ &+ n_e n_{q+2}\left[\alpha_r(q+2,T_e) + n_e\alpha_{3b}(q+2,T_e\right] \end{aligned} \tag{2.38}$$

The rate equation is important to explain the polarisation effect observed in the experimental part of this thesis for both continuum and line emission where recombination plays a role in both [17]–[21].

The collisional ionisation rate is given by [16] :

$$S = \frac{9\times10^{-6}\xi_q\left(T_e/\chi_q\right)^{1/2}}{\chi_q^{3/2}\left(T_e/\chi_q\right)} \exp\left(-\frac{\chi_q}{T_e}\right) \tag{2.39}$$

where χ_q is the ionisation potential and ξ_q is the electron occupying in the outer shell.

The simplified form of the rate of recombination is given by [16]:

$$\alpha_r = 5.2\times10^{-14}\left(\frac{\chi_q}{T_e}\right)^{1/2} q\left[0.429+\frac{1}{2}\log\left(\frac{\chi_q}{T_e}\right)+0.469\left(\frac{T_e}{\chi_q}\right)^{1/2}\right] \tag{2.40}$$

The rate of the three-body recombination is given by [16]:

$$\alpha_{3b} = 2.97\times10^{-27}\frac{\xi_q}{T_q\chi_q}\left(4.88+\frac{T_q}{\chi_q}\right) \tag{2.41}$$

Where T_e is the plasma temperature in eV and ne the electron density is in cm^{-3}

In CRM, the temperature is given by [6]:

$$T_e = 5.2\times10^{-6} A^{1/5}\left(I\lambda^2\right) \tag{2.42}$$

where λ is the laser wavelength $1.064\times10^{-4}\,cm$, A is the atomic number and I is the power density or intensity in Wcm^{-2}.

2.6 Polarised Emission from Laser Produced Plasmas

As briefly discussed in the introduction, both continuum and line emission can be partially polarised. Several attempts have been made to explain the origin of the anisotropy in the polarisation state of both types of radiation emitted from the laser-produced plasma. Some mechanisms underlying the origin of polarisation anisotropy in plasma are discussed briefly in this section.

2.6.1 Degree of Polarisation

The *degree of polarisation* (*P*) is the key quantity that can be used to quantify the anisotropy in the polarisation of the radiation emitted by a laser-produced plasma. It is the ratio of the intensity of the polarised component of the light emitted to the total intensity of the light [17]–[21]. The degree of polarisation (P) can be determined from the anisotropy in the orthogonally polarised emission of plasma light [17]–[21]. This can be achieved experimentally by placing a polariser in front of a detector. Plasma is resolved into ‘‘Horizontal’’ and ‘‘Vertical’’ components. ‘Horizontal’ refers to the direction parallel and ‘‘Vertical’’ refers to

perpendicular to the laser axis of incidence. Mathematically, P at a fixed wavelength is given by:

$$P_{\lambda} = \left(\frac{I_H - I_V}{I_H + I_V} \right) \tag{2.43}$$

where $I_{H,\,V}$ are the intensities of the ‘‘Horizontal’’ and ‘‘Vertical’’ components respectively at a wavelength of λ.

2.6.2 Polarisation of Continuum Radiation

As stated in section (**2.4**), the continuum emission in a plasma can arise either from bremsstrahlung or electron-ion radiative recombination processes. Previous studies have shown that the dominant mechanism for polarisation of continuum radiation starts with an anisotropy in velocity distribution of electrons in the plasma. For very strong laser fields some of the emitting species become aligned in the direction of the field of the laser [18]. As a result, electron recombination with such ions results in the corresponding continuum emission becoming (usually partially) polarised [22] with the axis being defined by the laser polarisation direction. It has also been suggested that reflection by the target surface of unpolarised plasma radiation is itself polarised in accordance with the Fresnel equations [23] albeit this applies to the case of plasma formed by ultrashort pulses and not thermal plasmas as is the case here. For the table top nanosecond laser plasmas under discussion in the thesis, it is more likely that an anisotropy in the electron velocity distribution function or EVDF (and hence preferred electron velocity direction) is transferred into an anisotropy in the polarisation of the radiation emitted in electron-atom or electron-ion processes. The recombination of electrons (with such an anisotropic EVDF) with ions is more generally used to explain the polarisation of continuum emission [22], [24].

When collisional processes dominate over radiative processes, LTE is satisfied and the electron velocity distribution function can be represented by a simple *Maxwell-Boltzmann Distribution (MBD)* [9], [25]. Excitation-induced by electrons with such an isotropic distribution leads to equal populations of atomic species between the different magnetic

sublevels of the levels involved in the transition of interest and gives rise to the emission of unpolarised radiation [26]. However, for a non-equilibrium system, which does not obey the isotropic Maxwell electron velocity distribution, it has been observed that two different temperatures are obtained from spectra that have been polarisation resolved parallel and perpendicular to the quantisation axis of the experiment. Such an observation is consistent with a plasma that is not in LTE. Clearly the EVDF of such a system is anisotropic and is typically represented by a bi-Maxwellian function [19]. The *isotropic Maxwell-Boltzmann equation* is given by [26]:

$$f(v) = n_0 \left(\frac{m_e}{2\pi k_B T} \right)^{3/2} \exp\left[\frac{-m_e v^2}{2k_B T} \right] \tag{2.44}$$

where n_0, m_e, and v are electron density, mass and velocity respectively. The *non-equilibrium* EVDF generally follows a *bi-Maxwellian distribution function* which is given by [24], [27]:

$$f(v) = n_0 \left(\frac{m_e}{2\pi k_B T_H} \right) \left(\frac{m_e}{2\pi k_B T_V} \right)^{1/2} \exp\left[-\frac{m_e v_H^2}{2k_B T_H} - \frac{m_e v_V^2}{2k_B T_V} \right] \tag{2.45}$$

where v_V and v_H are the velocities in the directions perpendicular and parallel to the laser quantisation axis while T_H and T_V are temperatures in the corresponding directions. With the above in mind we follow the derivation of expressions for the polarization of continuum emission in recombining plasmas is given in [22].

The number of photons per unit time, per unit solid angle with polarization aligned with the direction of the vector $\hat{e}$ generated in electron recombination with an ion leaving the ion in the state |Γ> is given by the expression [22]:

$$\frac{dN(\hat{e},\omega)}{d\Omega} \propto \int d\Omega(\vec{v}) f(\vec{v}) v \frac{d\sigma_\Gamma(\hat{e},v)}{d\Omega} \tag{2.46}$$

where f(v) is the electron velocity distribution function (EVDF) and the differential (velocity dependent) cross section for recombination into state |Γ> and is given by:

$$\frac{d\sigma_\Gamma(\hat{e},v)}{d\Omega} = \frac{d\sigma_\Gamma(\hat{e},v)}{4\pi}\left[1+\beta_\Gamma p_\Gamma(\vec{v}.\hat{e}/v)\right] \tag{2.47}$$

where β is the so-called asymmetry parameter and varies with electron energy. β values have been determined in photoionisation studies for many atoms [28] as well as in polarization studies [29].

The EVDF can expanded as a sum of Legendre polynomials:

$$f(\vec{v}) = \sum_0^\infty f_n(v)P_n(\cos\theta) \tag{2.48}$$

With a coordinate system defined in the figure below.

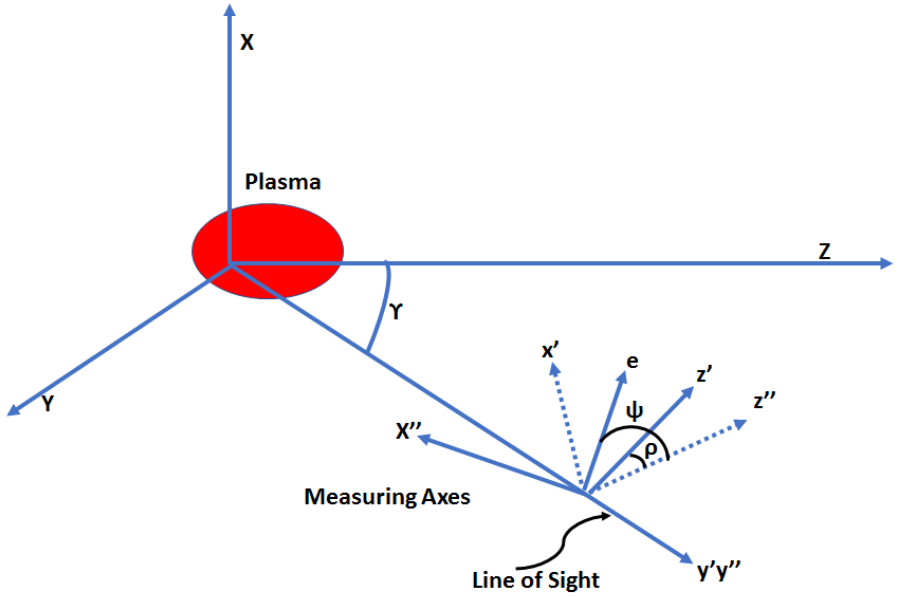

Figure 2.8: Geometry for observation of recombination radiation. Line of sight lies in yz plane [22].

The recombination radiation intensities for beams with electric fields aligned along the orthogonal x" (angular position φ=ρ+π/2) and z" directions (angular position φ=ρ) are given by the expressions:

$$J_{z''}(\omega) \propto \left.\frac{dN(\hat{e},\omega)}{d\Omega}\right|_{\psi=\rho}, \tag{2.49}$$

$$J_{z''}(\omega) \propto \left.\frac{dN(\hat{e},\omega)}{d\Omega}\right|_{\psi=\rho+\pi/2} \tag{2.50}$$

The degree of linear polarization of the recombination radiation is then:

$$\Pi(\omega) = \frac{J_{z''} - J_{x''}}{J_{z''} + J_{x''}} = \frac{3\beta_\Gamma \cos 2\rho \sin^2\gamma f_2}{20 f_0 + \beta_\Gamma f_2 (3\sin^2\gamma - 2)} \tag{2.51}$$

To determine $\Pi(\omega)$ for some specific useful cases it is necessary to determine the f_0 and f_2 expressions. The case of a bi-Maxwellian distribution, with temperatures T_H and T_V parallel and perpendicular respectively to the axis of symmetry (or quantization axis) for the polarization experiment, sometimes with a drift velocity along that axis U_D, is often met in laser plasma studies. Such an EVDF is given by the expression:

$$f(\vec{v}) = \left(\frac{m_e}{2\pi k_B T_H}\right)^{3/2} \frac{T_H}{T_V} \times \exp\left[-\frac{m_e v^2 \sin^2\theta}{2k_B T_V} - \frac{m_e (v\cos\theta - u_D)^2}{2k_B T_H}\right] \tag{2.52}$$

The expressions for f_0 and f_2 are [22]:

$$f_0 \propto S(\eta,\xi) \tag{2.53}$$

$$f_2 \propto -\frac{5}{2} S(\eta,\xi) + \frac{15}{2} \frac{\partial^2 S(\eta,\xi)}{\partial \eta^2} \tag{2.54}$$

Where

$$S(\lambda,\xi) = 2\sum_0^\infty \frac{(-\xi)^n}{n!} \frac{d^{2n}}{d\lambda^{2n}} \left[\frac{\sinh\lambda}{\lambda}\right] \tag{2.55}$$

And the two dimensionless quantities (λ ξ) are given by:

$$\lambda = \left[2m_e(\hbar\omega - E_b(nl)\right]^{1/2} \frac{u_D}{k_B T_H} \tag{2.56}$$

and

$$\xi = \left(\frac{\hbar\omega - E_b(nl)}{k_B T_H}\right)(1 - T_H / T_V) \tag{2.57}$$

Where $E_b(nl)$ is the electron binding energy for an electron in the quantum state *nl* into which it has been captured in the recombination process. $S(\lambda, \xi)$ is given by:

$$S(\lambda,\xi) = \int_{-1}^{1} dx \exp(-\xi x^2 + \lambda x) \tag{2.58}$$

$$= 2\sum_{0}^{\infty}\left(\frac{\xi^n}{n!}\right)\frac{d^{2n}}{d\lambda^{2n}}\left[\frac{\sinh\lambda}{\lambda}\right] \tag{2.59}$$

If the drift velocity (U_D) is small so that $\lambda << 1$, this expression simplifies to:

$$S(\lambda \ll 1,\xi) \simeq 2\sum_{0}^{\infty}\left(\frac{\xi^n}{n!}\right)\left[\frac{1}{2n+1} + \frac{\lambda^2}{2(2n+3)}\right] \tag{2.60}$$

So that f_0 and f_2 can be determined directly and substituted back to determined $\Pi(\omega)$ for an almost pure bi-Maxwellian. In this case, we have that the degree of polariation:

$$\tilde{\Pi}_{2T} = \frac{2\beta_\Gamma \sum_{0}^{\infty}(-\xi)^n n/(2n+3)(2n+1)n}{\sum_{0}^{\infty}\left[2+\beta_\Gamma n/(n+3)\right]\left[(-\xi)^n/(2n+1)n!\right]} \tag{2.61}$$

where the series converges rapidly with 'n'. For capture into a state *nl* where the symmetry parameter $\beta = 2$, e.g., K-shell capture, figure 3 in reference [22] shows the degree of linear polarization as a function of ξ. In the case of our experiments we look in the optical region so that $h\nu$-X_Γ takes quite small values and if T_H and T_V are close in value so that the terms in square brackets in equation (**2.61**) is also small it becomes clear that we are dealing with small values of ξ and we should expect absolute *P* values to be below 0.5. In our case the formula reduces to:

$$\tilde{\Pi}_{2T} \underset{\xi \to 0}{\sim} -\frac{\beta_\Gamma \xi}{10} \tag{2.62}$$

2.6.3 Polarisation of Line Radiation Emission

Discrete lines emitted by plasmas are polarised due to a non-statistical distribution of the population of the emitting species amongst the available magnetic sub-levels [12], [27]. Previous studies have suggested a number of origins for polarised line emission from laser produced plasmas including an anisotropy in the EVDF [19], [21], the dependency of the gain

cross-section on reabsorption [30], laser polarisation [12], [23] and self-generated magnetic fields [21]. Self-generated magnetic fields in laser produced plasmas are thought to arise from the Rayleigh-Taylor (RT) instability which has its origin in differences in the density of the plasma and the surrounding gas. For small perturbations with a spatial dimension $\lambda = 2\pi/k$, the RT growth rate scales as $exp(\gamma t)$ where $\gamma = (A_t ak)^{1/2}$ where A_t is the Atwood Number and a is the acceleration of the ablated plume [31]. A_t is the ratio of the difference to the sum of the plasma and gas densities. Magnetic field generation requires charge separation and subsequent current generation [32]. The RT instability provides the non-collinear density and temperature gradients required for magnetic field generation. Splitting of the energy levels combined with recombination into such levels can give rise to a magnetic sub-level imbalance [21] and hence anisotropically polarised light emission. However, in what follows the fundamentals of the velocity dependence of polarisation for line emission in electron atom or ion collisions, which is a well-established mechanism, is discussed.

Let us designate the upper state of the transition as ‘p’. All other states, including the lower state in the transition of interest designated ‘r’. ‘p’ is specified in greater detail by the ket vector $|\alpha J\rangle$ and ‘r’ by $|\alpha' J'\rangle$ where J specifies the total angular momentum of the state, e.g., J = 3/2 for the np $^2P_{3/2}$ single electron state. α is the set of all other quantum number needed to specify the state ‘p’. If one wishes to select out a particular magnetic sub-state of ‘p’ with quantum number M the ket vector becomes $|\alpha JM\rangle$.

The emission of polarised radiation has been observed in experiments on electron collisions with atomic targets for decades [33]. When an atom or ion is excited in such a collision the target retains a memory of the excitation conditions. For example, at low collision energy one can consider (classically) the collision to result in the induction of the excited electron to oscillate along the direction of travel of the exciting electron (e.g., along the z-direction). In this case, the radiation will be polarized in the z-direction [33]. If the radiation is observed in the x-y plane the radiation will be π polarized. On the other hand, for high energy electron

beams, where the electron energy starts to become relativistic, the atomic target senses an ultrashort electromagnetic pulse as the exciting electron passes by it. In this case, the electric field will be orthogonal to the propagation direction (z) and will lie in the x-y plane. In this case if the radiation is observed in the x-y plane the polarization direction will orthogonal to the low beam energy case, i.e., it will be σ polarized. Hence one should expect that the degree of polarization for radiation emitted from an atom or ion will depend on the viewing angle and also on the energy of the exciting electron. For a plasma with a single temperature and hence average electron energy one would not expect to observe any preferred polarization of the radiation. On the other hand, if there is an anisotropy in the electron velocity distribution function (EVDF), e.g., if there is a two-temperature distribution with fast and slow electrons, one could expect to observe a difference in the intensity of π and σ polarized light and hence a non-zero degree of linear polarization:

$$P = \left(\frac{I_\pi - I_\sigma}{I_\pi + I_\pi} \right) = \left(\frac{I_H - I_V}{I_H + I_V} \right) \tag{2.63}$$

From a quantum mechanical perspective, the anisotropy in the polarization of line radiation from plasmas reflects the generation of a non-statistical population distribution amongst the magnetic sublevels of the levels involved in the transition. To this end partial (magnetic quantum number resolved) electron excitation cross sections are needed for the specific transitions involved. These have been calculated for a number of well-studied transitions in a restricted number of atomic targets, mainly rare gases [18] .

Fujimoto and Kazantsev have developed an anisotropic line emission formulism based on density matrix theory [18].

$$\rho(p) = \rho_0^0(p) T_0^{(0)}(p) + \rho_0^2(p) T_0^{(2)}(p) + \cdots \tag{2.64}$$

Where

$$\rho_q^k(p) = \sum_{MN} (-)^{J-N} \langle JJM\ -N \mid kq \rangle \rho_{M,N}(p) \tag{2.65}$$

And

$$T_q^{(k)}(p) = \sum_{MN} (-)^{J-N} \langle JJM - N | kq \rangle | \alpha JM \rangle \langle \alpha JN |$$ (2.66)

Where

$$\langle JJM - N | kq \rangle$$ (2.67)

is a Clebsch-Gordon (angular momentum) coefficient.

Each atomic state is characterized as |αJM> where *J* and *M* refer to total and magnetic angular momentum numbers and α encompasses all other quantum numbers need to specify the state.

For some simple atomic systems, it is possible to extract experimentally the alignment from the degree of polarization from the following. Say one takes the case of a p-s transition and looks at the degree of linear polarization observing the radiation normal to the quantization axis of the system. The intensities of the orthogonal p and s polarization radiation components are given by [18]:

$$I_H = \frac{1}{8\pi l^2} n(p) A(p,s) \hbar\omega \left[1 + (-1)^{J_P + J_S} \sqrt{6} (2J_P + 1) \begin{Bmatrix} J_P & J_P & 2 \\ 1 & 1 & J_S \end{Bmatrix} \frac{a(p)}{n(p)} \right]$$ (2.68)

and

$$I_V = \frac{1}{8\pi l^2} n(p) A(p,s) \hbar\omega \left[1 - (-1)^{J_P + J_S} \frac{\sqrt{6}}{2} (2J_P + 1) \begin{Bmatrix} J_P & J_P & 2 \\ 1 & 1 & J_S \end{Bmatrix} \frac{a(p)}{n(p)} \right]$$ (2.69)

where *A(p,s)* is the spontaneous transition rate (in $\sec^{-1}$), J_P and J_S are total angular momentum quantum numbers of the upper and lower states, the term in chain brackets is the Wigner *6-J* symbol, *n(p)* represents the depopulation amongst the magnetic sublevels of level *'p'* and *a(p)* is the alignment parameter for level *'p'*. Here l is the distance between the emitting atoms and the detector and the incident intensity is given by the term outside square brackets, namely:

$$I_0 = \frac{1}{4\pi l^2} n(P) A(p,s) \hbar\omega$$ (2.70)

It is also given by:

$$I_0 = \frac{2}{3}\left(I_H + 2I_V\right) \tag{2.71}$$

Generally, the intensity obtained for the detector (spectrometer and the camera) has a contribution from the alignment of the population of atoms and ions. Therefore, the term $I_H + I_V$ contributes to the observed alignment. The longitudinal alignment can be described as:

$$A_L = \frac{\left(I_H + I_V\right)}{\left(I_H + 2I_V\right)} = \frac{2P}{3-P} \tag{2.72}$$

For line emission arising from states formed in electron ion recombination one can expect a degree of alignment of the excited state *'nl'* (or *Gamma* in Milchberg & Weisheit) formed in the recombination process and hence partially polarised line emission. In other words, if the state *Gamma* was not aligned then one would not observe anisotropic continuum emission or if the continuum is polarised so also will the corresponding line emission.

2.7 Summary

In this chapter, the fundamental physics of laser produced plasmas formed on solids is introduced. Emission of radiation from laser produced plasmas is explained in terms of the plasma parameters (density and temperature, effective charge state and etc) and the atomic parameters (eg. ionisation energy). The power radiation losses for both the continuum and line emission are discussed which are relevant to the degree of polarisation of the plasma radiation. As the focus of this study is the degree of polarisation of the emission which the dominant physical mechanisms underlying the partial polarisation of the continuum and the line emission are summarised. The physics of continuum polarisation is discusssed mainly in the framework of radiative recombination. Finally, the fundamental physics for the cause of the line emission polarisation is discussed within the framework of the non-statistical distribution of the atomic species amongst the available magnetic sublevels.

References

[1] P. K. Carroll and E. T. Kennedy, "Laser-produced plasmas," *Contemp. Phys.*, vol. 22, no. 1, pp. 61–96, 1981.

[2] C. Fallon, "Optical Diagnostics of Colliding Laser Produced Plasmas : Towards Next Generation Plasma Light Sources," Dublin City University, 2013.

[3] K. D. Kavanagh, "Image and Spectroscopy of Laser produced Colliding Plasmas," Dublin City University, 2006.

[4] J. Dardis, "Interactions Of Intense Optical and Extreme-Ultraviolet Lasers with Atoms and Solids," Dublin City University, 2009.

[5] N. Hans, D. W. and Omenetto, "Laser-Induced Breakdown Spectroscopy (LIBS), Part I: Review of Basic Diagnostics and Plasma-Particle Interactions: Still-Challenging Issues Within the Analytical Plasma Community," *Appl. Spectrosc.*, vol. 64, p. 335A–366A, 2010.

[6] S. S. Harilal, T. Sizyuk, A. Hassanein, D. Campos, P. Hough, and V. Sizyuk, "The effect of excitation wavelength on dynamics of laser-produced tin plasma," *J. Appl. Phys.*, vol. 109, no. 6, 2011.

[7] W. Nicola, "Laser Produced Plasmas in Liquid Environments," Dublin City University, 2016.

[8] F. Anabitarte, A. Cobo, and J. M. Lopez-Higuera, "Laser-Induced Breakdown Spectroscopy: Fundamentals, Applications, and Challenges," *ISRN Spectrosc.*, vol. 2012, pp. 1–12, 2012.

[9] J. P. Singh and S. N. Thanku, *Laser Induced Breakdown Spectroscopy*, no. 1. Elisevier, 2007.

[10] D. Salzmann, *Atomic Physics in Hot Plasmas*. Oxford University Press, 1998.

[11] N. Farid, S. S. Harilal, H. Ding, and A. Hassanein, "Emission features and expansion dynamics of nanosecond laser ablation plumes at different ambient pressures," *J. Appl. Phys.*, vol. 115, no. 3, pp. 1–9, 2014.

[12] A. Eslami Majd, A. S. Arabanian, and R. Massudi, "Polarization resolved laser induced breakdown spectroscopy by single shot nanosecond pulsed Nd:YAG laser," *Opt. Lasers Eng.*, vol. 48, no. 7–8, pp. 750–753, 2010.

[13] D. Giulietti and L. A. Gizzi, "X-Ray Emission from Laser Produced Plasmas," *Riv. Del Nuovo Cim.*, vol. 21, no. 1, pp. 1–93, 1998.

[14] W. C. Nunnally, "High Temperature Theta Pinch Plasma," Texas Tech University,

1974.

[15] M. J. Bernstein and G. G. Comisar, “X-ray production in laser-heated plasmas,” *J. Appl. Phys.*, vol. 41, no. 2, pp. 729–733, 1970.

[16] D. Colombant and G. F. Tonon, “X-ray emission in laser-produced plasmas,” *J. Appl. Phys.*, vol. 44, no. 8, pp. 3524–3537, 1973.

[17] A. Al-Qasimi, O. Korotkova, D. James, and E. Wolf, “Definitions of the degree of polarization of a light beam.,” *Opt. Lett.*, vol. 32, no. 9, pp. 1015–1016, 2007.

[18] T. Fujimoto and S. A. Kazantsev, “Plasma polarization spectroscopy Review Article,” *Plasma Phys. Control. Fusion*, vol. 39, pp. 1267–1294, 1997.

[19] J. C. Kieffer, J. P. Matte, M. Chaker, Y. Beaudoin, C. Y. Chien, S. Coe, G. Mourou, J. Dubau, and M. K. Inal, “X-ray-line polarization spectroscopy in laser-produced plasmas,” *Phys. Rev. E*, vol. 48, no. 6, pp. 4648–4658, 1993.

[20] J. Kim and D. E. Kim, “Measurement of the degree of polarization of the spectra from laser produced recombining Al plasmas,” *Phys. Rev. E - Stat. Nonlinear, Soft Matter Phys.*, vol. 66, no. 1, pp. 1–4, 2002.

[21] A. K. Sharma and R. K. Thareja, “Anisotropic emission in laser-produced aluminum plasma in ambient nitrogen,” *Appl. Surf. Sci.*, vol. 253, no. 6, pp. 3113–3121, 2007.

[22] H. M. Milchberg and J. C. Weisheit, “Polarization of recombination radiation from nonequilibrium plasmas,” *Phys. Rev. A*, vol. 26, no. 2, pp. 1023–1029, 1982.

[23] J. S. Penczak, Y. Liu, R. D. Schaller, D. H. Rich, and R. J. Gordon, “The mechanism for continuum polarization in laser induced breakdown spectroscopy of Si(111),” *Spectrochim. Acta - Part B At. Spectrosc.*, vol. 74–75, pp. 3–10, 2012.

[24] J. Liu, H.-Y. Tao, X. Gao, Z.-Q. Hao, and J.-Q. Lin, “The polarization characteristics of single shot nanosecond laser-induced breakdown spectroscopy of Al,” *Chinese Phys. B*, vol. 22, no. 4, p. 44206, 2013.

[25] R. F. and S. P. F. Colao, V.Lazic, “A comparison of single and double pulse laser-induced breakdown spectroscopy of aluminium sample,” *Spectrochim. Acta Part B*, vol. 57, no. 1167–1179, 2002.

[26] A. K. Sharma and R. K. Thareja, “Polarization-resolved measurements of picosecond laser-ablated plumes,” *J. Appl. Phys.*, vol. 98, no. 3, p. 33304, 2005.

[27] J. S. Penczak, Y. Liu, and R. J. Gordon, “Polarization-resolved laser-induced breakdown spectroscopy of Al,” *Opt. Lett.*, vol. 34, no. 4, p. 494, 2009.

[28] V. Schmidt, “Photoionization of atoms using synchrotron radiation,” *Reports Prog.*

Phys., vol. 55, no. 9, pp. 1483–1659, 1992.

[29] D. A. Shaw, D. M. P. Holland, E. E. Rennie, and L. G. Shpinkova, "A vibrationally resolved fluorescence polarization study of the CO+ A 2Π→X 2Σ+ transition in the 16.5–20 eV excitation range," *J. Phys. B At. Mol. Opt. Phys.*, vol. 36, no. 21, pp. 4233–4244, 2003.

[30] M. E. Asgill, H. Y. Moon, N. Omenetto, and D. W. Hahn, "Investigation of polarization effects for nanosecond laser-induced breakdown spectroscopy," *Spectrochim. Acta - Part B At. Spectrosc.*, vol. 65, no. 12, pp. 1033–1040, 2010.

[31] M. J. E. Manuel, C. K. Li, F. H. Séguin, J. A. Frenje, D. T. Casey, R. D. Petrasso, S. X. Hu, R. Betti, J. Hager, D. D. Meyerhofer, and V. Smalyuk, "Rayleigh-Taylor-induced magnetic fields in laser-irradiated plastic foils," *Phys. Plasmas*, vol. 19, no. 8, 2012.

[32] J. M. Stamper, J. A., Papadopoulos, K., Sudan,R.N., McLean, E.A., and Dawson, "Spontaneous Magnetic Fields in Laser-Produced Plasmas - PhysRevLett.26.1012-1.pdf." 1971.

[33] T. Fujimoto and S. a Kazantsev, "Plasma polarization spectroscopy," *Plasma Phys. Control. Fusion*, vol. 39, no. 9, p. 1267, 1997.

3 Experimental System

In this chapter, the experimental system used for measuring the anisotropic emission from nanosecond laser produced plasmas on solid targets is presented.

3.1 Introduction

The main components of the experimental systems comprising of the Q-switched laser, the vacuum chamber, targets, laser and plasma focusing optics, spectrometer, ICCD camera and polarisers are introduced and described in this chapter. A number of the experimental procedures that are unique to this experiment are also described. These include polarisation sensitivity calibration of the spectrometer system and the optical components needed to resolve the polarisation states of line and continuum emission from the plasmas studied.

The complete experimental system is shown in **Figure 3.1**. Briefly, a Q-switched Nd: YAG laser was used to create a laser produced plasma on a metallic target that was housed in an aluminium vacuum vessel. The emission from the plasma was collected at a viewing angle of 90^{o} to the target normal be means of a relay lens system. A dichroic polariser was used in conjunction with a compact mini-spectrometer (Stellarnet^{TM} EPP2000) for time integrated plasma emission measurements. For time-resolved imaging and spectroscopy a Wollaston prism was used to resolve the plasma emission into orthogonal polarisation states before recording it. An ICCD camera was used to perform time resolved imaging measurements while a space-resolving Czerny-Turner spectrometer equipped with the same ICCD was used to perform time resolved spectroscopy measurements.

3.2 The Laser System

Laser produced plasmas on solids were generated using a Q-switched Nd: YAG laser, model Spectron^{TM} SL-800. A part of establishing optimum operation of the laser was the determination of the optimum Q-Switch delay. Basically, the active medium of the laser (the Nd: YAG rod) is pumped into population inversion by a Xe flash lamp. The Q-switch is an electro-optic gate which acts to release the energy from the cavity in the form of a short laser pulse lasting a few to a few tens of nanoseconds. There exists an optimal delay between the

flashlamp and the Q-switch trigger pulses where the energy stored in the laser rod is highest and the maximum energy is released in the form of a short optical pulse when the Q-switch is activated. Measuring this was an important part of setting up the experiment. The intensity of the laser output was measured as a function of Q-switch delay by means of both a fast photodiode and by measuring the emission from a laser produced plasma with an optical spectrometer. The laser was operated at a wavelength of 1064 nm for all experiments. The laser specifications are shown in **Table 3.1**.

Table 3.1: Spectron™ SL-800 laser specification.

Parameters	Output
Laser type	Spectron™ SL-800
Lasing medium	Nd: YAG
Wavelength	1064 nm
Energy	400 mJ (max), 53±3 mJ, 142±3 mJ and 173±3 mJ for the experiments
Pulse duration	≈ 14 ns
Repetition rate	10 Hz
Trigger Jitter	+/- 1 ns

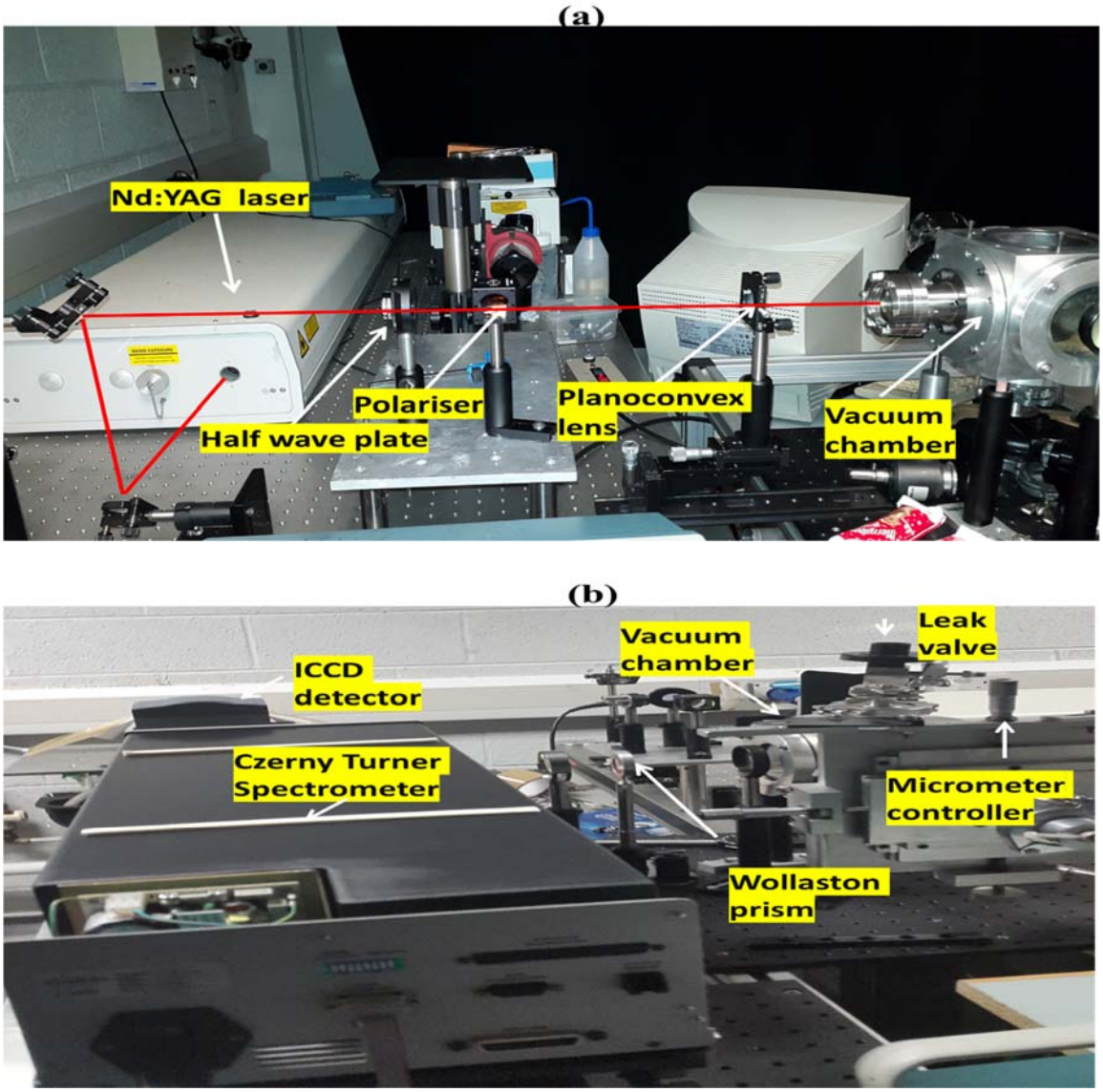

Figure 3.1: (a) Photograph showing the laser, laser focusing optics and vacuum chamber with the entrance window for the laser beam. (b) Photograph of the Czerny-Turner spectrometer with its cover removed. The ICCD camera (hidden) is mounted on the opposite end of the spectrometer. The micrometer controlled target holder is also indicated on the figure.

Figure 3.2 (a) and **(b)** shows the laser pulse height (in volts) and spectrally integrated intensity (in counts) of an Al plasma respectively as a function of a Q-switch delay respectively. In both figures, the pulse height and spectrally integrated intensities were

maximum for a Q-switch delay of 160 µs. To attenuate the laser intensity, a polariser and half-wave plate were placed in the beam path before the beam was delivered to the plasma chamber. The transmission axis of the polariser was kept fixed and by rotating the half-wave plate, the laser intensity was varied. **Figure 3.3** shows how the average laser power varied with half-wave plate angle.

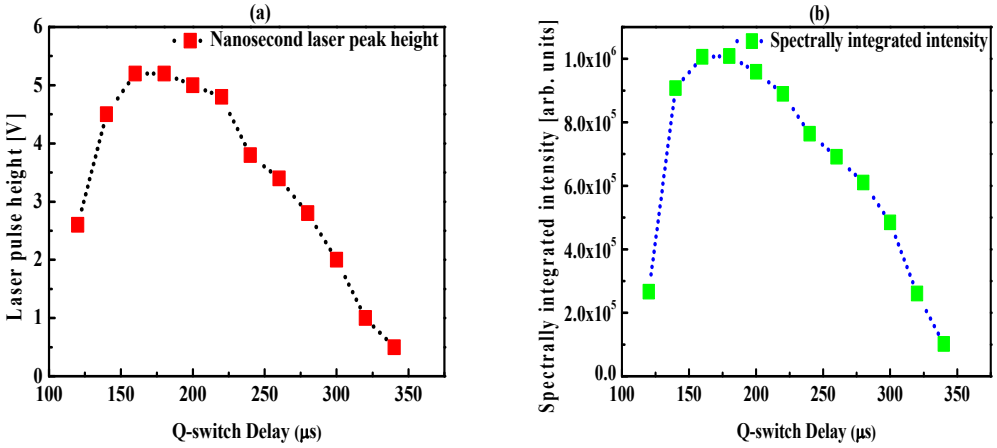

Figure 3.2: The optimal signal of the laser at each Q-switch delay using (a) a fast photodiode and oscilloscope and (b) a Stellarnet^{TM} 2000 spectrometer.

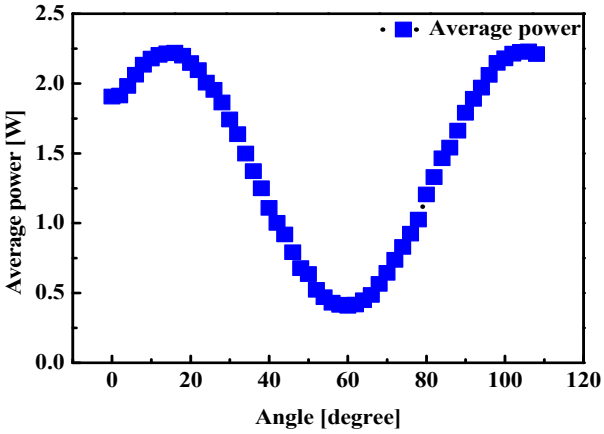

Figure 3.3: Average laser power vs half wave plate angle in degrees.

3.3 The Vacuum Chamber and Target Motion System

A small evacuable chamber was used to house the targets for the various plasma experiments. The chamber was made from an aluminium block and comprised a cube with equal sides of length 12.5 cm. The cube had been hollowed out to yield holes along x,y and z directions, each of diameter 7.2 cm. All six open sides could be enclosed by O-ring sealed flanges. The target was mounted on a vacuum sealed XYZ motion stage which was mounted in turn on the back of the vacuum chamber via one of the O-ring sealed flanges so that the target could be moved independently in the X, Y or Z directions to ensure a fresh target spot after each laser shot. A turbo-molecular pump was used to evacuate the chamber if experiments were being performed under vacuum and a small leak valve allowed the background pressure to be varied. **Figure 3.1 (b)** shows the vacuum chamber with the target holder mounted on it.

3.4 Polarisers

The polarisation state of the emitted radiation was measured in two ways. Firstly, a thin dichroic polariser was variously placed in front of the ICCD camera, the optical fiber coupled to a compact Stellarnet^{TM} EPP2000 compact spectrometer or the entrance slit of a Chromex 0.5m spectrometer equipped with ICCD readout. The latter spectrometer was stigmatic and hence space resolving. An image or spectrum could be taken with the polariser aligned at 0^{o} and then 90^{o} to the target normal. The degree of polarisation could then be determined by taking the difference between both measurements. However, because the use of a dichroic polariser required taking a laser shot for each polarisation state separately, the repeatability of the measurement was limited by shot-to-shot fluctuations in the laser pulse energy. To address this problem, a Wollaston prism was used to split the image of the plasma into two spatially separated, orthogonally polarised images which were simultaneously recorded thus eliminating any contributions from shot to shot laser output fluctuations. This was not possible with the Stellarnet^{TM} EPP2000 spectrometer which was fiber coupled and not space resolving.

3.4.1 Dichroic Polariser

A dichroic polariser is designed to transmit one specific polarisation state whilst blocking all other states. It is made from a polymer sheet material that is stretched, aligning the molecules along a preferred direction. Light polarised along that direction is strongly absorbed while the orthogonal while light polarised in the orthogonal direction is transmitted. In analogy to a wire grid polarizer only the performance of the polariser was measured using a Cary 5 UV-Vis spectrometer. **Figure 3.4** shows the transmission for various combinations of dichroic polarisers. Of interest is the purple trace in **Figure 3.4** which shows the transmission when two dichroic polarisers (P_1 and P_2) are placed at angles of -45^0 and 45^o respectively. Here 0^0 is chosen to be along the vertical direction and 90^0 for the horizontal direction. The trace shows almost zero transmission indicating good performance of the polariser over the spectral range of interest (400 - 700 nm).

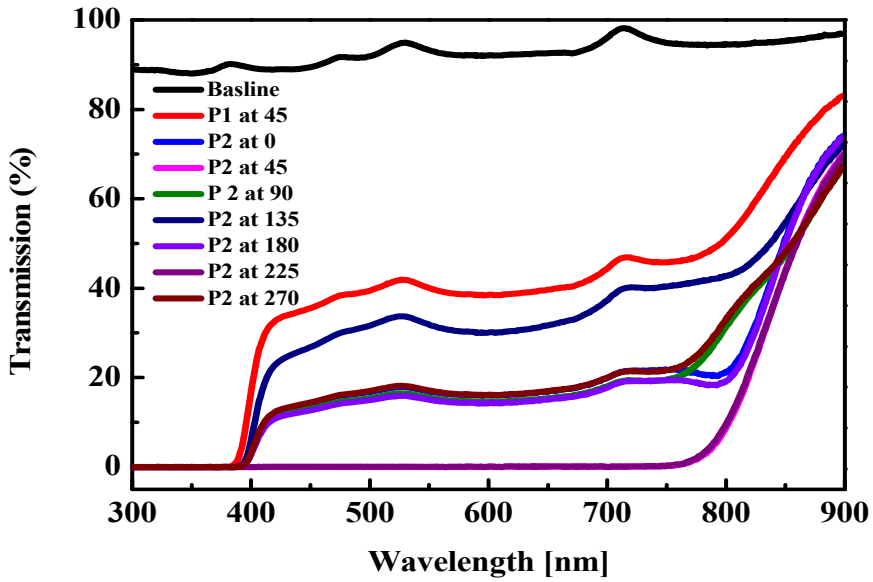

Figure 3.4: Polarisation efficiency of a dichroic film.

3.4.2 Wollaston Prism

Figure 3.5 shows the Wollaston prism. It is composed of two triangular birefringent calcite crystals that are optically cemented at their hypotenuses. When unpolarised light is passed

through the prism, it splits the light into two orthogonally polarised components via double refraction. The refractive index for the light waves passing through the prism is different depending on whether the polarisation direction is aligned with (e-ray) or orthogonal to (o-ray) the optic axis of the prism. In the Wollaston prism used in this work, the optic axes of the two calcite wedges are orthogonal to each other. This means that at the interface, the e and o-waves experience refractive index changes of opposite sign and hence refract in different directions, resulting in a spatial separation between the two polarisation components. In an ideal world, if the light entering the Wollaston prism is completely polarised at 45° to the optic axis of the first wedge, the two emerging beams should be of equal intensity. Thus, the polarisation response of the whole detection system could be measured in this way. For this reason, we installed a dichroic polariser in front of a Wollaston prism and imaged a backlighted pin at the plasma position onto an ICCD detector. **Figure 3.6** displays an image of the pin where it can be seen that the intensity of the two images, i.e., in the horizontally and vertically polarised directions, is as close as possible to equal. In this sense, the detection system in imaging mode is deemed robust.

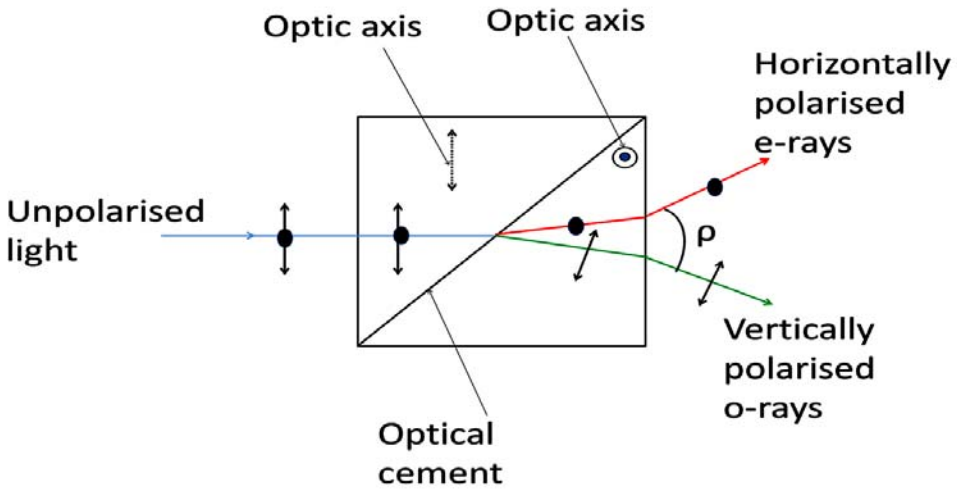

Figure 3.5: Wollaston prism polariser (Calcite).

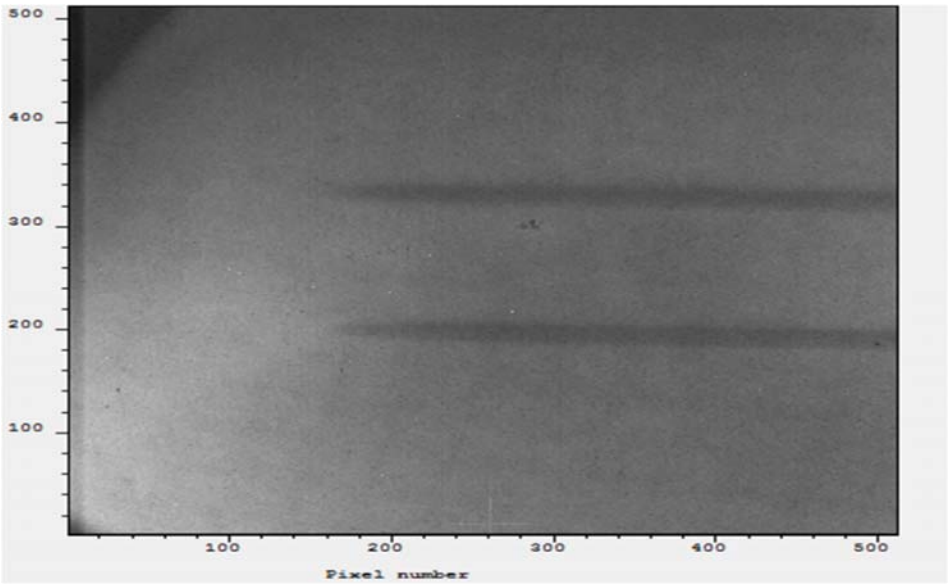

Figure 3.6: Images of the backlit pin resolved into orthogonal polarisation states.

3.5 Detection System

3.5.1 Czerny-Turner Spectrometer

Time and polarisation resolved plasma emission spectroscopy was performed using a 0.5 m focal length Chromex^{TM} Czerny-Turner spectrometer equipped with gated ICCD readout. The spectrometer is equipped with a plane grating of 1200 g/mm, a blaze wavelength of 500 nm and a mean spectral resolution of 0.07 nm at a slit width of 60 μm (at FWHM) [1,2]. The entrance slit of the spectrometer can be varied from 10 μm to 1 mm [3]. Specifically, for our experiments, the slit width was set at 200 μm. At this slit width the instrumental broadening, measured using a narrow emission line at 404 nm from a Mercury (Hg) lamp, was found to be 0.17 nm (at FWHM). Plasma light is focused onto the entrance slit located at the focus of a concave mirror (**Figure 3.7**) which collimated the radiation travelling to the plane grating. The dispersed radiation from the grating was then focused by the second Al mirror onto the ICCD camera. The grating disperses radiation according to the equation given below:

$$2d\left(\sin\alpha \pm \sin\beta\right) = m\lambda \tag{3.1}$$

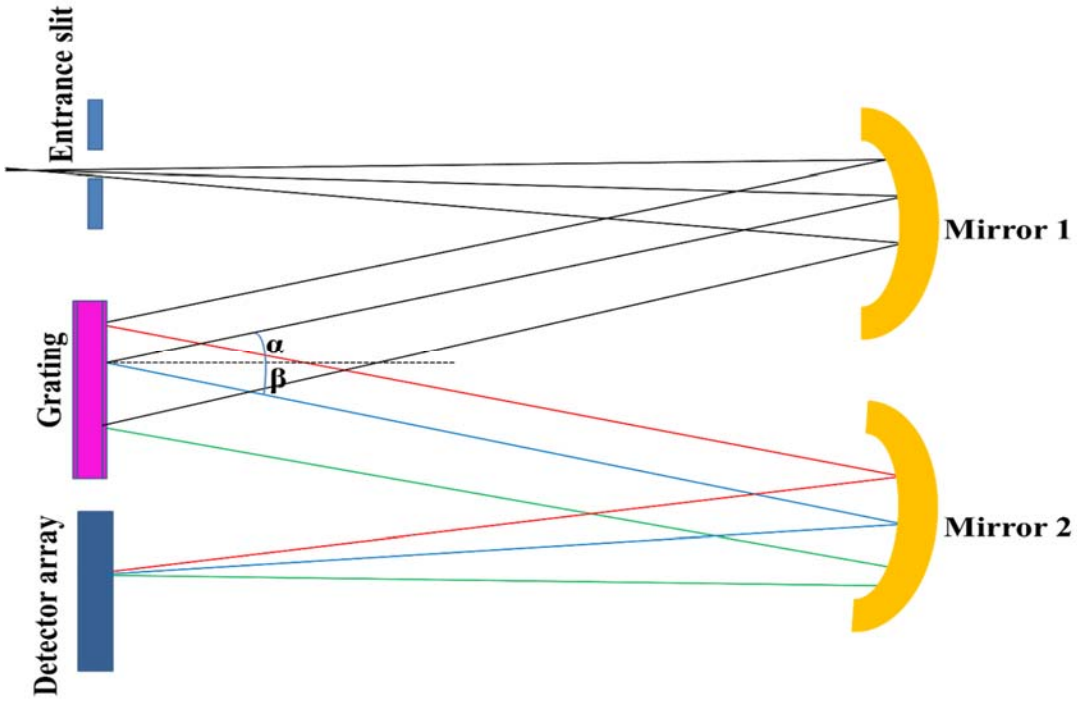

Figure 3.7: Schematic diagram of the spectrometer [4].

where d is the distance between grooves, α is the angle of incidence for light in impinging on the grating and β is the angle between the normal and the diffracted light beam, m is the diffraction order and λ is the wavelength of the light.

Figure 3.8 shows the spectral efficiency of the 1200g/mm grating used in the 190 to 700 nm spectral range. It can be seen that it peaks at close to 35% in the UV and stays above 20% out to 500 nm.

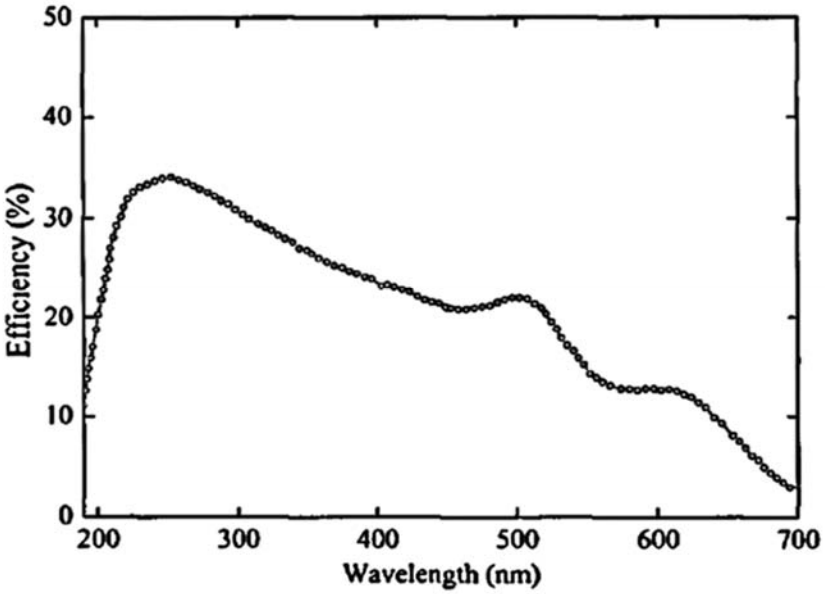

Figure 3.8: Efficiency curve for the 1200 grooves/mm grating supplied with the Chromex^{TM} visible spectrometer [3].

3.5.2 The ICCD Camera

Two ANDOR^{TM} ICCD cameras were used in this work reported in this thesis:

(1) ANDOR^{TM} i-Star Technology model DH734 was used for the experimental results presented in Chapters 4 and 5 and Appendix B. The ICCD sensor consisted of 1024 ×1024 pixels, each with an image area of 13 μm ×13 μm with the corresponding total area of 13.3×13.3 mm^2.

(2) ANDOR^{TM} model DH5H7 was used for the experimental results discussed in Chapter 6. The ICCD sensor consisted of 512 ×512 pixels, each with an image area of 24 μm ×24 μm or 12.3 x 12.3 mm^2.

For both ICCD detectors, the electronic gate pulse width was set at 10 ns for all measurements with yielded an achievable optical time resolution of ≈3 ns [3] and the time delay ranged from 1 ns to 5 μs depending on the experimental requirements. When photons fall onto a pixel, that pixel generates electron-hole pairs. Once generated, the electrons are collected in ‘‘wells’’ during the integration time of the CCD [5], [6]. The image is moved vertically row by row

to a readout section of the CCD, in which each pixel in the row is read out. In this manner, the image collected by the CCD can be reconstructed.

3.5.3 Synchronization

An important aspect of the experiment was synchronising the arrival of the laser pulse (which initiated plasma formation) with the gating of the intensifier of the ICCD camera. The output from a delay generator (model 9515 Quantum Composer) (operated at a pulse repetition rate of 10 Hz) was used as a local oscillator to trigger the flashlamps via 15 V active low pulses of 10 μs duration. A separate 10 Hz pulse train (also 15 V active low, 10 μs duration), synchronised to the flashlamps and delayed by 160 μs was used to trigger the Q-switch. This second pulse train was fed to the input of an AND gate. The other input of the AND gate was a TTL pulse generated in the software for the camera acquisition system (designated FIRE on the Andor^{TM} trigger pulse unit). The output of this AND gate was used to trigger the Q-switch. In this way, the Q-switch is activated, and a high-power laser pulse is emitted by the laser, only when an acquisition cycle is initiated by the ICCD data acquisition and control software. This ensured that while the laser flash lamps were continuously triggered at a repetition frequency of 10 Hz to ensure they reach their equilibrium temperature and the laser only outputted a pulse when requested to do so by the ICCD software. A third pulse, which could be delayed by a known amount t_d was required to trigger the intensifier of the ICCD to capture time resolved images and spectra. This third pulse was referenced to the Q-switch trigger pulse. The value of t_d was varied to probe different times during the plasma evolution. The width of the electronic gate pulse, which represents the time resolution of the experiment (essentially the exposure time of the camera), was generally fixed at 30 ns but could be as low as 10 ns resulting in an optical gate width of 3 ns. The full timing diagram is shown in **Figure 3.9**. The ‘‘time-zero’’ corresponding to plasma initiation, that is, the value of t_d =0 which represents the moment the laser pulse arrives at the target, was found by measuring the scattered light from the laser with a photodiode and displaying its output signal on an oscilloscope. The TTL pulse for the intensifier was also monitored on the same oscilloscope.

t_d was then varied until the rising edge of the TTL pulse and the photodiode signal coincided in time.

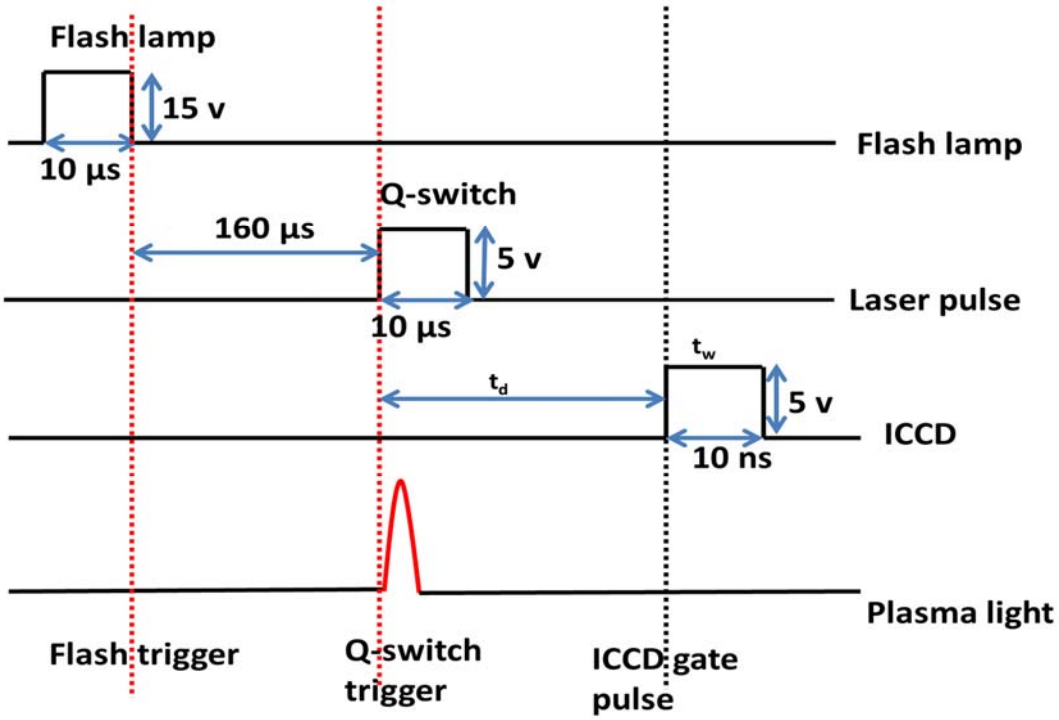

Figure 3.9: Timing diagram showing the synchronisation of the laser and the camera.

3.5.4 Stellarnet™ Spectrometer

Time-integrated polarisation resolved spectra were obtained using a Stellarnet™ EPP2000 UV-Vis spectrometer with readout via a linear CCD. It has a toroidal grating of 1200 g/mm with a recipricoal linear dispersion of 1 nm/pixel. The CCD has a pixel size of 14 µm × 200 µm and the detector integration time could be adjusted from 1ms to 65s. To improve the signal to background ratio (SBR) the dark current was subtracted. An optical fiber of core diameter equal to 50 µm was connected to the spectrometer to collect the plasma radiation. Wavelength calibration was done internally by the software.

3.5.5 Oscilloscope and Fast Photodiode

A Tektronix™ oscilloscope (model TDS3032) was used to record the synchronisation signals that come from the fast photodiode and ICCD camera. It was also used to measure the laser

pulse shape for each Q-switch delay to determine optimal value of that delay. In this way, it permitted the determination of the range of times around the optimal delay for which no ringing was observed (ringing indicates leakage and sub-optimal Q-switching). The combination of fast photodiode and oscilloscope indicated the time zero of the plasma emission. Data transfer was taken by capturing the signal trace on the Oscilloscope screen.

3.6 Calibration

3.6.1 Intensity Calibration for the Spectrometer

The intensity calibration of the Chromex^{TM} 0.5m spectrometer is one of the most important parts of the measurement and unique to this experiment because the diffraction grating efficiency is different for different polarisation states. The emission from a xenon lamp was polarised to 45^0 with respect to the optic axis of the Wollaston prism. This ensured that the intensity of the two polarisation components on the entrance slit of the spectrometer was equal. The relative polarisation sensitivity of the grating is then defined as the ratio of the horizontally to vertically polarised measured intensity. The measurement was repeated at several different central wavelengths of the spectrometer focusing on those spectral windows that were used in this experiment. As an example, **Figure 3.10** displays the polarization sensitivity at 395 nm, 465 nm, 512 nm and 569 nm central wavelengths of the Czerny-Turner spectrometer. Of note is the close to unity sensitivity of the grating at 465 nm which is close to the blaze wavelength of the spectrometer.

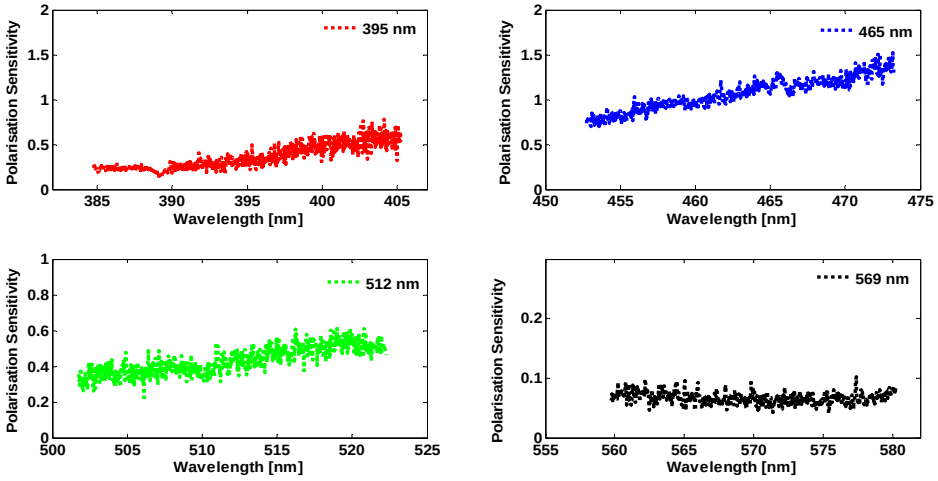

Figure 3.10: The polarisation sensitivity calibration of the horizontal and vertical directions for the 395 nm, 465 nm, 512 nm and 569 nm central wavelengths obtained with the aid of an intensity calibrated xenon lamp.

3.6.2 ICCD Gain Calibration

The spectra are further corrected to account for the gain of the ICCD camera. This was achieved by measuring a silicon plasma at a central wavelength of 556 nm for different gains. The Si II spectral line (at 556 nm) corresponding to the transition ($8s\ ^2S_{1/2} \rightarrow 5p^2P^0_{1/2}$) is unpolarised [7]. Spectra were measured for gain values from 0 to 255 in steps of 25 units. The following is the procedure for gain calibration:

(1) Determine the intensity as a function of the gain I(G) for both horizontal and vertical states of polarised emission for all values of G from 0 to 255;

(2) Calculate the correction factor defined as $\alpha = \frac{I(G)}{I(G=0)}$ for the orthogonal emissions,

(3) Divide each spectrum by the correction factor 'α' for the gain used to record it.

The variation of signal intensity was plotted as a function of the gain for both vertical and horizontal polarisations as shown in **Figure 3.11**. The data were then fitted to a function of the form:

$$I(G) = I_0 + A_0 e^{\left(\frac{G - x_0}{t}\right)} \tag{3.2}$$

Where I_0 is the initial intensity, i.e., at G=0 and t=0,

$$I(G=0) = I_0 + A_0 e^{-\frac{x_0}{t_0}} \tag{3.3}$$

For $x_0 \to \infty \Rightarrow I(G=0) \approx I_0$ and A_0 is the added intensity when the gain G = x_0, i.e., I(G=x_0) = I_0+A_0. t is the growth rate of the gain. The correction α(G) is then given by:

$$\alpha(G) = \frac{I(G)}{I(G=0)} \tag{3.4}$$

α was calculated from the average intensities of the horizontal (H) and vertical (V) polarization states. **Table 3.2** shows the raw data of each polarisation state and the average intensity value for H and V states.

Table 3.2: Total spectral intensity for H and V polarisation states.

Gain	I_V(10^6×arb. units)	I_H(10^6×arb. units)	(I_H+I_V)/2 (10^6× arb. units)
0	0.22	1.02	0.62
25	0.143	0.25	0.19
50	0.144	0.39	0.27
75	0.19	0.75	0.47
100	0.29	1.47	0.88
125	0.5	3.04	1.77
150	0.51	3.07	1.79
175	0.89	5.90	3.39
200	3.34	24.3	13.8
225	4.76	34.5	19.6
250	10.8	76.6	43.7

Values of I(G=0), A_0, x_0 and t_0 obtained from fitting equation 3.2 to the raw data in Table 3.2 are shown in Tables 3.3 and 3.4.

Table 3.3: Values of I(G=0) and A_0 obtained by fitting equation 3.1 to the raw H and V intensity data.

Parameters	Horizontal (H) x10^6	Vertical (V)x10^6	H/V
I (G=0)	0.14	0.24	0.58
A_0	0.014	0.13	0.10

Table 3.4: The average value of the gain cross-section from the exponential growth fit for the vertical and horizontal intensities for the average initial value of the gain x_0 and initial growth rate t_0.

Parameters	Horizontal (H)	Vertical	(H+V)/2
x_0	26.87	27.00	27.61
t_0	33.86	35.00	34.57

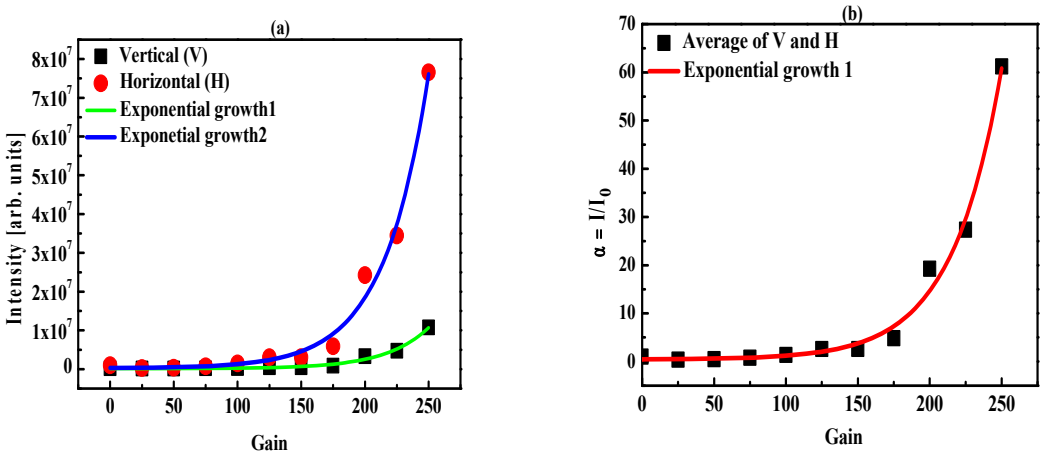

Figure 3.11: (a) Vertical and horizontal polarisation gain cross-section calibration with exponential growth curve fits. (b) Average gain calibration extracted from the orthogonal polarisations and the exponential fit.

3.7 Polarisation Imaging

Different plasma diagnostics have been employed to capture plasma dynamics. The orthogonally polarised images are tracked by the use of a Wollaston prism placed in front of an ICCD camera. These images are polarised parallel and perpendicular to the quantisation axis of the laser which will be described in detail in Chapter 4. In the past different models, have been proposed by different authors to explain to plume dynamics. For example, Sharma et. al. [7] proposed that an Al plasma plume expanding in ambient nitrogen can be understood in terms of a shock wave model for low pressure and a Drag model for high pressure. In the results presented in Chapter 4 the focus was on the spatial and temporal resolution with respect to the degree of polarisation. A broadband filter transmitted plasma radiation in the 380 – 600 nm band. Polarisation imaging was used to support time, space and polarisation resolved spectroscopic studies carried out with the stigmatic spectrometer.

Figure 3.12 (a) illustrates the orthogonally polarised images of an Al plasma plume at a background pressure of 1×10^{-5} mbar and at a time delay of 30 ns. The exposure time was 10 ns. Taking lineouts along directions normal to the target one can see from **Figure 3.12 (b)** that the ICCD intensity peaks occur at slightly different longitudinal positions but that the shapes of the plume light curves are very similar for both polarisation directions.

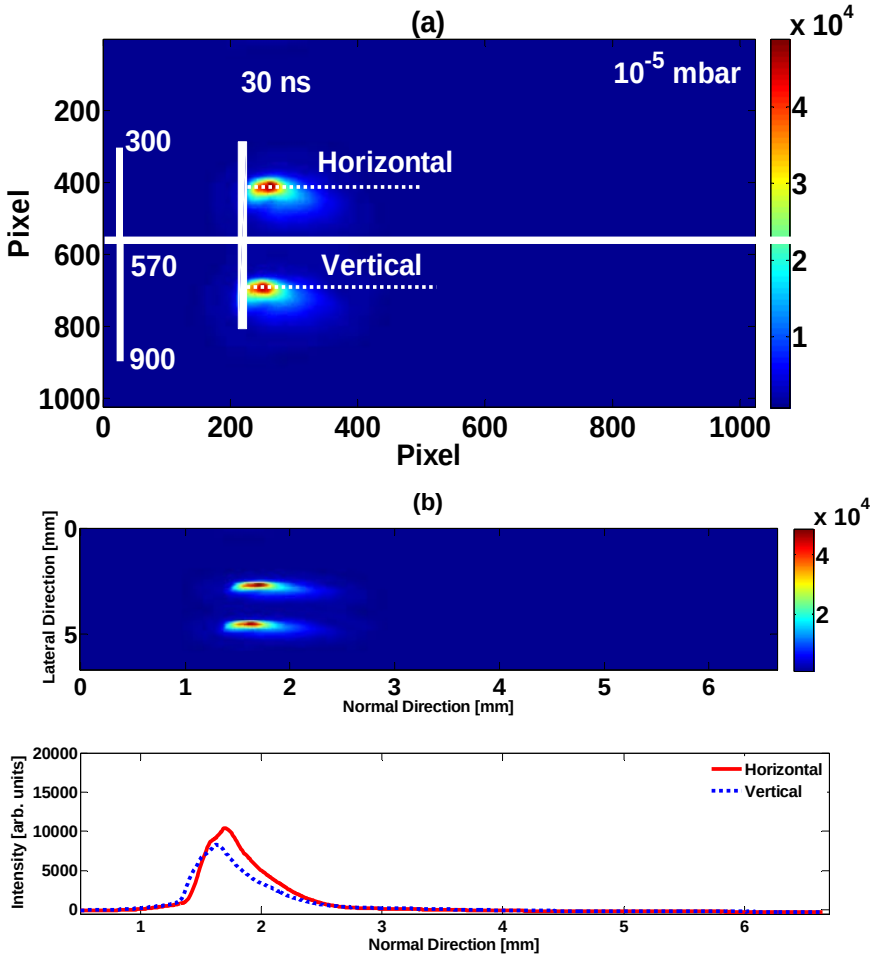

Figure 3.12: (a) Polarisation resolved images obtained at a time delay of 30 ns and (b) Lineouts for each image in figure 3.12(a). The laser fluence was 296 J/cm^2 at a background pressure of 1×10^{-5} mbar with a camera time resolution of 10 ns.

3.8 Optical Emission Spectroscopy

The emission spectrum of a laser produced plasma can be very useful for diagnosing the plasma itself, namely determining the plasma density and temperature. Time and space resolved spectroscopy allow for these parameters to be mapped in space and time. Line spectra are particularly useful in this regard with the intensity or the width allowing the determination of the temperature and density respectively. In practice, the measured line can be distorted (e.g., broadened or shifted) by the plasma along with instrumental effects [8], [9]. It turns out that many lines can be fitted with a Voigt profile, a convolution of a Gaussian profile with a Lorentzian profile with the latter component being dominated by the Stark effect [2]. **Figure 3.13** serves to illustrate the interaction of a Q-switched laser pulse with a solid target leading to plasma formation and its subsequent evolution. The main point is to indicate the likely timescales on which different types of radiation might be emitted.

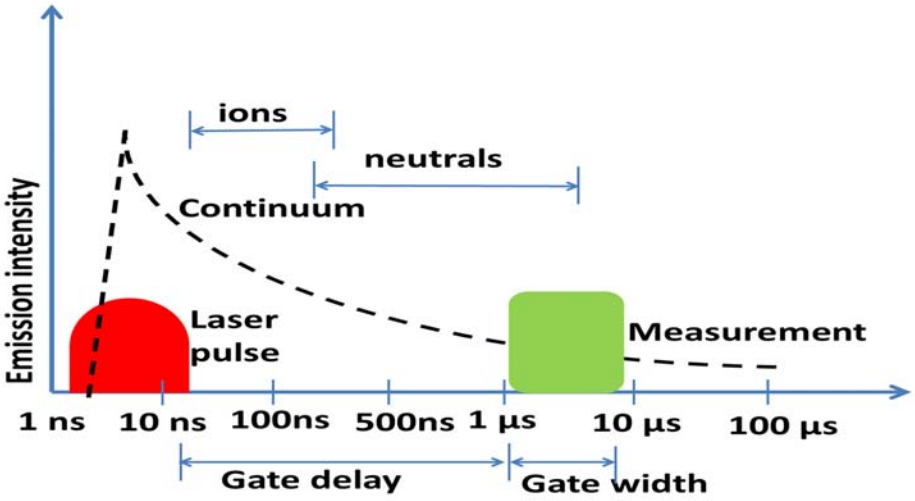

Figure 3.13: Schematic diagram showing plasma evolution with time.

The intensities of the spectral lines are greatly dependent on the environment in which the atomic or molecular species that emit the lines reside [5]. Since, as mentioned above, they play a key role in diagnosing the plasma, the various mechanisms that lead to spectral line broadening are outlined below.

3.8.1 Natural Broadening

This broadening arises from the inherent quantum nature of the excited state in any atomic system and is governed by the Heisenberg uncertainty principle [2], [5]. The uncertainty in the lifetime of the upper state gives rise to a minimum uncertainty in its energy which is turn leads to line broadening and is expressed as:

$$\Delta E \Delta t \geq \frac{\hbar}{2} \tag{3.5}$$

More rigorously, assume at some instant that the excited state population for a specific atom or ion is $N(t=0) = N_0$. The population decays spontaneously so that the excited state population at any subsequent instant in time t is given by $N(t) = N_0 e^{-t/\tau}$ [10] where, τ is defined as the excited state lifetime, i.e., the time taken for the population to decay to 1/e of its initial value N_0. This equation can also be expressed as $N(t) = N_0 e^{-\gamma t}$ where γ is referred to as a radiation damping factor. Thus, the finite upper state lifetime of the excited state results in an exponentially decaying line radiation signal. As the line intensity depends linearly on N(t), I(t) = N(t) x A, where A is the spontaneous emission rate, the frequency distribution of the corresponding emission line is obtained by taking the Fourier transform of N(t) which leads to a Lorentzian intensity distribution function expressed as [10]:

$$I(\nu) = \frac{I_0(\gamma/4\pi)^2}{\left[(\nu-\nu_0)^2 + (\gamma/4\pi)^2\right]} \tag{3.6}$$

I_0 is the peak intensity of line profile for the line centred at a frequency $\nu_0 = \frac{\omega_0}{2\pi}$ and γ is the radiation damping factor.

3.8.2 Doppler Broadening

It arises due to the random thermal motion of emitting atoms [1], [5]. The resulting line profile is Gaussian and the full-width half maximum (FWHM) of the line profile is given by:

$$\Delta\lambda_{1/2} = 7.6\times10^{-6}\lambda_0\sqrt{T/m} \tag{3.7}$$

where m is the atomic mass, T is the temperature and λ_0 are the central wavelengths.

3.8.3 Stark Broadening

Mutual collisions of the plasma species (electrons, ions and atoms) with their surrounding environment can create pressure broadening [11]. Collisions can include electron-electron, electron-atom, electron-ion, ion-ion or atom-atom collisions. However, there are two main contributions to Stark broadening of a spectral line emitted by an excited atom or ion [1], [2], namely electron-emitter or ion-emitter collisions. In dense plasmas, electron collisions with the surrounding plasma occur in a very short period of time compared to the natural lifetime of the electronic spontaneously emitted state. Theses collisions randomize the phase of the emitted radiation and for frequent collisions the life time is significantly shorter than the inverse natural line width [12]. In addition, the collisions perturb the atoms/ions which are interacting with the radiation which can lead not just to a broadening of the spectra of the atomic/ionic line profile emitted but also to a frequency shift [10].

Stark broadening occurs predominantly in the dense part of the plasma and is due mainly to collisions of electrons with atoms and ions in the plasma [4], [5]. The resulting shortened excited state lifetimes yield spectrally broadened emission lines. In that sense, as alluded to above, it can be compared to pressure broadening except that here it is the electron and ion densities rather than simply the gas density which impacts the collision frequency and hence the degree of broadening.

The FWHM of a Stark broadened line is given by [4]:

$$\Delta\lambda_{stark} = 2w\frac{n_e}{10^{16}} + 3.5A\frac{n_e^{1/4}}{10^{16}} + \left[1 - BN_D^{-1/3}\right]w\frac{n_e}{10^{16}} \tag{3.8}$$

where w is the electron impact width parameter, A is an ionic broadening parameter, and B is atomic and ionic coefficient. The first term arises from electron collisions with the excited atoms or ions which forces to them emit prematurely thereby shortening the lifetime of the state and thus increasing the width of the line emitted. The second term accounts for the effect

of the residual ion microfield and is usually negligible in table-top laser produced plasmas. The third term is also usually negligible in laser produced plasmas. N_D is the number of particles in the Debye sphere.

3.8.4 Instrumental Broadening

This contribution to line broadening depends on the spectrometer and the ICCD detector. It can be determined by measuring the spectrum of a low-pressure spectral lamp which emits lines with very narrow widths. It is in effect the spectral impulse response of the spectrometer and is used to deconvolve the instrumental broadening from a line profile before analysing the residual profile for density and/or temperature. The following measurements were made on the spectrometers used at DCU and MUT.

(1) The spectrum of a Hg lamp at a wavelength of 404 nm was measured using the 0.5 m Chromex Czerny-Turner Spectrometer operated with a slit width aof 200 μm. The spectrum was fitted with a Gaussian profile of width of ≈ 0.17 nm (at FWHM) which represented the instrument function for those settings.

(2) The emission spectrum of Hg I at a wavelength of 435.832 nm was fitted with a Gaussian profile and used to determine the instrument function of an Echelle spectrometer used to obtain spectra at MUT (Appendix D). The instrumental resolution here was found to be on the order of 0.02 nm (at FWHM) as shown in **Figure 3.14**.

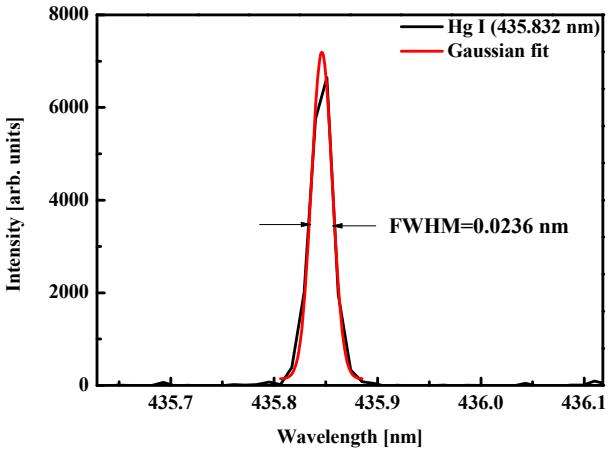

Figure 3.14: Instrumental broadening for an Echelle spectrometer using the Hg I 435.832 nm [$5d^{10}6s7s\ (^3S_1) \rightarrow 5d^{10}6s6p\ (^3P^0_1)$] line.

3.8.5 Estimation of Temperature

Plasma temperature and electron density are the key parameters to be determined. Using the condition of local thermodynamic equilibrium (LTE), electron energies follow a Maxwell-Boltzmann distribution function [2,4]. For a discrete line arising from a transition from state '1' to state '2', the integrated intensity for the transition is given by [2,4]:

$$I_{12} = \frac{h\omega_{12}}{8\pi^2} A_{12} N_1 l_{sight} \tag{3.9}$$

Where h is Planck's constant, $\omega_{12} = 2\pi\nu_{12} = 2\pi\frac{c}{\lambda}$ is the angular frequency, c is the speed of light, λ is the line wavelength, A_{12} is the transition rate in s^{-1} and l_{sight} is the length of plasma along the line of sight.

Assuming LTE, the temperature can be calculated from the intensity ratio of the pair of spectral lines that originate from different ion stages of the same element. The intensity ratio is related to the basic atomic parameters by the equation [4]:

$$\frac{I_1}{I_2} = \left(\frac{A_1\lambda_2 g_1}{A_2\lambda_1 g_2}\right) e^{-\frac{E_1 - E_2}{k_B T_e}} \tag{3.10}$$

Where I_1 and I_2 are the relative intensities of the emitted lines, A_1 and A_2 are the corresponding transition rates in units of sec^{-1}, g_1 and g_2 are the statistical weights of the levels involved, i.e., $2J+1$ where J is the total angular momentum, and E_1 and E_2 the energies of those states. Assuming LTE, it is possible to obtain the electron temperature T_e from the experimentally determined ratio. Knowing the temperature, the corresponding Stark broadening parameters can be obtained and used in equation (**3.8**) to determine the electron density [1], [2], [4]. Finally, it is clearly critical for LTE to hold in a plasma if equation (**3.8**) is to be applied. For LTE to hold it is essential that electron collisional processes dominate in

the plasma over radiative ones. McWhirter developed a criterion which must hold if a plasma can be assumed to be in LTE namely [1], [2], [13]:

$$n_e \geq 1.6 \times 10^{12} T_e^{1/2} \left(E_2 - E_1\right)^3 \quad (3.11)$$

where n_e is the electron density in cm^{-3}, T_e is the electron temperature in eV and $E_1 - E_2$ in eV is the transition energy for the emission line being used to diagnose the plasma. It is clear from this expression that the lower the transition energy, the more likely it is to satisfy the McWhirter criterion and hence lines in the visible and infrared regions of the spectrum are most often used for this purpose.

Dense plasmas with a temperature gradient are prone to opacity which can significantly affect relative line intensities ranging from a slight deviation from the statistical intensity ratio, e.g., 2:1 for the ratio of the 3s ($^2S_{1/2}$) to 3p ($^2P_{3/2,\ 1/2}$) to complete line reversal in extreme cases [3]. In that sense, it is an important consideration in plasma polarisation spectroscopy and could interfere with measurements of line polarisation in cases where the 1/2 to 1/2 transition is used for polarisation calibration. In order to check for opacity, the line intensity ratios for the unpolarised Al^0 and Al^{2+} spectra were monitored to check for the presence of opacity during the studies reported here. The greatest potential effect was on the Al^0 doublet since the lower state in the transition is the ground state of the atom, which is likely to have the greatest population in the cooler corona of the plasma plume.

3.9 Data Processing

Time and polarisation resolved spectroscopy data were captured by a combination of the spectrometer and the ICCD camera and could be displayed as raw images, i.e., spatially resolved spectra since the spectrometer is stigmatic, or as a single space integrated trace by fully vertically binning the image. The data were plotted in two-dimensional spaces as intensity vs wavelength using an in-house developed Matlab code. The flow chart for orthogonally polarised emission spectra is shown in **Figure 3.15**. The processes for data analysis are summarised briefly as follows. First, the ICCD ‘‘.sif’’ image file is read in and

the image split into spectra corresponding to the orthogonally polarised states. Secondly, we subtracted the background of the camera which was approximately 5 pixels along the vertical and the horizontal direction from the zero value. Thirdly the vertically polarised spectrum was corrected by multiplying it by the appropriate gain correction factor. Fourthly, we developed a separate MATLAB code to extract the polarisation sensitivity from the ratio of the horizontal to vertical spectra of a Xe lamp at a different central wavelength of the spectrometer. This was mainly used to calibrate the continuum emission from an Al plasma described in the results chapters. Lastly, to extract the degree of polarisation (P) of the line, the unpolarised neighbouring line was used to calibrate the spectra of the orthogonally polarised states. The area under each spectrum line, polarised and unpolarised, was used to reduce the error in obtaining its relative intensity.

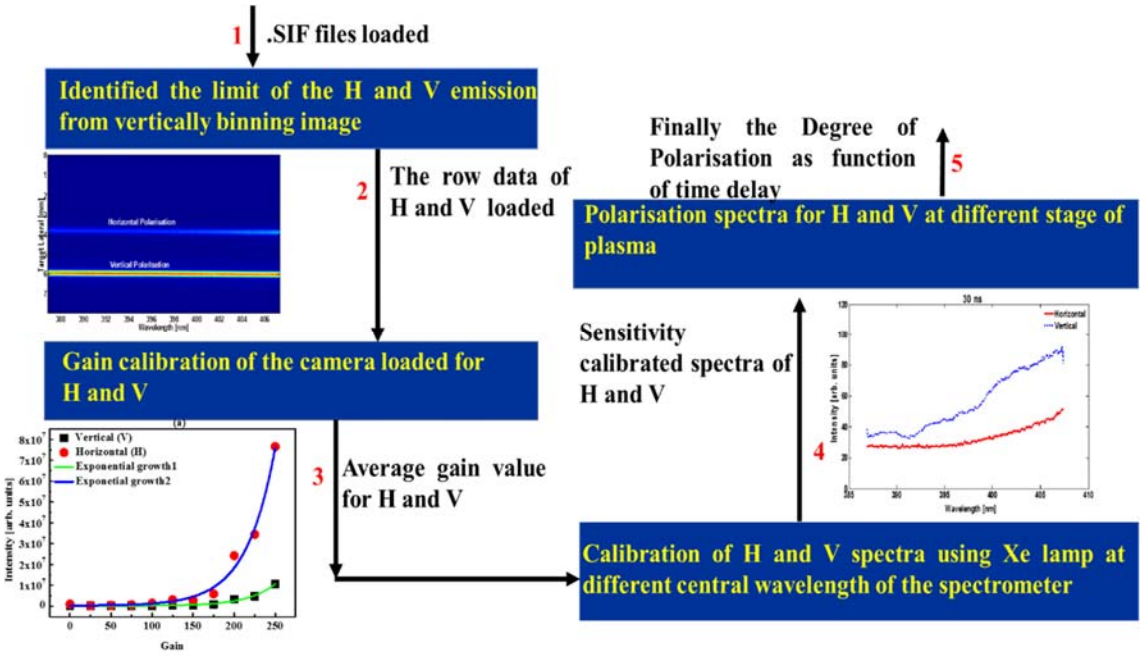

Figure 3.15: A flow chart for the analysis of the time-resolved horizontal (H) and vertical (V) plasma polarisation emission spectra.

References

[1] J. Dardis, "Interactions Of Intense Optical and Extreme-Ultraviolet Lasers with Atoms and Solids," Dublin City University, 2009.

[2] C. Fallon, “Optical Diagnostics of Colliding Laser Produced Plasmas : Towards Next Generation Plasma Light Sources,” Dublin City University, 2013.

[3] K. D. Kavanagh, “Image and Spectroscopy of Laser produced Colliding Plasmas,” Dublin City University, 2006.

[4] J. P. Singh and S. N. Thanku, *Laser Induced Breakdown Spectroscopy*, no. 1. Elisevier, 2007.

[5] D. W. Hahn and N. Omenetto, “Laser-Induced Breakdown Spectroscopy (LIBS), Part II: Review of Instrumental and Methodological Approaches to Material Analysis and Applications to Different Fields,” *Appl. Spectrosc.*, vol. 66, no. 4, pp. 347–419, 2012.

[6] R. Gaudiuso, M. Dell’Aglio, O. De Pascale, G. S. Senesi, and A. De Giacomo, “Laser Induced Breakdown Spectroscopy for Elemental Analysis in Environmental, Cultural Heritage and Space Applications: A Review of Methods and Results,” *Sensors*, vol. 10, no. 8, pp. 7434–7468, 2010.

[7] A. K. Sharma and R. K. Thareja, “Polarization-resolved measurements of picosecond laser-ablated plumes,” *J. Appl. Phys.*, vol. 98, no. 3, p. 33304, 2005.

[8] N. Hans, D. W. and Omenetto, “Laser-Induced Breakdown Spectroscopy (LIBS), Part I: Review of Basic Diagnostics and Plasma-Particle Interactions: Still-Challenging Issues Within the Analytical Plasma Community,” *Appl. Spectrosc.*, vol. 64, p. 335A–366A, 2010.

[9] F. Anabitarte, A. Cobo, and J. M. Lopez-Higuera, “Laser-Induced Breakdown Spectroscopy: Fundamentals, Applications, and Challenges,” *ISRN Spectrosc.*, vol. 2012, pp. 1–12, 2012.

[10] J. F. Christopher, *Atomic Physics*. Oxford University Press, 2005.

[11] W. Nicola, “Laser Produced Plasmas in Liquid Environments,” Dublin City University, 2016.

[12] A. W. Allen, M. Blaha, W. W. Jones, A. Sanchez, and H. R. Griem, “Stark-broadening measurement and calculations for a singly ionized aluminum line,” *Phys. Rev. A*, vol. 11, no. 2, pp. 477–479, 1975.

[13] P. N. . Burgess D.D, Fawcett B.C, “Vacuum ultra-violet emission spectra from laser-produced plasmas,” *PROC PHYS. SOC*, vol. 92, 1967.

4 Comparison of the Polarisation of Line (Al I and Al II) and Continuum Emission in Laser Produced Plasmas

Anisotropic emission from a laser-produced aluminium plasma is studied using time and polarisation resolved imaging and spectroscopy at different ambient pressures of air. The time-resolved degree of polarisation for discrete lines emitted by the plasmas, namely Al^0 (396.15 nm) and Al^+ (466.3 nm), is compared to nearby continuum emission. The results are interpreted in the framework of radiative recombination and statistical imbalances in the populations of magnetic sub-states. A stronger anisotropy in air than in vacuo is observed. It is also found that continuum emission is more strongly polarised than line emission.

4.1 Introduction

Plasma polarisation spectroscopy (PPS) has been shown to be a powerful diagnostic technique which reveals information about the electron velocity distribution function (EVDF) and population imbalance within the magnetic sub-shells of atoms and ions within a plasma [1]. PPS has been applied to laser produced plasmas where partial polarisation has been observed in the X-ray and visible spectral ranges [2], [3]. Importantly, a particular application of PPS known as Polarisation Resolved Laser Induced Breakdown Spectroscopy (PRLIBS) exploits this partial polarisation in order to enhance the signal to background ratio over traditional LIBS measurements [4]. In various wide-ranging studies [4]–[6], it was shown that the continuum radiation tends to have a greater degree of polarisation than the line emission. For this reason, placing a polariser in front of a spectrometer results in lower background continuum, thus increasing the signal-background ratio, which is one figure of merit for LIBS. The origin of the polarisation in this study was postulated to be an anisotropic electron distribution function caused by steep density gradients which result in polarised recombination radiation [6]. Similarly, studies on the visible emission from an Al plasma showed that line emission can also be partially polarised. In [3] the degree of polarisation of the Al^{2+} at 569.6 was found to be about 3 %. The origin of the polarisation in this study is attributed to an inherent population imbalance in the magnetic sub-shells of the ionic system arising from anisotropic recombination from more highly charged ions. This study was extended in [7] where the degree of polarisation of the Al^{2+} doublet was measured with time resolution and in a variety of background gas pressures. The degree of polarisation was found to oscillate with time and its origin was attributed to anisotropic electron distribution functions caused at the plasma–gas interface.

In this chapter, we extend the studies [6], [7] and make a time-resolved comparison of the degree of polarisation from both plasma imaging and spectral line emission in an Al plasma (the Al^0 at 396.15 nm and Al^+ at 466.3 nm lines) and nearby continuum emission at a different air pressures.

4.2 Experimental Setup

4.2.1 Imaging setup

The time and polarisation resolved imaging of a radiation emitted from an Al plasma setup is shown in **Figure 4.1**. The Nd:YAG laser was focused on to an Al target, plasma was formed and then the first lens collect and collimated an pass through the Wollaston prism split into orthogonally polarised beam and the second lens and pass through the filter and focused on to the ICCD readout. The detail of the imaging setup is similar to the spectroscopy setup described below.

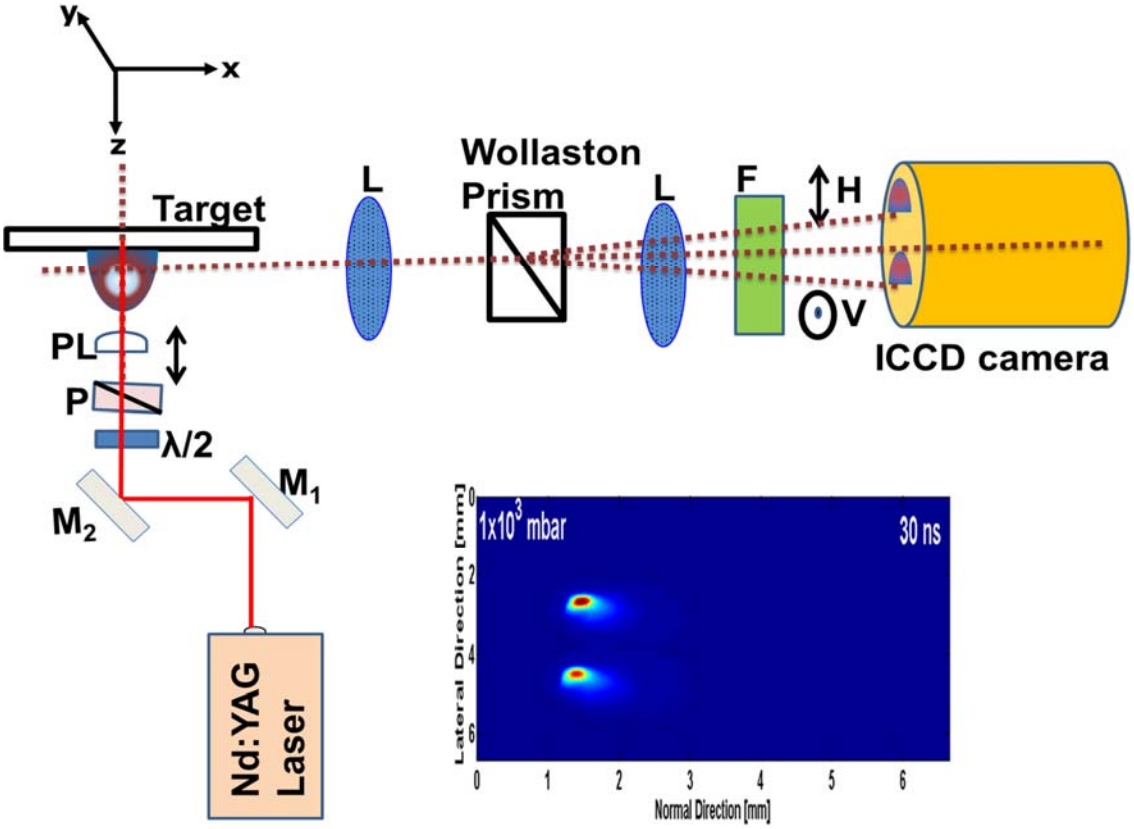

Figure 4.1: **Schematic of time and polarisation resolved imaging of laser produced plasma setup (M, mirror; λ/2, half wave plate; P, polariser; PL, planoconvex lens; L, lens; W, Wollaston prism, F, Filter). Two plasma images are created screen of an ICCD camera. Inset is a typical image obtained by the experiment**.

4.2.2 Spectroscopy setup

Figure 4.2 shows the experimental setup. A Nd: YAG laser (Spectron^{TM} SL800, 14 ns pulse width, 1064 nm wavelength) was focused onto an aluminium (99.99% pure) target at normal incidence using a planoconvex lens (f = 250 mm). A combination of a half-wave plate and polariser were placed before the planoconvex lens to attenuate the incident laser. The on-target laser fluence was measured to be ~550 J/cm^2 (corresponding to an irradiance of 4×10^{10} W/cm^2). The target was mounted on a precision x-y-z translation stage to ensure a fresh target surface after each laser shot. Spectra were recorded by means of a 0.5 m Czerny-Turner spectrometer (Chromex^{TM} 500is) which was coupled to an ICCD camera (Andor^{TM} i-Star DH734) with a time resolution of ~10ns. The spectrometer was equipped with a grating of 1200 g/mm blazed at 500 nm which provided a mean spectral resolution of 0.17 nm. The plasma formed was imaged with a magnification of 2:1 at right angles to the laser propagation axis by a combination of two lenses of focal lengths f_1= 100 mm and f_2 = 50 mm onto the entrance slit of the spectrometer (slit width = 200 μm). A Wollaston prism was used to split the plasma emission into orthogonally polarised components so that both polarisation states to be measured in a single shot.

The spectra presented in this chapter were taken at a distance of 1 mm from the target surface and each represents the average of 10 single laser shots. The optic axis of the experiment (defined here as the axis of quantization) was chosen to be normal to the target. Thus, the Wollaston prism was aligned to produce images polarised parallel and perpendicular to this axis (and parallel to the entrance slit of the spectrometer). The system was calibrated to account for the polarisation dependent sensitivity of the spectrometer as described in Chapter 2. The degree of polarisation was then calculated from the resultant spectra from using equation (**2.43**) reproduced here as equation (**4.1**) and given by:

$$P_\lambda = \left(\frac{I_H - I_V}{I_H + I_V} \right) \tag{4.1}$$

Where I_H is the intensity of the light polarised normal to the target and I_V is light polarised parallel to the slit.

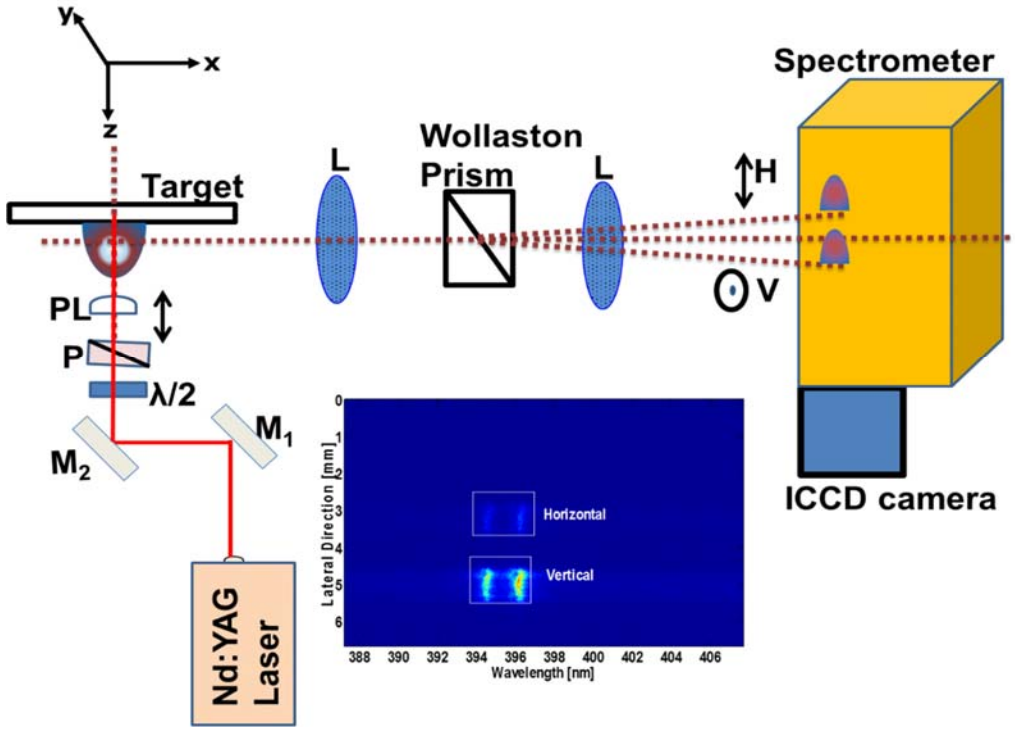

Figure 4.2: Schematic of polarisation resolved laser produced plasma spectroscopy setup (M, mirror; λ/2, half wave plate; P, polariser; PL, planoconvex lens; L, lens; W, Wollaston prism). Two plasma images are created on the entrance slit of a spectrometer gated with an ICCD readout. Inset is a typical image obtained by the experiment.

4.3 Imaging Results

In **Figure 4.3**, **Figure 4.4** and **Figure 4.5** ICCD images of an aluminium plasma are shown for a range of time delays and a range of background pressures. Each image comprises two plumes corresponding to the horizontal and vertical polarisation. The top image in each photograph corresponds to horizontally polarised light, whereas the bottom image was formed by vertically polarised light only. Here, horizontal refers to a direction parallel to the axis of incidence of the laser and the vertical corresponds to light perpendicular to its axis of incidence. Visual inspection of **Figure 4.3** (which corresponds to a base pressure of 1×10^{-5} mbar) shows that the plasma plume expands adiabatically and undergoes free expansion [8]. Ablation occurs along the direction perpendicular to the target surface [9]. In **Figure 4.5**

(which corresponds to a base pressure of 1×10^3 mbar) it can be readily seen that the plume is much more confined. This agrees with previous studies [10] and is attributed to plasma confinement due to the atmospheric pressure ambient gas. **Figure 4.3** shows the orthogonally polarised image of Al plasma at a background pressure of 1×10^{-5} mbar at a time delay of 30 ns. In **Figure 4.4** (which corresponds to a base pressure of 10^{-2} mbar) the plasma expands but then seems to form a double structure. At 1×10^{-2} mbar, a peculiar effect of bifurcation of the plume into slow and fast moving components can be distinguished. This is attributed to excitation of the low-pressure background gas by the expanding plasma [10].

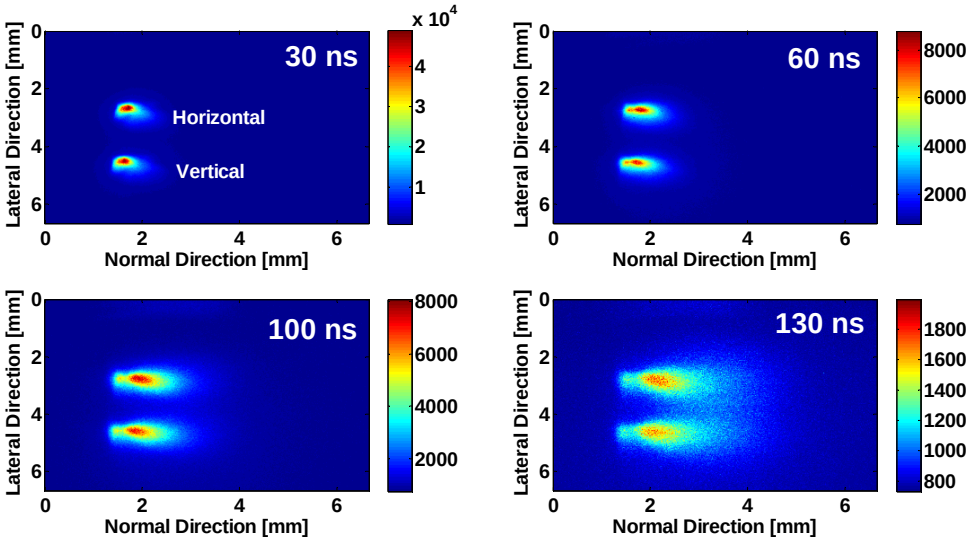

Figure 4.3: Orthogonal polarisation images recorded at various time delays following plasma formation. The laser fluence was 296J/cm^2 at a background pressure of 1×10^{-5} mbar. For all time delays, the camera time resolution was 10 ns.

For each image, the degree of polarisation (P) is calculated by extracting a region of interest around each polarisation image and summing of the pixel counts (relative intensity values). P is then found from the variance of the two intensities (the difference over the sum). In this way, the variation in the degree of polarisation with both time delay and background pressure could be observed. **Figure 3.12 (a)** illustrates the limit of the integration of the data points for the orthogonally polarised states. The degree of polarisation (P) vs time delay is shown in **Figure 4.6** for different background pressures.

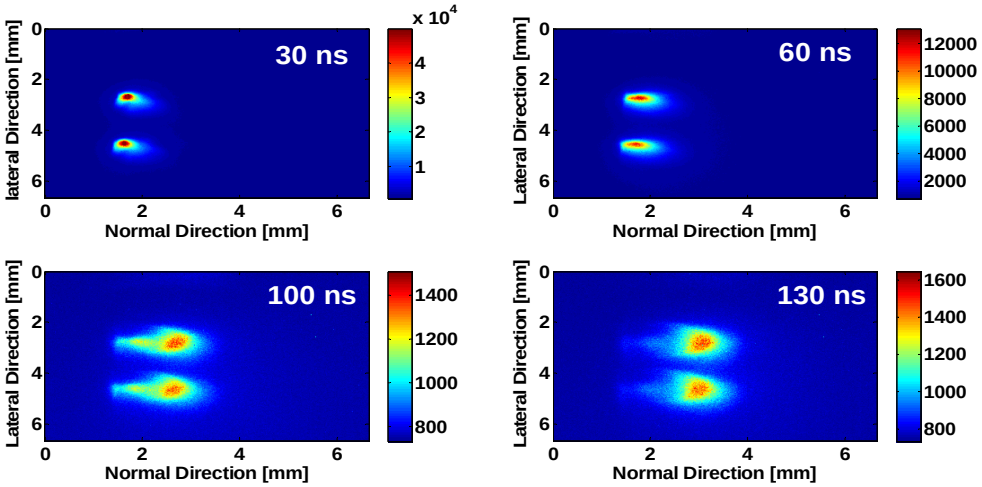

Figure 4.4: Orthogonal polarisation images recorded at various time delays following plasma formation. The laser fluence was 296 J/cm^2 at a background pressure of 1×10^{-2} mbar. For all time delays, the camera time resolution was 10 ns.

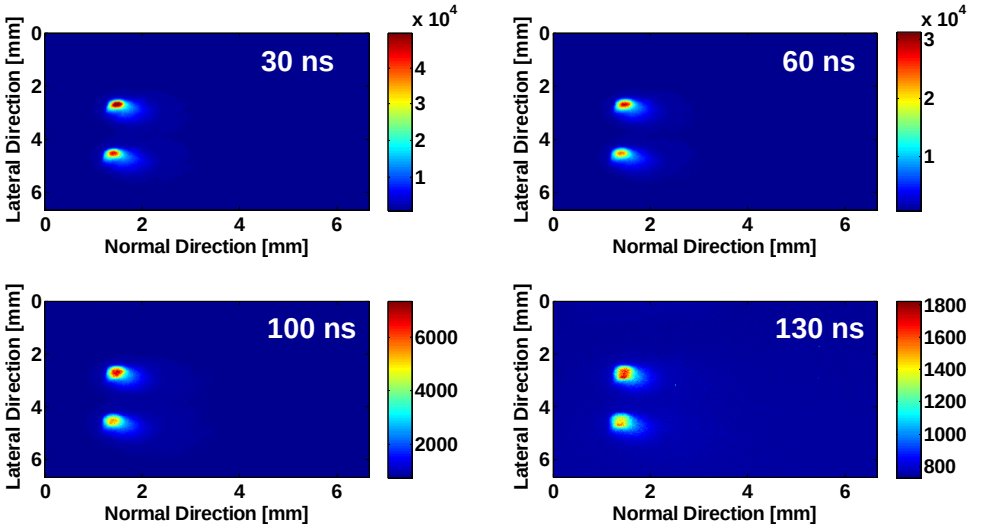

Figure 4.5: Orthogonal polarisation images recorded at various time delays following plasma formation. The laser fluence was 296 J/cm^2 at background pressures of 1×10^3 mbar. For all time delays, the camera time resolution was 10 ns.

It is clear that the emission from plasmas created at atmospheric pressure is more strongly polarised than for those plasmas created at lower background pressures. Similarly, while the radiation emitted at low background pressures tends to show minimal polarisation at all time delays, whereas the plasma emission created at atmospheric pressure becomes initially more

anisotropic with time before returning to a more isotropic state. However, the polarisation values are close for all time delays for the low background pressure cases. To further investigate the mechanisms underlying these observations, spectrally resolved measurements were made.

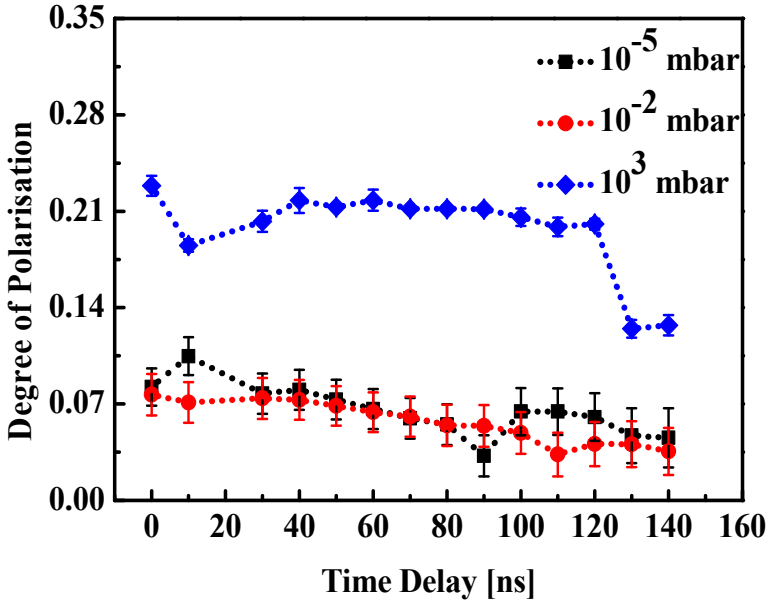

Figure 4.6: The degree of polarisation of emission vs time delay at various background pressures. The laser fluence was 296 J/cm^2 with an ICCD camera gate width of 10 ns.

4.4 Spectroscopy Results

4.4.1 Time Integrated Al Plasma Emission

Figure 4.7 shows emission spectra of Al plasmas at background pressures of 1×10^{-5}, 1×10^{-2} and 1×10^{3} mbar respectively in the visible spectral range (380 - 700 nm) for an integration time of 100 ms obtained. The spectra were recorded by a Stellarnet^{TM} EPP2000 spectrometer at a location approximately 1 mm distant from the target surface at a fluence of 550 J/cm^2 (corresponding to an irradiance of 3.9×10^{10} W/cm^2). For all pressures, the spectra display discrete line emission superimposed on a continuum background. For spectra formed in air neutral emission is stronger than ion emission. However, for the plasma formed in vacuo, the

spectrum is dominated by emission from ions. For this reason, the time-resolved studies in air focused on the spectral range of 390-400 nm where lines are due to resonant neutral transitions and on the 460-470 nm spectral range to where emission from Al^{+} can be observed.

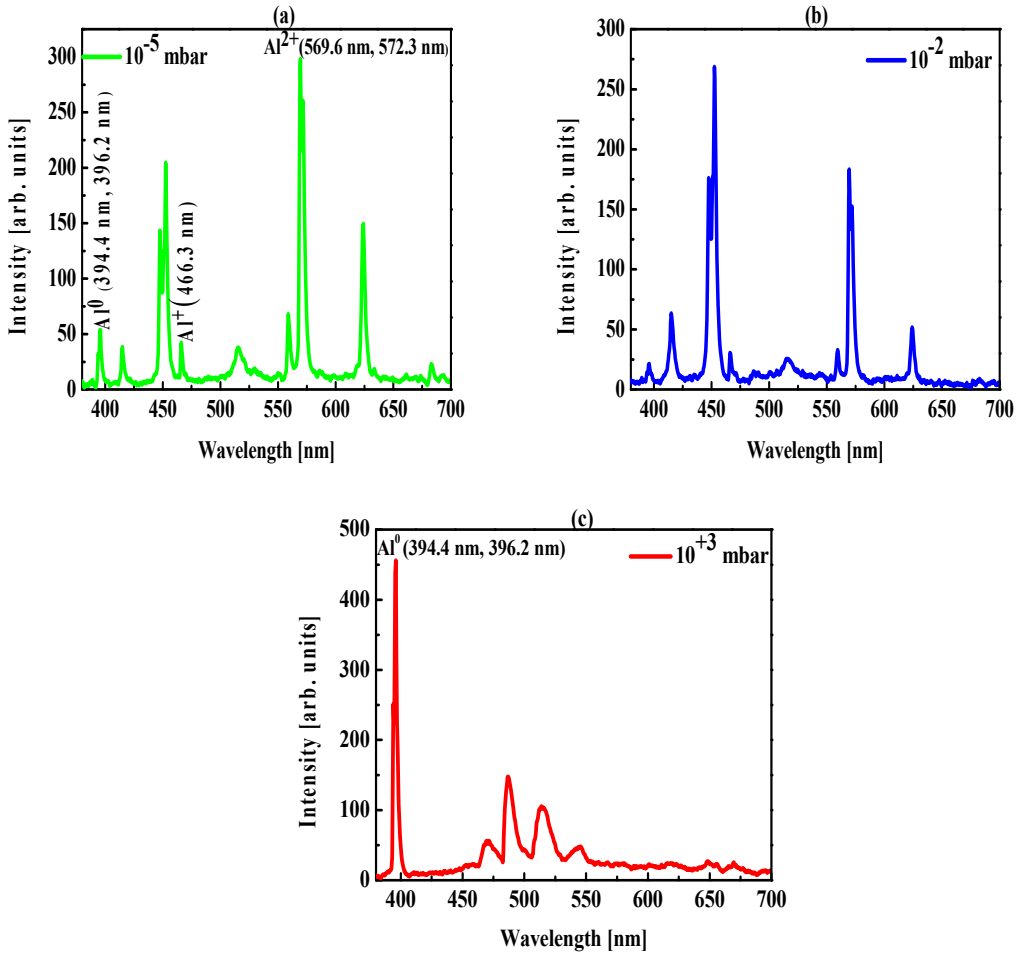

Figure 4.7: Emission spectra of Al plasmas at a laser fluence of 550 J/cm^2 taken at background pressures of (a) 1×10^{-5}, (b) 1×10^{-2} and (c) 1×10^3 mbar, respectively and at an integration time of 100 ms.

On the other hand, studies in vacuo focused on the spectral range 565-575 nm, where Al^{2+} ion emission is present. **Table 4.1** shows the spectroscopic parameters and electronic transition of the neutral and ionic emission. To avoid any confusion, the time integrated spectra were

taken with a different spectrometer and CCD detector (Stellarnet^{TM} EPP2000 spectrometer) from the time resolved spectra.

Table 4.1: Spectroscopic parameters for Al^0 (at 394.4 nm and 396.15 nm), Al^+ (at 466.3 nm), and Al^{2+} (at 569.6 nm and 572.3 nm) lines with assignments from the NIST database. Here g_kA_{ki} is the product of transition probability and statistical weight and E is the upper state energy in eV

Wavelength [nm]	Transition	g_kA_{ki} $\times 10^8$ [1/s]	E [eV]
Al^0 (394.4, 396.15 nm]	4s ($^2S_{1/2}$) →3p ($^2P^o_{1/2,3/2}$)	1, 1.97	3.14, 3.14
Al^+ (466.3 nm)	3s 4p ($^1P^o_1$) →$3p^2$ ($^1D_2$)	1.74	13.26
Al^{2+} (569.6 nm, 572.3 nm)	4p ($^2P^o_{3/2,1/2}$) → 4s ($^2S_{1/2}$)	3.51, 1.73	17.82

4.4.2 Al Neutral Doublet

Polarisation resolved emission spectra of an aluminium plasma showing the Al^0 doublet measured at a central wavelength of the spectrometer of 395nm at a number of time delays following plasma formation and for two different pressures of 1×10^{-2} and 1×10^{3} mbar are shown in **Figure 4.8** and **Figure 4.9** respectively. In **Figure 4.8** it can be seen that the early stages of plasma formation and evolution (<70 ns) are dominated by broadband continuum emission. Line emission appears at the later stages of the plasma evolution as evidenced by the appearance of the 394.4 and 396.15 nm features. These features are associated with the characteristic transitions in the Al neutral atom: 4s ($^2S_{1/2}$) →3p ($^2P^o_{1/2}$) and 4s ($^2S_{1/2}$) →3p ($^2P^o_{3/2}$) respectively as shown in the Appendix A **Figure A.1 (a)** and **(b).** There are clear differences in the intensities of the horizontal and vertically polarised spectra in the figures for the early phases of plasma formation and expansion, i.e., in the continuum spectra. However, weak polarisation of the spectra has been observed for line emission in the time delay range of 100-130 ns. In **Figure 4.9**, where plasmas were formed in ambient air at atmospheric pressure, continuum emission dominates in the first 100 ns with significant differences in the vertically polarised component compared to horizontally polarised emission. Line emission began to appear after a time delay of approximately 230 ns following plasma breakdown. This is evident by the appearance of discrete features at 394.4 nm, 396.15

nm and 399.2 nm respectively. The feature at 399.2 nm is associated with excitation of singly ionised oxygen via the $2s^2 2p^2(^3P)3d\ (^2P_{3/2}) \rightarrow 2s^2 2p^2(^3P)3p\ (^4P^o_{3/2})$ transition. This feature starts to appear approximately 130 ns earlier than the aluminium features. At a time delay of 530 ns, the emission is completely dominated by neutral aluminium lines. This emission lasts for up to approximately 5 μs following plasma formation. At this pressure, vertically polarised continuum emission is stronger than the horizontally polarised component. As time goes on, for both background pressures, the plasma seems partially polarised mainly in the outer wings of the spectrum where the continuum emission is brightest.

Comparison of the emission features at the two pressures show that the plasma is highly anisotropic at early times with polarised continuum radiation emanating from the plasma. On the other hand, the degree of polarisation of line radiation is significantly smaller. There is little or no polarisation anisotropy detected at the wings of the spectrum for the time delay range of 70- 130 ns where the emission is mainly line-like in appearance.

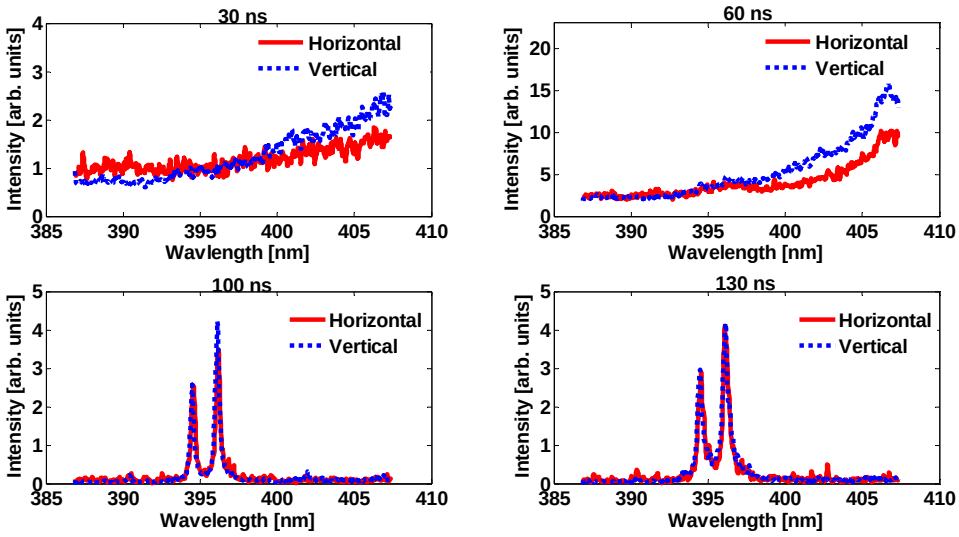

Figure 4.8: The sensitivity calibrated spectra of time and polarisation resolved Al^0 (394.4 nm and 396.15 nm) lines at a laser fluence of 550 J/cm^2 and background pressure of 10^{-2} mbar for the continuum (upper plots) and the lines (lower plots) at various time delays following plasma formation.

The degree of polarisation (P) was computed at two wavelengths, one for the continuum emission at 402 nm and the other for line emission of Al^0, at 396.15 nm. **Figure 4.10** shows several trends for both line and continuum emission. Firstly, the degree of polarisation (P) oscillates with time delay. Further modulation of P is different at the two pressures. It can be seen that the modulation is greater for both the line and continuum emission at 10^{-2} mbar compared to atmospheric pressure.

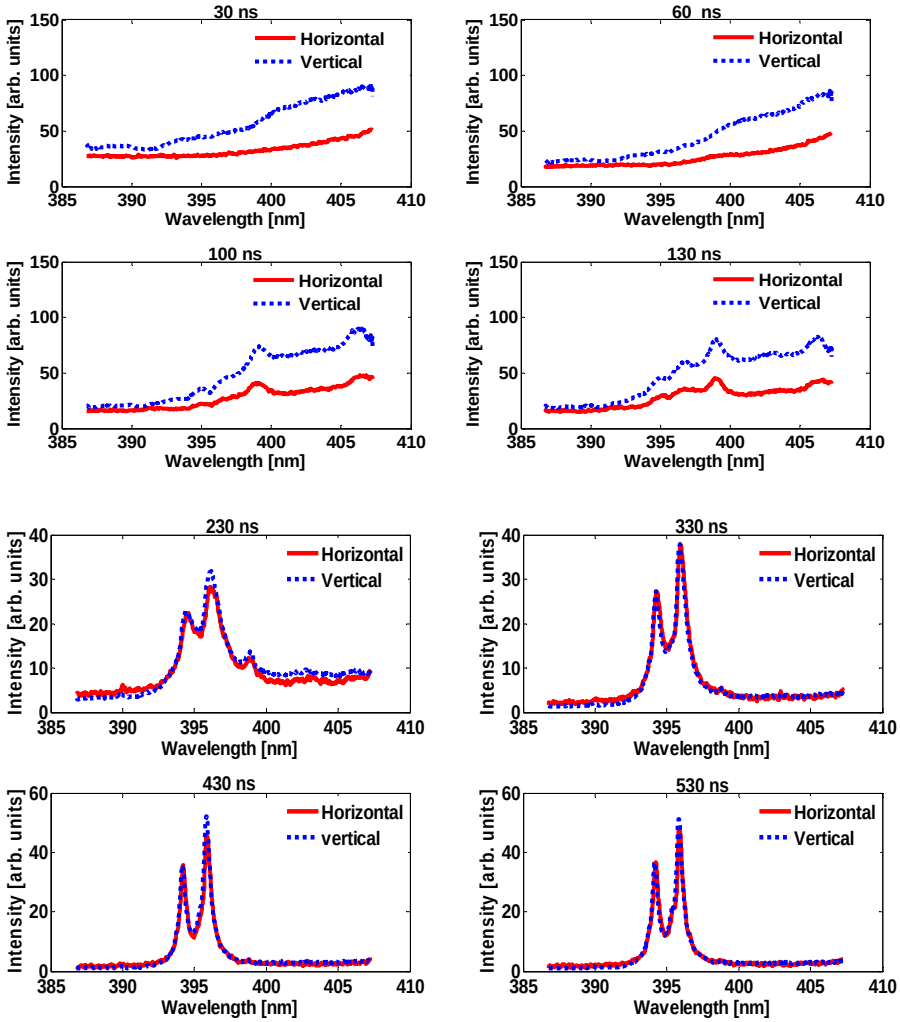

Figure 4.9: The sensitivity calibrated spectra of time and polarisation resolved spectra of Al at a laser fluence of 550 J/cm^2 and background pressure of 1×10^3 mbar for the continuum (the upper four graphs) and the Al^o (394.4 and 396.15 nm) lines (the lower four graphs) at various time delays following plasma formation.

For line emission, the degree of polarisation P is close to zero at atmospheric pressure and is equally distributed about zero, lying in the range -0.1 < P < +0.1, for an ambient air pressure of 10^{-2} mbar. On the other hand, for continuum radiation it is negative (-0.2 < P < -0.01 at 10^{-2} mbar) and (-0.4 < P < -0.25 at 10^{3} mbar). It can be seen that P is remarkably constant at around -0.3 for continuum emission at atmospheric pressure. On the other it is clearly oscillatory at the 402 nm wavelength point at 10^{-2} mbar decreasing to -0.2 at a time delay of 130 ns compared to a value of zero at a delay of 30 ns. Distinct oscillations in time for line radiation are clear from figure 4.9 for both ambient pressures, albeit the amplitude of the oscillations are smaller than for those seen at 402 nm and 10^{-2} mbar (**Figure 4.10 (a)**). Sharma et al. [7] reported that the oscillation in P with time delay is related to the growth in Rayleigh-Taylor (RT) instabilities due to the density difference between the plasma and background gas. The weak polarisation of the line emission is in a good agreement with Kim et al. [3].

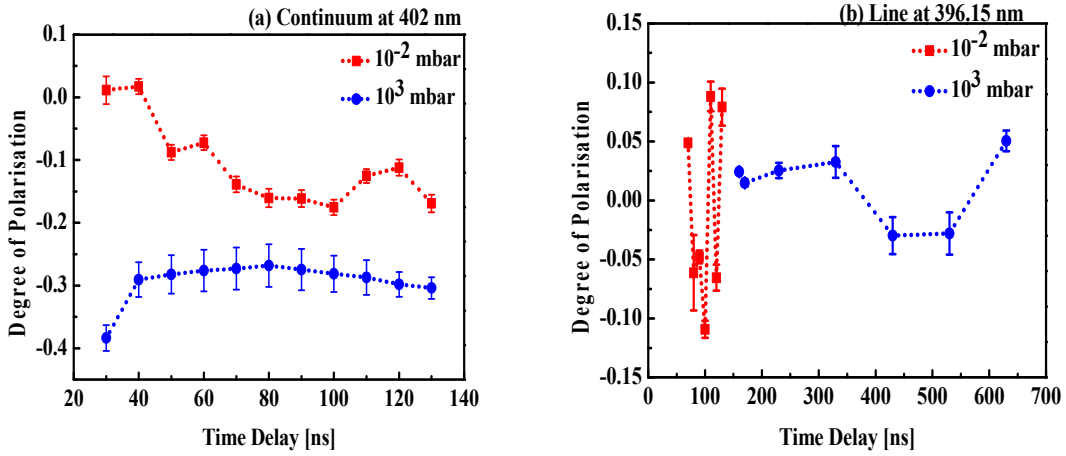

Figure 4.10: Degree of polarisation vs time delay at a background pressure of 1 ×10^{-2} and 1×10^{3} mbar at a laser fluence of 550 J/cm^2 for (a) continuum emission at 402 nm (inset) and (b) line emission at 396.15 nm.

The alignment parameter can be extracted from the degree of polarisation (P) emission as mentioned in section **2.6.3** using equation (**2.72**) which is repeated below for convenience:

$$A_L = \left(\frac{I_H + I_V}{I_H + 2I_V} \right) = \frac{2P}{3 - P} \tag{4.2}$$

Figure 4.11 shows the alignment parameter as function of the time delay for the Al^0 line at 396.15 nm. As the alignment parameter is directly related to the function *P*, the modulation trend at 10^{-2} and 10^3 mbar follow a similar trend.

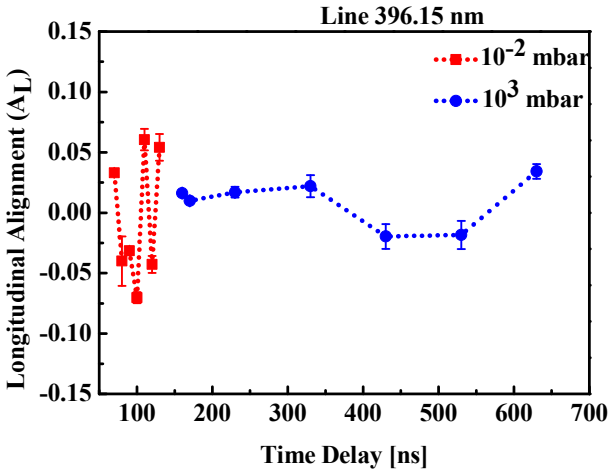

Figure 4.11: Longitudinal alignment parameter as a function of time delay for the Al^0 396.15 nm line.

4.4.3 Singly Ionised Al

Figure 4.12 and **Figure 4.13** show polarisation resolved emission spectra at a central wavelength of the spectrometer of 463 nm as a function of time delay at pressures of $1x10^{-5}$ and 1×10^3 mbar respectively. It can be seen from both figures that the spectrum emitted by the plasma in vacuo is quite different to that emitted by the plasma in air at atmospheric pressure. For both pressures, continuum emission dominates the spectra for the first 60 ns or so. At 1×10^{-5} mbar (in vacuo) the 466.3 nm line of Al^+ arising from 4p ($^1P^o_1$) $\rightarrow$3p^2 ($^1D_2$) transition as shown in the (Appendix **Figure A.2 (c)**) is already well developed with a strong signal to background ratio (SBR). On the other hand, it only becomes well distinguished in air at time delays of some hundreds of nanoseconds. In addition, the 466.3 nm line was observed in atmospheric pressure air for delays of up to 5 μs.

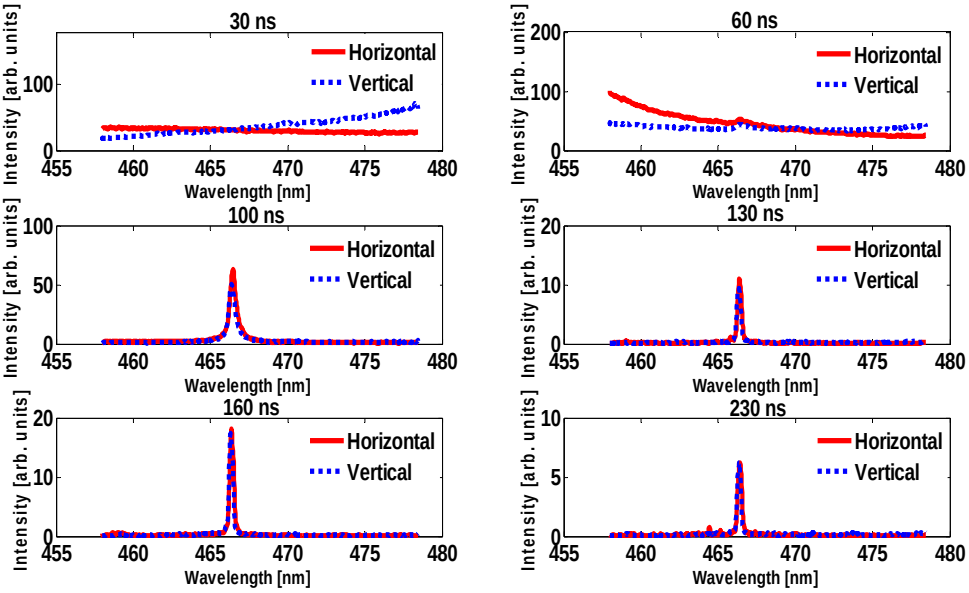

Figure 4.12: Sensitivity calibrated time- and polarisation resolved spectra showing Al^+ (at 466.3 nm) emission at a laser fluence of 550 J/cm^2 for a background pressure 1×10^{-5} mbar at various time delays following plasma formation.

Figure 4.13 shows at broadband featured at 463.1 nm which is due to the 3p ($^3P_2$) →3s ($^3P^o_2$) transition of N^+ in the delay time range of 100-330 ns in air at atmospheric pressure. The crossover between horizontal and vertical polarisation observed in both figures for line and/or continuum emission variously depends on the background pressure and time delay.

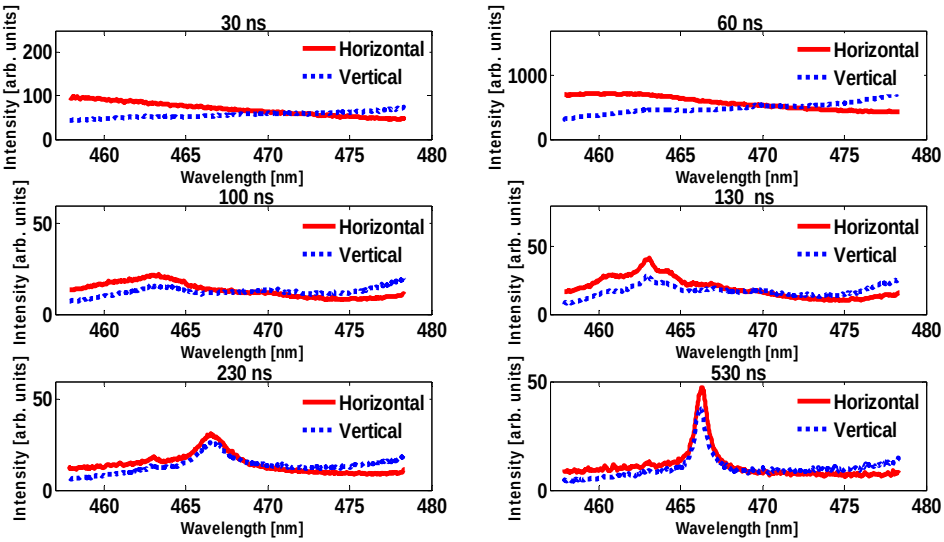

Figure 4.13: Sensitivity calibrated spectra of time- and polarisation resolved showing Al^+ (at 466.3 nm) emission at a laser fluence of 550 J/cm^2 for a background pressure 1×10^3 mbar at various time delays following the plasma formation.

P is plotted as a function of time delay on **Figure 4.14(a)** for a background pressure of 1×10^{-5} mbar and on **Figure 4.14(b)** for a pressure of 1×10^3 mbar for Al^+ line emission at 466.3 nm and continuum emission at a wavelength of 459 nm in each case. In contrast to **Figure 4.10** the degree of polarisation (P) is positive at all time delays. Once again P varies with time delay and the modulation depth is greatest at the lower pressure. There is also a significant difference in P for line and continuum radiation. For the former, the degree of polarisation varies from ≈ 0.03 to 0.1 and from ≈ 0.05 to 0.1 at atmospheric pressure. For continuum emission at the 459 nm wavelength point it varies from ≈ 0.30 to 0.35 in air at atmospheric pressure. The greatest variation in P is seen for continuum emission at 459 nm in ambient air at atmospheric pressure. Close to plasma formation P ≈ 0.2 growing to 0.3 at 50 ns and dropping rapidly to ≈ 0.07 at delays in excess of 125 ns. It is interesting to note that P switches sign from approximately -0.3 at 402 nm to +0.3 at 459 nm at time delays around the centre value of 70 ns or so.

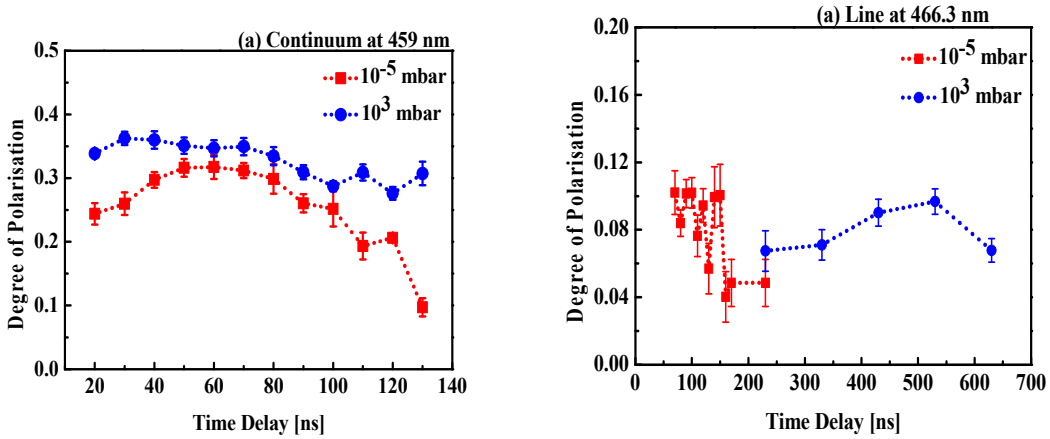

Figure 4.14: Degree of polarisation vs time delay at a background pressure of 1 ×10^{-5} and 1×10^{3} mbar at a laser fluence of 550 J/cm^2 for (a) continuum emission at 459 nm (inset) and (b) line emission at 466.3 nm.

Figure 4.15 shows the alignment parameter as a function of the time delay of the Al^+ line at 466.3 nm. It can be seen that the degree of alignment for this line the trend is similar at both pressures of 1×10^{-5} and 1×10^{3} mbar and as expected since P is small, A_L is also small using equation (**4.2**).

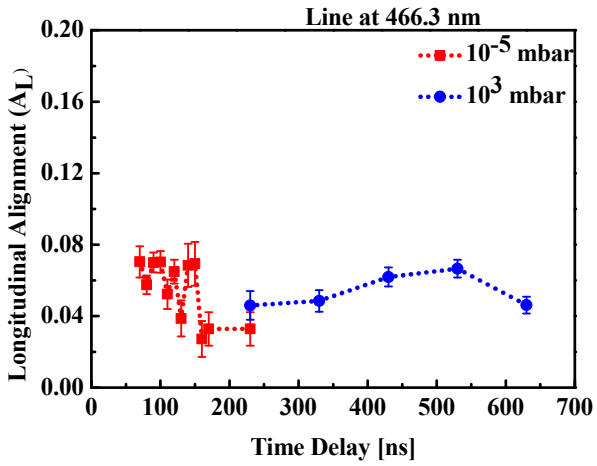

Figure 4.15: Alignment parameter as a function of time delay for the Al^+ line at 466.3 nm.

4.5 Electron Density and Temperature

4.5.1 Electron Density

Stark broadening is a well-established technique to estimate the electron density using an isolated line in a spectrum [11], [12]. The profile of a Stark broadened line is well described by a Lorentzian function [13]. From our time-resolved measurements, the Al^+ line at 466.3 nm is well isolated compared to the Al^0 doublet (at 394.4 and 396.15 nm) and Al^{2+} doublet (at 569.6 and 572.3 nm). During the early lifetime of the plasma (0-100 ns), continuum emission from the core dominates the emission spectrum of laser produced plasmas and tends to overwhelm line emission [14]. Spectra in which lines of ions were clearly observed occurred only for time delays in the range 100 to 230 ns in vacuo (i.e, at a pressure of 1×10^{-5} mbar). Stark broadening, given by equation **(3.8)**, is described in section (**3.8.3**). For dense laser produced plasmas it is possible to approximate Stark broadening by the electron impact term only [13]. In this case, perturbations caused by ions are negligible and the ion correction factor can be neglected from the equation of the Stark broadening [11]. In this case where line broadening is dominated by electron collisions the approximate value of the line profile of such isolated line is given by:

$$\Delta\lambda_{1/2} \approx \frac{2wN_e}{10^{16}} \tag{4.3}$$

where $\Delta\lambda_{1/2}$ is the Stark width, w=0.0615 nm at half width [15] is the electron impact parameter for the Al^+ at 466.3 nm line (which varies with temperature) and N_e is the electron density respectively. The standard method to obtain the Stark broadening contribution to a spectral line is by fitting the line with a Voigt profile since the measured line profile is the result of the convolution of a Gaussian profile (mainly because of instrumental broadening) and a Lorentzian profile as mentioned in section (**3.8**) [12], [13].

Figure 4.16 shows the horizontal (parallel to the laser axis of incidence) and vertical (perpendicular to the laser axis of incidence) polarisation spectra for an Al plasma showing

the Al^+ line at 466.3 nm at a background pressure of 1×10^{-5} mbar for time delays of 100 and 120 ns respectively. A Voigt spectral profile which is a convolution of the instrumental function of 0.17 nm at FWHM and a Lorentzian function is found from the fit to each measured line. The electron densities are then calculated using equation (**4.2**). The densities of the different polarisation states are extracted from the different Lorentzian fits. As an example, for horizontal and vertical polarisation at a time delay of 100 ns, the densities were $6.5\pm0.2\times10^{16}$ cm^{-3} and $6.8\pm0.2\times10^{16}$ cm^{-3} respectively at a pressure of 1×10^{-5} mbar. Similarly, for these polarisation states at atmospheric pressure (**Figure 4.17**) the densities at a time delay of 530 ns were $1.4\pm0.1\times10^{17}$ cm^{-3} and $1.5\pm0.1\times10^{17}$ cm^{-3} for the orthogonal polarisation states so little difference in densities are observed as one would expect (in contrast to temperature).

The variation in density with time delay obtained from the 466.3 nm line at a background pressure of 1×10^{-5} mbar as shown in **Figure 4.18 (a)**. It is observed that the density drops as time progresses for both polarisation states which is an indication that P decreases with time delay in the range 100 to150 ns. The single data point at 230 ns may indicate that the degree of polarisation may be flat between 160 and 230 ns. **Figure 4.18 (b)** displays the density drop with time delay in the range of 230 to 630 ns at a background pressure of 10^3 mbar.

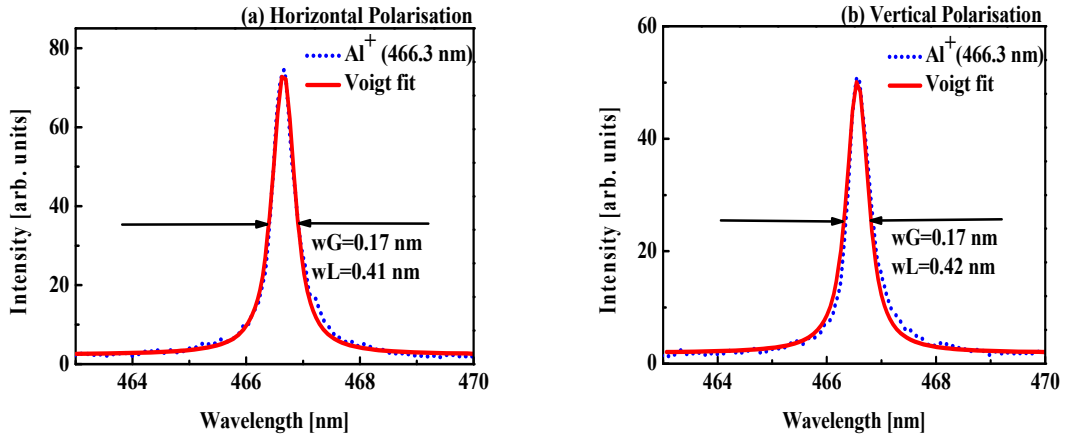

Figure 4.16: Voigt profile fits for horizontal and vertical polarisation spectra showing Al^+ (at 466.3 nm) at time delays of 100 ns at a background pressure of 1×10^{-5} mbar.

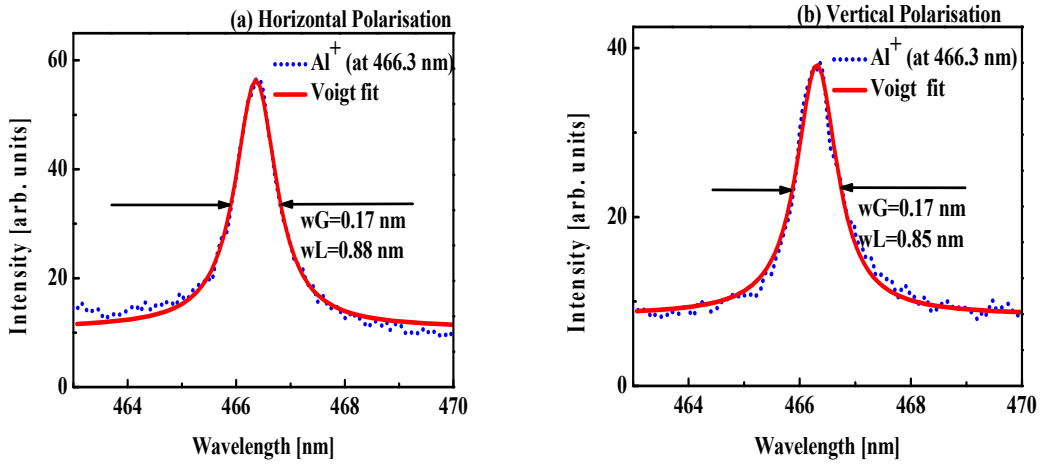

Figure 4.17: Voigt profile fits for horizontal and vertical polarisation spectra showing Al^+ (at 466.3 nm) at a time delay of 530 ns at a background pressure of 1×10^3 mbar.

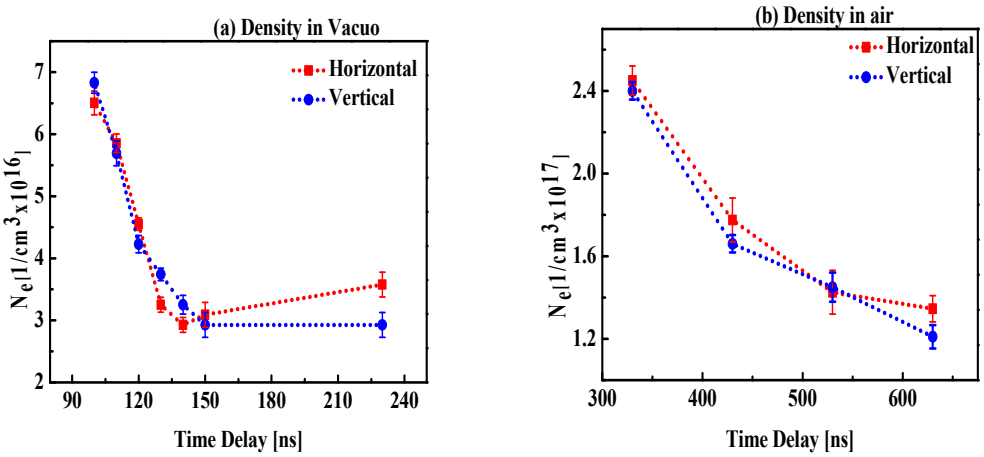

Figure 4.18: Electron density vs time delay for both horizontal and vertical polarisation spectra showing Al^+ (at 466.3 nm) at a background pressure of (a) 1×10^{-5} and (b) 1×10^3 mbar respectively at a laser fluence of 550 J/cm^2.

4.5.2 Electron Temperature

As only a small number of lines were present in our spectra it was not possible to use the Boltzmann plot method to determine plasma temperatures. Instead, the line ratio method was used. The method was applied to successive ion stages using the Al^+ (at 466.3 nm) and Al^{2+}

(at 569.6 nm) lines in the time delay range 100 to 130 ns where orthogonally polarised lines were clearly visible at a background gas pressure of 1×10^{-5} mbar. However, the emission spectra in air were more broadened especially at short time delays. The dominant emission features in air came from Al^0 and Al^+. For Al^0, the 394.4 and 396.15 nm close lying lines interfere with each other which makes temperature estimation using these lines difficult. Therefore, we did not include the evaluation of the electron temperature in air. We also excluded temperature estimation during the early lifetime of the plasma emission even in vacuo as the continuum emission interferes with the line emission. As discussed in section (**3.8**) a simplified form of equation (**3.10**) was used here to determine electron temperature from the line intensity ratio:

$$\ln\left(\frac{I_1}{I_2}\right)=\ln\left(\frac{A_1 g_1 \lambda_2}{A_2 g_2 \lambda_1}\right)-\left(\frac{E_1-E_2}{k_B T_e}\right) \tag{4.4}$$

The simplified form of the equation (**4.4**) is given by

$$k_B T_e=\frac{E_2-E_1}{\ln\left(\frac{A_2 g_2 \lambda_1 I_1}{A_1 g_1 \lambda_2 I_2}\right)} \tag{4.5}$$

where I_1 is the line intensity from the higher ionisation stage, I_2 the line intensity from the lower ionisation stage, A_1 and A_2 are the Einstein coefficients, g_1 and g_2 are statistical weight of the levels of interest E_1 and E_2 are the excitation energies in eV of the transitions. $k_B=1.4\times10^{23}m^2kg/s^2k$ (or 8.6×10^{-5} eV/k) is the Boltzmann constant. **Table 4.2** contains the values of these parameters obtained from the NIST database [16]. In addition, **Table 4.3** shows the measured integral intensities from the Voigt fits for orthogonally polarisation spectra for Al^{2+} (at 569.6 nm) and Al^+ (at 466.3 nm) lines respectively.

Table 4.2: Spectroscopic parameters used to determine electron density and the temperature as per the NIST database [16].

Wavelength [nm]	A_{ki} [1/s] $\times10^7$	g_k	Upper state energy [eV]
466.3 (Al^+)	5.81	3	13.26
569.6 (Al^{2+})	8.77	4	17.82

Table 4.3: Integrated intensities from the Voigt fit for the horizontal (H) and vertical (V) polarisation emission spectra for the Al^{2+} (at 569.6 nm) and Al^{+} (at 466.3 nm) lines, used to extract electron temperature.

Time delay [ns]	H for 569.6 nm	V for 569.6 nm	H for 466.3 nm	V for 466.3 nm
100	198	65	2298	1583
110	181	56	2174	1580
120	86	22	1678	1189
130	20	3.4	244	181

Figure 4.19 illustrates the orthogonally polarised spectra of an Al plasma showing the Al^{2+} doublet at a time delay of 100 ns. The estimated electron temperatures from equation (4.2) as a function of time delay is shown in **Figure 4.20** with finite temperature differences for horizontal and vertically polarised emission for the time delay in the range of 100-130 ns.

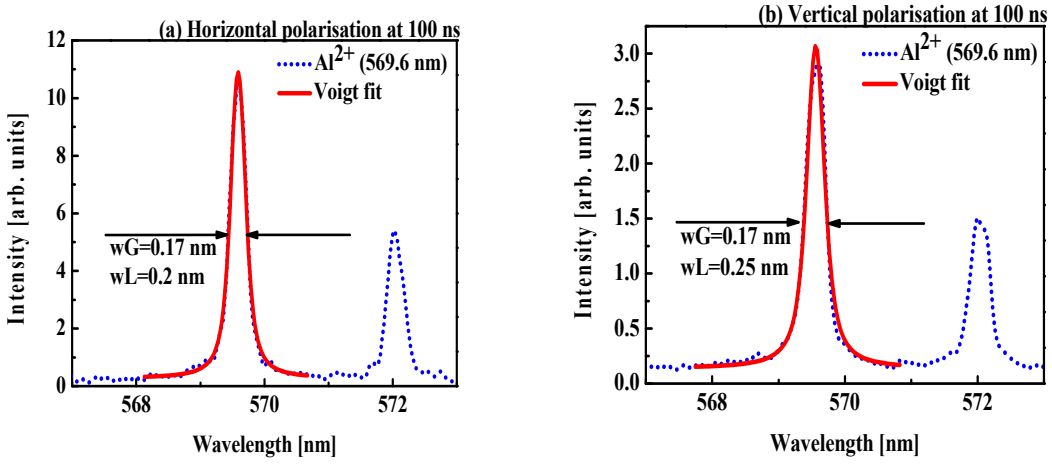

Figure 4.19: Voigt profile fits for horizontal and vertical polarisation spectra showing Al^{2+} (at 569.6nm) at a time delay of 100 ns, a background pressure of 1×10^{-5} mbar and a laser fluence of 550 J/cm^2.

To verify that the plasma is in LTE, we applied the McWhirter criterion given by equation (**4.6**) below. The threshold density for the transition of interest (taking the 466.3 nm line as it's the shortest wavelength) at a photon energy of 2.7 eV, and a temperature value not exceeding 2 eV, is $\approx10^{15}$ cm^{-3} [13], [17].

$$n_e \geq 1.6\times10^{12} T_e^{1/2} \left(E_1 - E_2\right)^3 \tag{4.6}$$

Where here T_e is electron temperature in eV, E_1 and E_2 are the successive ion stage of the same element in eV. The lowest measured density was 2.9×10^{16} cm^{-3} which is greater than the threshold 10^{15} cm^{-3} and so our assumption of LTE holds. However, if we consider the whole plasma emission, it is believed that it is well described by bi-Maxwellian expression (**2.45**) with different temperatures in the parallel T_H and perpendicular T_V directions [1], [2].

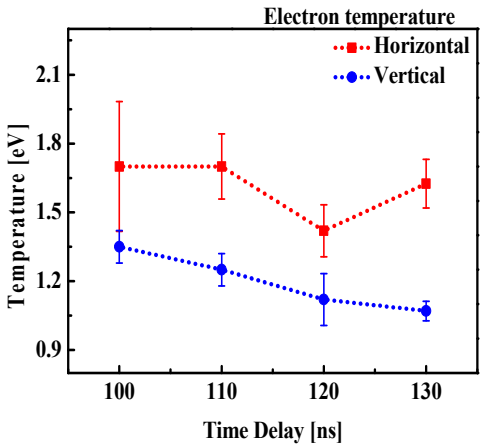

Figure 4.20: Electron temperature vs time delay for both horizontal and vertical polarisation spectra determined from Al^+ (at 466.3 nm) and Al^{2+} (at 569.6 nm) lines at a background pressure of 1×10^{-5} mbar and laser fluence of 550 J/cm^2.

T_H and T_V are used here in the sense that we define the plasma temperature normally as being irrespective of the orientation of the polarisation direction of the radiation. However, in our case we obtain different values which of course affect other plasma processes such as recombination rates and processes which depend on those primary processes such as the distribution of population amongst the magnetic sublevels. **Figure 4.20** shows how the parallel T_H and perpendicular T_V temperatures evolve with time in the 100 to 130 ns range.

4.6 Collisional Radiative Model (CRM) for Polarisation

To determine the dominant radiative processes in our plasmas, we employ the collisional radiative model of Colombant and Tonon [18] which has been applied frequently for Nd:YAG plasmas at the laser power densities encountered in our experiments. The collisional ionisation, radiative recombination and the three body recombination rates are calculated from the experimentally determined plasma parameters (density and temperature) for the in-vacuo case. The temperatures obtained for orthogonal polarisations are used to determine rates specific to each polarisation direction. **Figure 4.21**, **Figure 4.22** , and **Figure 4.23** illustrate the rate of collisional ionisation, rate of radiative and three-body recombination, for the horizontal and vertical polarisation emission directions, on a logarithmic scale as a function of time delay. The rate coefficients for Al^{+}, Al^{2+} and Al^{3+} using equations (**2.37**) to (**2.40**) [18]–[20] are shown in these figures. It can be seen that radiative recombination rate is greater than three-body (3B) recombination for Al^{2+} and that Al^{2+} consistently has the highest rate of radiative recombination (RR) with Al^{3+} close by. The greatest difference in polarisation resolved RR rates occurs for Al^{3+} while the Al^{+} RR rate is virtually negligible compared to doubly and triply charged ions. From the above we can conclude that we can ignore 3B recombination, that RR dominates for doubly and triply charged ions. On the other hand, 3B recombination is somewhat higher for the singly charged ion than RR. We may also propose that neutral line emission must be due to electron excitation of Al atoms rather than recombination from Al^{+} leaving Al in excited states. With the greatest difference in RR rates occurring for Al^{3+} one could conclude that this process has an important contribution to make to polarisation anisotropy for continuum emission and to line emission from excited Al^{+} and Al^{2+} formed in the RR process.

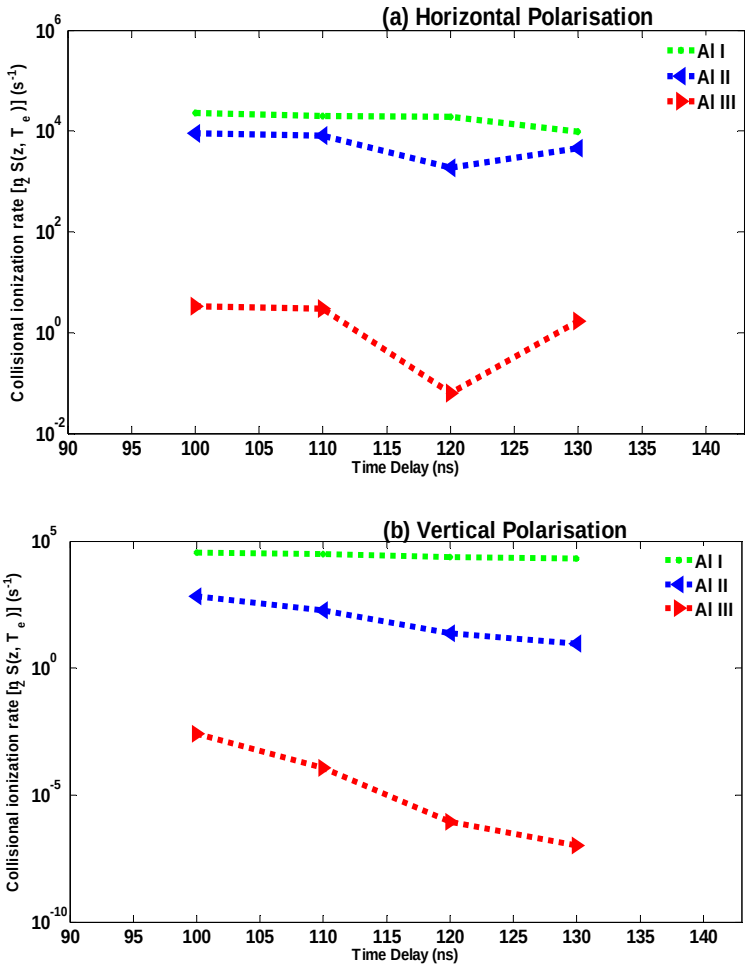

Figure 4.21: **Collisional ionization rate for the horizontal and vertical polarisation directions.**

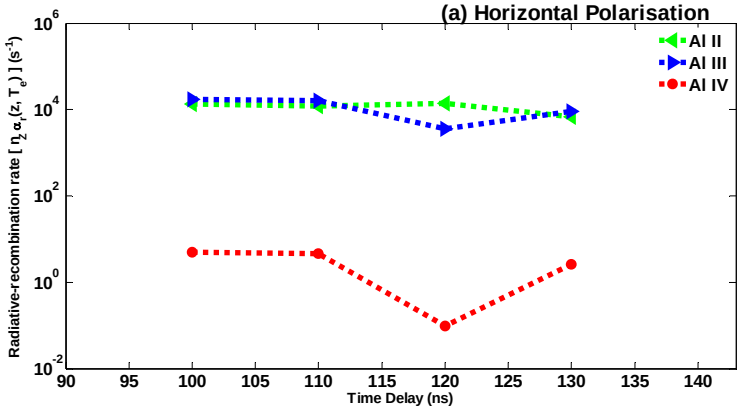

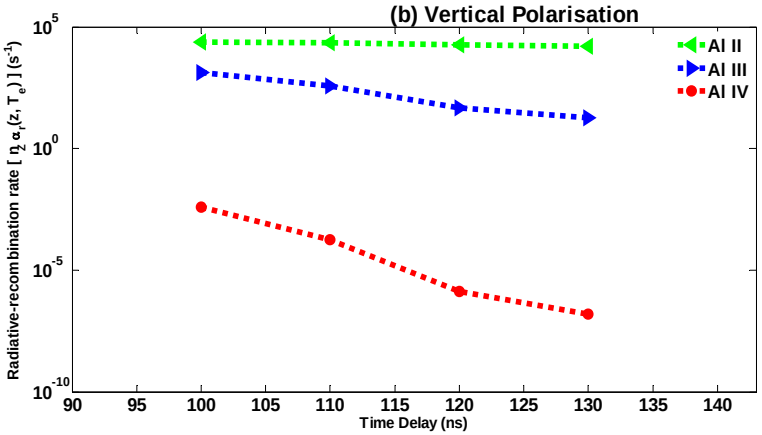

Figure 4.22: Rate of radiative recombination for the horizontal and vertical polarisation directions.

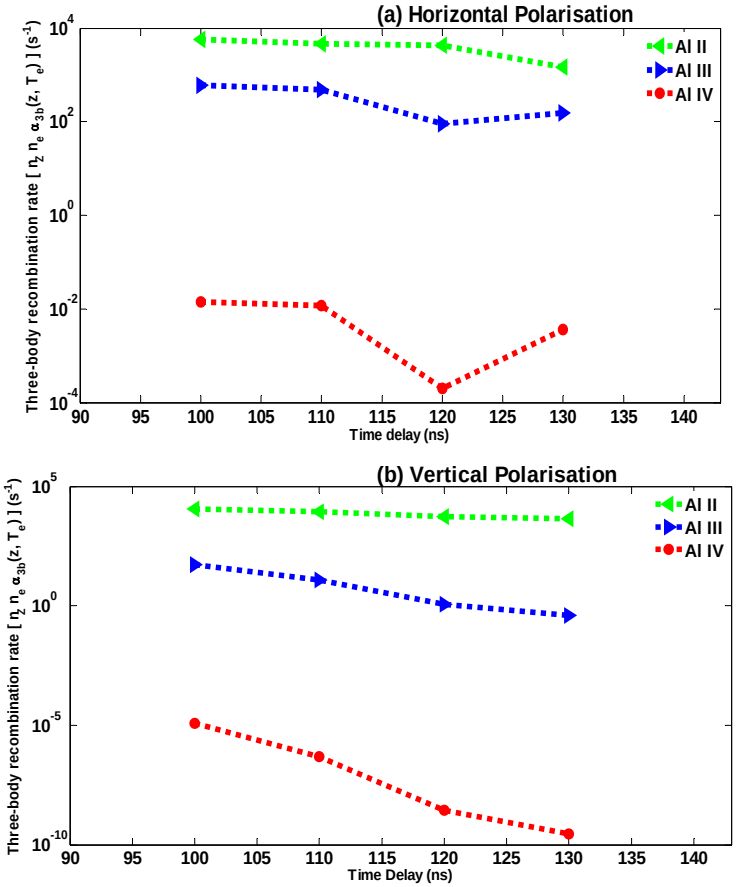

Figure 4.23: Rate of three body recombination for the horizontal and vertical polarisation directions.

4.7 Discussion

In the present study, polarisation resolved imaging and spectroscopy of Al plasma emission are studied in air and in vacuo. The imaging results show stronger anisotropy in air than in vacuo. P is stronger for continuum than line emission for the atoms and ions studied as shown in **Figure 4.10** and **Figure 4.14** respectively.

In relation to continuum emission it is clear that an anisotropic EVDF with a partially preferred direction for the electron motion in the plasma translates into an anisotropic polarisation distribution. This is observed to be quite strong in our case with quite large P values, especially in air. We see from **Figure 4.22** that the RR rate computed for lowly charged Al ions for horizontal and vertical equivalent temperatures are quite different and hence one would expect the resulting anisotropy in the polarisation of the resulting continua to be significant as observed. As the RR rate scales, linearly with degree of ionisation in equation (**2.40**), one would expect the anisotropy to increase or continua generated be recombination into more highly charged ions.

In relation to line emission it is clear that non-zero atomic alignment (non-statistical distribution of the atomic/ionic population amongst the available magnetic sublevels) is present in our plasmas. Computation of the degree of polarisation for the Al^0 doublet comprising 3p – 4s transitions would be possible using the simplified equations (**2.68**) and (**2.69**) for the horizontal and vertically polarised component intensities. However, they require a code to compute the corresponding Clebsch-Gordon coefficients as well as knowledge of the alignment parameters and states population. On the face of it computation of the degree of polarisation for the 466.3 nm line would be even more challenging and a task for a fully theoretical study since this is a $3p^2$ to 3p4s transition. That said it is also clear that radiative recombination is an important process in the formation of ions in excited states such as Al^{2+} and especially Al^+ [21] in the context of the current chapter. For Al^+, with the electron captured into the nl = 4p state from which the 466-nm line originates, although β values

(asymmetry parameters) have not been experimentally determined for this Al^+ transition, taking a typical value of 1.5 and using equation (**2.57**) we find that ξ which has a value of approximately 0.1. Substituting these numbers into equation (**2.62**) the degree of polarisation for the resulting line emission comes out at 0.01 in the right order of magnitude as **Figure 4.14 (b)**.

In relation to other mechanisms suggested in the literature, polarisation induced by the laser field is not a valid argument because our target was normal to the incident laser and Kieffer et al. [2] have observed that the polarisation at normal incidence is independent of the laser field. This also observed here for optical spectroscopy (**Chapter 6**).

At 10^{-2} mbar, P exhibits oscillations with time delay for continuum radiation as shown in **Figure 4.10**. At a pressure of 10^{-5} mbar P also oscillated with time delay for both Al^+ orthogonally polarised spectra as shown in **Figure 4.14**. Such an oscillation is an indication of the growth of the Rayleigh-Taylor (RT) instability produced by the difference in the density of the plasma and background gas [7]. The RT instability gives rise to oscillations in the EVDF and hence in the degree of polarisation P.

One potential application of this is using plasma polarisation spectroscopy as an alternative to gated spectroscopy in LIBS. This has been alluded to in the past and is noted here again. It seems that the continuum can be suppressed with the use of a polariser in front of the spectrometer with little loss in the intensity of the line emission.

4.8 Conclusion

The degree of polarisation for different charge states of an Al plasma emission was studied using time and polarisation resolved imaging and spectroscopy in the visible spectral range. The imaging results show stronger anisotropy in air than in vacuo. The spectroscopy results indicate that the plasma has a high degree of polarisation at early times during its evolution and that this scales with background pressure. From the rate equations for various radiation

losses in the plume, it is inferred that continuum radiation should dominate at high background pressures. In vacuo, for all charge states, the degree of polarisation oscillated with time delay as the result of a dynamical non-statistical distribution of the magnetic sub-levels as the plasma evolved due to the growth of a RT instability. We interpret the results in the framework of radiative recombination of electrons with an anisotropic velocity distribution.

References

[1] T. Fujimoto and S. A. Kazantsev, "Plasma polarization spectroscopy Review Article," *Plasma Phys. Control. Fusion*, vol. 39, pp. 1267–1294, 1997.

[2] J. C. Kieffer, J. P. Matte, M. Chaker, Y. Beaudoin, C. Y. Chien, S. Coe, G. Mourou, J. Dubau, and M. K. Inal, "X-ray-line polarization spectroscopy in laser-produced plasmas," *Phys. Rev. E*, vol. 48, no. 6, pp. 4648–4658, 1993.

[3] J. Kim and D. E. Kim, "Measurement of the degree of polarization of the spectra from laser produced recombining Al plasmas," *Phys. Rev. E - Stat. Nonlinear, Soft Matter Phys.*, vol. 66, no. 1, pp. 1–4, 2002.

[4] J. S. Penczak, Y. Liu, and R. J. Gordon, "Polarization-resolved laser-induced breakdown spectroscopy of Al," *Opt. Lett.*, vol. 34, no. 4, p. 494, 2009.

[5] Y. Zhao, S. Singha, Y. Liu, and R. J. Gordon, "Polarization resolved laser-induced breakdown spectroscopy," *Opt. Lett.*, vol. 34, no. 4, pp. 494–496, 2009.

[6] A. Eslami Majd, A. S. Arabanian, and R. Massudi, "Polarization resolved laser induced breakdown spectroscopy by single shot nanosecond pulsed Nd:YAG laser," *Opt. Lasers Eng.*, vol. 48, no. 7–8, pp. 750–753, 2010.

[7] A. K. Sharma and R. K. Thareja, "Anisotropic emission in laser-produced aluminum plasma in ambient nitrogen," *Appl. Surf. Sci.*, vol. 253, no. 6, pp. 3113–3121, 2007.

[8] S. S. Harilal, C. V Bindhu, M. S. Tillack, F. Najmabadi, and a C. Gaeris, "Plume splitting and sharpening in laser-produced aluminium plasma," *J. Phys. D. Appl. Phys.*, vol. 35, no. 22, pp. 2935–2938, 2002.

[9] A. K. Sharma and R. K. Thareja, "Polarization-resolved measurements of picosecond laser-ablated plumes," *J. Appl. Phys.*, vol. 98, no. 3, p. 33304, 2005.

[10] Y. Liu, J. S. Penczak, and R. J. Gordon, "Nanosecond polarization-resolved laser-induced breakdown spectroscopy.," *Opt. Lett.*, vol. 35, no. 2, pp. 112–114, 2010.

[11] N. Hans, D. W. and Omenetto, "Laser-Induced Breakdown Spectroscopy (LIBS), Part

I: Review of Basic Diagnostics and Plasma-Particle Interactions: Still-Challenging Issues Within the Analytical Plasma Community," *Appl. Spectrosc.*, vol. 64, p. 335A–366A, 2010.

[12] F. Anabitarte, A. Cobo, and J. M. Lopez-Higuera, "Laser-Induced Breakdown Spectroscopy: Fundamentals, Applications, and Challenges," *ISRN Spectrosc.*, vol. 2012, pp. 1–12, 2012.

[13] C. Fallon, "Optical Diagnostics of Colliding Laser Produced Plasmas : Towards Next Generation Plasma Light Sources," Dublin City University, 2013.

[14] R. F. and S. P. F. Colao, V.Lazic, "A comparison of single and double pulse laser-induced breakdown spectroscopy of aluminium sample," *Spectrochim. Acta Part B*, vol. 57, no. 1167–1179, 2002.

[15] A. W. Allen, M. Blaha, W. W. Jones, A. Sanchez, and H. R. Griem, "Stark-broadening measurement and calculations for a singly ionized aluminum line," *Phys. Rev. A*, vol. 11, no. 2, pp. 477–479, 1975.

[16] NIST, "Atomic lines." NIST, p. none, 2016.

[17] J. Dardis, "Interactions Of Intense Optical and Extreme-Ultraviolet Lasers with Atoms and Solids," Dublin City University, 2009.

[18] D. Colombant and G. F. Tonon, "X-ray emission in laser-produced plasmas," *J. Appl. Phys.*, vol. 44, no. 8, pp. 3524–3537, 1973.

[19] S. S. Harilal, T. Sizyuk, A. Hassanein, D. Campos, P. Hough, and V. Sizyuk, "The effect of excitation wavelength on dynamics of laser-produced tin plasma," *J. Appl. Phys.*, vol. 109, no. 6, 2011.

[20] M. G. Su, B. Wang, Q. Min, S. Q. Cao, D. X. Sun, and C. Z. Dong, "Time evolution analysis of dynamics processes in laser-produced Al plasmas based on a collisional radiative model," *Phys. Plasmas*, vol. 24, no. 1, p. 13302, 2017.

[21] G. A. Wubetu, H. Fiedorowicz, J. T. Costello, and T. J. Kelly, "Time resolved anisotropic emission from an aluminium laser produced plasma," *Phys. Plasmas*, vol. 24, no. 1, p. 13105, 2017.

5 Time Resolved Anisotropic Emission from an Aluminium Laser Produced Plasmas

The polarisation anisotropy of the emission from a laser produced aluminium plasma has been studied using time and polarisation resolved spectroscopy at various background pressures of air. A Wollaston prism was used to resolve the emission from the plasma into polarisation components that are parallel and orthogonal to the plasma expansion axis. Spectroscopy reveals that as the background pressure is increased, strongly polarised continuum emission dominates at early stages of the plasma formation. The results are compared and contrasted to similar experiments and discussed in the framework of a recombining plasma.

5.1 Introduction

The polarisation state of the light emitted from a laser produced plasma has recently become an area of interest in the wider laser plasma community. The observation that the continuum emission from a laser plasma tends to be more polarised than the line emission [1]–[7] which could improve the signal-to-background ratio (SBR), potentially a useful feature for analytical techniques such as laser-induced breakdown spectroscopy (LIBS), is one reason underlying this interest. To date the degree of polarisation (P) of the light emitted from a laser-produced plasma was measured for various focal positions [1], laser energies [2], [7], background pressures [8], incident laser polarisations [6], detection directions [1] and pulse durations [4]. In many cases, the use of a polariser in front of the spectrometer during a LIBS measurement suppressed the continuum and improved the limit of detection (LOD) by increasing the SBR [1], [6]. In one study [9], it was found that no significant polarisation of either the continuum or line emissions could be observed. This apparent null result compared with previous studies was resolved by taking the laser fluence into account [1]–[6].

In this chapter, we present a systematic study of the time- and polarised-resolved emissions from an aluminium laser plasma in different background environments. Emission spectra are measured simultaneously for plasma components parallel and perpendicular to the quantization axis of the experiment (take here as the normal to the target). We measure the polarisation of lines arising from different charge states of the aluminium plasma and correlate the degree of polarisation to the various radiation losses in the plasma. The results are discussed in the framework of class 1 and class 2 polarisation, as discussed in the introductory chapter, and also the potential usefulness of this technique for LIBS.

5.2 Experimental Setup

Figure 5.1 shows the experimental setup used in this work. A Q-Switched Nd: YAG laser was focused onto an aluminium target to create a laser produced plasma. The laser used (Spectron SL800) had a 14 ns pulse duration and was operated at its fundamental wavelength of 1064nm. The fluence of the laser was varied using a combination of a half-wave plate and

a polariser. For this experiment, the laser was focused normal to the target using a planoconvex lens (f = 250 mm) onto an Al slab (purity 99.99 %) target to give a maximum fluence of 550 J/cm^2 (corresponding to an irradiance of 4×10^{10} W/cm^2). The target was housed in a square vacuum sealed chamber which was evacuated to a pressure of 1×10^{-5} mbar and mounted onto a micrometer controlled x-y-z translation stage which could be manipulated from outside the vacuum chamber. This ensured that a fresh target spot could be revealed after each laser shot. The plasma light emission was imaged normal to the laser propagation axis with a magnification of 0.5 using a two-lens imaging system. A Wollaston prism was placed in the path of the imaging system to resolve the plasma image into two orthogonally polarised states. Thus, two images were formed in the image plane of the lens system. The optic axis of the Wollaston prism was aligned such that the plasma light was resolved into polarisation components parallel and perpendicular to the laser propagation direction. The plasma light was imaged onto the entrance slit of a Czerny-Turner spectrometer with a 1200 g/mm grating and a focal length of 0.5m giving an ultimate mean resolution of 0.17 nm. At the exit of the spectrometer, the light was detected by a gated, intensified CCD camera (Andor i-Star) whose ultimate time resolution was $\simeq$ 10 ns.

5.3 Methodology

Despite its usefulness, polarisation spectroscopy is somewhat obfuscated by many variable parameters. Thus, a clear methodology is required to interpret results correctly. Firstly, accurate and precise values for the degree of polarisation can only be obtained if there exist no random intensity fluctuations between the polarisation components. We have observed here that line and continuum emission from a laser produced plasma will fluctuate naturally in intensity by typically ±10%. Thus, making separate measurements of the different polarisation states limits the precision of the measurement. To account for this, the Wollaston prism method is used such that both polarisation states are measured in a single shot, eliminating the possibility for shot-to-shot fluctuations.

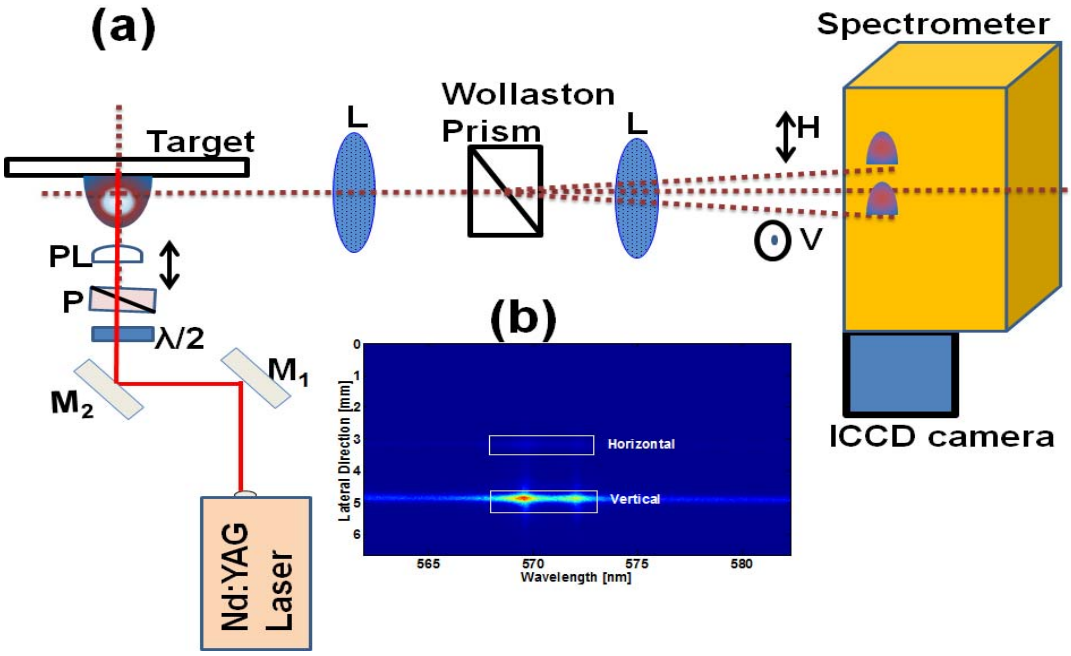

Figure 5.1: Experimental setup (not to scale) showing the geometry of the experiment. A laser plasma is formed on a flat target. The plasma is imaged through a Wollaston Prism. Two plasma images are created on the entrance slit of an ICCD Camera. Inset is a typical image obtained by the experiment.

To measure the precision and accuracy of our system, repeated measurements were made with an unpolarised light source. The standard deviation of the degree of polarisation was determined to be 0.01 %. Secondly, any measurement of polarisation must be done with respect to some reference axis, often called the axis of quantization. In our experiment, we use the following terminology: The plasma light was resolved into ‘‘Horizontal’’ and ‘‘Vertical’’ components. ‘Horizontal’ refers to the direction normal to the target. ‘‘Vertical’’ refers to the direction parallel to the entrance slit of the spectrometer. It was determined that the efficiency of the ICCD camera and imaging system had no polarisation dependence in the wavelength ranges of interest to this study. However, the spectrometer was far more efficient for light polarised in the ‘‘Vertical’’ direction because this is also along the direction of the grating rulings. Normally, this is accounted for by normalising to some unpolarised emission line (for example, the $3s^2 4s\ (^2S_{1/2}) \rightarrow 3s^2 3p\ (^2P^0_{1/2})$ transition [10]. However, line emission from a laser plasma tends to sit on top of continuum emission at the same wavelength. While

the line emission from this transition is unpolarised the continuum may, in fact, contain a partial polarisation. Thus, it is not always clear if the measurement can be normalised at this point. To account for the difference in efficiency for the different polarisations, emission from a xenon spectral lamp was polarised to 45^0. This ensured that the intensity of the polarisation components at the entrance slit was equal. The measured difference through the spectrometer optical system was then used to calibrate further measurements. The degree of polarisation at a particular wavelength (P_λ) is the key parameter to measure the anisotropy emission from laser produced plasma. It is determined by the variance on the polarisation states. Mathematically, it is given by:

$$P_\lambda = \left(\frac{I_H - I_V}{I_H + I_V} \right) \tag{5.1}$$

Where $I_{H,V}$ are the intensities of the 'Horizontal' and 'Vertical' components respectively at a wavelength of λ.

The experiment was performed as follows. To benchmark the system, the time-resolved value of P was measured with the PPS technique for the Al^{2+} spectrum centred at 569 nm. This was performed with a laser fluence of 550 J/cm^2 and a background pressure of 1×10^{-5} mbar to compare with similar experimental results [10]. Air was then leaked into the chamber such that the base pressure rose to 1×10^{-2} mbar and the measurements were repeated. The experiment was then performed for the optical spectrum of Al^0 (centred at 395nm) at base pressures of 1×10^{-2} mbar and 1×10^{3} mbar at the same laser fluence. This gave a wide parameter space under which to compare and contrast the anisotropy of the laser plasma.

5.4 Results and Discussion

5.4.1 Spectroscopy Results

Figure 5.2 and **Figure 5.3** show polarisation resolved spectra at different stages of the plasma evolution for two different background pressures (1×10^{-2} mbar and 1×10^{-5} mbar respectively). In **Figure 5.2**, the spectrum is dominated by continuum emission. The spectra taken at later times are dominated by line emission. **Figure 5.3** shows that as the pressure is lowered, the

continuum emission dies away more quickly and the line structure of the spectrum appears sooner. As time progresses, for both background pressures, the plasma seems partially polarised mainly in the outer wings of the spectrum where the continuum emission is brightest. The degree of polarisation at 569 nm oscillates about zero as time proceeds. This is evidenced in **Figure 5.4** where the degree of polarisation (P) was calculated using Equation (**5.1**) and plotted for both background pressures.

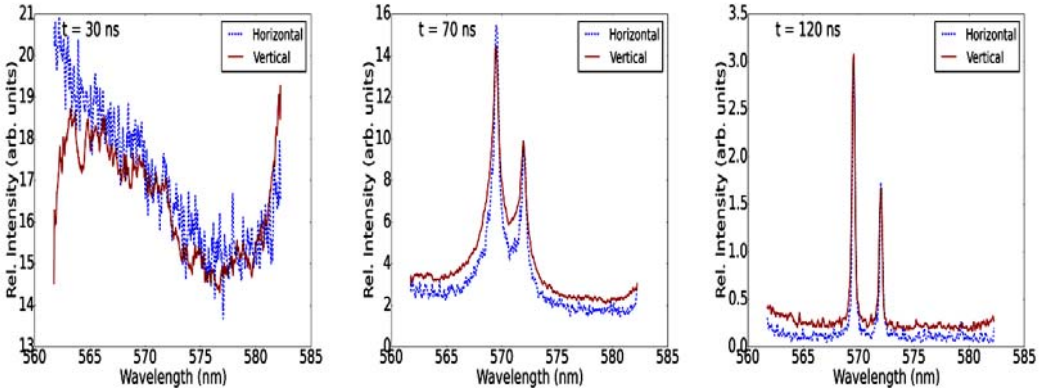

Figure 5.2: Polarisation resolved spectra of an Al plasma, showing a mix of continuum emission and the Al^{2+} doublet, for different stages of plasma evolution at a background pressure of 1×10^{-2} mbar. The laser fluence was 550 J/cm^2 with an ICCD camera gate width of 10 ns.

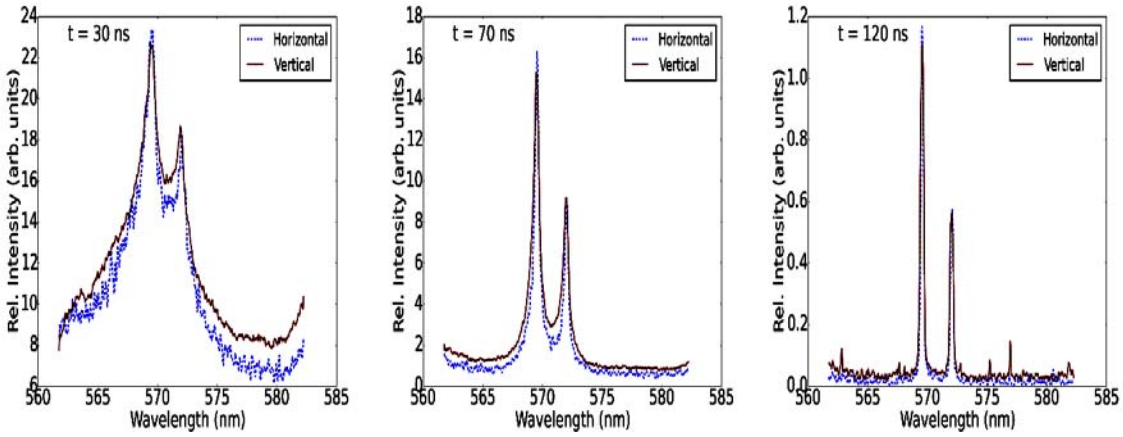

Figure 5.3: Polarisation resolved spectra of an Al plasma, showing a mix of continuum emission and the Al^{2+} doublet, for different stages of plasma evolution at a background pressure of 1×10^{-5} mbar. The laser fluence was 550J/cm^2 with an ICCD camera gate width of 10ns.

The degree of polarisation of the Al^{2+} spectrum has been measured before in different contexts [10], [11]. The results in this study are in good agreement with these other reports. Previous reports [10] have shown that P will be transient in nature and generally very small for the case of a plasma expanding into vacuum, which is in agreement with **Figure 5.3**. In previous reports [10], the degree of polarisation (of the Al^{2+} line at 569nm) increased with background pressure and eventually became vanishingly small as the pressure was increased further. **Figure 5.4** shows that as the background pressure is increased from 1×10^{-5} mbar to 1×10^{-2} mbar, the degree of polarisation is, in general, higher.

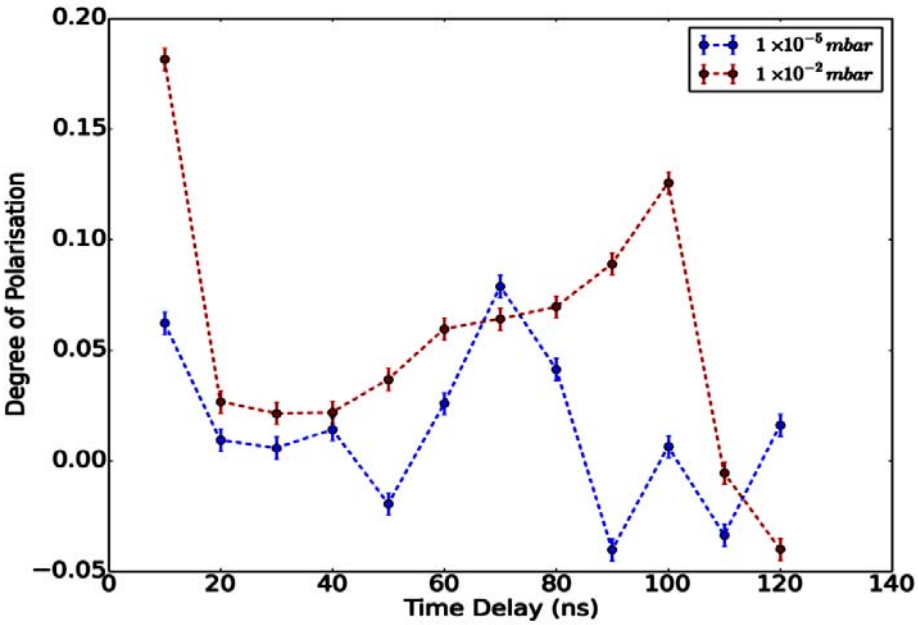

Figure 5.4: Degree of polarisation extracted from the time resolved spectra in Figure 5.2 and Figure 5.3. The centre wavelength of the spectrometer was set at 569 nm.

However, in this study, it was found that if the background pressure was increased to atmospheric pressure, the visible emission was dominated by singly charged ions and neutral emission. The polarisation resolved spectrum of Al^0 at different stages of the plasma evolution at a background pressure of 1×10^{-2} mbar is shown in **Figure 5.5**. The general trend is roughly

in line with the spectrum of Al^{2+}. No neutral emission was observed at 1×10^{-5} mbar. The polarisation resolved spectrum of Al^{0} at atmospheric pressure is shown in **Figure 5.6** to be highly anisotropic and dominated by continuum emission.

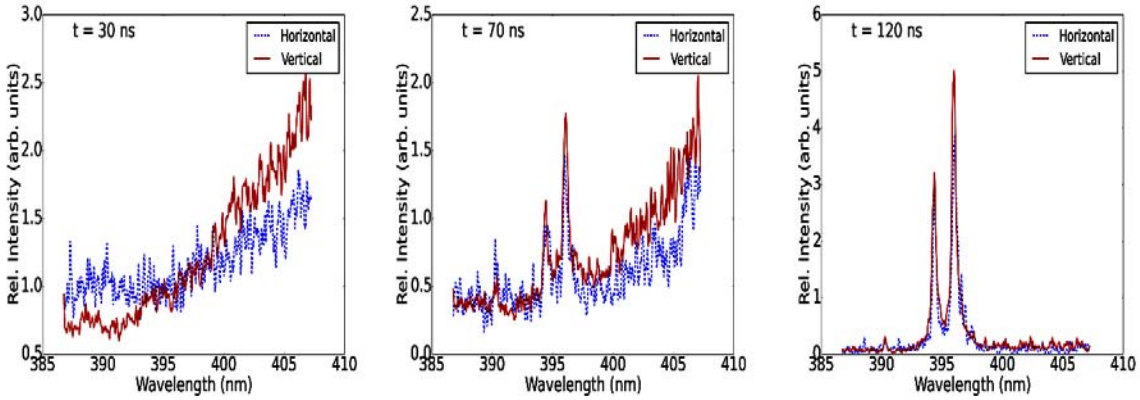

Figure 5.5: Polarisation resolved spectra of an Al plasma, showing a mix of continuum emission and the Al^{0} doublet, for different stages of plasma evolution at a background pressure of 1×10^{-2} mbar. The laser fluence was 550 J/cm^2 with an ICCD camera gate width of 10 ns.

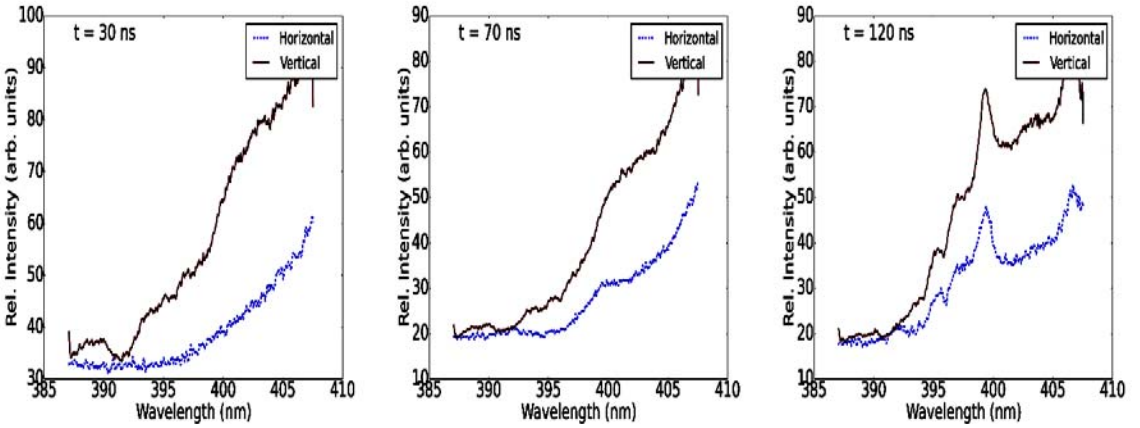

Figure 5.6: Polarisation resolved spectra of an Al plasma, showing a mix of continuum emission and the Al^{0} doublet, for different stages of plasma evolution at a background pressure of 1×10^{3} mbar. The laser fluence was 550 J/cm^2 with an ICCD camera gate width of 10ns.

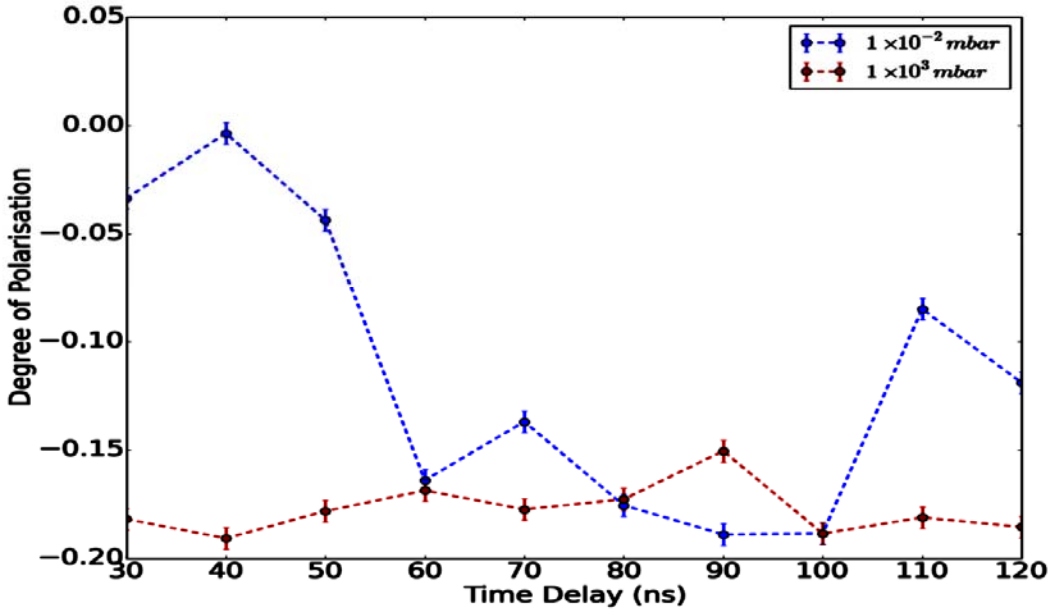

Figure 5.7: Degree of polarisation extracted from the time resolved spectra in Figure 5.5 and Figure 5.6. The wavelength of the spectrometer here was 395 nm.

5.4.2 Discussion

The data presented would seem to indicate the following. Firstly, as the background pressure is decreased, the spectrum becomes dominated by ionic emission over neutral emission, as is expected. Secondly, a higher background pressure is correlated with a longer lasting continuum spectrum. Thirdly, the line emission seems to be weakly polarised whereas the continuum emission seems to be more strongly polarised. This is seen not only in **Figure 5.6** but also in **Figure 5.3** where there is a minimal polarisation in the spectrum and it is mainly in the wings where continuum emission is present. In the past, various mechanisms have been proposed to explain anisotropic emission in laser plasmas including self-generated magnetic fields, radiation trapping and anisotropic electron distribution functions. It seems most appropriate here to describe the anisotropy as arising from radiative recombination in the laser plasma. For the same laser intensity, the initial and average temperatures of a plasma formed in vacuum and at atmospheric pressure should be similar [12]. Thus, for a plasma in LTE, one would expect a similar charge state distribution present within the plumes. However, our

observations indicate that the vacuum spectrum is dominated by doubly charged Al^{2+} ions and the atmospheric spectrum is dominated by Al^{0} emission.

The long-sustained continuum emission in the atmospheric case must then be due to forced recombination in the laser plasma which means the plasma is not in equilibrium because its radiative temperature is not equal to its kinetic temperature. This arises from the confinement of the plume in the background gas which causes free electrons to recombine with ions resulting in a lower average charge state. Another possibility lies in the fact that as the electrons in the atmospheric case try to expand away from the target, the plasma is stopped by the background gas. One would expect a planar expansion under atmospheric conditions and so the direction of deceleration of the electrons will be in the direction of expansion, i.e. along the target normal. In this case, the continuum emission would arise from this deceleration. If the deceleration of the electrons has a preferred direction, as we expect, then the emission should be polarised. This is one plausible explanation for the strong anisotropy in the atmospheric case. In the vacuum case, there is no background gas to confine the plume and so it expands and rapidly cools. The rates of free-free (P_{ff}), free-bound (P_{fb}) and bound-bound (P_{bb}) emission are all temperature dependent in a laser plasma. For the reader's convenience the important equations in section (**2.4**) are summarised as follows [13]:

$$P_{ff} = 1.5\times10^{-26} n_e \left(T_e\right)^{1/2} q^2 n_i \frac{W}{m^3} \tag{5.2}$$

where n_i is the ion density and q is the charge of the ion. Similarly, the recombination radiative power density is given by

$$P_{fb} = 1.5\times10^{-26} n_e \left(T_e\right)^{1/2} q^2 n_i \frac{E_I}{T_e}\frac{W}{m^3} \tag{5.3}$$

Where E_I is the ionisation potential of the species, therefore,

$$P_{fb} = P_{ff}\frac{E_I}{T_e}\frac{W}{m^3} \tag{5.4}$$

$$P_{bb} = P_{ff} \frac{2\times10^{7} e^{-\frac{E_r}{T_e}}}{T_e q^2} \tag{5.5}$$

Where energy and temperature are in eV, n_e is the electron density in m^{-3}, n_i is the ion density in m^{-3}, q is ion charge in C, E_I is the ionisation potential, and E_r is the excitation energy in eV.

This explains the higher levels of continuum radiation in the plasma formed in the atmosphere. In vacuo (taken here to mean 1 $\times10^{-5}$mbar), the plasma expands rapidly which lowers its density n_e thus lowering the value of P_{ff} and P_{fb}. Eventually, the radiative losses lower the electron temperature T_e to a value close to the resonance energy for a transition in an atom or ion in the plasma, increasing the value of P_{bb}. This explains the dominance of ionic line emission under vacuum. For a plasma formed in air, the confinement causes a higher n_e value which increases the rate of P_{ff} and hence P_{fb}. Thus, it can be concluded that, for any given time, the continuum radiation power should scale with background pressure. It is now perhaps useful to consider whether the rate of P_{ff} is higher or lower than the rate of P_{fb}. Equation (**5.4**) shows that if the electron temperature T_e is lower than the ionisation energy of the bound state to which the electron is captured E_I then radiative recombination will be preferred. Under these experimental conditions, temperature analysis is not possible by optical spectroscopy however it can be inferred that just after ablation, radiative recombination is the main energy dissipation channel in the plasma. Detailed frequency and time-resolved measurements of plasmas under similar experimental conditions to this work have shown that the preferential energy dissipation method just after laser heating will be radiative recombination which populates the lowly charged ions and neutral atom [14]. Thus, to explain the results here, the model of anisotropic emission from radiative recombination can be used. Previous theoretical analysis has shown that the degree of polarisation of the recombination emission is inversely proportional to the electron temperature in the plasma

[15], [16]. This explains why the degree of polarisation is generally higher in the atmospheric case. The high density leads to a higher level of continuum radiation from free-free and radiative recombination processes. The adiabatic and radiative losses lower the plasma temperature and increase the value of the anisotropy. Similarly, the plasma confinement due to the background gas sustains the electron density, the continuum radiation and therefore the polarisation.

It is perhaps wise to make some mention as to the sign of the polarisation in both **Figure 5.4** and **Figure 5.7**. In general, the polarisation is generally positive in **Figure 5.4** and negative in **Figure 5.7** at a pressure of 10^{-2} mbar for the continuum. One possible explanation for this is to consider the total polarisation of the emission at a specific wavelength, as being the combination of anisotropy from two sources: (a) the bound-bound emission and (b) the free-free or free-bound emission. The direction of the free-free or free-bound polarisation is along the expansion axis of the plasma, which, in our experimental scheme, is a negative polarisation direction. The second polarisation is from the bound-bound emission. The polarisation of this emission arises from angular momentum conservation in transitions between magnetic sublevels which have a statistical imbalance in their populations. The direction of this polarisation should be perpendicular to the quantisation axis of the experiment, which in our scheme is along the expansion axis. This results in a positive polarisation. Hence the overall direction of polarisation at a wavelength/time/pressure is dependent on whether continuum of line emission dominates.

There is empirical evidence from our data to support this as a valid hypothesis. Perhaps it is most readily shown in **Figure 5.3**, middle panel (t= 60 and 100 ns). Looking a wavelength of 569 nm, it is clear the polarisation is in the positive direction (Horizontal > Vertical). However, looking at a wavelength of 565 nm the polarisation is negative (Vertical > Horizontal). We believe this is since under the conditions that the spectrum was taken, at 569 nm the line emission dominates the emission. In cases where the continuum emission dominates, the polarisation should be negative.

Regarding the efficacy of this technique for LIBS, the data here would seem to indicate that the PRLIBS technique is effective at suppressing the background continuum when radiative recombination is the dominant radiation loss process. This appears to be true for the atmospheric but not for the vacuum case. The power of the recombination process depends on the experimental parameters such as plasma temperature and density and background pressure. Similarly, the continuum radiation appears to be sustained for a longer time in the atmospheric case. This is due to confinement of the plume by the background gas. Again, the duration of this sustained radiation and hence the duration of the times during which there is large anisotropy will be dependent on experimental parameters. PRLIBS is often touted as an advantageous alternative to gated-LIBS due to the fact that the parameters of gated-LIBS are tied to the experimental conditions [17]. It would appear from this study that PRLIBS also depends on the experimental conditions and therefore care must be taken when using this technique effectively. Similarly, our data indicate that the origin of the polarisation can be explained without the need to consider the target experimental geometry. It is most likely the case, then, that the totality of the polarised emission results from a combination of sources such as polarisation of line emission [17], experimental configuration (such as Fresnel reflection resulting from oblique laser incidence on the surface) [18] and recombination emission and is unlikely to be explained by any single mechanism.

5.5 Conclusion

In this study, the time and polarisation resolved spectroscopy of an aluminium laser produced plasma was performed. The results indicate that the plasma has a high degree of polarisation at early times during its evolution and that this scales with background pressure. From rate equations for various radiation losses in the plume, it is inferred that continuum radiation should dominate at high background pressures. Similarly, conclusions from a theoretical model for anisotropy in radiative recombination emission seems to describe the trends found in this data. Thus, we present strong evidence that the anisotropy in the plasma plume is driven

by radiative recombination during the early phase of the plume when the plasma is out of LTE.

References

[1] J. S. Penczak, Y. Liu, and R. J. Gordon, "Polarization resolved laser-induced breakdown spectroscopy of Al," *J. Phys. Chem. A*, vol. 113, no. 47, pp. 13310–13317, 2009.

[2] Y. Liu, J. S. Penczak, and R. J. Gordon, "Nanosecond polarization-resolved laser-induced breakdown spectroscopy.," *Opt. Lett.*, vol. 35, no. 2, pp. 112–4, 2010.

[3] N. Agnes, Z.-Q. Hao, J. Liu, H.-Y. Tao, X. Gao, C.-K. Sun, and J.-Q. Lin, "The high dependence of polarization resolved laser-induced breakdown spectroscopy on experimental conditions," *Chinese Phys. B*, vol. 21, no. 7, p. 74204, 2012.

[4] Y. Zhao, S. Singha, Y. Liu, and R. J. Gordon, "Polarization resolved laser-induced breakdown spectroscopy," *Opt. Lett.*, vol. 34, no. 4, pp. 494–496, 2009.

[5] N. Agnes, H. Tao, Z. Hao, C. Sun, X. Gao, and J. Lin, "A comparison of single shot nanosecond and femtosecond polarization-resolved laser-induced breakdown spectroscopy of Al," *Chinese Phys. B*, vol. 22, no. 1, p. 14209, 2013.

[6] A. Eslami Majd, A. S. Arabanian, and R. Massudi, "Polarization resolved laser induced breakdown spectroscopy by single shot nanosecond pulsed Nd:YAG laser," *Opt. Lasers Eng.*, vol. 48, no. 7–8, pp. 750–753, 2010.

[7] Y. Liu, J. S. Penczak, and R. J. Gordon, "Nanosecond polarization-resolved laser-induced breakdown spectroscopy.," *Opt. Lett.*, vol. 35, no. 2, pp. 112–114, 2010.

[8] D. Zhao, N. Farid, R. Hai, D. Wu, and H. Ding, "Diagnostics of First Wall Materials in a Magnetically Confined Fusion Device by Polarization-Resolved Laser-Induced Breakdown Spectroscopy," *Plasma Sci. Technol.*, vol. 16, no. 2, pp. 149–154, 2014.

[9] M. E. Asgill, H. Y. Moon, N. Omenetto, and D. W. Hahn, "Investigation of polarization effects for nanosecond laser-induced breakdown spectroscopy," *Spectrochim. Acta - Part B At. Spectrosc.*, vol. 65, no. 12, pp. 1033–1040, 2010.

[10] A. K. Sharma and R. K. Thareja, "Anisotropic emission in laser-produced aluminum plasma in ambient nitrogen," *Appl. Surf. Sci.*, vol. 253, no. 6, pp. 3113–3121, 2007.

[11] J. Kim and D. E. Kim, "Measurement of the degree of polarization of the spectra from laser produced recombining Al plasmas," *Phys. Rev. E - Stat. Nonlinear, Soft Matter Phys.*, vol. 66, no. 1, pp. 1–4, 2002.

[12] B. Wu, "High-intensity nanosecond-pulsed laser-induced plasma in air, water, and vacuum: A comparative study of the early-stage evolution using a physics-based predictive model," *Appl. Phys. Lett.*, vol. 93, no. 10, 2008.

[13] M. J. Bernstein and G. G. Comisar, "X-ray production in laser-heated plasmas," *J. Appl. Phys.*, vol. 41, no. 2, pp. 729–733, 1970.

[14] G. Bertuccelli, H. O. Di Rocco, D. I. Iriarte, M. Romeo Y Bidegain, and H. F. Ranea-Sandoval, "Radiative mechanisms in laser-produced plasmas in Xe," *J. Quant. Spectrosc. Radiat. Transf.*, vol. 61, no. 3, pp. 309–317, 1999.

[15] J. Liu, H.-Y. Tao, X. Gao, Z.-Q. Hao, and J.-Q. Lin, "The polarization characteristics of single shot nanosecond laser-induced breakdown spectroscopy of Al," *Chinese Phys. B*, vol. 22, no. 4, p. 44206, 2013.

[16] T. Fujimoto and S. A. Kazantsev, "Plasma polarization spectroscopy Review Article," *Plasma Phys. Control. Fusion*, vol. 39, pp. 1267–1294, 1997.

[17] J. S. Penczak, Y. Liu, and R. J. Gordon, "Polarization-resolved laser-induced breakdown spectroscopy of Al," *Opt. Lett.*, vol. 34, no. 4, p. 494, 2009.

[18] J. S. Penczak, Y. Liu, R. D. Schaller, D. H. Rich, and R. J. Gordon, "The mechanism for continuum polarization in laser induced breakdown spectroscopy of Si(111)," *Spectrochim. Acta - Part B At. Spectrosc.*, vol. 74–75, pp. 3–10, 2012.

6 Effect of Target Geometry and Incident laser Polarisation on Al Plasma Emission

In this study, the polarisation state of the emission from a laser produced Al plasma has been studied for different target geometeries and at different incident laser polarisations. Time and polarisation resolved emission spectroscopy was used to characterise the plasma radiation at a central wavelength of the spectrometer of 395 nm, measured in air. The degree of polarisation (P) was quantified for the line emission 396.15 nm and the nearby continuum as the function of time delay and fluence. A strong polarisation effect was observed for the continuum emission at oblique laser incidence, compared to normal incidence.

6.1 Introduction

In this chapter, experimental results on polarisation resolved emission spectra at different stages of plasma formation/evolution for different target geometries and incident laser angles and polarisation states are investigated. Al plasma emission at a central wavelength of the spectrometer of 395 nm is studied simultaneously for orthogonally polarised states, in air ambient (1×10^3 mbar). As discussed in Chapter 2, both the continuum and the line emission from a laser produced plasma can be partially polarised. However, the nature of this polarisation is a relatively unexplored area with little data over a wide parameter of space available in the literature. For example, the earliest studies on the polarisation of line emission from laser produced plasmas date back to the early 1990s and were limited to investigations in the X-ray region of the spectrum [1]. More recently, studies have focused on polarised emission in the visible region of the spectrum. However, these studies have tended to be either time integrated measurements on alloys for LIBS applications [2] or on femtosecond laser ablation [3]. The polarisation of light emitted by a laser-produced plasma on an aluminium target has been studied previously but only either in a time-integrated measurement [4] or over a very limited experimental parameter space [5].

Several authors proposed possible explanations for the observation of the partial polarisation of continuum and line emission from laser produced plasmas on solids [2], [6], [7]. Different mechanisms were speculated upon to explain the how the various plasma emissions became partially polarised. Depending on the power density, the polarisation of the emitted radiation can depend on the incident laser polarisation [8], target geometry [6], [7], thermalisation effect within the plasma [9] and radiative recombination [10]. In all of these papers, it was agreed that the plasma is out of equilibrium [1], [10]. For example, Majd et al. [2] reported polarised emission from plasmas formed on a Cu target observed at 30^0 to the incident laser for vertical, horizontal or circular laser polarisation for a pulse duration of 6ns, 1064 nm in time integrated studies. They found the degree of polarisation for the continuum emission produced by a vertically polarised incident laser was larger than for horizontal and circular incident laser polarisation. Penczak et al. [7] compared the time-integrated spectra of an Al plasma formed

by nanosecond scale laser pulses of different polarisation directions which were incident onto the target both normally and at 45^0. They demonstrated that for normal incidence the continuum emission dropped by 10 % for s polarisation (i.e., polarisation perpendicular to the plane of incidence) and p polarisation (i.e., polarisation parallel to the plane of incidence) compared to 45^0 laser incidence on the target. Thus, the degree of polarisation was sensitive to both the incident laser polarisation and the target geometries for these spectra. Another interesting time resolved and time integrated plasma emission study using nanosecond laser pulses focused into gases and onto solids (copper and steel) was performed by Asgill et al. [6]. They observed emission at 45^0 with respect to incident laser direction to be more strongly polarised than for normal laser incidence for which the emission was very weakly polarised. The stronger polarisation at a laser incidence of 45^0 was explained based on Fresnel reflection of the plasma light from the surface of the target and the plasma plume itself [6], [7].

In this study, the effect of target geometry (angle of laser incidence on the target) and the incident laser polarisation on the plasma emission are investigated using time and polarisation resolved spectroscopy. The variation of P is shown for different stages of the plasma formation and evolution.

6.2 Experimental Setup

Figure 6.1 shows the schematic diagram of the set-up. A Q-switched Nd:YAG laser (wavelength 1064 nm, pulse duration 14 ns FWHM at a repetition rate of 10 Hz) was focused by a plano-convex lens (f = 250 mm) onto an Al target in air to two different laser pulse energy of ~53 mJ (corresponding to laser fluence of 169 J/cm^2 and the laser irradiance 1.2×10^{10} W/cm^2) and ~142 mJ (corresponding to laser fluence of 452 J/cm^2 and the laser irradiance of 3.3×10^{10} W/cm^2). The target was located inside a square chamber either normal or at 45^0 to the laser quantisation axis or at 45^0 to the optic axis of the detector. The plasma emission was collected, collimated and focused by a combination of two lenses of focal lengths f_1 =100 mm and f_2 = 50 mm, onto the entrance slit (width = 200 μm) of a 0.5 m Czerny-Turner spectrometer (Chromex^{TM} 500-is) equipped with a grating of 1200 g/mm

coupled to an ICCD camera of 512×512 pixels (Andor^{TM} DH5H7). The ICCD camera was operated with a gate width of 10 ns and the time delay was increased in steps of 10 ns for the study of the continuum emission in the range 0-130 ns and the for the line emission from 230-530 ns in steps of 100 ns. To change the incident laser intensity and polarisation, the combination a half wave plate, horizontal polariser and a second half wave plate were used. Both horizontal (second half wave plate set at 0^0) and vertical (second half wave plate set at 45^0) incident laser polarisations were used. In addition, a quarter wave plate replaced the second half wave plate to change to the circular laser polarisation. To study the effect of the target geometry on the polarisation state of the emitted radiation, the target was set at 45^0 with respect to the incident laser direction (quantisation axis) and at 45^0 with respect to the optic axis of the detector (spectrometer with gated with ICCD). A Wollaston prism was used to split the plasma emission into two orthogonally linearly polarised states thereby eliminating any errors due to shot to shot fluctuations from the laser. These orthogonally polarised states are "Horizontal", i.e., parallel to the laser quantisation axis and "Vertical", i.e., perpendicular to the laser quantisation axis. Particularly for this set of experiments, we set the central wavelength of the spectrometer at 395 nm to study the Al neutral doublet emission and the nearby continuum. For the 396.15 nm line the unpolarised neighboring line at a wavelength of 394.4 nm arising from the 4s ($^2S_{1/2}$) → 3p ($^2P^o_{1/2}$) transition was used for the polarisation sensitivity calibration. As mentioned in section **2.5** the degree of polarisation anisotropy is given by:

$$P_\lambda = \left(\frac{I_H - I_V}{I_H + I_V} \right) \tag{6.1}$$

where I_H is the intensity parallel to the laser quantisation axis and I_V is the intensity perpendicular to it.

Another important parameter is the incident angle dependent laser fluence F in Jcm^{-2} given by:

$$F = \frac{E \cos\theta}{\pi r^2} \tag{6.2}$$

Where E is the pulse energy, θ is the angle of incidence and $r \approx 100\,\mu m$ is the spot size of the laser.

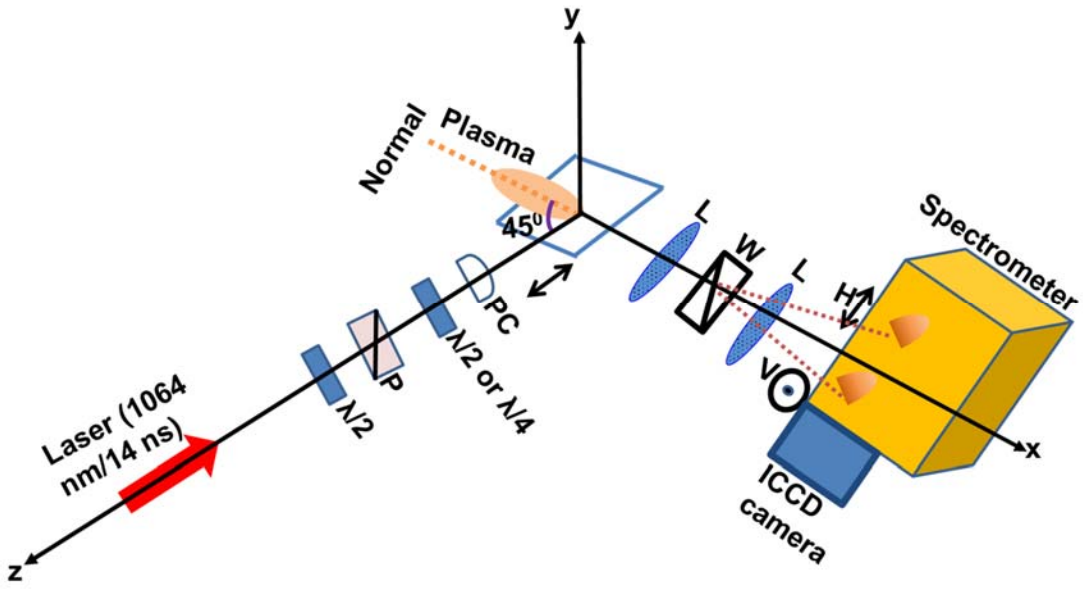

Figure 6.1:Schematic of time-resolved PRLIBS setup for the target at 45⁰ to the incident laser (M, mirror; λ/2, half-wave plate; λ/4, quarter-wave plate; P, polariser; PL, planoconvex lens; L, lens; W, Wollaston prism).

6.3 Spectroscopy Results

6.3.1 Polarisation as a Function of Time Delay

Figure 6.2 (a-c), Figure 6.3 (a-c) and **Figure 6.4 (a-c)** show the variation of the orthogonally polarised (H and V) states for continuum (upper four panels) and line emission (lower four panels) for different time delays. Continuum emission dominated in the time delay range 0-130 ns following plasma breakdown. Comparing relative intensities, the plasma emission is generally stronger for vertical than for horizontal polarisation independent of the state of polarisation of the incident laser field. Starting at around 100 ns, an O^+ feature at 399.2 nm, due to the transition $2s^22p^2(^3P)3d\ (^2P_{3/2}) \rightarrow 2s^22p^2(^3P)3p\ (^4P^0_{3/2})$, was observed. It persisted for approximately 330 ns and exhibited a small degree of polarisation (P). Weak polarisation anisotropy was observed for the Al neutral doublet at 394.4 and 396.15 nm which appeared in the time delay range 230-530 ns. The doublet arises from 4s $(^2S_{1/2}) \rightarrow$3p $(^2P^0_{1/2,\ 3/2})$ transition in atomic aluminium and persists for a period of up to 5 μs in air ambient. We

observed a very weak polarisation effect in the time delay range of 230-530 ns for the 396.15 nm line with the little difference in the relative intensities for vertical and horizontal polarisation respectively. The spectrum for each polarisation was integrated over the wavelength range of the $^2S_{1/2} - {}^2P_{3/2}$ member of the doublet (i.e., from 395.5 nm to 396.6 nm).

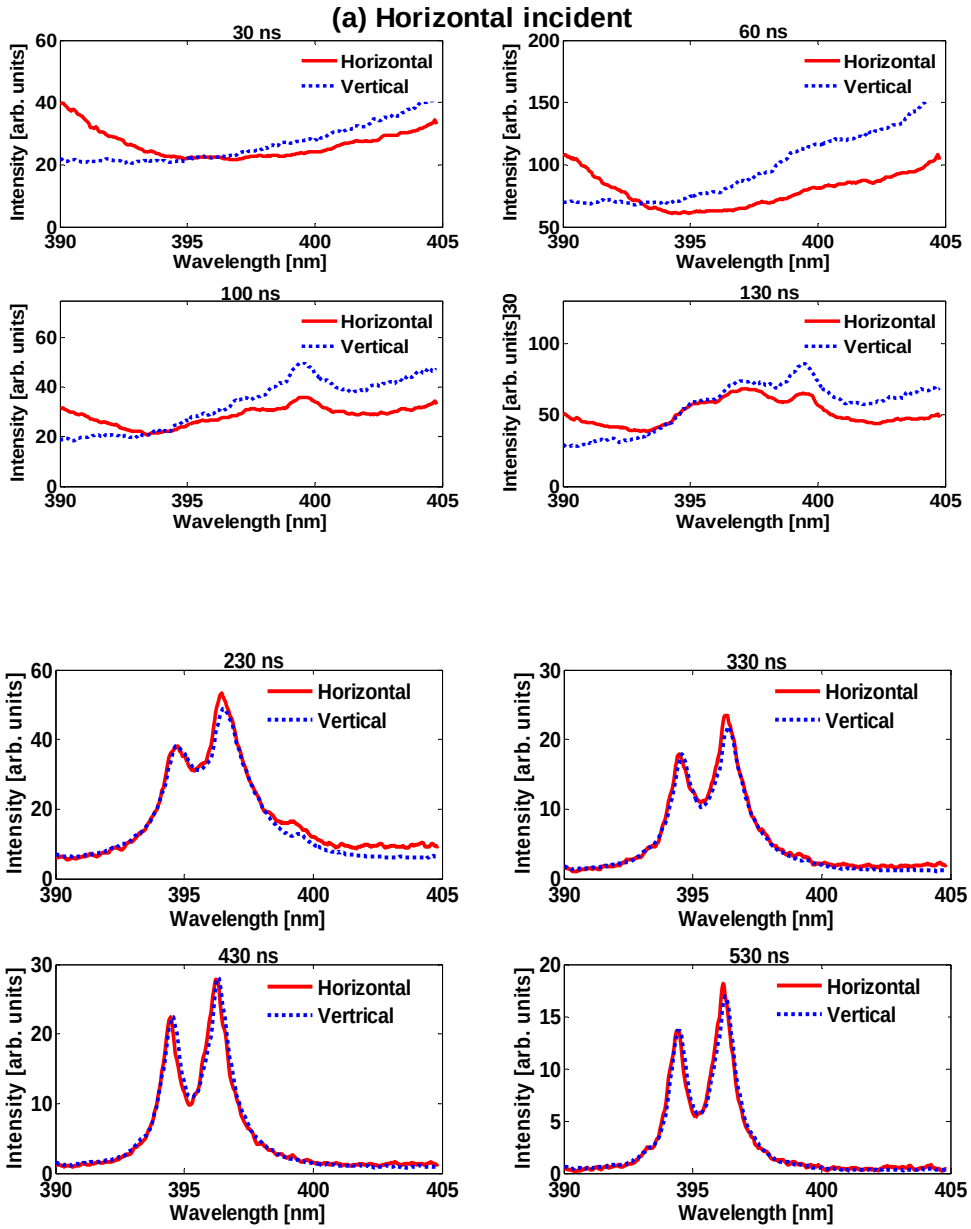

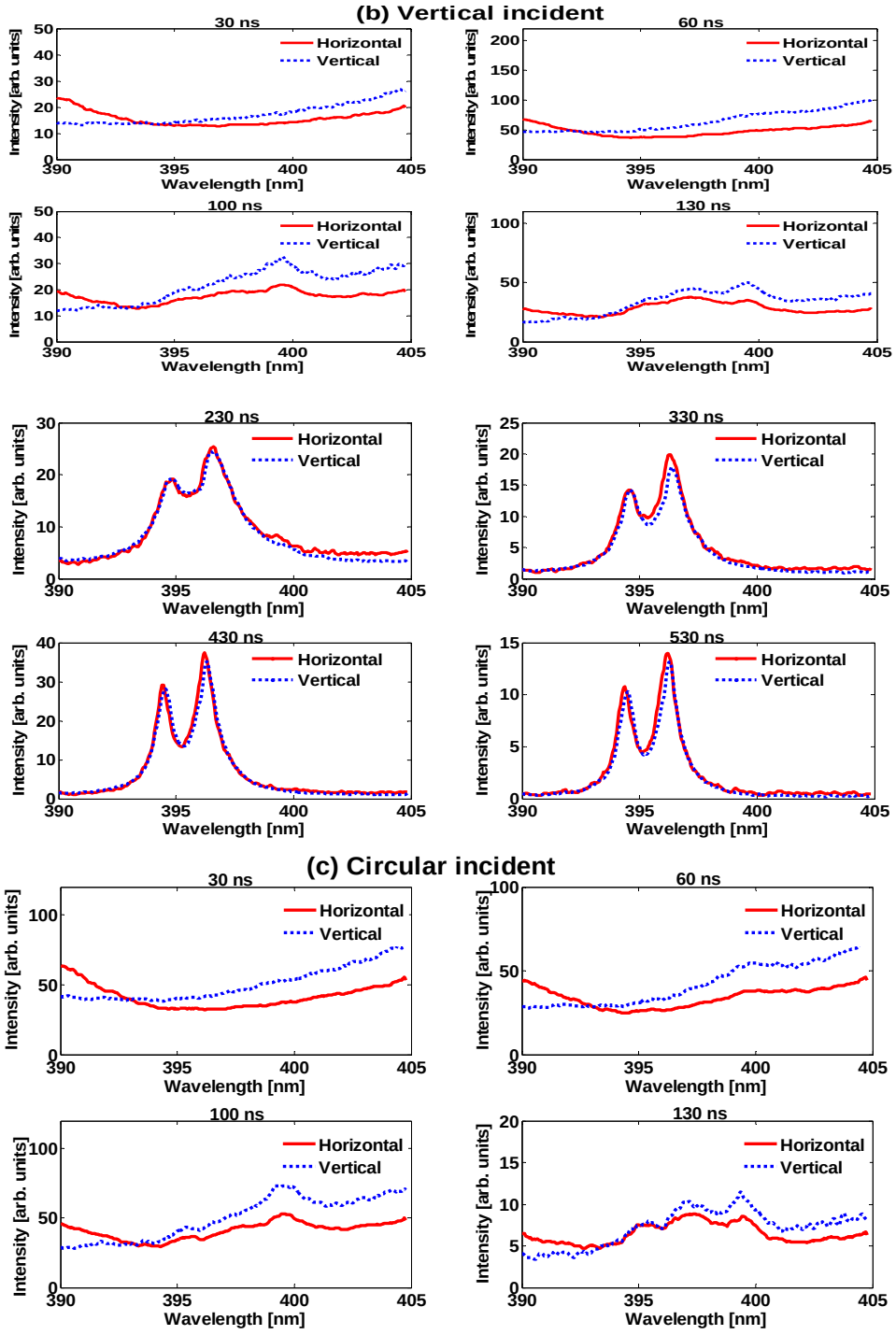
(b) Vertical incident
30 ns
60 ns
100 ns
130 ns
230 ns
330 ns
430 ns
530 ns
Horizontal
Vertical
Intensity [arb. units]
Wavelength [nm]
(c) Circular incident
30 ns
60 ns
100 ns
130 ns
Horizontal
Vertical
Intensity [arb. units]
Wavelength [nm]

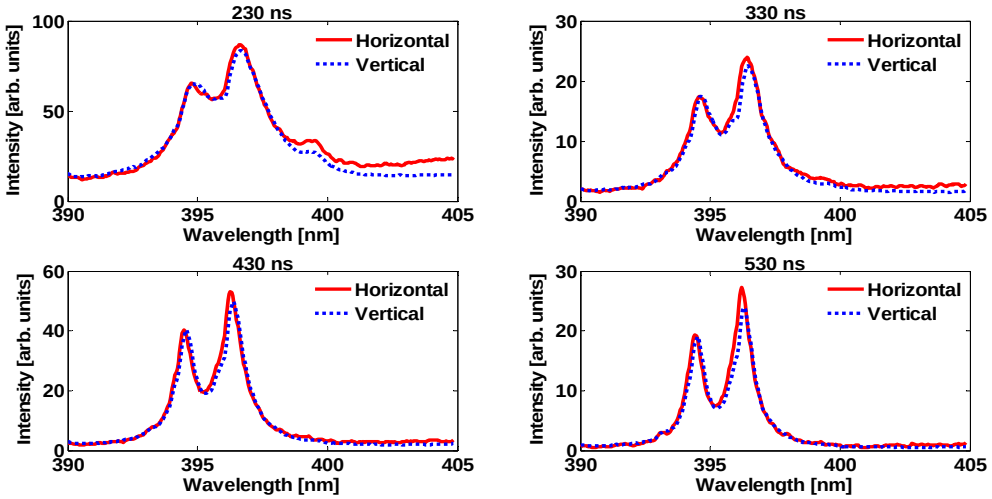

Figure 6.2: Polarisation resolved spectra of an Al plasma, showing a mix of continuum emission and the Al^0 doublet for different stages of plasma evolution at a background pressure of 1×10^3 mbar for a laser at normal incidence on the flat target. The spectra were obtained for different incident laser polarisation states at a fluence of 452 J/cm^2 for continuum (upper four panels) and line (lower four panels) emission for each of (a) horizontal, (b) vertical, and (c) circular incident laser polarisation. The ICCD gate width was set at 10 ns.

The degree of polarization formula in equation (**2.43**) was modified to account for polarization sensitivity to yield:

$$P_\lambda\left(396.15nm\right)=\left(\frac{\left(\frac{I_H^{396.15nm}}{I_H^{394.4nm}}\right)-\left(\frac{I_V^{396.15nm}}{I_V^{394.4nm}}\right)}{\left(\frac{I_H^{396.15nm}}{I_H^{394.4nm}}\right)+\left(\frac{I_V^{396.15nm}}{I_V^{394.4nm}}\right)}\right) \tag{6.3}$$

Where $I^{394.4nm}$ is the polarisation insensitive component of the Al^0 doublet.

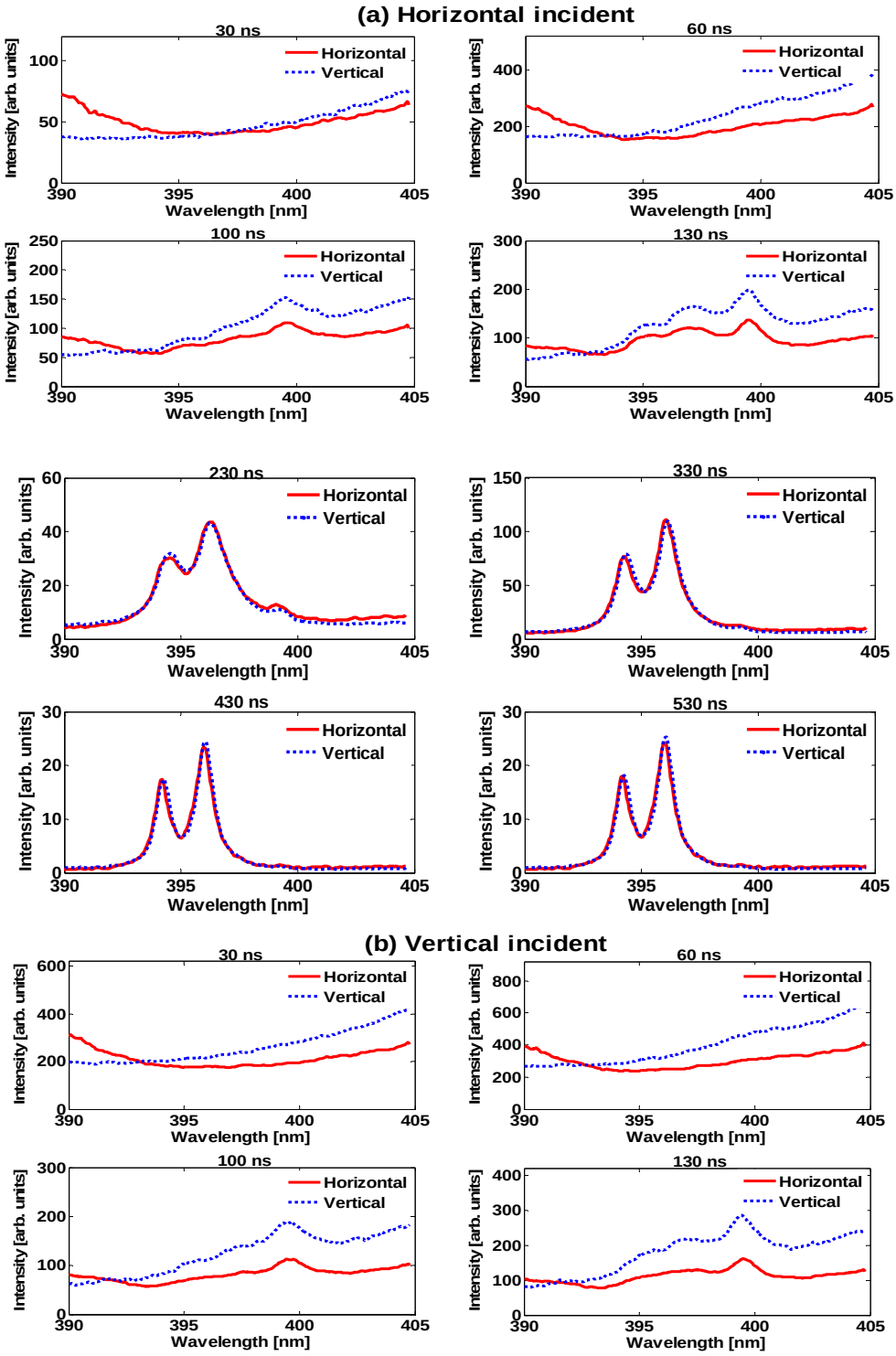
(a) Horizontal incident
30 ns
60 ns
100 ns
130 ns
230 ns
330 ns
430 ns
530 ns
(b) Vertical incident
30 ns
60 ns
100 ns
130 ns
Horizontal
Vertical
Intensity [arb. units]
Wavelength [nm]

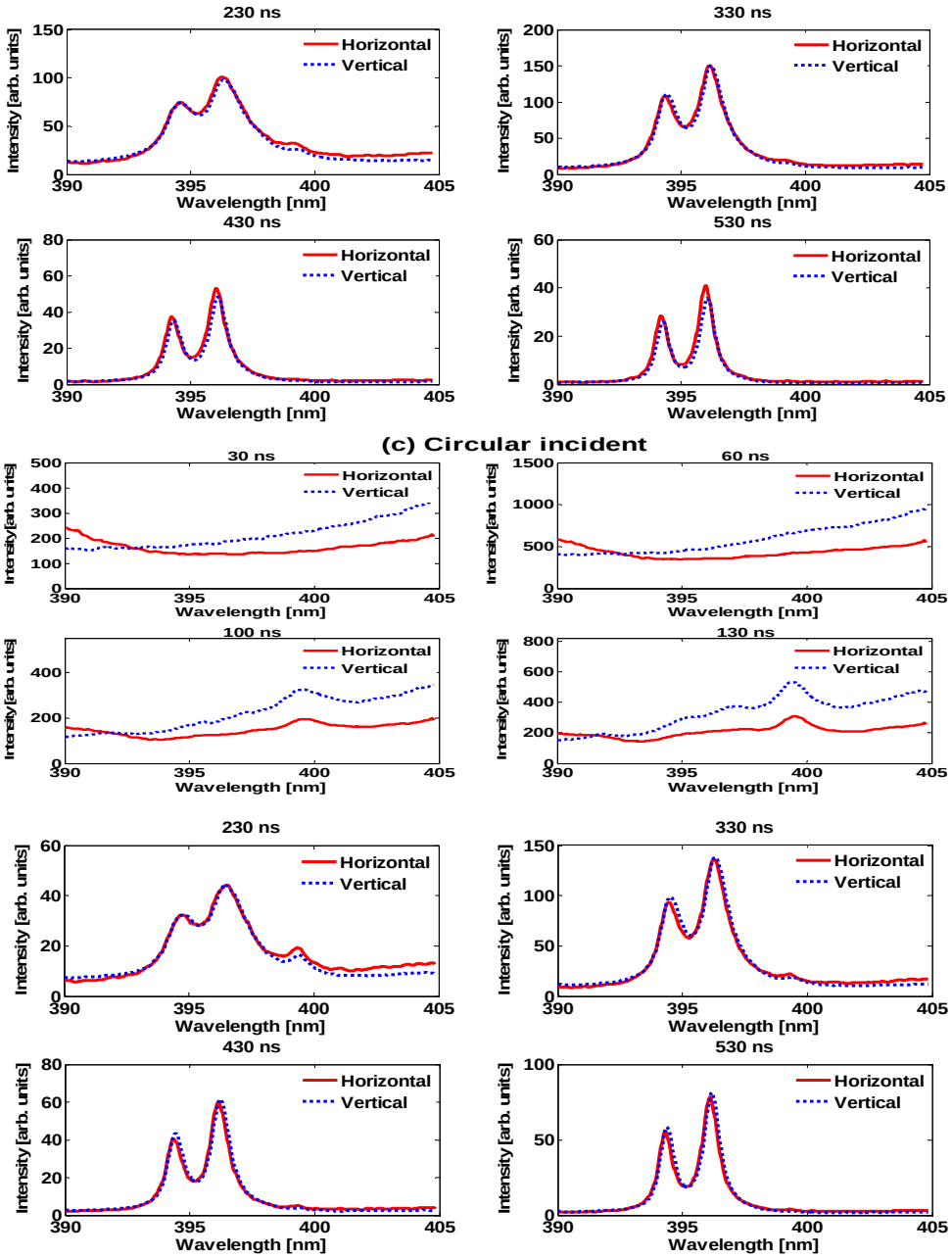

Figure 6.3: **Polarisation resolved spectra of an Al plasma, showing a mix of continuum emission and the Al^0 doublet for different stages of plasma evolution at a background pressure of 1×10^3 mbar for a laser incident at 45^0 to the target normal. The spectra were obtained for different incident laser polarisation states at a fluence of 452 J/cm^2 for continuum (upper four panels) and line (lower four panels) emission for each of (a) horizontal, (b) vertical, and (c) circular incident laser polarisation. The ICCD gate width was set at 10 ns.**

The degree of polarisation (P) was computed at a wavelength of 402 nm for the continuum emission and at 396.15 nm for the line emission using equation (**6.3**). The continuum polarisation emission was obtained by integrating the signal between 401 and 403 nm in the time delay range 0-130 ns for both vertical and horizontal polarisation directions. On the other hand, the line emission spectrum was integrated over the wavelength range 395.5 nm to 396.6 nm for time delays in the range 230-530 ns.

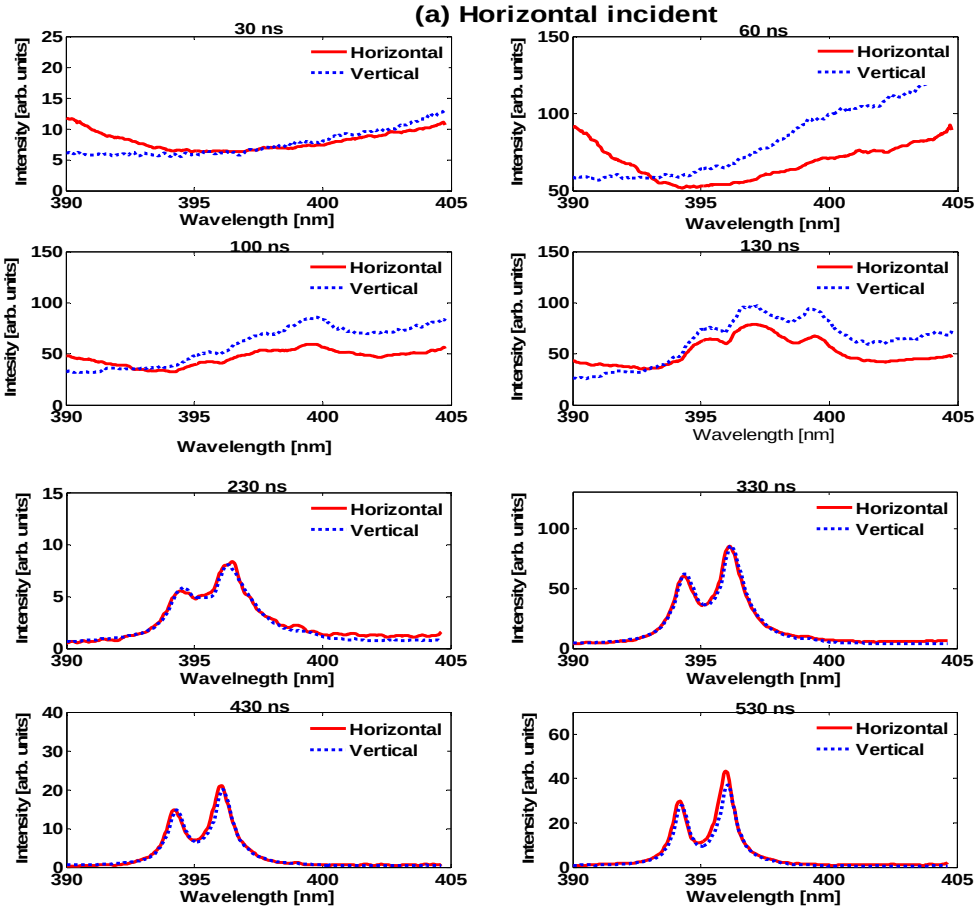

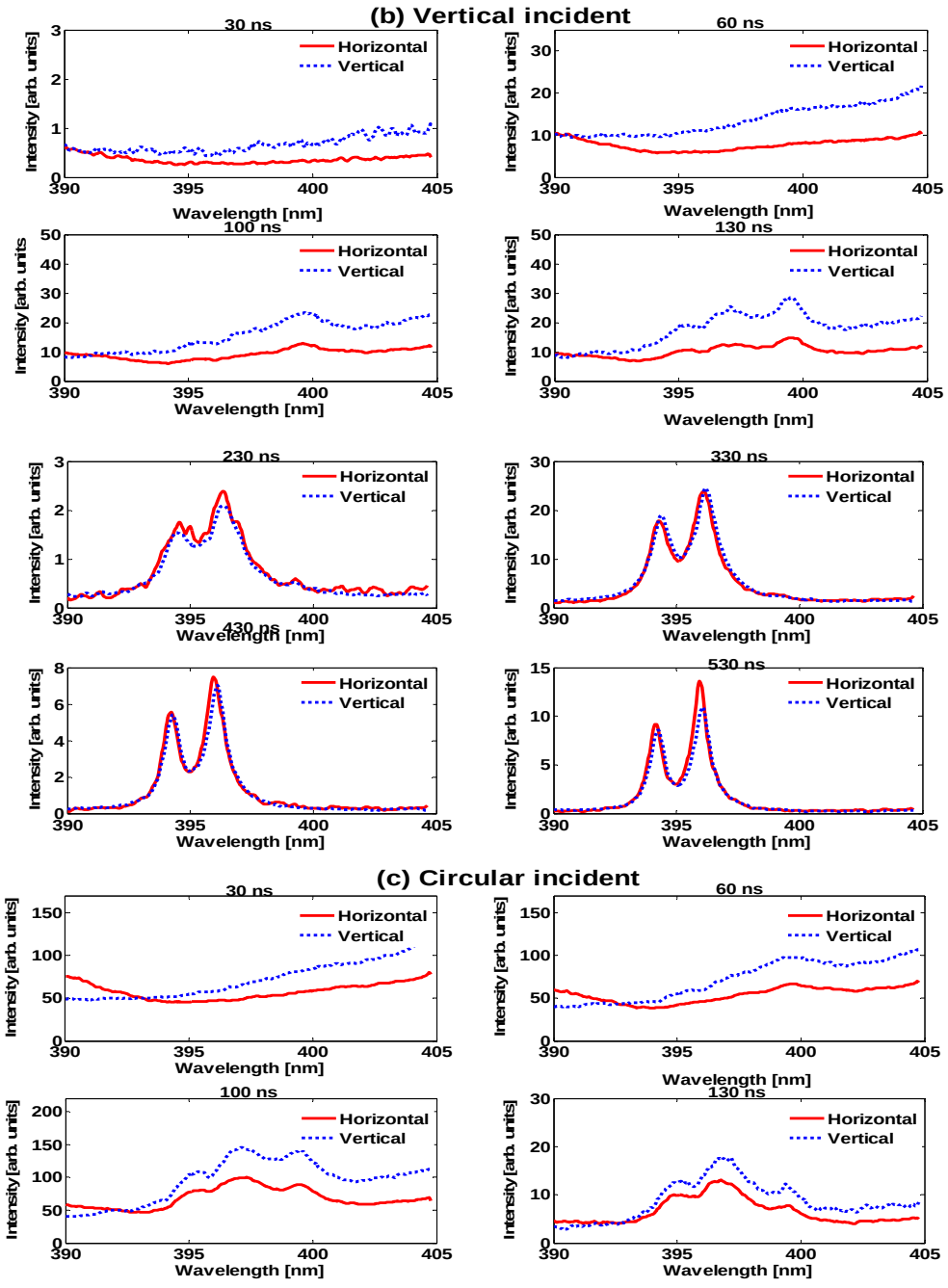
(b) Vertical incident
30 ns
60 ns
100 ns
130 ns
230 ns
330 ns
430 ns
530 ns
Horizontal
Vertical
Intensity [arb. units]
Wavelength [nm]
(c) Circular incident
30 ns
60 ns
100 ns
130 ns
Horizontal
Vertical
Intensity [arb. units]
Wavelength [nm]

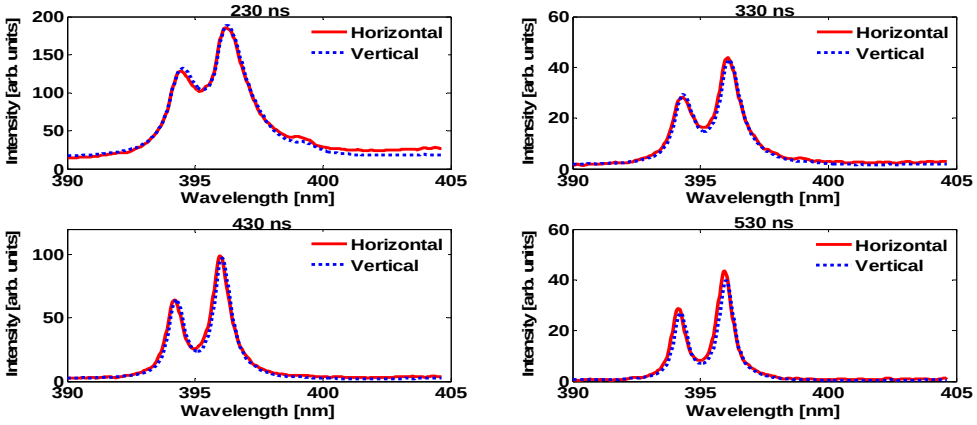

Figure 6.4: **Polarisation resolved spectra of an Al plasma, showing a mix of continuum emission and the Al^0 doublet for different stages of plasma evolution at a background pressure of 1×10^3 mbar at 45^0 to the detector optic axis. The spectra were obtained for different incident laser polarisation states at a fluence of 452 J/cm^2 for continuum (upper four panels) and line (lower four panels) emission for each of (a) horizontal, (b) vertical, and (c) circular incident laser polarisation. The ICCD gate width was set at 10 ns.**

Figure 6.5 (a) shows that P is approximately the same for the continuum emission from plasmas produced by a laser incident normally on the target surface for each different laser polarisation state. The variation of P at early times was in the range of -0.27<P<-0.12 with a modulation of 10% only in first 40 ns and remained almost constant in the time delay range 40-130 ns. However, a clear variation of the continuum polarisation was observed for the emission produced by having a target set at 45^0 to the incident laser direction as shown in **Figure 6.5 (b).** The result is consistent with Majd et al. [2] who reported on the time integrated emission spectra of a Cu plasma produced by nanosecond laser (1064 nm, 8 ns and 51 mJ) ablation of the target set at an angle of 30^0 to the incident laser direction with variable polarization**.** First, the degree of polarisation for plasma emission produced by vertically and circularly polarised laser pulses overlap well and are hence quite similar. For plasmas produced by horizontally polarised laser pulses P is smaller at all time delays but follows a similar trend, with the absolute value of P increasing slowly with time delay. **Figure 6.5 (c)** displays P as a function of time delay for the continuum emission with the target set at 45^0 to both laser incident direction and the optic axis of the detector. At early time delays P is quite different for plasmas formed by laser pulses of different polarisation states with values of ≈

40% for vertically polarised laser pulses, followed by ≈ 20% for circularly polarised pulses and ≈ 5% for horizontally polarised laser pulses respectively. As time progresses the values of P for the different laser polarisation states start to converge to values in the range of -0.2 to -0.3. In all these cases, we find that the continuum is more strongly polarised for oblique angles of incidence of the laser and indeed also the detector. However, for line emission the corresponding values of P were <10 % as observed in **Figure 6.6 (a-c)**. Our observation is in a good agreement with the time integrated polarisation emission study reported by Penczak et. al. [11].

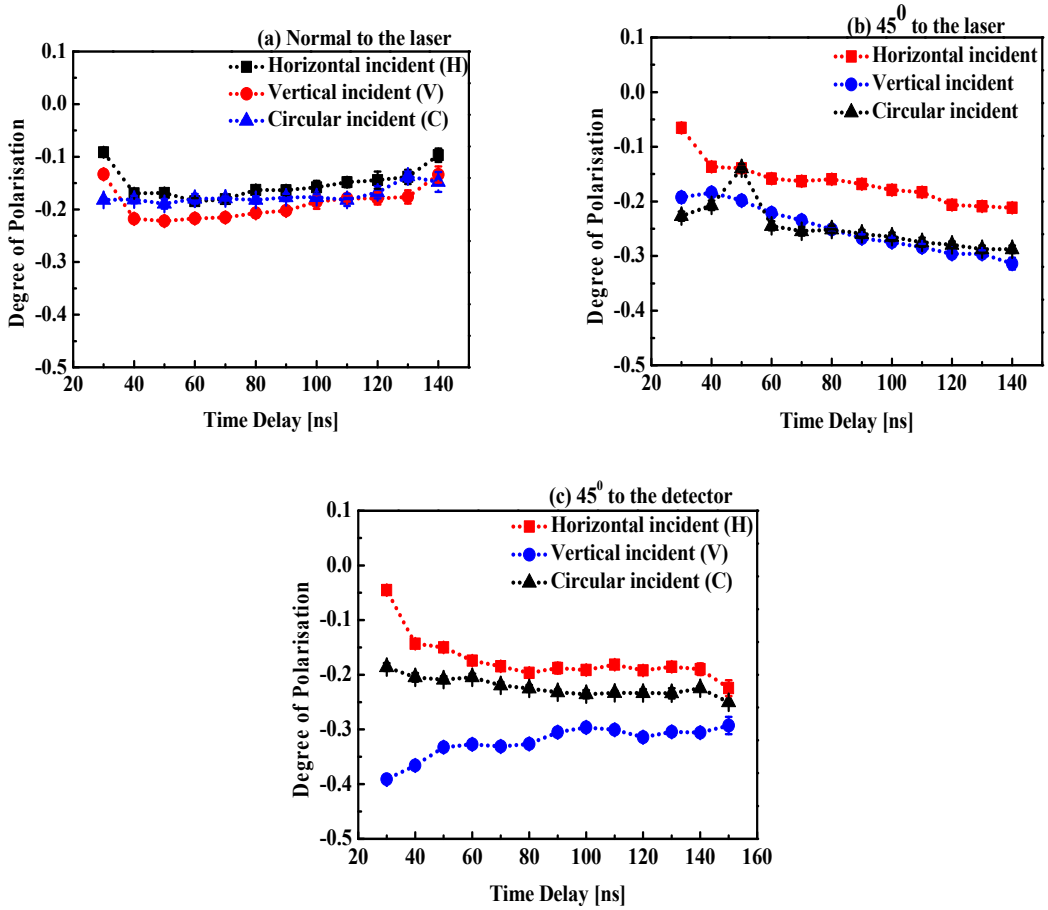

Figure 6.5: Degree of polarisation as a function of time delay for Al^0 at a laser fluence of 452 J/cm^2 at a background pressure of 1×10^3 mbar for continuum emission at 402 nm for different incident laser polarisation states. (a) The target normal to the incident laser direction (b) 45^0 to the incident laser and (c) 45^0 to the detector axis.

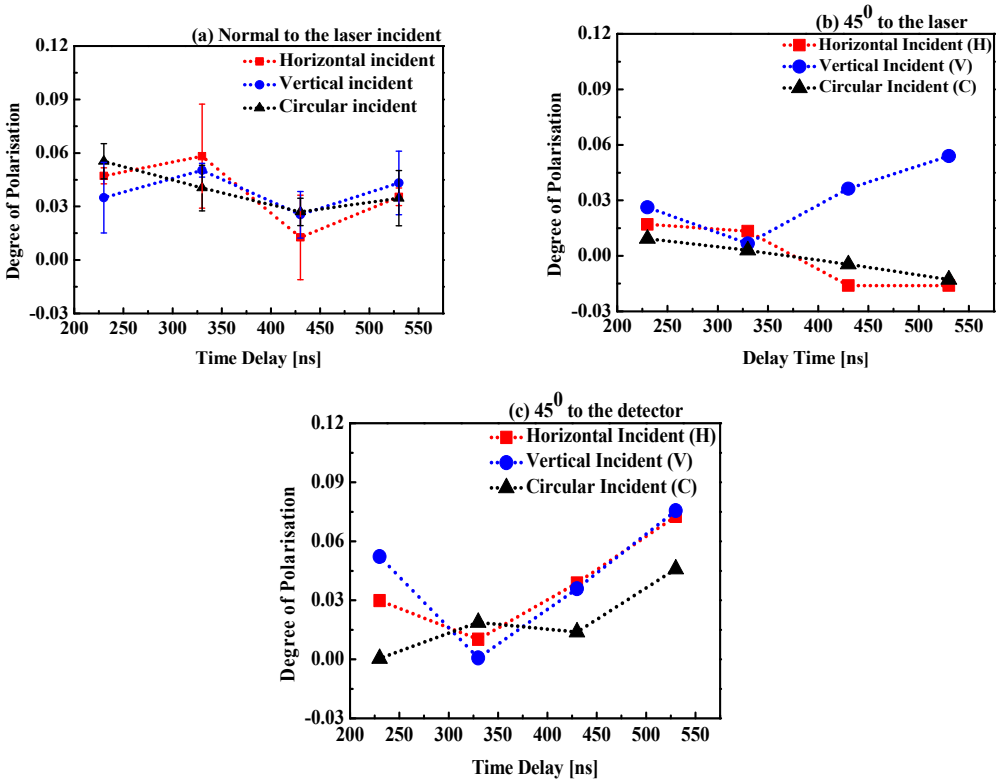

Figure 6.6: Degree of polarisation as a function of time delay for Al^0 at a laser fluence of 452 J/cm^2 at a background pressure of 1×10^3 mbar for the line at 396.15 nm for different incident laser polarisation states. (a) The target normal to the incident laser direction (b) 45^0 to the incident laser and (c) 45^0 to the detector axis.

The underlying mechanisms of the different in the degrees of polarisation (P) for different laser polarisation states and angles of incidence require the taking into account the angle of the detector with respect to the quantisation axis (namely the laser direction 'z'). For the target normal to the incident laser direction, similar to the discussion in chapter 4, the dominant mechanism for the observation of polarised emission is the transfer of an anisotropic electron velocity distribution (EVDF) into an anisotropy in the polarisation of the emitted radiation [12], [13]. There is no significant additional effect due to the polarisation state of the laser as **Figure 6.5 (a)** shows. However, as noted above, when the target is rotated through 45 degrees firstly about the vertical axis (and hence also with respect to the incident laser direction, **Figure 6.5 (b)** and subsequently also rotated through 45 degrees about the horizontal axis (i.e., also with respect to the detector axis) the degree of polarisation is not

only different to **Figure 6.5 (a)** but also now depends on the polarisation state of the laser. Asgill et. al. [6] undertook a time resolved study of the polarisation of plasma emission for Fe and Cu targets and suggested that additional polarisation was due to the difference in reflectivity of the target for horizontally and vertically polarised light which becomes significant at angle of 45 degrees and greater. They computed the Fresnel reflection coefficients and obtained values of ca. 20% at an angle of incidence of 45 degrees for plasma radiation at 600 nm for Fe and 400 nm for Cu respectively. They suggested that the dynamic nature of the degree of polarisation measured was due to the temporal development of the plasma and the effect of subsequent plasma–surface interactions on the relative reflectivities. Although this proposal may help explain an additional contribution for oblique laser incidence over normal incidence it does explicitly explain the dependence also on the laser polarisation state. It can only be speculated at this stage that the EVDF depends also on the laser polarisation state at oblique incidence. Some support for this suggestion may come from the fact that there is a component of the component of the laser field in the target direction depends on whether it is vertically or horizontally polarised and so one would expect potentially different plasma conditions to pertain in these two cases for **Figure 6.5 (b)**. For the target tilted at 45 degrees with respect to both the laser and detector axes the P values H and V polarisations lie on either side of the circularly polarised laser case as noted earlier and as expected. Confirmation would require and explicit study of the plasma parameters at early times when only continuum emission is observed. For line emission in **Figure 6.6** the P values are small and so it difficult to be definitive on the laser polarisation dependence. Although there does appear to be a small effect of the target orientation with respect to the laser and detector directions.

Four conclusions can be drawn from these sets of experimental results. (1) With the flat target normal to incident laser, the polarisation state of the emission does not vary very much with incident laser polarisation state, albeit it does vary with time delay, (2) for the target set at 45^0 to the incident laser direction, the values of P for plasmas formed by vertically and circularly polarised laser pulses are larger than for plasmas formed by the horizontally polarised laser,

(3) for the target and the detector both set at 45^0 with respect to the direction of the incident laser, P values are largest for vertically polarised laser produced plasmas while for circularly polarised laser produced plasmas the P values are intermediate between V and H at all time delays, (4) for all these studies, the line polarisation is less affected by geometrical and incident laser polarisation state effects.

6.3.2 Polarisation as a Function of Fluence

In this section, the role of the different target geometries, incident laser polarisation and laser fluences on the degree of polarisation for Al continuum emission at 402 nm is explored. Laser fluences of 452 and 169 J/cm^2 were used to produce the plasmas. **Figure 6.7** shows that the absolute value of P is larger at the higher fluence for the target set normal to the incident laser in the delay range of 20-140 ns.

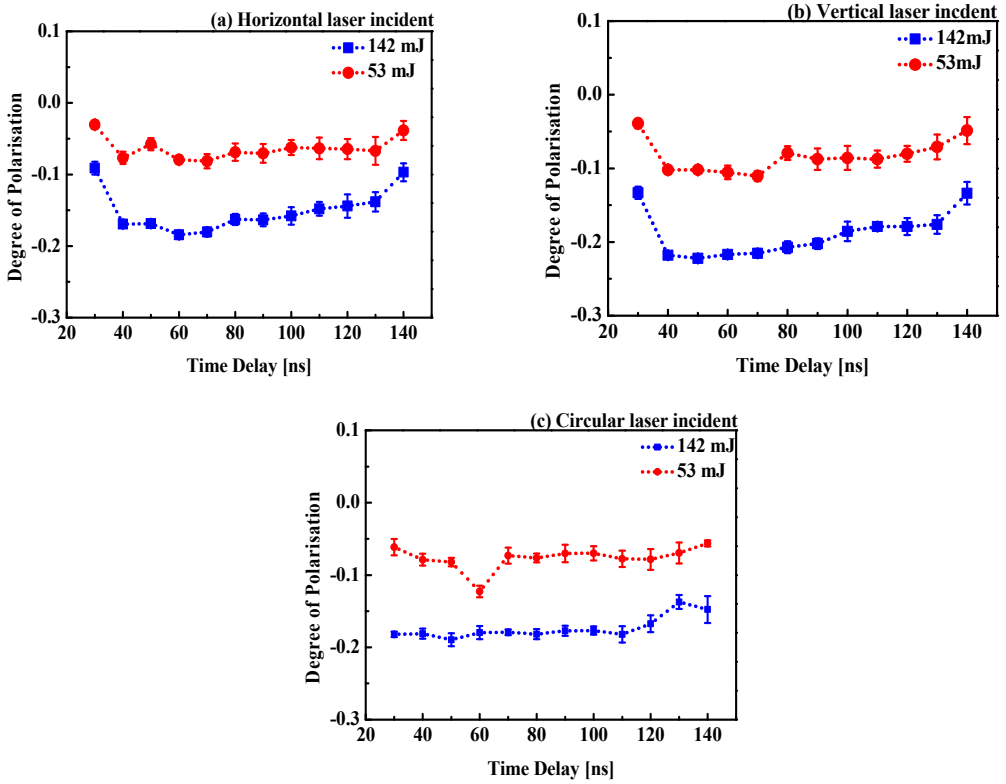

Figure 6.7: Degree of polarisation as a function of time delay for Al^0 at laser fluences of 452 J/cm^2 and 169 J/cm^2 at a background pressure of 1×10^3 mbar for continuum

emission at 402 nm. (a) Horizontally polarised, (b) vertically polarised and (c) circularly polarised laser pulses incident normal to the target.

Figure 6.8 shows the case for the target set at 45^0 to the incident laser direction. For a horizontally polarised laser P is minimally different for the two fluences used. On the other hand, for both circularly and vertically polarised lasers, P is quite different in each case and the absolute value is actually higher for the lower fluence by values in the range of 40-70%.

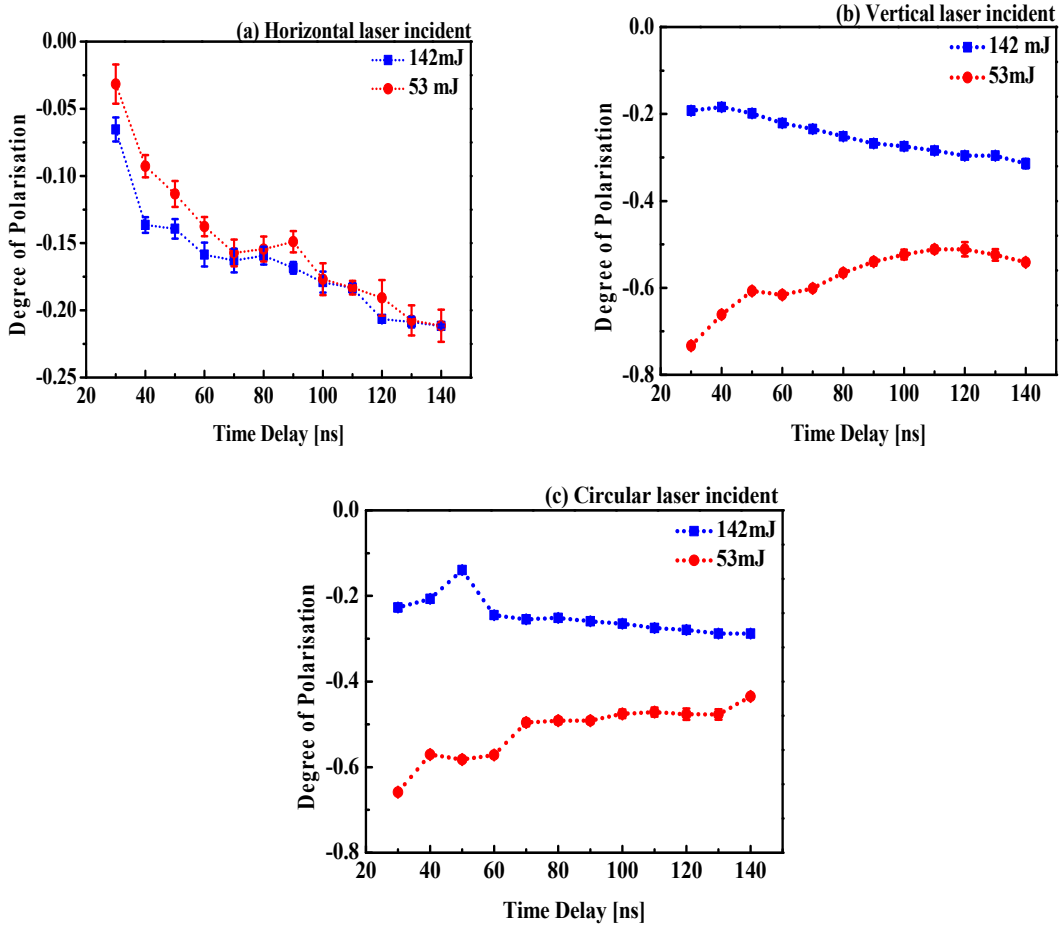

Figure 6.8: Degree of polarisation as a function of time delay for Al^0 at a laser fluence of 452 J/cm^2 and 169 J/cm^2 at a background pressure of 1×10^3 mbar for continuum emission at 402 nm. (a) Horizontally polarised, (b) vertically polarised and (c) circularly polarised laser pulses for the target set at 45^0.

Finally, **Figure 6.9** displays P for the target set at 45^0 to the optic axis of the detector and the incident laser direction. Here, for a horizontally polarised laser P was quite different for the two fluences at short time delays but converged in the range of 60-140 ns. For a vertically polarised laser, P was yet again quite different for the two different fluences at short time delays but started to converge as time proceeded to a maximum time delay of 140 ns. For a circularly polarised laser, no such convergence with time delay was observed with the difference in P values being consistently close to 0.1. This result is consistent with the time integrated measurement by Pencazak et al [7], [11] and Majd et al. [2].

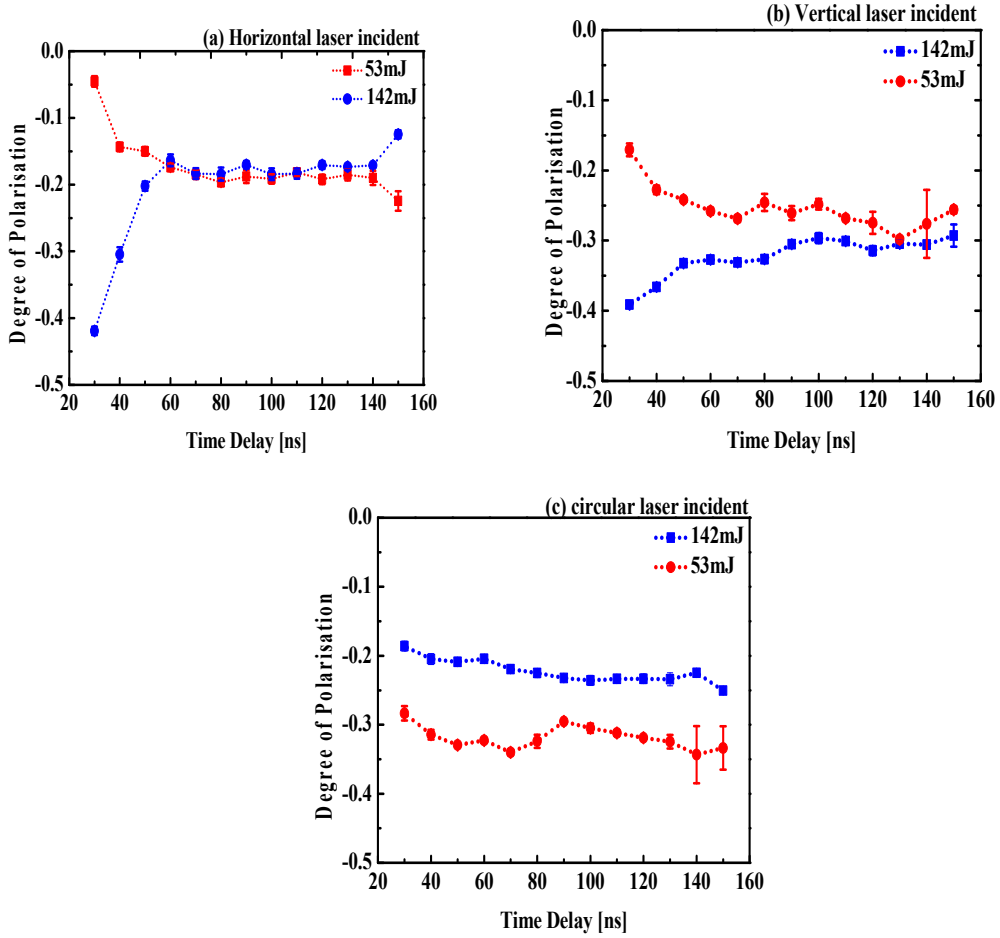

Figure 6.9: Degree of polarisation as a function of time delay for Al^0 at a laser fluence of 452 J/cm^2 and 169 J/cm^2 at a background pressure of 1×10^3 mbar for continuum emission at 402 nm. (a) horizontally polarised, (b) vertically polarised and (c) circularly polarised laser pulses for the target at 45^0 wrt to the optic axis of the detector.

6.4 Discussion

In order to interpret the results shown in the section 6.3 it is useful to refer to **Figure 6.10** which shows the three different target geometries at which spectra for different polarisation states of the laser were taken. **Figure 6.10 (a)** shows the case for the laser incident normal to the target surface. The corresponding spectra are shown in **Figure 6.2** and the degree of polarisation (P) data extracted for continuum and line emission are shown in **Figure 6.5 (a)** and **Figure 6.6 (a)** respectively.

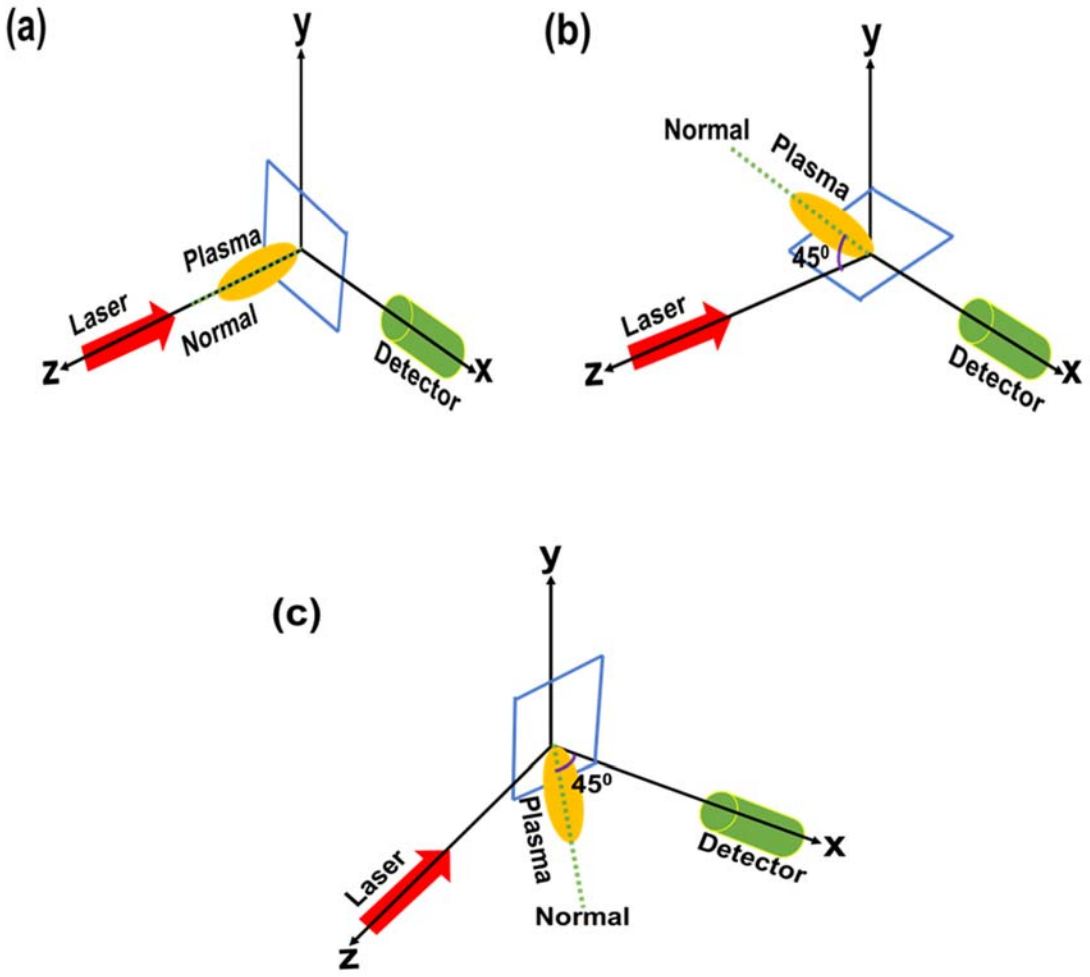

Figure 6.10: The target at (a) normal, (b) at 45^0 wrt to the laser and (c) at 45^0 wrt the ICCD camera respectively.

Looking at **Figure 6.5 (a)** P appears largely independent of the state of polarisation of the incident laser. This is to be expected since the electric field vector of the laser field is parallel to the target surface and hence one would not expect the laser polarisation to have a significant effect. The same is observed for the Al^0 doublet in **Figure 6.6 (a)** where once again P is largely constant with time delay. In this case, the laser pulse has long passed and so any residual effect one might expect to be quite small with P largely determined by the EVDF anisotropy.

In the second case in **Figure 6.10 (b)**, the target is tilted along the horizontal axis and so is now set at 45^0 to the incident laser direction. In this case for horizontal polarisation of the laser field the situation is as for the target normal to the laser direction, i.e., the electric field oscillates along the target surface. However, for a vertically polarised laser field, the vector can be resolved into one component along the target surface and one normal to the surface. This later will result in stronger penetration of the laser field into the surface and hence a stronger impact on P. This is clear from **Figure 6.5 (b)** where one can see that the absolute value of P is larger than for a horizontally polarised laser and the difference in P for horizontally and vertically polarised laser fields remains constant with time delay (albeit both drop off as time proceeds). As the circularly polarised laser field can be resolved into horizontal and vertical components this case is very similar to the vertically polarised laser field case. For the Al^0 doublet in **Figure 6.6 (b)** the P values are very small and interpretation is not so simple. It is unlikely that the laser polarisation continues to have an effect at such long-time delays and it is once again time variations in the EVDF that gives rise to the temporal behavior of P observed.

In the final case the flat target is turned through 45^0 with respect to both its horizontal and vertical axes so that the target normal is tilted with respect to the incident laser direction and also tilted towards the detector. In this case both horizontally and vertically polarised laser fields will have a component the penetrates into the target and so one would expect P values

to be quite similar in absolute value but opposite in sign and for the circularly polarised case to lie between them (as it is a superposition of both horizontally and vertically polarised cases with a simple phase shift). This is observed in **Figure 6.5 (c)**. As time proceeds, one can see that all three cases tend to converge to P close to 0.25 at delays near 160 ns. One could reasonable expect that the effect (or plasma memory) of the laser polarisation will have subsided at this stage and so the plasma polarisation anisotropy is mainly determined by the EVDF anisotropy at that time. Once again for the line emission in **Figure 6.6 (c)** the P values are small and quite close. However, for the long-time delays concerned it is unlikely there is any memory of the laser polarisation state. In summary, any effect of the laser polarisation state on P for plasma emission seems mostly to occur for continuum emission, which dominates at short time delays following plasma ignition. The attitude of the target with respect to the incident laser direction is also a factor as having a component of the laser field normal to the target surface appears to increase P for short time delays when the laser field is present on the target.

The degree of polarisation for two different laser pulse energies (53 mJ and 142 mJ) and hence fluences (452 J/cm^2 and 169 J/cm^2) are shown in section 6.3 for normal incidence on the target in **Figure 6.7**, with the target tilted through 45^0 along its horizontal axis in **Figure 6.8** and tilted through 45^0 along both its horizontal and vertical axes in **Figure 6.9**. Data are once again provided for horizontally, vertically and circularly polarised laser fields for continuum emission in the wavelength region of 402 nm.

From **Figure 6.7**, it is clear that the absolute value of P is larger at the higher fluence rising from an average value of approximately -0.1 at 169 J/cm^2 to ca. -0.2 at 452 J/cm^2 and remaining rather constant and independent of the laser polarisation state as observed in **Figure 6.5 (a)**. For the case where the target is tilted through 45^0 along its horizontal axis the behavior of P depends on the incident laser polarisation state. For horizontally polarised laser light there appears to be little or no difference in P for the two fluences. In this case, the laser field lies in the plane of the target surface and the evolution of P with time seems to be driven by

the plasma EVDF with little effect of the laser. For vertically polarised laser fields, there is a significant variation in P with fluence with the absolute value of P larger at the lower fluence. Exactly similar values and behavior are observed for circularly polarised laser fields, consistent with **Figure 6.5 (b)**. In both vertically and circularly polarised cases the values of P move closer to each other as time proceeds. It is not yet clear why larger absolute P values are observed at the lower fluence. Finally, for the target rotated through 45^0 along both its horizontal and vertical axes the trends are quite different in **Figure 6.9**. For horizontally and vertically polarised fields, in contrast to **Figure 6.8**, the absolute value of P is larger at the higher fluence. Although quite different at early times when the laser field is present, they converge at longer time delays where one would expect the laser polarisation state memory has all but faded away. The steady state values of -0.2 (horizontally polarised laser) and -0.3 (vertically polarised laser) are consistent with **Figure 6.5 (c)**.

6.5 Conclusion

In summary, the effects of target geometry and incident laser polarisation on Al neutral doublet emission and the nearby continuum emission at 402 nm have been studied by time resolved plasma polarisation spectroscopy in air ambient. Weaker line emission polarisation was observed for different incident laser polarisations and target geometries. It would appear that the laser polarisation has little or no effect on the Al^0 doublet, perhaps to be expected as these lines are only clearly observed after long time delays (>250 ns) long after the laser pulse has terminated. In general, the effect of laser field polarisation state is greater in those cases where the field has a component that penetrates the target surface and for shorter time delays, as one might expect. However, some of the trends remain to be fully understood, especially the inversion of the dependence of P on fluence which is diametrically opposite in **Figure 6.8** compared to **Figure 6.7** and **Figure 6.9**.

References

[1] J. C. Kieffer, J. P. Matte, M. Chaker, Y. Beaudoin, C. Y. Chien, S. Coe, G. Mourou, J. Dubau, and M. K. Inal, "X-ray-line polarization spectroscopy in laser-produced plasmas," *Phys. Rev. E*, vol. 48, no. 6, pp. 4648–4658, 1993.

[2] A. Eslami Majd, A. S. Arabanian, and R. Massudi, "Polarization resolved laser induced breakdown spectroscopy by single shot nanosecond pulsed Nd:YAG laser," *Opt. Lasers Eng.*, vol. 48, no. 7–8, pp. 750–753, 2010.

[3] Y. Zhao, S. Singha, Y. Liu, and R. J. Gordon, "Polarization resolved laser-induced breakdown spectroscopy," *Opt. Lett.*, vol. 34, no. 4, pp. 494–496, 2009.

[4] J. Kim and D. E. Kim, "Measurement of the degree of polarization of the spectra from laser produced recombining Al plasmas," *Phys. Rev. E - Stat. Nonlinear, Soft Matter Phys.*, vol. 66, no. 1, pp. 1–4, 2002.

[5] A. K. Sharma and R. K. Thareja, "Anisotropic emission in laser-produced aluminum plasma in ambient nitrogen," *Appl. Surf. Sci.*, vol. 253, no. 6, pp. 3113–3121, 2007.

[6] M. E. Asgill, H. Y. Moon, N. Omenetto, and D. W. Hahn, "Investigation of polarization effects for nanosecond laser-induced breakdown spectroscopy," *Spectrochim. Acta - Part B At. Spectrosc.*, vol. 65, no. 12, pp. 1033–1040, 2010.

[7] J. S. Penczak, Y. Liu, R. D. Schaller, D. H. Rich, and R. J. Gordon, "The mechanism for continuum polarization in laser induced breakdown spectroscopy of Si(111)," *Spectrochim. Acta - Part B At. Spectrosc.*, vol. 74–75, pp. 3–10, 2012.

[8] J. S. Penczak, Y. Liu, and R. J. Gordon, "Polarization and fluence dependence of the polarized emission in nanosecond laser-induced breakdown spectroscopy," *Spectrochim. Acta - Part B At. Spectrosc.*, vol. 66, pp. 186–188, 2011.

[9] A. K. Sharma and R. K. Thareja, "Polarization-resolved measurements of picosecond laser-ablated plumes," *J. Appl. Phys.*, vol. 98, no. 3, p. 33304, 2005.

[10] H. M. Milchberg and J. C. Weisheit, "Polarization of recombination radiation from nonequilibrium plasmas," *Phys. Rev. A*, vol. 26, no. 2, pp. 1023–1029, 1982.

[11] J. S. Penczak, Y. Liu, and R. J. Gordon, "Polarization-resolved laser-induced breakdown spectroscopy of Al," *Opt. Lett.*, vol. 34, no. 4, p. 494, 2009.

[12] G. A. Wubetu, H. Fiedorowicz, J. T. Costello, and T. J. Kelly, "Time resolved

anisotropic emission from an aluminium laser produced plasma," *Phys. Plasmas*, vol. 24, no. 1, p. 13105, 2017.

[13] T. Fujimoto and S. A. Kazantsev, "Plasma polarization spectroscopy Review Article," *Plasma Phys. Control. Fusion*, vol. 39, pp. 1267–1294, 1997.

7 Conclusion and Outlook

In summary, a time and polarisation state resolved imaging and spectroscopic study of laser produced Al plasmas has been undertaken. Spectra of Cu and Al alloy plasmas were also recorded and discussed in the appendix. Time resolution for the widest parameter ranges sets the current study apart those published to date. Al plasmas were studied in different spectral windows, target geometries and incident laser polarisation states. For future work, similar experiments on colliding plasmas formed on these solids could be undertaken and compared with the single plasma case reported here. Further and more detailed plasma modelling to quantify the dominant polarisation emission mechanism from our experimental plasma parameters is another important future study. Of course, plasma polarisation spectroscopy (PPS) could be extended to UV and vacuum-UV wavelengths where resonance lines of more highly charged ions in the plasma could be explored. Finally, studies on femtosecond laser generated plasmas, where the plasma formation mechanism is non-thermal and the intense laser field is will create a strong initial quantisation axis could be a fruitful area of study.

7.1 Conclusions

In this work, a time and polarisation resolved imaging and spectroscopy study of an Al plasma for different charge states were studied at different time delays, background pressures, target geometries, incident laser polarisation states and fluences is carried out. Chapters 1 and 2 include the motivation for this work, present laser produced plasma fundamentals and the origin of the polarisation anisotropy for line and continuum radiation and summarise the literature to date.

Experimental details are given in Chapter 3. An Al slab was irradiated by Q-switch Nd: YAG laser pulse duration of 14 ns at a central wavelength of 1064 nm. A Wollaston prism was used to split the plasma light into an orthogonal linearly polarised beams in front of the 0.5 m Czerny-Turner spectrometer (spectral resolution of 0.17 nm) which was equipped with an ICCD camera (time resolution of 10 ns). To account for the difference in efficiency for the different polarisation states, emission from a xenon spectral lamp was polarised at 45^0. The measured difference in orthogonally polarised Xe spectra was then used to calibrate for polarisation sensitivity. In addition, unpolarised lines near the polarised lines of interest were used to ensure corrections arising from the polarisation state sensitivity of the spectrometer.

Chapter 4 focused mainly polarisation anisotropies in the Al^0 (at 394.4 and 396.15 nm) and Al^+ (at 466.3 nm) lines and the nearby continuum in air and in vacuo. Polarisation resolved imaging results show stronger anisotropy in plasma emission in air compared to in vacuo. The polarisation spectroscopy results show the continuum emission to be more strongly polarised than the line emission at different time delays. However, in vacuo for all the charge states, the degree of polarisation (P) oscillates with time delay. Such an oscillation is an indication of the growth of the Rayleigh-Taylor (RT) instability produced by the difference in the density of the plasma and background gas.

Chapter 5 extends the study in Chapter 4 to include time resolved plasma polarisation spectroscopy (PPS) on Al^{2+} (at a central wavelength of 569 nm) at different background air pressures. The study also considers Al^{0} (at a central wavelength of 395 nm) again and the impact of lines superposed on continua on the degree of polarisation P. High values of P in air for continuum emission in the early life time of the plasma at high ambient pressure were measured. From the rate of power radiation losses at this pressure, the dominant polarisation effect is related to radiative recombination for low temperature plasma. The line emission at a lower pressure oscillated with time delay. This is yet again evidence of an RT instability which a self-generated magnetic field can arise affecting both the EVDF and potentially lifting the degeneracy in the magnetic sublevels. However, a definitive explanation would need very detailed modelling of the plasma and associated atomic processes.

In Chapter 6 the effects of target geometry and incident laser polarisation state on an Al plasma (at a central wavelength of 395 nm) formed in air were considered. The degree of line polarisation was observed to be weaker than for continuum emission for different incident laser polarisation states and target geometries. Significant enhancements in the degree of polarisation for continuum emission were observed at oblique laser incidence on the target compared to normal incidence for different incident polarisation. The strong degree of polarisation for the continuum emission produced by Vand C incident laser at oblique target due to additional electric field component perpendicular to the target surface compared to H incident laser. As a result, it modulate the EVDF and hence the degree of polarisation. As the line emission was captured at longer time delays it would appear that the memory of the laser polarisation will have faded away and so no significant effect on P is expected.

7.2 Outlook

7.2.1 Time Resolved Polarisation Imaging and Spectroscopy of Stagnation Layers

As mentioned in the introduction to this chapter fundamental investigations of anisotropic polarised emission from nanosecond laser produced plasmas could be extended to colliding

plasmas and the stagnation layer formed at the collision plane between multiple plasmas. Previously in our research group, colliding plasmas formed on solids were studied for several PhD projects. For example, Fallon et al. [1] studied the target geometrical effect on the stagnation layer and dual pulse LIBS for the improvement of the limit of detection (LOD) for the stagnation layers formed by nanosecond ablation of Cu target at different wedge angles. Time and polarisation resolved imaging and spectroscopy could also be used to study the anisotropic emission of the stagnation layer formed at different background pressures and the work extended to determine whether the LOD can be further improved.

7.2.2 Time Resolved Polarisation Imaging and Spectroscopy of Femtosecond Ablation of Solids

Time integrated femtosecond laser ablation of solids for application in LIBS was studied in the Gordon group at the University of Illinois Chicago. For example, Panczak et al. [2] reported an almost >90% anisotropy in continuum polarisation for an plasma produced by the incident laser (800 nm, 50 fs). Extension to time and polarisation resolved imaging and spectroscopy and for different target geometries is clearly worth pursuing.

7.2.3 Polarisation Modelling using Experimentally Determined Parameters

In this thesis, the experimentally determined parameters were used to calculate the power radiation losses to help with understanding the relative importance of different types of emission in our plasmas. Clearly more detailed and rigorous quantum mechanical calculations are needed and should be performed to determine the dominant polarisation emission process e.g electron-ion recombination rate, line vs continuum emission intensities, atomic population distribution amongst the available magnetic sublevels which could then be included as input to a plasmas radiative spectral code.

References

[1] C. Fallon, “Optical Diagnostics of Colliding Laser Produced Plasmas : Towards Next Generation Plasma Light Sources,” Dublin City University, 2013.

[2] J. S. Penczak, Y. Liu, and R. J. Gordon, “Polarization-resolved laser-induced breakdown spectroscopy,” *Opt. Lett.*, vol. 34, no. 4, p. 494, 2009.

A. Partial Grotrian Diagrams for Al I, Al II and Al III lines of interest

Figure A.1 (a) and **(b)** display the energy level diagram for atomic aluminium showing the fine and magnetic sublevel splitting for the Al^0 at 396.15 nm corresponding to the transition $3s^24s\ (^2S_{1/2}) \rightarrow 3s^23p\ (^2P°_{3/2})$ and 394.4 nm corresponding to the transition $3s^24s\ (^2S_{1/2}) \rightarrow 3s^23p\ (^2P^0_{1/2})$ respectively.

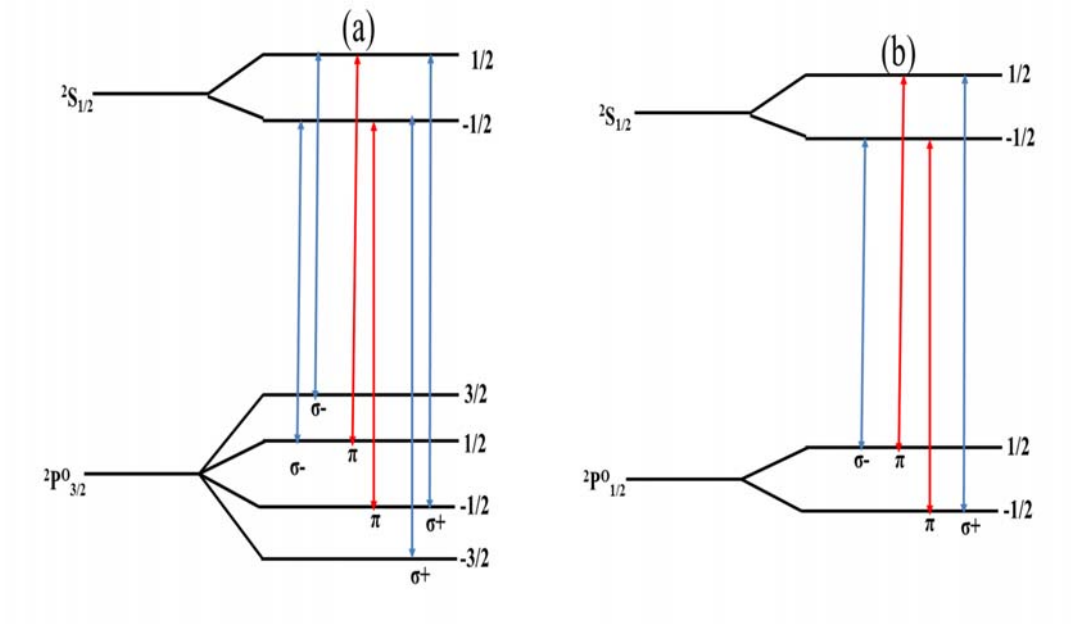

Figure A.1: Energy level splitting for atomic Al at (a) 396.15 nm ($3s^24s\ ^2S_{1/2} \rightarrow 3s^23p\ ^2P°_{3/2}$) and (b) 394.4 nm ($3s^24s\ ^2S^0_{1/2} \rightarrow 3s^23p\ ^2P^0_{1/2}$).

In transitions between the above levels, when the change of magnetic quantum number is zero, i.e., $\Delta m = 0$, the light is linearly polarised and represented as π polarisation. However, when the magnetic quantum number changes by unity, i.e., $\Delta m = \pm 1$, the light is right circularly or left circularly polarised which is represented by $\pm\sigma$. The 394.4 nm line is unpolarised with four multiplets having two σ and two π polarisation transitions [2].

Consequently, the net degree of polarisation (P) is zero due to equal strength in this counter-rotating polarisation. However, the 396.15 nm line is polarised due to the difference in the strength of four σ and two π polarised transitions. The net degree of polarisation (P) is thus different from zero for due to unequal strength in these counter-rotating polarisations. The unpolarised 394.4 line is used in conjunction with the 396.15 nm polarised line to calibrate the spectrometer for polarisation state sensitivity.

Figure A.2 (a) to **(c)** displays the energy level diagram showing the splitting of level for the transitions of Al^{2+} 4p ($^2P^o_{3/2}$) → 4s ($^2S_{1/2}$) at 569.6 nm, 4p ($^2P^o_{1/2}$) → 4s ($^2S_{1/2}$) at 572.3 nm and Al^+ (3s4p ($^1P^o_1$) →$3p^2$ ($^1D_2$)) at 466.3 nm, respectively. The magnetic sublevel structure for the transitions of interest are shown. The 572.3 nm line is unpolarised and can thus be used to calibrate the polarised neighbouring 569.6 nm line. Kim et al. [1] and Sharma et al. [2] used the 572.3 nm line for polarisation sensitivity calibration for the Al^{2+} doublet. The discrete lines become polarised in the plasma due to a non-statistical distribution of the atomic and ionic population amongst magnetic sublevels in selected parts of the plasma where there is an anisotropy in the EVDF [3].

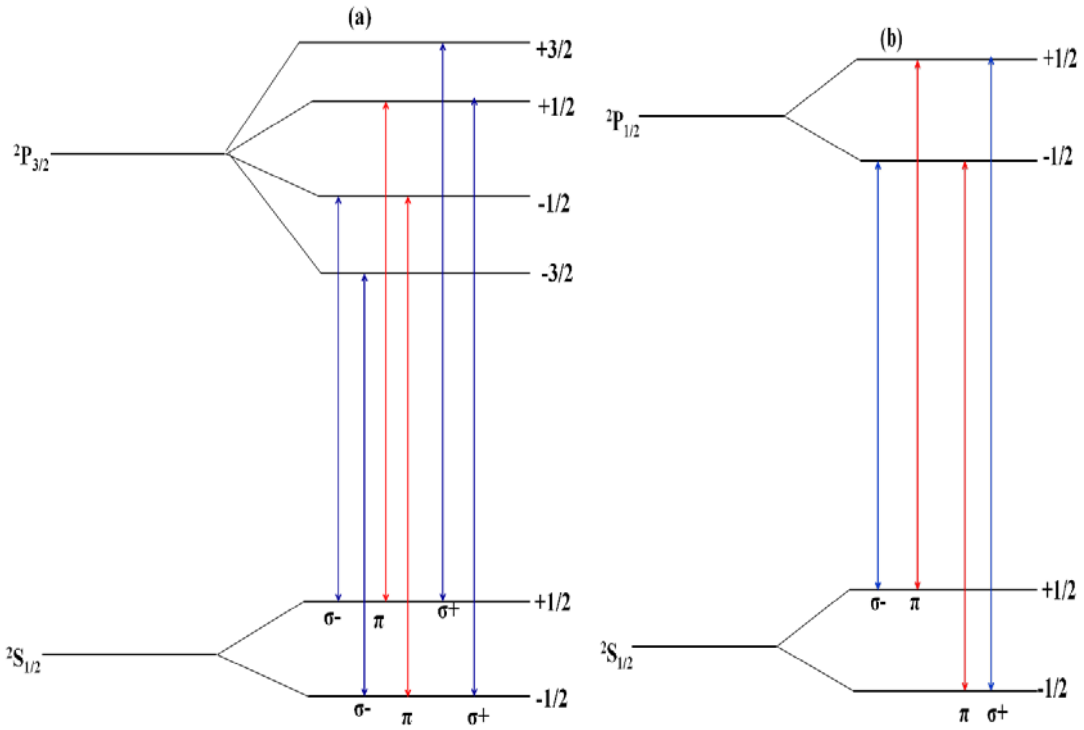

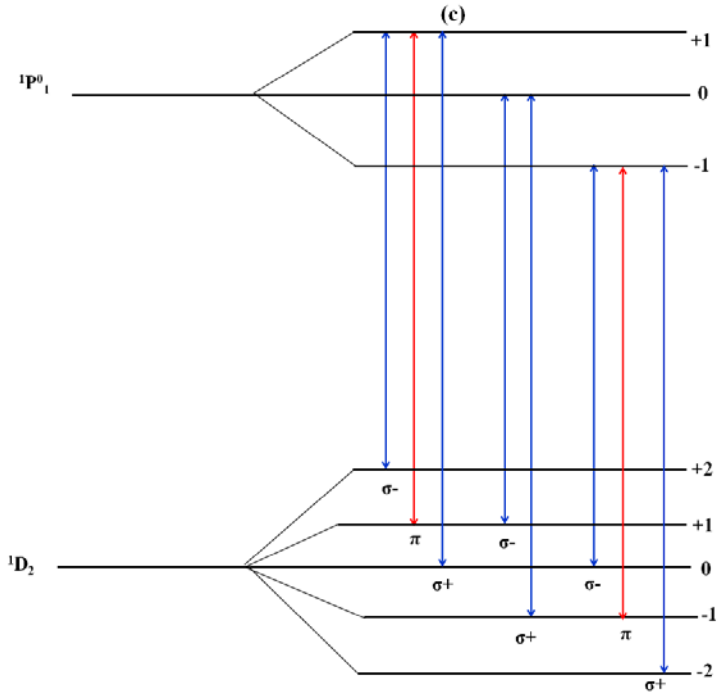

Figure A.2: Magnetic sublevel structure for the (a) 569.6 nm, (b) 572.3 nm and (c) 466.3 nm lines.

References

[1] J. Kim and D. E. Kim, "Measurement of the degree of polarization of the spectra from laser produced recombining Al plasmas," *Phys. Rev. E - Stat. Nonlinear, Soft Matter Phys.*, vol. 66, no. 1, pp. 1–4, 2002.

[2] A. K. Sharma and R. K. Thareja, "Anisotropic emission in laser-produced aluminum plasma in ambient nitrogen," *Appl. Surf. Sci.*, vol. 253, no. 6, pp. 3113–3121, 2007.

[3] J. S. Penczak, Y. Liu, and R. J. Gordon, "Polarization-resolved laser-induced breakdown spectroscopy," *Opt. Lett.*, vol. 34, no. 4, p. 494, 2009.

B. Polarisation of Cu plasma emission

Polarised emission from nanosecond laser produced Cu plasmas at a central wavelength of 512 nm was also investigated and some of the results summarised in this appendix. The radiation emitted was studied using time and polarisation resolved spectroscopy at chamber pressures of 1×10^{-2} and 1×10^{-5} mbar. The degree of polarisation of the emission was determined for both line and continuum emission and plasma parameters (electron density and temperature) extracted to help elucidate the dominant mechanisms for the anisotropies in the polarisation of the plasma radiation. As the recombination radiation rate is larger than the free-free rate, it is suggested that anisotropic continuum polarisation results from a transfer of the anisotropy on the EVDF (and hence the directed motion of electrons) into partially polarised recombination radiation as it did for aluminium plasmas. The partial polarisation of line emission arises from a non-statistical distribution of the relevant atomic (or ionic) population amongst the magnetic sub-levels. Once again, as recombination appears to be a significant radiation process in the plasma, it is suggested that the imbalance amongst the m-sublevels of the upper state of the relevant transitions, arises from the anisotropy in the EVDF.

B.1 Introduction

In this appendix, the polarised emission from laser produced Cu plasmas at a central wavelength of 512 nm is discussed for two low pressures. The same spectral windows and fluence are used to investigate the plasma emission for different time delays and pressures. The dominant mechanisms that can explain the observed partial polarisation effect for the Cu continuum and line emission are studied and correlated with the plasma parameters (electron density and temperature). In a laser produced plasma both background continuum emission [1] and the discrete line emission can be partially polarised [2], [3]. The broadband continuum partial polarisation can be explained on the basis of an anisotropic electron velocity distribution [4]. On the other hand, the existence of population imbalances in the magnetic sublevels is used to explain the partial polarisation of line emission [5].

Here the degree of polarisation is quantified for Cu plasmas at a central wavelength of 512 nm for both the line and the nearby continuum emission at pressures of 1×10^{-2} and 1×10^{-5} mbar. The plasma parameters were determined using the Stark broadening for electron density and the Boltzmann plot method for the electron temperature.

B.2 Experimental setup

The experimental setup is the same as that used in Chapter 4**.** A Spectron^{TM} laser (wavelength = 1064 nm, pulse duration = 14 ns) was used to ablate a Cu target (99.99% pure). The ablation fluence was varied from 127-889 J/cm^2 (corresponding laser irradiance of 9-63 GW/cm^2). The system was calibrated to account for a polarisation dependent efficiency in the spectrometer. This was achieved by imaging a small pinhole illuminated with unpolarised light through the system. This allowed for correction of the polarisation sensitivity.

B.3 Results and Discussion

B.3.1 Polarisation Emission of Cu Plasma

At a pressure of 1×10^{-5} mbar, broadband continuum with broad super imposed lines dominated for time delays <50 ns following plasma breakdown. More discrete emission lines of atomic Cu were observed during the period 60 - 230 ns following plasma formation. The ionic lines of Cu^+ at 505.89 and 506.7 nm were also observed and exhibited significant Stark broadening. Clear differences in the orthogonally polarised spectra were observed in each panel as shown in **Figure B.1**. The emission lines narrowed significantly in the time delay range 230 - 530 ns. Lines of Cu^0 at wavelengths of 510.554 nm, 515.809 nm and 521.82 nm with weaker intensity difference in the orthogonally polarised spectra were also observed. These transitions are shown in **Table B.1.**

Table B.1: Spectroscopic parameters for Cu^0 (510.554 nm, 515.809 nm, and 521.82 nm) with assignments from the NIST database. Here g_kA_{ki} is the product of transition probability and statistical weight and E is the upper state energy in eV.

Wavelength [nm]	Transition	g_kA_{ki} x10^8 [1/s]	E [eV]
Cu^0 (510.554nm)	$3d^{10}4d\ (^2P^o_{3/2}) \rightarrow 3d^{10}4p\ (^2D_{5/2})$	2	3.82
Cu^0(515.809nm)	$3d^{10}4d\ (^2D_{3/2}) \rightarrow 3d^{10}4p\ (^2P^\circ_{1/2})$	6	6.2
Cu^0(521.82 nm)	$3d^{10}4d\ (^2D_{5/2}) \rightarrow 3d^{10}4p\ (^2P^\circ_{3/2})$	7.5	6.2

At a pressure of 1×10^{-2} mbar, **Figure B.2**, similar observations were made. Pure broadband continuum was observed at earlier time delays <30 ns with superimposed lines appearing only at later times. The degree of polarisation was computed as a function of time delay for the continuum at 505 nm and the line emissions at a characteristics transition Cu^0 at 510.6 nm, 515.3 nm and 521.82 nm as shown in **Figure B.3**. Stronger anisotropy in the continuum polarisation in the range $0.2 < P < 0.4$ was observed at a pressure of 10^{-2} mbar and $0.10 < P < 0.35$ for a pressure of 10^{-5} mbar. However, for line emission the degree of polarisation values were in the range of $-0.15 < P < 0.1$ at a pressure of 10^{-2} mbar while at a pressure of 10^{-5} mbar the degree of polarisation lay in the range $-0.2 < P < 0.1$.

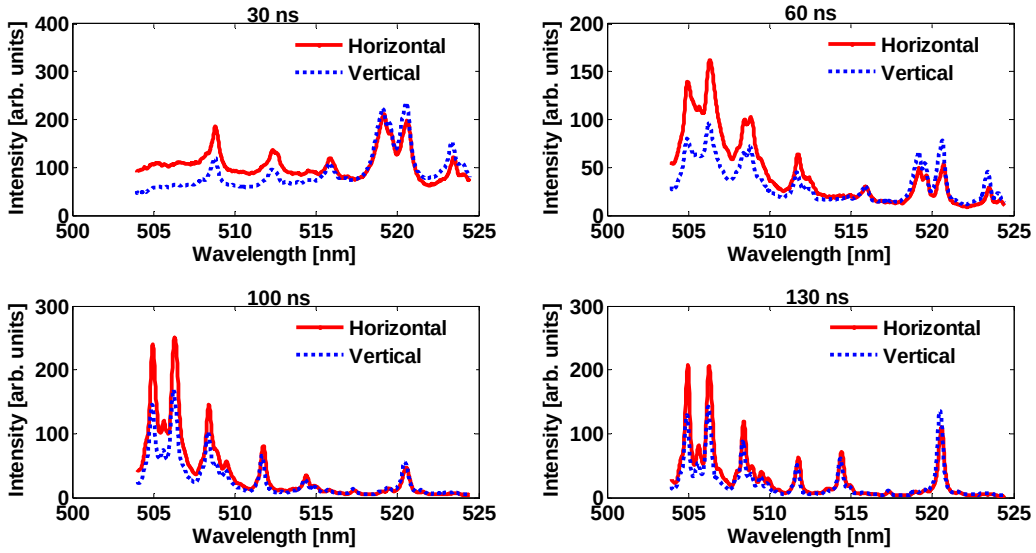

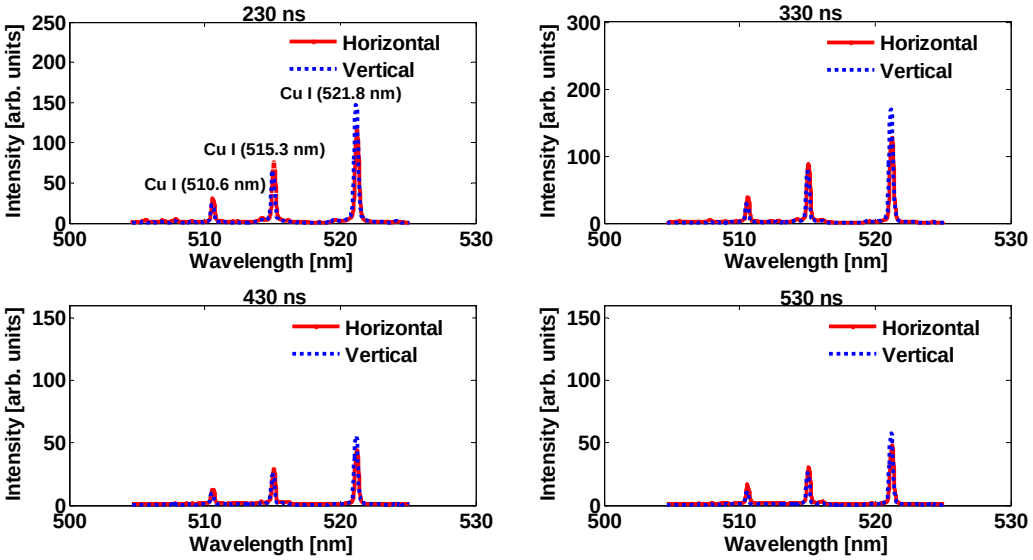

Figure B.1: Polarisation sensitivity calibrated emission spectra of a Cu plasma at a central wavelength of 512 nm at a laser fluence of 550 Jcm^{-2} for a pressure of 10^{-5} mbar. The top four panels show emission in the time delay range 0-130 ns while the lower four panels cover the range 230-530 ns. The time resolution for all was 10 ns.

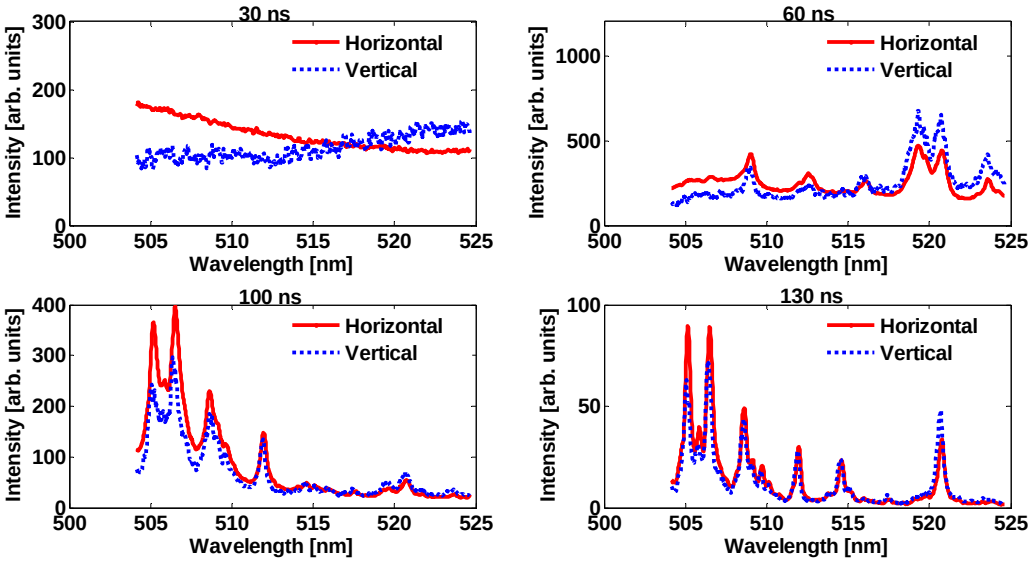

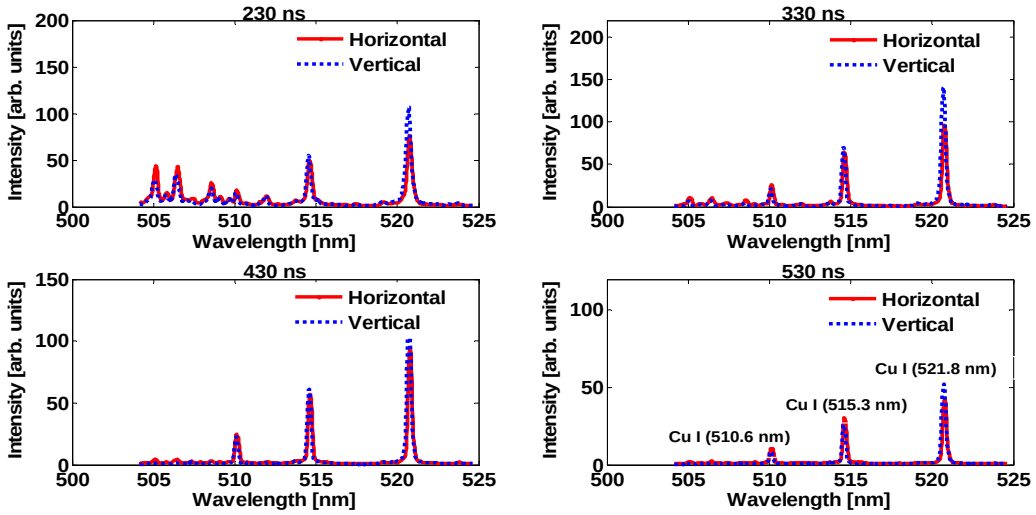

Figure B.2: Polarisation sensitivity calibrated emission spectra of a Cu plasma at a central wavelength of 512 nm at a laser fluence of 550 Jcm^{-2} for a pressure of 10^{-2} mbar. The top four panels show emission in the time delay range 0-130 ns while the lower four panels cover the range 230-530 ns. The time resolution for all was 10 ns.

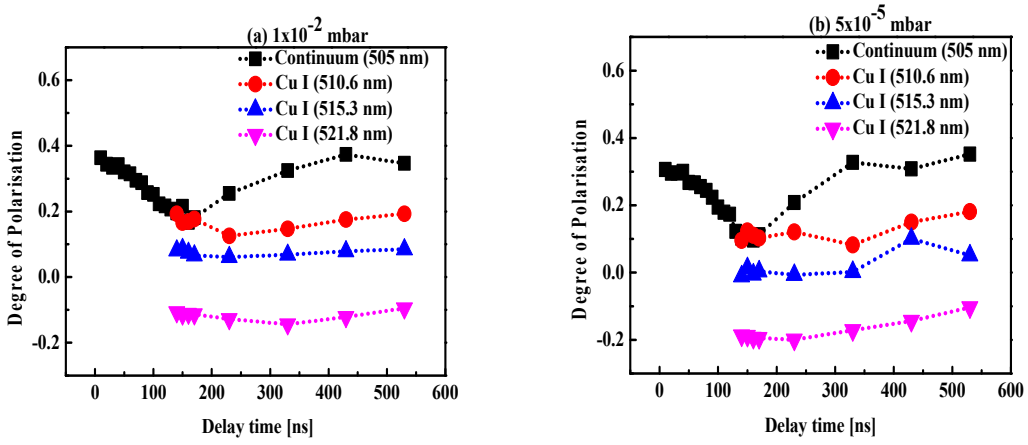

Figure B.3: The degree of polarisation as the function of time delay at a pressure of (a) 10^{-2} mbar and (b) 10^{-5} mbar for a Cu plasma for broadband continuum (at a wavelength of 505 nm) and line emission.

B.3.2 Electron Density and Temperature

To determine the electron density, Stark broadening of an isolated line at 521.8 nm was employed. A Voigt profile was fitted to this spectral line in the time delay interval of 140-530

ns following plasma breakdown. As mentioned in the experimental chapter, the instrumental resolution was 0.17 nm FWHM. Keeping this value for the Gaussian component, the Lorentzian width (FWHM) was determined. This value was used to determine the electron density using equation (**4.3**). **Figure B.4** shows the decay of the electron density with time delay. The density for the horizontally and vertically polarised spectra are minimally different for the studied pressures. The density at a pressure of 10^{-2} mbar was significantly less than the density at 10^{-5} mbar.

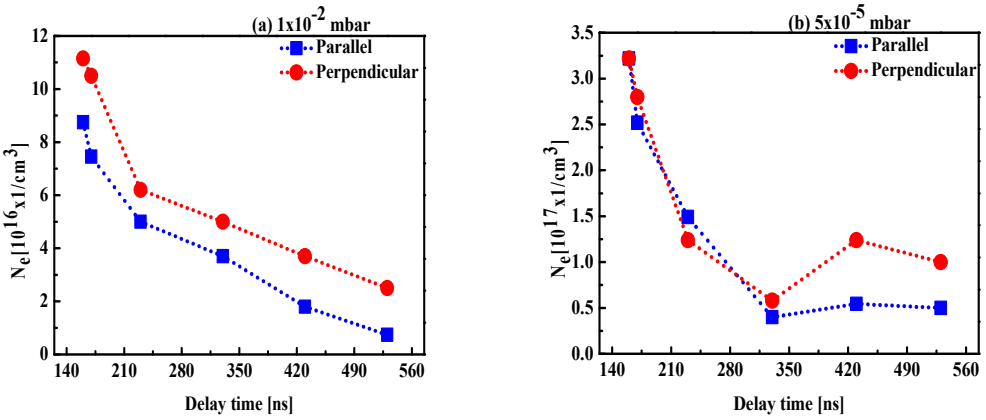

Figure B.4: Electron density estimated using the Cu I (at 521.8 nm) line.

The Boltzmann plot method was used to determine the temperatures of the orthogonal polarised states from the neutral emissions of Cu^0 of 520.6, 515.3 and 521.8 nm respectively using equation (**2.32**). It is clear that the two temperatures are different indicating an anisotropic EVDF and hence an anisotropy in the polarisation of radiation emitted in electron collisional processes.

The sources of the continuum emission are free-free electronic transitions (Bremsstrahlung radiation) and/or free-bound electronic transitions (radiation recombination). On the other hand, the line emission is due to bound to bound transitions within excited atoms or ions in the plasma [6]. It has been proposed previously that the continuum polarisation is due to an anisotropy in the EVDF which when the electrons recombine with ions in the plasma they transfer their directed motion into an anisotropy in the polarisation of the recombination

radiation emitted [7]. The line polarisation emission is usually based on a non-statistical imbalance of magnetic sublevels of the atoms and ions in the upper states [6].

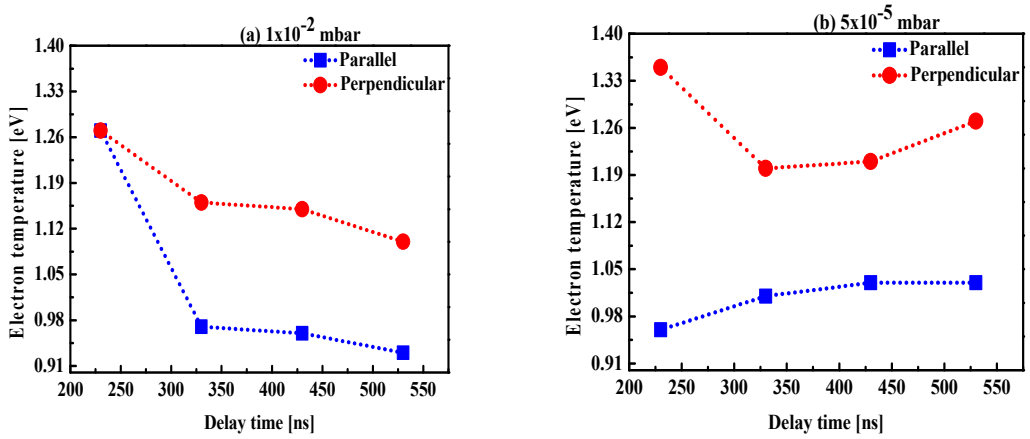

Figure B.5: Electron temperature determined from Boltzmann plot of Cu I (at 510.6, 515.3 and 521.8 nm).

The calculated electron-electron and electron-ion thermalization times for Copper plasmas equations (2.29) & (2.30) were found to be t_{ee}≈280 ps and t_{ei}≈47 ps respectively. The electron density from equation (4.2) is n_e≈10^{17} cm^{-3}, the electron temperature in Figure B.5 is T_e≈1.3 eV and the ionisation energy of atomic Cu is E_I=7.7264 eV were used to calculate t_{ee} and t_{ei}. This indicated that a good thermalization is expected for the target materials at a laser pulse duration ≈14 ns used in our experiment. This indicates that collisional excitation is likely to be a less probable cause for the polarised emission for Cu at low charge states in lower atmospheric pressure as the electron density and temperature are too low.

B.4 Conclusion

In summary, the polarisation of atomic lines and the nearby continuum emitted by Cu plasmas at a central wavelength of 512 nm was studied using time and polarisation resolved emission spectroscopy. The dominant mechanism for the continuum and line polarisation are suggested to radiative recombination combined with an anisotropic EVDF.

References

[1] A. Eslami Majd, A. S. Arabanian, and R. Massudi, “Polarization resolved laser induced breakdown spectroscopy by single shot nanosecond pulsed Nd:YAG laser,” *Opt. Lasers Eng.*, vol. 48, no. 7–8, pp. 750–753, 2010.

[2] J. Kim and D. E. Kim, “Measurement of the degree of polarization of the spectra from laser produced recombining Al plasmas,” *Phys. Rev. E - Stat. Nonlinear, Soft Matter Phys.*, vol. 66, no. 1, pp. 1–4, 2002.

[3] A. K. Sharma and R. K. Thareja, “Anisotropic emission in laser-produced aluminum plasma in ambient nitrogen,” *Appl. Surf. Sci.*, vol. 253, no. 6, pp. 3113–3121, 2007.

[4] J. C. Kieffer, J. P. Matte, M. Chaker, Y. Beaudoin, C. Y. Chien, S. Coe, G. Mourou, J. Dubau, and M. K. Inal, “X-ray-line polarization spectroscopy in laser-produced plasmas,” *Phys. Rev. E*, vol. 48, no. 6, pp. 4648–4658, 1993.

[5] K. B. C. Nore´n and J. W. McConkey, P. Hammond, “Near-threshold study of the polarization of He resonance radiation using an energy-selected electron beam,” *Phys. Rev. A*, vol. 53, no. 5, pp. 2249–2252, 1996.

[6] J. S. Penczak, Y. Liu, and R. J. Gordon, “Polarization-resolved laser-induced breakdown spectroscopy,” *Opt. Lett.*, vol. 34, no. 4, p. 494, 2009.

[7] H. M. Milchberg and J. C. Weisheit, “Polarization of recombination radiation from nonequilibrium plasmas,” *Phys. Rev. A*, vol. 26, no. 2, pp. 1023–1029, 1982.

C. Time Integrated Polarisation Emission from Aluminium Laser Produced Plasmas

The partially polarised emission from an Aluminium (Al) laser produced plasma has been studied using time integrated spectroscopy. It was achieved by placing a dichroic polariser in front of a time integrated optical spectrometer and the results have been interpreted in the frame work of a radiatively recombining plasma. We find that the plasma emission exhibits a small but distinct polarisation anisotropy. Depending on the power density of the incident laser we find that either the line emission or the continuum exhibit a greater polarisation effect. In the work presented here, we present results which show strongly polarised line emission.

C.1 Introduction

Laser Induced Breakdown Spectroscopy (LIBS) is a widely used analytical technique for detection and characterization of materials [1]. The polarisation of both the discrete line emission and the continuum has been studied before in elements like Cu [2] and Al [2]–[4]. The polarisation of the line emission is generally ascribed to an asymmetry in the populations of the magnetic sublevels in the transition under study [5]. Continuum emission polarisation in nanosecond laser produced plasmas is generally ascribed to an anisotropy in the electron distribution function [4], [5]. Previous studies have indicated that, depending on the intensity regime, either the lines or the continuum will exhibit a stronger degree of polarisation [3], [6]. This means that in a polarisation resolved experiment, the continuum can be suppressed to a greater degree than the line emission which increases the line in continuum ratio. This ratio (often called the signal to background ratio) governs the figure of merit in a LIBS measurement which is called the Limit of Detection (LOD).

In our time-integrated experiment, we observed that the line emission is more strongly polarised than the continuum. We have studied in detail also the polarisation of the emission of radiation for both the continuum and selected line emission from an Al plasma. Namely,

Al^0 (394.4 nm and 396.15 nm), Al^+(466.3 nm) and Al^{2+} (569.6 nm and 572.3 nm) in the optical spectral range. Specifically, we have investigated the dependence of the degree of polarisation of emission on the laser fluence, position of the plasma and the background gas pressure.

C.2 Experimental

Figure C.1 shows the experimental setup used in this work. Briefly, a Q-switched Nd: YAG laser (from the Spectron™ Laser System, pulse width 14 ns, 1064 nm at a repetition rate of 10 Hz) was focused normal to the target by a planocovex lens (f = 220 mm) onto an Al target (99.99% pure) to produce the plasma. The target was housed in a square chamber to facilitate experiments under vacuum. It was mounted on a high precision x-y-z translation stage so that a fresh surface was revealed for each measurement. The plasma formed was imaged normal to the incident laser beam direction. The plasma radiation was collected, collimated and then focused onto an optical fibre which was coupled to the spectrometer using a pair of convex lenses with focal length (f_1 = 100 mm and f_2 = 170 mm). A dichroic polariser was placed before the fibre optic to select a particular polarisation state. The spectrometer (StellarNet™ EPP200 Spectrometer, with a toroidal grating of 1200 g/mm, resolution = 0.3 nm) was set at an integration time at 100 ms. For all the measurements performed the dark current background of the detector was subtracted from the measured spectroscopic data.

In our experiment, we compared spectra with no polariser in place (called LIBS spectra) with spectra where a polariser was placed in front of the spectrometer (called PRLIBS spectra). The degree of polarisation is given by:

$$P_\lambda = \left(\frac{I_{//} - I_\perp}{I_{//} + I_\perp} \right) \tag{C.1}$$

Where $I_{//}$ is an intensity of the light parallel to the incident laser propagation axis and $I_\perp$ is the intensity perpendicular to the incident laser propagation axis.

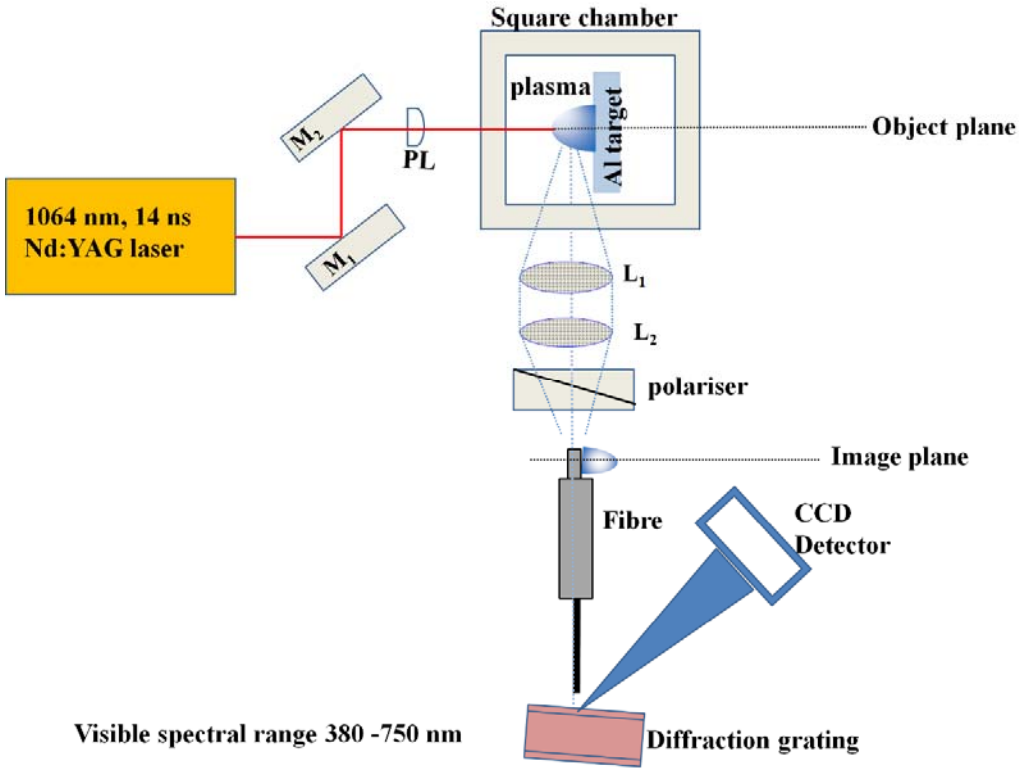

Figure C.1: Schematic diagram of PRLIBS (M, mirror; PL, planoconvex lens; L, lens).

C.3 Results and Discussions

C.3.1 Time Integrated LIBS and PRLIBS

Figure C.2 displays the time integrated LIBS and PRLIBS optical emission spectra of an Al plasma. The plasma was produced in air ambient at a pressure of 10^{-2} mbar. The spectra were recorded from a spatial region approximately 1 mm away from the target surface at a laser fluence of 600 J/cm^2. The spectra display a mix of lines (neutrals and ions) superimposed on a continuum background. They also exhibit the dominance of ionic over neutral emission. The PRLIBS spectrum was produced by placing the dichroic polariser at 0^0. In this case, we state that vertically polarised plasma radiation can pass through it. This experimental result is consistent with the study by with Kim et al. [4]. However, we note that the time integrated PRLIBS spectra shown in [7] do not coincide with [5].

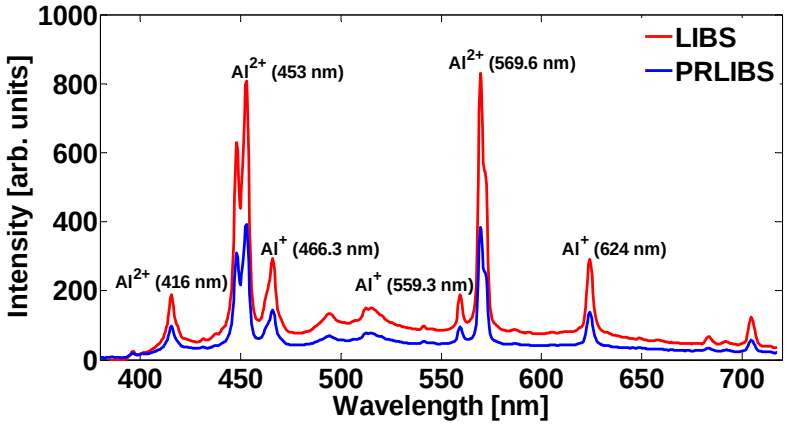

Figure C.2: LIBS and PRLIBS spectrum at a laser fluence of 600 J/cm^2 at a pressure of 10^{-2} mbar.

C.3.2 Effect of Laser Fluence on Polarisation

Figure C.3 displays time integrated orthogonal polarisation resolved emission from an Al plasma created by nanosecond pulses with energies of 25, 60 and 180 mJ respectively at a background pressure of 1x10^{-2} and an integration time of 100 ms. There is a clear variation (anisotropy) in the intensity of the emission for horizontal to the vertical polarisation for the lines Al^{2+} (at 453 nm), Al^{+} (at 466.3 nm), and Al^{2+} (at 569.6 nm).

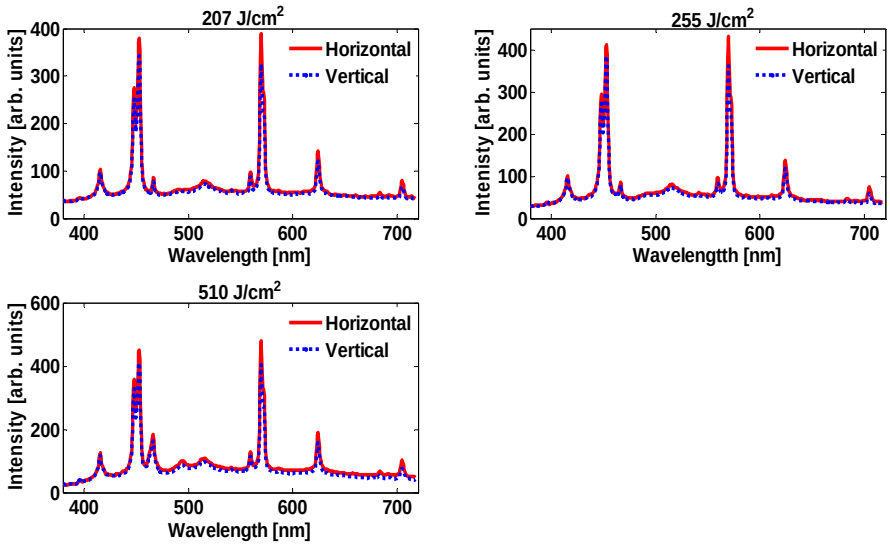

Figure C.3: (a) the PRLBS spectrum for vertical and horizontal polarisation and (b) Polarisation spectrum at a laser fluence of 600 J/cm^2 at a pressure of 1x10^{-2}mbar.

Figure C.4 shows the variation in the degree of polarisation (P) with laser irradiance. Singly and doubly charged ions are present and it is clear that the wavelength integrated value of P for the continuum varies most with laser fluence, consistent with time resolved measurements.

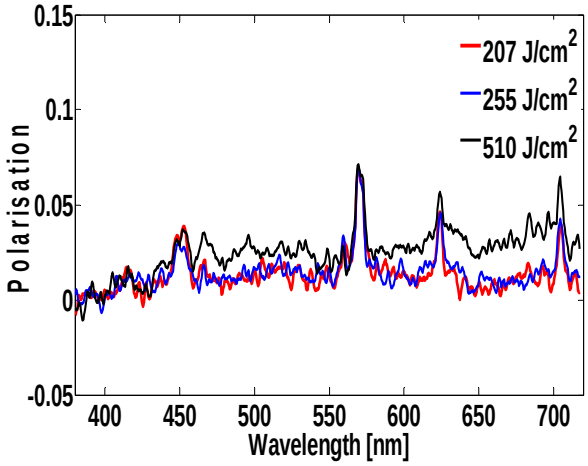

Figure C.4: The polarisation emission spectrum as a function of laser irradiance.

Figure C.5 displays the degree of polarisation P as a function of laser irradiance at a pressure of 10^{-2} mbar. P was extracted for the continuum at 600 nm, line emissions of Al^0 (at 396.15 nm), Al^+ (at 466.3 nm) and Al^{2+} (at 569.6 nm) respectively for different laser irradiance values. Our results show that at a pressure of 10^{-2} mbar, the degree of polarisation increases with the charge state, at least for the specific atomic or ionic lines under study. This is interpreted in the frame work of alignment of ions due to self-generated electric and magnetic fields within the plasma plume. This result is consistent with Kim et al. [4] and Sharma et al.[8] for Al^{2+} polarisation emission.

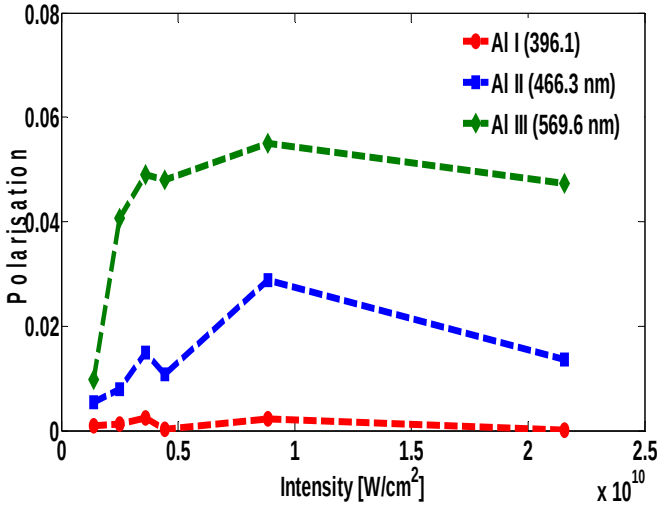

Figure C.5: Effect of laser fluence on the LIBS and PRLIBS at minimum transmission at a pressure of 1x10^{-2} mbar at a fluence of 1146 J/cm^2, 950 J/cm^2 and 790 J/cm^2.

C.3.3 Effect of Background Gas Pressure on Polarisation Emission

Figure C.6 shows the spectrally resolved degree of polarisation (P) as a function of background gas pressure. The value of P grows with background pressure. In the atmosphere, the plasma is confined by air which enhances the emission lifetime of the plasma [3]. However, in vacuo, the plasma particles expand freely resulting in less energy in absorption from the incident laser energy and a reduction in the number of particles available for collisional reheating [9]. It is likely that the additional free electrons from the air plasma increase the recombination rate and hence the recombination continuum and the density of excited ions and atoms which decay by line emission. In addition, the anisotropy in the EVDF (increasing the values of P) appears to be enhanced in the gas-plasma collision.

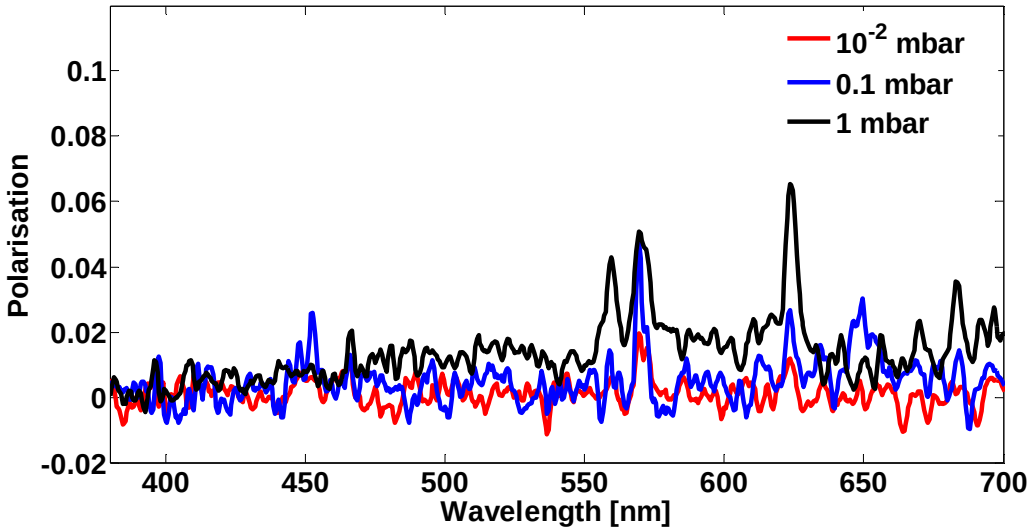

Figure C.6: Polarisation as a function of background pressure.

C.4 Conclusion

Time integrated spectra of Al laser produced plasma, where all radiation emitted is captured, show that discrete emission is more polarised than the continuum emission. We have compared the degree of polarisation of the Al^0 (396.15 nm), Al^+ (at 466.3 nm) and Al^{2+} (569.6 nm) measured at a pressure of 10^{-2} mbar. Al^0 is observed to be more weakly polarised compared to Al^+ and Al^{2+}.

References

[1] D. W. Hahn and N. Omenetto, "Laser-Induced Breakdown Spectroscopy (LIBS), Part II: Review of Instrumental and Methodological Approaches to Material Analysis and Applications to Different Fields," *Appl. Spectrosc.*, vol. 66, no. 4, pp. 347–419, 2012.

[2] A. K. Sharma and R. K. Thareja, "Characterization of laser-produced aluminum plasma in ambient atmosphere of nitrogen using fast photography Characterization of laser-produced aluminum plasma in ambient atmosphere of nitrogen using fast photography," *A*, vol. 4490, no. 2004, 2004.

[3] Y. Liu, J. S. Penczak, and R. J. Gordon, "Nanosecond polarization-resolved laser-induced breakdown spectroscopy.," *Opt. Lett.*, vol. 35, no. 2, pp. 112–114, 2010.

[4] J. Kim and D. E. Kim, "Measurement of the degree of polarization of the spectra from laser produced recombining Al plasmas," *Phys. Rev. E - Stat. Nonlinear, Soft Matter*

Phys., vol. 66, no. 1, pp. 1–4, 2002.

[5] Jaehoon Kim and Dong-Eon Kim, "Study of The Anisotropy of Electron Energy Distribution Ionized Oxygen Plasma by using Polarization Spectroscopy," *J. Opt. Soc. Korea*, vol. 7, no. 3, pp. 145–149, 2003.

[6] J. S. Penczak, Y. Liu, R. D. Schaller, D. H. Rich, and R. J. Gordon, "The mechanism for continuum polarization in laser induced breakdown spectroscopy of Si(111)," *Spectrochim. Acta - Part B At. Spectrosc.*, vol. 74–75, pp. 3–10, 2012.

[7] J. S. Penczak, Y. Liu, and R. J. Gordon, "Polarization-resolved laser-induced breakdown spectroscopy," *Opt. Lett.*, vol. 34, no. 4, p. 494, 2009.

[8] A. K. Sharma and R. K. Thareja, "Anisotropic emission in laser-produced aluminum plasma in ambient nitrogen," *Appl. Surf. Sci.*, vol. 253, no. 6, pp. 3113–3121, 2007.

[9] D. Zhao, N. Farid, R. Hai, D. Wu, and H. Ding, "Diagnostics of First Wall Materials in a Magnetically Confined Fusion Device by Polarization-Resolved Laser-Induced Breakdown Spectroscopy," *Plasma Sci. Technol.*, vol. 16, no. 2, pp. 149–154, 2014.

D. Comparison of LIBS and PRLIBS emission spectra for Al Alloy

Time and polarisation resolved optical emission spectroscopy from laser produced plasmas of Al alloys have been studied in the visible spectral range at a background pressure of 10^{-4} mbar. A comparative experimental investigation is done on the laser induced breakdown spectroscopy (LIBS) and polarisation resolved LIBS (PRLIBS) spectra. The polarised emission is obtained by placing a dichroic polariser in front of a time resolved Echelle optical spectrometer equipped with ICCD readout and the results have been interpreted in the frame work of a radiatively recombining plasma. The signal to background ratio (SBR) is increased significantly for the PRLIBS compared to the LIBS spectra. In addition, the degree of polarisation is quantified for Al^0 (at 396.15 nm) and Al^{2+} (569.6 nm) lines by using unpolarised lines close by. The plasma parameters are measured and compared to the degree of polarisation to determine the dominant mechanism for the polarised emission.

D.1 Introduction

Laser Induced Plasma Spectroscopy (LIBS) is a widely used analytical technique for the characterization of materials [1]–[3]. Polarisation resolved laser induced plasma can be potentially used as an alternative way to gated LIBS. It a simple way to potentially suppress the background continuum emission and increase the signal to background ratio for the classification and quantification of elements in materials [4], [5]. In a laser produced plasma anisotropies in the polarisation of emitted radiation can occur [6]. In some cases, the background broadband emission is found to be polarised [5], [7] and in other cases, the discrete line emission is found to be polarised [8]. However, these studies focussed on narrow spectroscopic windows and very little has been reported on the mechanisms that lead to anisotropies in the line emission. The nature of the continuum anisotropy is attributed to anisotropies in the electron velocity distribution function (EVDF) which leads to a bi-Maxwellian velocity distribution for the free electrons. The line emission is polarised due to

an imbalance of populations of the magnetic subshells which can be also due in part of an anisotropic EVDF.

In this study, we present results from a time resolved plasma polarisation spectroscopy at a background pressure of 1×10^{-4} mbar in the visible spectral range. Time and polarisation resolved optical spectroscopy was used to quantify the plasma parameters and correlate with the degree of polarisation of the neutral (at 396.15 nm) and ionic (at 569.6 nm) emission. The main mechanism of the polarisation effect observed is discussed. The SBR for the LIBS and PRLIBS spectra are quantified for low pressure and temperature plasmas.

D.2 Experimental Setup

Figure D.1 shows the time resolved PRLIBS setup to track the plasmas evolution with time. A BRIO^{TM} Nd:YAG laser, operating at 1064 nm was used to ablate the target, with a laser fluence of 223 Jcm^{-2} (corresponding to an irradiance of 5.6×10^{10} Wcm^{-2}) at a pulse duration of 4 ns with a repetition rate of 20 Hz. The intensity of the laser was varied using a combination of a half-wave plate and a polariser. A well-calibrated energy meter was used before and after each measurement to ensure the correct reading of the laser pulse energy. For this experiment, the laser was focused normal to the target using a planoconvex lens (f = 100 mm) onto an Al alloy target to produce the plasmas. The target was mounted on a micrometer controlled x-y-z translation stage in a sealed vacuum chamber at a background pressure of 10^{-4} mbar. This ensured that a fresh target spot could be revealed after each laser shot. The light emitted was imaged normal to the laser propagation axis by a C52 ANDOR^{TM} optical head (with a focal length of f = 150 mm to ∞) and then focused on to a 2m long fused silica fiber with a core diameter of 50 µm connected to an Echelle spectrometer ESA^{TM} 4000 spectrometer (LLA, GmbH, Berlin, Germany) equipped with an ICCD detector (Kodak^{TM} KAF 1001 camera). The spectrometer operated in the wavelength range of 200-700 nm with a spectral resolution $\lambda/\Delta\lambda \approx 20{,}000$. An OG3 (from OML^{TM} SKAWINA) Al alloy of circular disc target was used for the experiments. The concentrations of these alloys are shown in **Table D.1**.

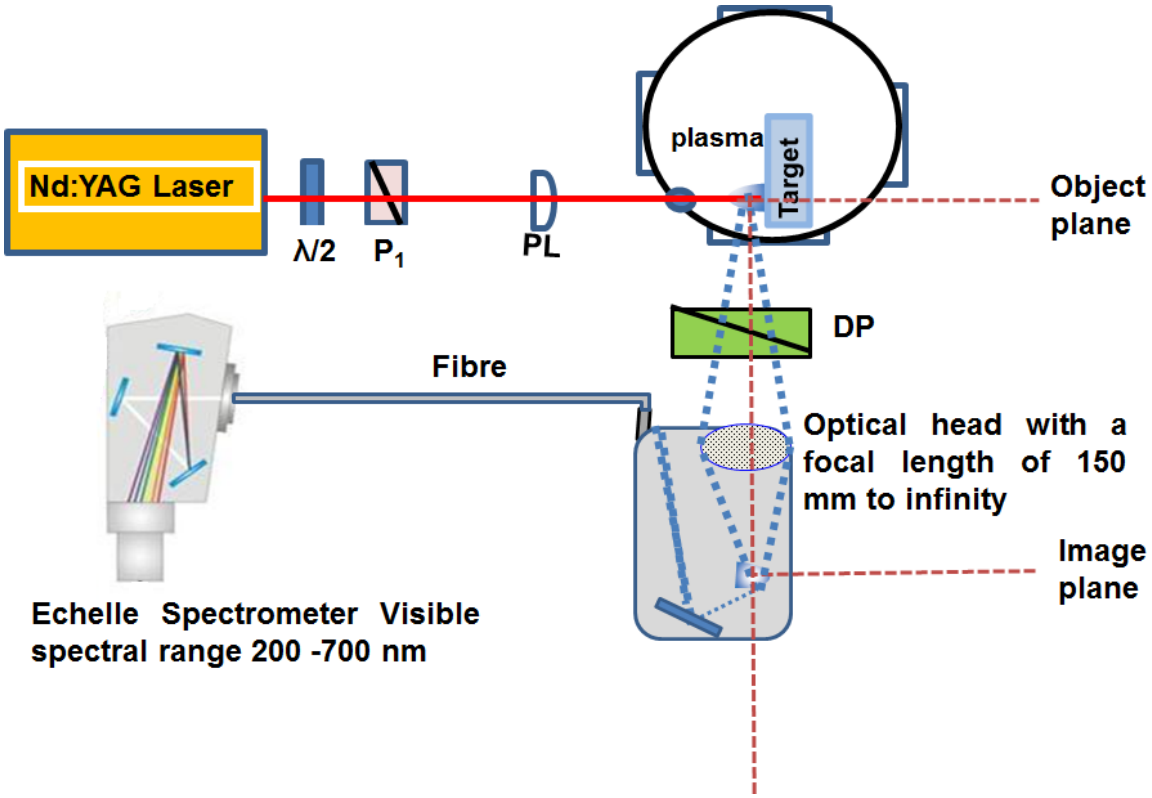

Figure D.1: Schematic diagram of TRLIBS (λ/2, half-wave plate; P_1, polariser; PL, planoconvex lens; DP, dichroic polariser).

Table D.1: A circular disc of an OG series standard (OML™ SKAWINA) OG3 Al alloy of different concentrations (in w/w %).

Elements	OG3
Cu	4.3
Mg	0.34
Ti	0.18
Fe	0.29
Si	0.27
Zn	0.2
Mn	0.08
Ni	0.04
Al	94.3

The measurements were performed at a gate width of 500 ns and a time delay of 50 ns respectively. In this experiment, we compared spectra with no polarizer in place (called LIBS spectra) with spectra where is polarizer is placed in front of the spectrometer (called PRLIBS spectra). The degree of polarization is found by:

$$P_{\lambda} = \left(\frac{I_H - I_V}{I_H + I_V} \right) \tag{D.1}$$

Where I_H is an intensity of the light parallel to the incident laser propagation axis and I_V is the intensity perpendicular to the incident laser propagation axis.

D.3 Results and Discussion

D.3.1 Emission from Laser Produced Plasmas

Figure D.2 shows a single shot time resolved optical emission spectra from an Al alloy plasma produced by a laser pulse energy with an of 70±3 mJ (corresponding fluence of 223±10 Jcm^{-2}) at a background pressure of 10^{-4} mbar in the visible spectral range. The spectra are averaged over 10 single shots for plasmas formed on an OG3 series circular disc standard target. The plasma emission was taken at approximately 1 mm away from the target surface at a gate width of 500 ns and a time delay of 50 ns.

Figure D.2 shows the comparison of LIBS and PRLIBS spectra for the wavelength range 380-600 nm. Each spectrum comprises Al^{2+}, Al^{+} and Al^{0} lines superimposed on broadband continuum. The dominant lines observed are Al^{0} (at 394.4 nm), Al^{0} (at 396.15 nm), Al^{2+} (at 452.9 nm), Al^{+} (at 466.3 nm), Al^{+} (559.3 nm) and Al^{2+} (at 569.6 nm) respectively. The corresponding the spectroscopic parameters and electronic transitions of the ionic and neutral line emissions are given in **Table D.2**. The assignments were made by data taken from the NIST database.

Table D.2: Spectroscopic parameters for Al^0 (at 394.4 nm and 396.15 nm), Al^+ (at 466.3 nm), and Al^{2+} (at 569.6 nm and 572.3 nm) with assignments from the NIST database. Here g_kA_{ki} is the product of transition probability and statistical weight and E is the upper state energy in eV.

Wavelength [nm]	Transition	$g_kA_{ki} \times 10^8$ [1/s]	E [eV]
Al^0 (394.4, 396.15 nm)	4s ($^2S_{1/2}$) →3p ($^2P^0_{1/2,3/2}$)	1.2	3.14
Al^{2+} (414.99 nm)	$3p^6 5f$ ($^2P^o_{7/2}$) → $2p^6$ 4d($^1D_2$)	16.4	23.54
Al^+ (466.3 nm)	3s 4p ($^1P^o_1$) →$3p^2$ ($^1D_2$)	1.74	13.26
Al^{2+} (452.9 nm)	$2p^6$4d($^2P_{5/2}$) →$2p^6$ 4p($^2P^o_{3/2}$)	14.9	20.55
Al^+ (458.97 nm)	3s7f($^3F^o_4$) →3s4d($^3D_3$)	0.078	17.765
Al+ (559.3302 nm)	3s4d$^1D_2$ → 4s4p$^1P^o_1$	4.63	15.47
Al^{2+} (569.6 nm, 572.3 nm)	4p ($^2P^o_{3/2,1/2}$) → 4s ($^2S_{1/2}$)	3.51, 1.73	17.82

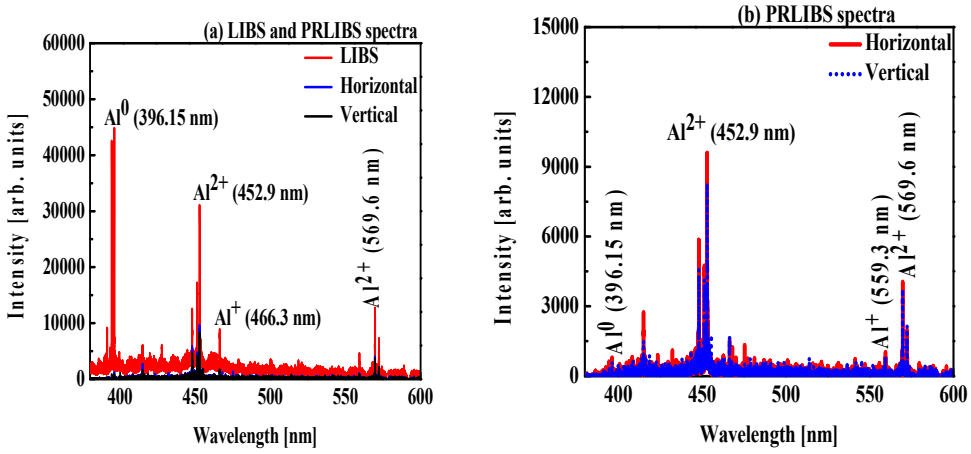

Figure D.2: The LIBS and PRLIBS spectra of an Al alloy (OG3) for a laser pulse energy of 70 mJ at a background pressure of 10^{-4} mbar. The laser fluence was 223 J/cm^2 with an ICCD camera gate width of 500 ns.

D.3.2 Electron Density and Temperature

An optical spectroscopic method was used to determine two plasma parameters (density and temperature). An isolated line of an Al^+ (at 466.3 nm) was used to estimate the electron

density. This line is broadened by Stark effect as the result of the interaction of the Al^+ with electrons. The FWHM of the stark broadened line is given by [9]:

$$\Delta\lambda_{stark} = 2w\frac{n_e}{10^{16}} + 3.5A\frac{(n_e)^{1/4}}{10^{16}} + \left[1 - BN_D^{-1/3}\right]w\frac{n_e}{10^{16}} \quad \text{(D.2)}$$

The approximate value of the linewidth for such an isolated line is given by [9] :

$$\Delta\lambda_{1/2} \approx \frac{2wn_e}{10^{16}} \quad \text{(D.3)}$$

Where $\Delta\lambda_{1/2}$ is the Stark width, w=0.0615 nm at half width is the electron impact parameter for the Al^+ at a wavelength 466.3 nm line for a temperature of 10,000 K [10] and n_e is the electron density respectively. **Figure D.3** shows the LIBS and PRLIBS spectrum with the Al^+ line at a wavelength of 466.3 nm.

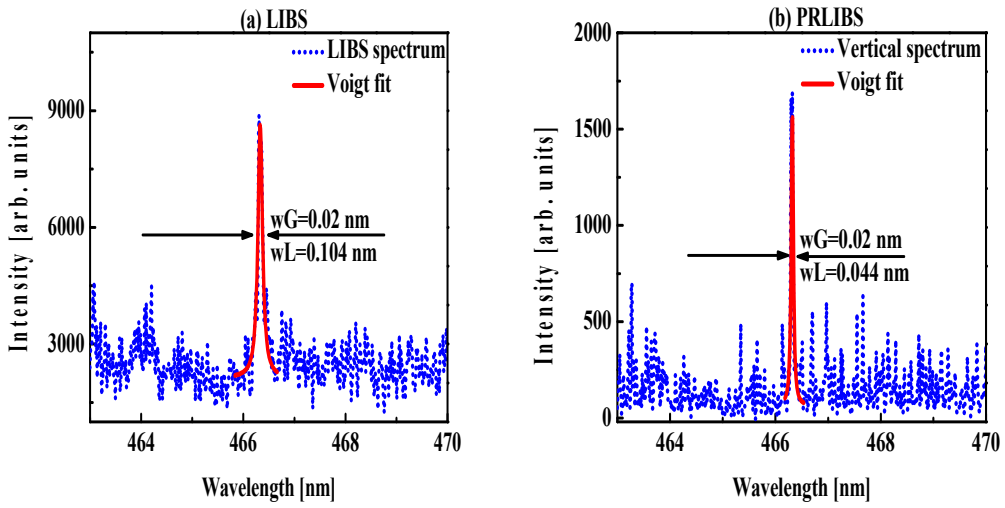

Figure D.3: The Voigt fits for the (a) LIBS and (b) PRLIBS spectra showing Al^+ (at 466.3 nm) for a time delay of 60 ns at a background pressure of 1×10^{-4} mbar. The laser fluence was 223 J/cm^2 with an ICCD camera gate width of 500ns.

This spectral line was fitted using a Voigt profile which is a convolution of the Gaussian (at 0.02 nm at FWHM) and the Lorentzian profile. The Lorentzian component of the profile was used to estimate the electron density in this study. The estimated densities were approximately 1.7×10^{16} cm^{-3} for the LIBS and 0.7×10^{16} cm^{-3} for the PRLIBS spectra respectively.

D.3.3 Electron Temperature

Assuming LTE, the temperature can be calculated from the intensity ratio of the pair of spectral lines that originate from different ion stages of the same element. The intensity ratio is related to the basic atomic parameters by the equation [9]:

$$\frac{I_1}{I_2} = \left(\frac{A_1 \lambda_2 g_1}{A_2 \lambda_1 g_2} \right) e^{-\frac{E_1 - E_2}{k_B T_e}} \tag{D.4}$$

where I_1 and I_2 are the relative intensities of the emitted lines, A_1 and A_2 are the corresponding transition rates in units of sec^{-1}, g_1 and g_2 are the statistical weights of the levels involved, i.e., $2J+1$ where J is the total angular momentum, and E_1 and E_2 the energies of those states. From equation (D.4) the electron temperature can be determined from the line ratio:

$$\ln\left(\frac{I_1}{I_2} \right) = \ln\left(\frac{A_1 g_1 \lambda_2}{A_2 g_2 \lambda_1} \right) - \left(\frac{E_1 - E_2}{k_B T_e} \right) \tag{D.5}$$

The intensity ratio from an Al^+ at a wavelength of 559.323 nm and Al^{2+} at a wavelength of 569.6 nm were used to quantify the plasma temperature from the LIBS and PRLIBS spectra. The summed intensity obtained by taking the area under the profile of each of these lines is given in **Table D.3**.

Table D.3: LIBS and PRLIBS total line intensities obtained by determining the area under each spectral line.

Spectrum	LIBS	Horizontal	Vertical
Al^+ (559.323 nm)	31144	5746	5564
Al^{2+} (569.6 nm)	211208	49182	39216

Using table 2 and substituting into equation (5) the LIBS spectrum temperature determined to be 1.1±0.3 eV. The horizontal and vertical PRLIBS spectra temperature values were 1±0.4 eV and 1.05±0.25 eV respectively.

In order to check the validity of the assuming LTE in the plasma the McWhirter criterion [11], [12] was used. This equation is given by:

$$n_e \geq 1.6 \times 10^{12} T_e^{1/2} \left(E_1 - E_2 \right)^3 \tag{D.6}$$

Where here n_e is the electron density, T_e is the electron temperature, E_1 is the upper state energy of Al^+ at a wavelength of 559.3 nm and E_2 is the upper state energy of Al^{2+} a wavelength of 569.6 nm respectively. Using equation D.6, n_e is estimated to be 2.9×10^{15} cm^{-3} which is less than the electron density obtained experimentally. Consequently, the McWhirter criterion is satisfied and the assumption of LTE to estimate plasma parameters [11], [12] is valid.

D.3.4 Polarisation Resolved Spectra

Figure D.4 shows a comparison of the LIBS and PRLIBS spectra where The Al^0 (at 394.4 and 396.15 nm) and Al^{2+} (at 569.6 and 572 nm) lines are present. It is known from Kim et al. [6], Sharma et al. [8] and Wubetu et al. [13] that the 394.4 and 572.3 nm lines are unpolarised. The normalized degree of polarisation of the 396.15 nm wavelength line can be re-written as from equation (1) is given by:

$$P_\lambda = \left(\frac{\left(\frac{\sum I_H^{396.15nm}}{\sum I_H^{394.4nm}} \right) - \left(\frac{\sum I_V^{396.15nm}}{\sum I_V^{394.4nm}} \right)}{\left(\frac{\sum I_H^{396.15nm}}{\sum I_H^{394.4nm}} \right) + \left(\frac{\sum I_V^{396.15nm}}{\sum I_V^{394.4nm}} \right)} \right) \tag{D.7}$$

The degree of polarisations using equation (D.7) were -0.07±0.02 for the 396.15 nm Al neutral line and 0.1±0.03 for the 569.6 nm Al^{2+} line respectively. The negative sign for the 396.15 nm line was due to the S to P transitions and for the 569.6 nm line, the sign is positive as it is a P to S bound to bound transition (**Table D.2**).

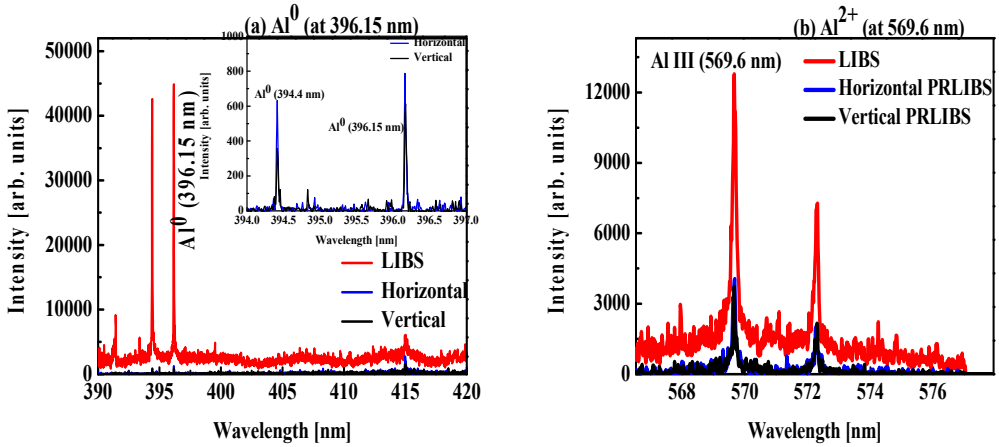

Figure D.4: Comparison of the LIBS and PRLIBS spectra produced at a laser pulse energy of 70 mJ. The spectra were taken at a time window of 500 ns and delay of 50 ns.

D.3.5 Comparison of SBR

Here the signal-to-background ratio (SBR) of the Al^0 (at 396.15 nm) and Al^{2+} (at 569.6 nm) lines are compared for the LIBS and PRLIBS spectra. Farid et al. [14] reported the SBR using the peak intensity of the signal and average intensity of the background. However, in our study to minimize the error the area under the curve of the signal intensity and the summation of the background intensities are used to extract the SBR. The equation to calculate the SBR is given by:

$$SBR = \left(\frac{\sum I_{signal} - \sum I_{background}}{\sum I_{background}} \right) \tag{D.8}$$

Where $\sum I_{signal}$ is the integrated intensity of the line and $\sum I_{background}$ is the integrated intensity of the background. A significant increase of the SBR for the PRLIBS spectra was observed for both lines as shown in
Table D.4 and **Table D.5.**

Table D.4: LIBS and PRLIBS total line intensities obtained by determining the area under each spectral line along with corresponding background intensities.

Spectrum	LIBS (counts)	Horizontal PRLIBS (counts)	Vertical PRLIBS(counts)
Al^0 (396.15 nm)	298998	2568	2058
Background	51353	222	183

Al^{2+} (569.6 nm)	211208	49182	20334
Background	138838	39216	22953

Table D.5: The SBR of the LIBS and PRLIBS spectra.

SBR	**Al^0 (396.15 nm)**	**Al^{2+} (569.6 nm)**
LIBS	4.82	0.52
Horizontal	10.6	1.42
Vertical	10.2	0.7

D.4 Discussion

The comparison of the SBR of the LIBS and PRLIBS spectra were done. It shows that the SBR was increased significantly by placing a polariser in front of a detector for the plasma formed at low pressure. The emitted degree of the polarisation was quantified for the Al^0 neutral and Al^{2+} ionic emission. Based on the Kim et al. [6] speculation and Saha equation, the calculated low density and temperature indicated that the upper states could be populated by radiation recombination of Al^+ for the neutral emission (at 396.15 nm) and Al^{3+} for the double ionic emission (at 569.6 nm) to the electrons. These upper state population could then create a population imbalance and lead emission line polarisation [15]. Since the density and the temperature are too low, the radiative interactions are dominant than the collision interactions to be the dominant mechanism for the polarisation effect observed.

D.5 Conclusion

The degree of polarisation was studied for the Al neutral line at a wavelength of 396.15 nm and the Al^{2+} line at a wavelength of 569.6 nm. A time and polarisation resolved Echelle spectrometer was used the visible spectral range for the plasmas formed at lower pressure. P_λ was estimated to be -0.07±0.02 for neutral and 0.1±0.03 for the doublet emission. The SBR was quantified for this emission for both the LIBS and PRLIBS spectra. The PRLIBS spectrum significantly increases the SBR compared to the LIBS spectrum. Spectroscopy was also used to quantify the plasma parameters and the low temperatures obtained indicated that

the polarisation effect observed was likely mainly due to radiative recombination in the plasma. Detail calculations are needed to confirm this.

References

[1] W. D. Hahn and N. Omenetto, "Laser-Induced Breakdown Spectroscopy (LIBS), Part I: Review of Basic Diagnostics and Plasma-Particle Interactions: Still-Challenging Issues Within the Analytical Plasma Community," *Appl. Spectrosc.*, vol. 64, p. 335A–366A, 2010.

[2] X. Jiang, P. Hayden, R. Laasch, J. T. Costello, and E. T. Kennedy, "Inter-pulse delay optimization in dual-pulse laser induced breakdown vacuum ultraviolet spectroscopy of a steel sample in ambient gases at low pressure," *Spectrochim. Acta - Part B At. Spectrosc.*, vol. 86, pp. 66–74, 2013.

[3] F. Anabitarte, A. Cobo, and J. M. Lopez-Higuera, "Laser-Induced Breakdown Spectroscopy: Fundamentals, Applications, and Challenges," *ISRN Spectrosc.*, vol. 2012, pp. 1–12, 2012.

[4] J. S. Penczak, Y. Liu, and R. J. Gordon, "Polarization-resolved laser-induced breakdown spectroscopy," *Opt. Lett.*, vol. 34, no. 4, p. 494, 2009.

[5] A. Eslami Majd, A. S. Arabanian, and R. Massudi, "Polarization resolved laser induced breakdown spectroscopy by single shot nanosecond pulsed Nd:YAG laser," *Opt. Lasers Eng.*, vol. 48, no. 7–8, pp. 750–753, 2010.

[6] J. Kim and D. E. Kim, "Measurement of the degree of polarization of the spectra from laser produced recombining Al plasmas," *Phys. Rev. E - Stat. Nonlinear, Soft Matter Phys.*, vol. 66, no. 1, pp. 1–4, 2002.

[7] Y. Zhao, S. Singha, Y. Liu, and R. J. Gordon, "Polarization resolved laser-induced breakdown spectroscopy," *Opt. Lett.*, vol. 34, no. 4, pp. 494–496, 2009.

[8] A. K. Sharma and R. K. Thareja, "Anisotropic emission in laser-produced aluminum plasma in ambient nitrogen," *Appl. Surf. Sci.*, vol. 253, no. 6, pp. 3113–3121, 2007.

[9] J. P. Singh and S. N. Thanku, *Laser Induced Breakdown Spectroscopy*, no. 1. Elisevier, 2007.

[10] A. W. Allen, M. Blaha, W. W. Jones, A. Sanchez, and H. R. Griem, "Stark-broadening measurement and calculations for a singly ionized aluminum line," *Phys. Rev. A*, vol. 11, no. 2, pp. 477–479, 1975.

[11] J. Dardis, "Interactions Of Intense Optical and Extreme-Ultraviolet Lasers with Atoms and Solids," Dublin City University, 2009.

[12] C. Fallon, "Optical Diagnostics of Colliding Laser Produced Plasmas : Towards Next Generation Plasma Light Sources," Dublin City University, 2013.

[13] G. A. Wubetu, H. Fiedorowicz, J. T. Costello, and T. J. Kelly, "Time resolved anisotropic emission from an aluminium laser produced plasma," *Phys. Plasmas*, vol. 24, no. 1, p. 13105, 2017.

[14] N. Farid, S. S. Harilal, H. Ding, and A. Hassanein, "Emission features and expansion dynamics of nanosecond laser ablation plumes at different ambient pressures," *J. Appl. Phys.*, vol. 115, no. 3, pp. 1–9, 2014.

[15] N. Agnes, Z.-Q. Hao, J. Liu, H.-Y. Tao, X. Gao, C.-K. Sun, and J.-Q. Lin, "The high dependence of polarization resolved laser-induced breakdown spectroscopy on experimental conditions," *Chinese Phys. B*, vol. 21, no. 7, p. 74204, 2012.

List of Publications Associated with this Work

Articles in Scientific Journals and Conference Proceedings

1) **G.A. Wubetu**, H. Fiedorowicz, J.T. Costello, and T. J. Kelly ‘‘Time-resolved anisotropic emission from an aluminum laser produced plasma’’ *Phys. Plasmas* **24**, 013105 (2017);
2) **G.A. Wubetu**, T. J. Kelly, P. van Kampen, H. Fiedorowicz, A. Bartnik, P. Wachulak, W. Skrzeczanowski, and J.T. Costello, ‘‘Comparison of the polarisation of line and continuum emission in a laser produced plasma’’ *IOP Conf. Series: Journal of Physics*: Conf. Series **810** (2017) 012063,
3) **G.A. Wubetu**, T. J. Kelly, P. Hayden, W. Skrzeczanowski, H. Fiedorowicz, and J. Costello, ‘‘Effect of target geometry and laser incident polarisationon on Al plasma emission’’ **(In preparation)**
4) **G.A. Wubetu**, T. J. Kelly, P. Hayden, W. Skrzeczanowski, H. Fiedorowicz, and J. Costello, ‘‘Time resolved polarisation imaging of an Al plasma at different pressures’’ **(In preparation)**
5) **G.A. Wubetu**, T. J. Kelly, P. Hayden, W. Skrzeczanowski, H. Fiedorowicz, A. Bartnik, P. Wachulak, W. Skrzeczanowski, and J.T. Costello, ‘‘Time-resolved emission spectroscopy of an Al alloy laser plasma in air’’- **(In preparation)**
6) **G.A. Wubetu**, T. J. Kelly, P. Hayden, W. Skrzeczanowski, H. Fiedorowicz, W. Skrzeczanowski, and J.T. Costello ‘‘Polarisation spectroscopy of a Cu plasma emission’’

Conference Oral Presentations:

1) **G.A. Wubetu**, T. J. Kelly, P. van Kampen, H. Fiedorowicz and J.T. Costello, “Polarisation-resolved laser-produced aluminum plasmas” EXTATIC Welcome Week Workshop, Warsaw, Poland, 20 - 24 October 2014
2) **G.A. Wubetu**, T. J. Kelly, P. van Kampen, H. Fiedorowicz and J.T. Costello, “Polarisation-resolved laser-produced aluminum plasmas” 29th International

Conference on Plasma and Nanotechnology, Mahatma Gandhi University, Kottayam, Kerala, India, 8 - 11 December 2014

3) **G.A. Wubetu**, T. J. Kelly, P. van Kampen, H. Fiedorowicz and J.T. Costello, "Anisotropic emission from an aluminum laser produced plasma" 2nd Workshop on Ultrafast Photonic Processes and Interactions, Dublin, Ireland, 28 - 29 January 2015
4) **G.A. Wubetu**, T. J. Kelly, P. van Kampen, H. Fiedorowicz and J.T. Costello, "Polarisation-resolved laser-produced aluminum plasmas" SFI Workshop, DCU, Dublin, Ireland, November 17, 2015
5) **G.A. Wubetu**, T. J. Kelly, P. van Kampen, H. Fiedorowicz and J.T. Costello, "Optical Diagnostics of Polarisation Resolved Spectroscopy of Laser Produced Al Plasma Emission" EXTATIC Welcome Week, Southampton, UK, 11 - 15 January 2016

Poster Presentations

1) **G.A. Wubetu**, T. J. Kelly, P. van Kampen, H. Fiedorowicz and J.T. Costello, "Polarisation-resolved laser-produced aluminum plasmas" 29th International Conference on Plasma and Nanotechnology, Mahatma Gandhi University, Kottayam, Kerala, India, 08 - 11 December 2014
2) **G.A. Wubetu**, T. J. Kelly, P. van Kampen, H. Fiedorowicz and J.T. Costello, "Anisotropic emission from an aluminum laser produced plasma" 42nd IOP Plasma Physics Conference, UK, 30 March - 02 April 2015
3) **G.A. Wubetu**, T. J. Kelly, P. van Kampen, H. Fiedorowicz and J.T. Costello, "Anisotropic emission from an aluminum laser produced plasma", PIRE Workshop, Purdue University, West Lafayette, USA, 11 - 12 May 2015
4) **G.A. Wubetu**, T. J. Kelly, P. van Kampen, H. Fiedorowicz and J.T. Costello, "Time-resolved anisotropic emission from an aluminum laser produced plasma", PIRE Workshop, Dublin City University, Dublin, Ireland, 01 - 03 July 2015
5) **G.A. Wubetu**, T. J. Kelly, P. van Kampen, H. Fiedorowicz and J.T. Costello, "Time-resolved anisotropic emission from an aluminum laser produced plasma", Photonics Ireland Workshop 2015, Cork, Ireland, 02 - 04 September 2015

6) **G.A. Wubetu**, T. J. Kelly, P. van Kampen, H. Fiedorowicz and J.T. Costello, "Optical Diagnostics of Polarisation Resolved Spectroscopy of Laser Produced Al Plasma Emission'', NCPST Workshop, DCU, Dublin, Ireland, December 12, 2015
7) **G.A. Wubetu**, T. J. Kelly, P. van Kampen, H. Fiedorowicz and J.T. Costello, "Anisotropic emission from an aluminum laser produced plasma", 23rd International Conference on Spectral Line Shape, Toruń, Poland, 19 - 24 June 2016

Conferences and Scientific meeting attended

1) EXTATIC Welcome Week, 02-04 Oct. 2013, Aachen, Germany
2) COST Action MP1203 Meeting, 21-22 Oct. 2013, Dublin, Ireland
3) VUV/EUV Workshop UCD, 02 Nov. 2013, Dublin, Ireland
4) Laser Ablation (LA) /Laser Induced Breakdown Spectroscopy (LIBS) Workshop, 02-04 Feb. 2015, Fremont, California, USA
5) NCPST Plasma/NanoScience Conference 19-20 March 2014, Dublin, Ireland
6) EXTATIC Welcome Week, 20-24 Oct. 2014, Warsaw, Poland
7) 29th International Conference on Plasma and Nanotechnology, 08-11 Dec. 2014, Mahatma Gandhi University, Kottayam, Kerala, India.
8) 2nd Workshop on Ultrafast Photonic Processes and Interactions, 28-29 Jan. 2015, DCU, Dublin, Ireland
9) 42nd IOP Plasma Conference 30 Mar-02 April 2015, Kents Hill Park Training and Conference Centre, Milton Keynes, UK
10) PIRE Workshop, 28-29 May 2015, Purdue University, West Lafayette USA
11) Purdue University PIRE Annual Meeting Jul. 2015, Dublin, Ireland
12) Photonics Ireland Workshop, 02-04 Sept 2015, Cork, Ireland
13) EXTATIC Welcome Week, 11-14 January 2016, Southampton, UK
14) 23rd International Conference on Spectral Line Shape, 19 - 24 June 2016, Toruń, Poland.

Awards

1) Oral presentation award certificate and Indian musical instrument in the 29th International Conference for Plasma and Nanotechnology, 08-11 Dec. 2014, Mahatma Gandhi University, Kottayam, Kerala, India

Course Completed

1) EXTATIC Foundation Module (FSH502)
2) Nanosecond Laser Ablation (FSH507)
3) Ultrafast lasers and Attosecond Technology (FSH506)
4) Special topics (FSH509)
5) Intellectual Property & Commercialization (GS601)
6) Research Ethics (GS604)